Analysis and Design of Reconfigurable MHD Antenna

THESIS

submitted in fulfillment of the requirement of the degree of

DOCTOR OF PHILOSOPHY

to

JC BOSE UNIVERSITY OF SCIENCE & TECHNOLGY

by

Taruna Sharma

Registration No: YMCAUST/PH16/2012

Under the Supervision of

Dr. MUNISH VASHISHATH
Professor, Department of Electronics Engg. J. C. Bose UST, YMCA, Faridabad, Haryana, 121006

Dr. RAJVEER YADUVANSHI
Professor, Department of ECE, NSUT, New Delhi, 110078

Department of Electronics Engineering,
J. C. Bose University of Science and Technology,
YMCA, Faridabad, Haryana, India, 121006

Jan, 2022

DECLARATION

I hereby declare that:

a) The work contained in the thesis is original and has been done by me, under the supervision of Professor Munish Vashishath and Professor Rajveer Singh Yaduvanshi.
b) The work has not been submitted to any other Institute for any degree or diploma.
c) I have followed the guidelines provided by the Institute in writing the thesis.
d) I have conformed to the norms and guidelines given in the Ethical Code of Conduct of the Institute.
e) Whenever, I have used materials (data, theoretical analysis and text) from other sources, I have given due credit to them by citing them in the text of the thesis and giving their details in the references.
f) Whenever, I have quoted written materials from other sources, I have put them under quotation marks and given due credit to the sources by citing them and giving required details in the references.

Signature of the Student

Name: Taruna Sharma

Roll no.: YMCAUST/PH16/2012

CERTIFICATE

This is to certify that this Thesis entitled **"Analysis and Design of Reconfigurable MHD Antenna",** being submitted in fulfillment of the requirement for the Degree of Doctor of Philosophy in **ELECTRONICS ENGINEERING** under the faculty of Engineering & Technology, J.C. Bose University of Science and Technology, YMCA, Faridabad, during the academic year 2019-2020, is a bonafide record of work carried out under our guidance and supervision.

We further declare to the best of our knowledge that the thesis does not contain part of any work which has been submitted for the award of any degree either in this university or in any other university.

Dr. MUNISH VASHISHATH
Professor, Department of Electronics Engg.
J. C. Bose University of Science and Technology, YMCA, Faridabad,
Haryana, 121006.

Dr. RAJVEER SINGH YADUVANSHI
Professor, Department of ECE,
NSUT, New Delhi 110078.

Dated:

ACKNOWLEDGEMENTS

Words are not sufficient to express my gratitude towards my supervisors Dr. Munish Vashsishath, Professor, Department of Electronics Engineering, J. C. Bose University of Science and Technology and Dr. Rajveer Singh Yaduvanshi, Professor, Department of Electronics and Communication Engineering, Ambedkar Institute of Advanced Communication Technology and Research, New Delhi for their invaluable guidance, everlasting encouragement and moral support with appreciation. I consider myself extremely fortunate to grab the opportunity to work and learn under them over the entire period of association with them. It is difficult to overstate my feelings towards my guide. Above all the reasons for which a student is grateful to his/her teacher, I am immensely grateful to my teachers for believing in me. They not only encouraged me from time to time but also took a lot of efforts to bring this work to conclusion. I not only owe them the contribution this work has made to science, but also every success in my future.

I am thankful to Dr. Parikshit Vasisht and Dr. Gaurav Varshney for their tremendous support and help during antenna fabrication and measurement work. I am deeply indebted to my father Mr. J. P. Sharma, who have always been my pillar of strength, my mother Mrs. Shanti Sharma for being epitome of courage, my siblings Bindu, Neeraj, Pankaj and Hidayat for their sheer support in whatever I do. My sincere heartiest thanks to my husband Mr. Manish Gautam for his constant encouragement and support. Without his support, completion of this thesis would not have been possible. I am at a short of words to express my loving gratitude to my sweet daughter Kashvi and son Abhiraj for their love which inspired me during my entire work.

In the end, I would like to express my deepest gratitude towards almighty God who has strengthen me in every struggle of life and provided enough perseverance and guidance in life.

Name: Taruna Sharma

Roll no.: YMCAUST/PH16/2012

ABSTRACT

Modern wireless information-oriented society needs wide bandwidth to support huge data transfers and that too with ease in space allocations. Antenna can be coined as key component of all wireless technologies. Vitality of antenna in any wireless communication system makes it crucial for antenna designers to design technology responsive antennae with desired characteristics. Micro-strip antenna have been emerged as an affable part of wireless system due to ease in fabrication, less weight, low cost and easy integration with other planar structures. High performance of micro strip antenna and arrays degraded due to low gain and low efficiency consequence of surface wave losses and conductor losses. Dielectric Resonator Antennas presented virtuous features such as high radiation efficiencies (97%) with high Quality Factor values, high gain, small size, light weight and low cost. DRAs offer high degree of flexibility versatility over wide range of frequencies. DRA's have another important factor such as low power losses and high-power handling capacity than a micro strip antenna.

DRA technology is emerging as a revolution in various fields including WBAN, Wi-Max, WLAN and cognitive radio. These are easy to fabricate and their operating bandwidth can be varied over wide range by choosing resonator parameters such as permittivity of the material. Simple coupling schemes are adopted for their integration into different planar structures and their performance is easily optimized. DRA operates in TE, TM and HEM modes and its impedance bandwidth is superior to micro strip antenna (MSA). Numerous techniques have been devised to increase the bandwidth of the DRA with a stable gain. These techniques can be broadly divided in three categories. First technique is lowering the Q-factor of the DRA. Second is making use of external matching networks to increase the impedance bandwidth. Third technique is combination of multiple DRA's in one form or another. It is possible to have different combination of shapes such as a dielectric disk, a rectangular DRA and a triangular DRA in the stacked antenna. Partial and Defected Ground structures presents a unique way of bandwidth increment by adding capacitive and reactive element to the circuit. Symmetrical and asymmetrical conducting strips not only decreases the dimensions but also increases the bandwidth.

A featured investigation on multi segment technique of bandwidth enhancement is applied in the proposed work. Total design can be segregated into four parts where

each segment is added sequentially one after another and their effect on gain and frequency response is observed accordingly. Presented work provides a novel design employing partial ground structure along with a slotted ground plane. Defected ground structure (DGS) technique not only reduces antenna size but also increases bandwidth. DGS is employed with stair step micro strip offers advantage of bandwidth enhancement and increases efficiency of antenna. Combination of multiple ring patch antenna with RRDRA yields best frequency response with an Ultra Wide Band and a high with increased average efficiency of 90% throughout the operating range. Compact size, high bandwidth along with high gain and efficiency makes it suitable candidate for UWB applications.

Re-configurability is an adjunct property of radiator due to which it can modify its frequency and can alter its radiating characteristics. Reconfigurability is a truly desired feature of an antenna system. This works presents a frequency reconfigurable antenna which makes use of fluids inside a resonator tube. Modes can be characterized as fields pattern set up due to excitation inside resonator tube. The word magneto hydrodynamics (MHD) is derived from magneto means magnetic field, hydro means liquid, and dynamics means movement. An oscillating rectangular fluid frame consisting of conducting fluid has been radiating under controlled electric field and magnetic field applied. Fluid molecules oscillate due to impact ionization inside the fluid and contribute to radiate energy. Resonant frequency depends on velocity of the fluid, volume, type of fluid, shape of tube, chemical properties of fluid used, magnetic bias and electric bias conditions. Hence, it has resulted into large design space for antenna reconfigurability mechanisms i.e. polarization reconfigurability and pattern reconfigurability.

Ultra wide band technologies are gaining momentum after Federal Communication Commission have approved and allocated frequency band of 3-10 GHz for this specified band. However, constant electromagnetic interference in Wi-Fi, W-LAN and X-band creates disturbance in the efficient working of system. Various techniques have been devised to suppress unwanted signal interference in WLAN, Wi-Fi and ITU bands. Insertion of stubs and parasitic strips and using modified DRA geometries with altered feed mechanism is serving the purpose. Presented work demonstrates a Fork shape feed, low profile DRA design for UWB communication. A compact antenna is proposed which not only solve the space constraint of the UWB systems but also can be fitted into any hand held device for 4.2-16.6 GHz range. DGS

technique of bandwidth enhancement is applied in the design. Partial ground structure with a slot in center and use of conducting strip not only increases the bandwidth but also increases gain of the antenna. Incorporation of the asymmetric ring in DRA reduces the quality factor of DRA which in turn improve cross and co polarization of the design.

Recent advancements in Wireless communication technologies have totally transformed the outlook of our society towards sharing and accessing the information via wireless media. Exponentially increasing modern day consumers are expecting super wide bandwidth, high data rate with high speed information for contemporary communication systems. Academia and Industry are rigorously searching for that viable spectrum whose frequency lies between overly crowded microwave region and deplored infrared region . Tera Hertz (THz) regime (0.1 -30 THz) is now envisioned as the potential candidate to alleviate scarcity of channel capacity and channel modelling with less fading and high spectral efficiency. An ultra-wideband (UWB) antenna covering the lower THz band has been implemented. The antenna response has been set with the single/dual/triple band notch characteristics depending upon the size and location of the applied graphene nano-ribbons.

Sensors designed using ultra-wideband (UWB) technology are considered powerful and emerging technique to extract information about the state of biological and physiological conditions of human organs for diagnostic purposes. MPA and DRA both are dual faces of microwave radiators and both offers own advantage and disadvantages.. A novel feed Ring rectangular Dielectric Resonator Antenna (RRDRA) is presented as a sensing element for Radar based microwave imaging Breast Cancer Detection technique. Proposed antenna is purposefully designed to radiate in Lower European Band so that penetrating tissue losses can be confined.

The main objective of this research work is to design and analyze Ultra Wide Band Dielectric Resonator Antenna with various bandwidth enhancement techniques. Implementation of Magneto Hydrodynamic Antenna, Multi-segmented DRA, Defected Ground Structure along with slots and strip combination yields desired response from the system. In this thesis, dual band notch creation and tunabilty in band notch has been implemented using grapheme nano ribbons. Design and analysis of Bio- medical applications of DRA have been incorporated in proposed work. All bandwidth enhancement techniques along with band notch creations have been explored. Specifically health related applications of the DRA’s such as lung and brain tumor and breast cancer have been explored in this thesis.

TABLE OF CONTENTS

DECLARATION i

CERTIFICATE ii

ACKNOWLEDGEMENTS iii

ABSTRACT iv

TABLE OF CONTENTS vii

LIST OF FIGURES xi

LIST OF TABLES xvi

LIST OF ABBREVIATIONS xvii

CHAPTER 1 **1-25**

INTRODUCTION

1. PREAMBLE 1

1.1 ANTENNA PERFORMANCE PARAMETER 2

1.1.1 Reflection Coefficient 2

1.1.2 Impedance 2

1.1.3 Voltage Standing Wave Ratio (VSWR) 2

1.1.4 Bandwidth 3

1.1.5 Radiation pattern and Half power beam width (HPBW) 4

1.1.6 Directivity 4

1.1.7 Efficiency 5

1.1.8 Gain 5

1.1.9 Polarization 5

1.2 DRA WORKING PRINCIPLE & SHAPES of DRA 8

1.2.1 The Hemispherical DRA 9

1.2.2 Cylindrical DRA Insight 11

1.2.3 The Rectangular DRA 12

1.2.4 Determination of Q-Factor and Resonant Frequency 14

1.3 DRA COUPLING METHODS 14

1.3.1 Micro strip line 16

1.3.2 Coaxial Probe 16

1.3.3 Aperture Coupled DRA 17

1.3.4 CPW fed DRA 18

1.4 ULTRA-WIDEBAND TECHNOLOGY 19
1.4.1 Frequency Bandwidth exploration in UWB Concepts 19
1.5 RE-CONFIGURABILITY, BAND NOTCH CREATION and TUNABILTY IN UWB SYSTM 20
1.6 BIO MEDICAL APPLICATIONS OF DRA 22
1.7 MOTIVATION 22
1.8 OBJECTIVES OF THESIS 23
1.9 METHODOLOGY 23
1.10 ORGANIZATION OF RESEARCH WORK 23
CHAPTER 2 **27-71**
LITERATURE SURVEY
2.1 INTRODUCTION 27
2.2 TRENDS IN DIELECTRIC RESONATOR ANTENNA STRUCTURES 28
2.3 BANDWIDTH ENHANCEMENT TECHNIQUES OF DRA 30
2.3.1 Review on Multi segment Multi Element DRA 30
2.3.2 Review on Defected Ground Structure 39
2.3.3 Review on Hybridization Techniques of Bandwidth Enhancements 43
2.3.4. Review on Array Structure 52
2.4 REVIEW on RE-CONFIGURABILITY and BAND NOTCH CREATION 54
2.4.1 Review on Band-Notch Multi-Mode & Multi-Band Reconfigurable antennas 61
2.5 REVIEW ON GRAPHENE BASED TUNABILITY 64
2.6 REVIEW on BIO-MEDICAL APPLICATIONS of DRA 66
2.6.1 Review on BREAST CANCER DETECTION SENSORS 68
CHAPTER 3 **73-85**
BANDWIDTH ENHANCEMENT TECHNIQUES of DRA
3.1 BANDWIDTH ENHANCEMENT USING MSRDRA 73
3.1.1 Geometry and Design of MSRDRA 74
3.1.2 Results and Discussions of MSRDRA 75
3.2 BANDWIDTH ENHANCEMENT of DRA with DEFECTED GROUND STRUCTURE 79
3.2.1 Geometry of DRA with Defected Ground Structure 79

3.2.2 Results and Discussions of DRA with Defected Ground Structure 80
3.2.3 Radiation Pattern 80
3.2.4 Impact of ground on bandwidth 82
3.2.5 Fabricated Results 83
3.3 CONCLUSION 84
CHAPTER 4 **87-110**
RECONFIGURABLE, BAND NOTCH AND TUNABLE ANTENNAS
4.1 Rectangular Moat shaped MHD Antenna 88
4.1.1 Mathematical modelling of Liquid Assisted Antenna 89
4.1.2 Software Based Design of Antenna 90
4.1.3 Results and Discussions for MHD Antenna 91
4.1.4. Parametric Analysis of Antenna 92
4.2 BAND NOTCH CREATION with DRA 93
4.2.1 Antenna Geometry and Design 94
4.2.2 Results and Discussion for Band Notch DRA 96
4.3 TUNABLE ANTENNA WITH GRAPHENE 98
4.3.1 Nano-Antenna with UWB response 101
4.3.2 The Tunable Dual-Band Notch Characteristics 104
4.4 CONCLUSION 110
CHAPTER 5 **111-131**
BIO-MEDICAL APPLICATIONS OF DRA
5.1 INTRODUCTION 111
5.1.1 Design and Development of DRA with Circular Patches. 113
5.1.2 Theoretical Consideration of DRA with Circular Patches 114
5.1.3 Results and Discussions for DRA with Circular Patches 115
5.1.4 Radiation Pattern of DRA with Circular Patches 118
5.1.5 Parametric Analysis of DRA with Circular Patches 119
5.1.6. Impact of Ground on antenna performance 120
5.1.7 Stepped Microstrip Parametric Variation 122
5.1.8 Phantom Design and SAR Calculation 123
5.2 DRA with SYMMETRICAL L-SHAPE STUB MICROSTRIP FEED 124
5.2.1 Design of DRA with Symmetrical L-shape microstrip feed 124

5.2.2 Optimization of the feed 125
5.2.3 Fabricated prototype of Antenna 127
5.2.4 Results and Discussions 127
5.3 CONCLUSION 130
CHAPTER 6 **133-136**
CONCLUSIONS AND FUTURE SCOPES
6.1 CONCLUSION 133
6.2 FUTURE SCOPE 135
REFERENCES 137-163
APPENDIX 165-167
BRIEF PROFILE OF RESEARCH SCHOLAR 169
LIST OF PUBLICATIONS 171-173

LIST OF FIGURES

Figure	Legend	Page No.
1.1	Frequency Response of Antenna	3
1.2	Radiation Pattern and Half Power Beam Width	4
1.3	Ceramic rectangular DRA with a, b, and d dimensions	9
1.4	Geometrical Representation of Hemispherical DRA	9
1.5	Geometrical Representation of Cylindrical DRA	11
1.6	Geometrical Representation of Rectangular DRA	13
1.7	Various Coupling Mechanism of DRA	15
1.8	Geometrical Representation of Micro-strip feed line	16
1.9	Geometrical Representation of Co-axial feed line	17
1.10	Geometrical Representation of Aperture feed line	18
1.11	Geometrical Representation of CPW feed line	18
1.12	UWB antenna with notch filter implementation	21
2.3.1	(a) Geometry of proposed antenna (b) Comparison of Simulated and Measured Input Reflection	32
2.3.2	Coefficient of Proposed Ring DRA with Annular-Shaped Microstrip Feed	32
2.3.3	Geometry of proposed antenna Top view	33
2.3.4	Simulated and Measured Reflection Coefficient	33
2.3.5	Fabricated prototype of antenna	34
2.3.6	Simulated and Measured Reflection Coefficient	34
2.3.7	(a) Top View of the DRA (b) Isometric View of DRA	35
2.3.8	Simulated and Measured Reflection Coefficient	36
2.3.9	Aperture coupled Asymmetric DRA (a) Top View Aperture coupled Asymmetric DRA (b) Side View	36
2.3.10	Measured and simulated Reflection Coefficient of the DRA	37
2.3.11	Schematic diagram of a proposed DRA symmetrically placed on a Defected Ground Structure: (a) Front Schematic diagram of a proposed DRA symmetrically placed on a Defected Ground Structure: (b) Top Schematic diagram of a proposed DRA symmetrically placed on a Defected Ground Structure: (c) Rear View	40
2.3.12	Measured and simulated Reflection Coefficient of the DRA	40
2.3.13	Geometry of proposed antenna (a) Top view Geometry of proposed antenna (b) Panoramic view	41
2.3.14	Comparison of Simulated and Measured Reflection Coefficient	41
2.3.15	Cubical-shaped dielectric resonator antennas (a) Microstrip feed line	42

	Cubical-shaped dielectric resonator antennas b) Reduced ground plane with slots	
	Cubical-shaped dielectric resonator antennas (c) Front View	
2.3.16	Measured and Simulated Reflection Coefficient	42
2.3.17	Geometry of Proposed Antenna (a) Panoramic	
	Geometry of Proposed Antenna (b) Top view	44
2.3.18	Comparison of Simulated and Measured Input Reflection Coefficient	44
2.3.19	Geometry of proposed antenna (a) Top view	
	Geometry of proposed antenna (b) Side view	45
2.3.20	Simulated and Measured Reflection Coefficient	45
2.3.21	Schematic Diagram of Proposed CDRA (a) Psi-Shaped Microstrip Line	
	Schematic Diagram of Proposed CDRA (b) Isometric View of Realized CDRA	47
2.3.22	Measured and Simulated Return Loss variation of Proposed Antenna	47
2.3.23	Schematic Diagram of Proposed CDRA	48
2.3.24	Simulated and Measured Reflection Coefficient	49
2.4.1	Categorization of antenna reconfiguration techniques	55
2.4.2	Top View of the DRA	60
2.4.3	Simulated and Measured Reflection Coefficient	60
2.4.4	Top View of the DRA	62
2.4.5	Simulated and Measured Reflection Coefficient	63
3.1.1	Geometrical Configuration of the MSRDRA	74
3.1.2	(a) Geometry of RDRA with No Segment	75
	(b) S11 Response of the RDRA with No Segment.	
3.1.3	(a) Geometry of RDRA with one segment	76
	(b) S11 response of the RDRA with one segment.	
3.1.4	(a) Geometry of RDRA with two segments	76
	(b) S11 response of the RDRA with two segments.	
3.1.5	(a) Geometry of RDRA with three segments	77
	(b) S11 response of the RDRA with three segments.	
3.1.6	(a) Geometry of RDRA with four segments.	77
	(b) S11 response of the RDRA with four segments.	
3.1.7	(a) Radiation Efficiency of the antenna	78
	(b) Gain v/s Frequency response of the antenna	
3.1.8	(a) Radiation Pattern at 9.29 GHz	78
	(b) Broadband Radiation Pattern	
3.1.9	Comparison of proposed MSRDRA parameters	79
3.2.1	(a) Top View	79
	(b) Side view	
	(c) Bottom view of DRA	

3.2.2	Reflection coefficient of Proposed Structure (PS) and Patch Only (PO) configuration of antenna.	80
3.2.3	Radiation Pattern at 5.3 GHz Radiation Pattern at 9.3 GHz Radiation Pattern at 12.57 GHz Broadband Radiation Pattern	81
3.2.4	(a) Gain of the antenna (b) Radiation Efficiency	82
3.2.5	Variation in dimensions of Ground Plane	82
3.2.6	(a) Fabricated Microstrip Patch (b) Ground plane of antenna without DRA	83
3.2.7	(a) Assembled antenna with DRA (b) Measured S11 parameter	84
3.2.8	Comparitive Graph of Measured and Simulated (a) Reflection Coefficient Comparitive Graph of Measured and Simulated (b) Gain	84
4.1.1	(a) Geometrical structure of DRA (b)Geometry of Square Annular Ring MHD shows Magnetic and Electric bias.	90
4.1.2	Optimized Return Loss results	91
4.1.3	Return Loss results for various frequency bands when NaCl is taken as fluid element.	91
4.1.4	Obtained radiation pattern of X-Y plane of antenna	92
4.1.5	Gain obtained by the antenna	92
4.1.6	Return Loss Graph for frequencies when different probe lengths are taken	93
4.2.1	(a) Top View (b) Bottom View of the antenna (c) Without slot feed structure (d) with slot feed structure	95
4.2.2	(a) S11 with and without Slot in CST (b) VSWR with and without slot in CST	97
4.2.3	(a) Gain Drop in DRA with and without Slot (b) Depicts Drop in Efficiency at Band Rejection Frequencies	97
4.2.4	(a) Co-polarized and Cross Polarized Simulated Radiation Patterns in $\phi = 0^o$ and $\phi = 90^o$ Planes at Operating Frequency 4.5 GHz (b) Co-polarized and Cross Polarized Simulated Radiation Patterns in $\phi = 0^o$ and $\phi = 90^o$ Planes at Operating Frequency 7.5 GHz	98
4.3.1	The antenna structure	101
4.3.2	(a) Antenna Evolution (b) S-parameter Response	103

	(c) Electrical Equivalent circuit of UWB antenna.	
4.3.3	S-Parameter Response of UWB Antenna with Variable, l_s S-Parameter Response of UWB Antenna with Variable, w_s S-Parameter Response of UWB Antenna with Variable, l_p S-Parameter Response of UWB Antenna with Variable, w_p	103
4.3.4	Effect of placing the dielectric slab with grown graphene nano-ribbons on (a) S_{11} parameter response (b) phase (c) real (d) imaginary part of impedance	104
4.3.5	(a) Impedance Plot of the Antenna with and without Graphene Nano-Ribbons showing the generation of multiple modes (b) Equivalent Circuit of Antenna with Graphene Nano-Ribbons.	105
4.3.6	Antenna Response with variable μ_c.	105
4.3.7	E −field distribution on antenna without graphene nano-ribbons at frequency without graphene ribbon	108
4.3.8	E −field distribution on antenna without graphene nano-ribbons at frequency with graphene ribbons	108
4.3.9	S_{11}-parameter response of antenna with (a) different values of offset of graphene nano-ribbons from the bottom edge of metallic radiator S_{11}-parameter response of antenna with (b) variable s S_{11}-parameter response of antenna with (c) variable w_{st}	108
4.3.10	Radiation pattern of antenna at frequency	109
4.3.11	(a) Gain with and without graphene nano-ribbons. radiation efficiency of antenna with and without graphene nano-ribbons (b) radiation efficiency of antenna with and without graphene nano-ribbons	109
5.1.1	Depicts (a) Top View, Depicts (b) Top View without DRA Depicts (c) Side view Depicts (d) Bottom View	113
5.1.2	(a) Reflection Coefficient comparison (b) VSWR comparison (c) Gain comparison, (d) Radiation Efficiency comparison	116
5.1.3	Impedance Plot of the Proposed Structure	117
5.1.4	E field distribution inside RDRA	117
5.1.5	Radiation Pattern with Co-Polarization and Cross Polarization at	118

5.1.6	Evolution of the Patch to be used in sensor	119
5.1.7	(a)Various response of patch from evolution stages (b)Response of various ground structures	120
5.1.8	Various modifications in partial ground structure	121
5.1.9	Current Density of Ground Plane (a) Without slot Current Density of Ground Plane (b) With slot	122
5.1.10	Length variation of Micro strip feed Width variation of Micro strip feed	122
5.1.11	Breast Phantom for calculation of SAR	124
5.2.1	(a) Top View (b) Side View (c) Feed structure of Antenna	125
5.2.2	(a) Simple feed (b) Inductive feed (c) Capacitive feed	125
5.2.3	(a) Imaginary Impedance of the three stages (b) Reflection coefficients of the three stages.	126
5.2.4	Electrical equivalent circuit of Structure	126
5.2.5	(a) Fabricated prototype of antenna (b) Measured Refection-coefficient (c) Screen shot of VNA	127
5.2.6	(a) represents comparison between measured and simulated parameter (b) impedance plot of the antenna.	128
5.2.7	Electric field at configuration	129
5.2.8	(a) Gain (b) Radiation Efficiency of Antenna	129
5.2.9	Simulated and measured Co-polarization and Cross-polarization radiation patterns of the proposed antenna structures at frequencies 4.1, 5.2 and 6.8 GHz respectively along $\phi = 0^o$ and $\phi = 90^o$.	129

LIST OF TABLES

Table	Legend	Page No.
1.1	Comparison between MPA and DRA	6
2.3.1	Multi-segment DRA for Bandwidth Enhancement	38
2.3.2	DGS based Bandwidth Enhanced DRA	42
2.3.3	Mixed Methods implemented DRA designs to Enhance Bandwidth	51
2.4.1	Reconfigurable DRA in present state of art	61
2.4.2	Summarizing Narrow Band Structure in UWB Technology	62
2.4.3	Band Notch DRA's in present state of Art	63
2.5	Comparison table of THz Patch Antenna	66
2.6	Radiators Proposed for BAN Networks	67
2.6.1	Sensor comparison for early detection of Breast Cancer	70
3.2.1	Dimensions of antenna structure	80
3.2.2	Impact of Ground Dimensions on Band Width	83
4.1.1	Dimensions of Rectangular MHD Antenna	90
4.1.2	Parametric Variation of Probe Inside Fluid	93
4.2.1	Dimensions table of DRA	96
4.3	Dimensions of antenna structure	101
4.3.1	Performance of antennas	103
5.1.1	Dimensions of Proposed Structure	114
5.1.2	Dimensions of Jumbled ring structure	119
5.1.3	Variation in Bandwidth with variation in Patch	120
5.1.4	Variation in Bandwidth due to Defected Ground Structure	121
5.1.5	Material properties of the multilayer human tissue model	123
5.2.1	Dimensions of Proposed Structure	125

LIST OF ABBREVIATIONS

CDRA	Cylindrical Dielectric Resonator Antenna
CPW	Co-Planar Waveguide
DRA	Dielectric Resonator Antenna
FBW	Fractional Bandwidth
FCC	Federal Communication Commission
FR1	Frequency Range 1
FSS	Fixed Service Satellite
IEEE	Institute for Electrical and Electronics Engineers
LTE	Long Term Evolution
LTE-A	Long Term Evolution- Advance
MSRDRA	Multi Segment Rectangular Dielectric Resonator Antenna
RDRA	Rectangular Dielectric Resonator Antenna
RRDRA	Rectangular Ring Dielectric Resonator Antenna
UWB	Ultra Wideband
VSWR	Voltage Standing Wave Ratio
WLAN	Wide Local Area Network
BAN	Body area network

CHAPTER 1

INTRODUCTION

1.PREAMBLE

Wireless Communication has been emerging as a skyrocketing industry after World War II due to excellent inventions and technological advancements. Complex and efficient systems consequent as a breakthrough caused by transistor followed by integrated circuits and compact & low profile antennas. The data to be transmitted from Point A to Point B through the atmosphere has to be converted from its electrical form inside the transmitter into an electromagnetic wave that can propagate through the atmosphere to reach the receiver station where it is converted back to an electrical signal for further processing. Antenna can be defined as a transducer in the system which converts electrical signals into electromagnetic waves and vice versa. An antenna is a pivotal element in a radio communication system which is required in both the transmitting and receiving terminals.

Antenna is the device for radiating or receiving electromagnetic wave in free space. The antenna is the interface between transmission line and free space. An antenna has various shape and geometries such as wire antennas, aperture antennas and printed antennas. Dipole antennas, loop antennas and helix antennas are classified as wire antennas while horn antennas and slot antennas are classified as aperture antennas. For printed antennas, there have patch antennas and printed slot antennas. An antenna works when there is variation in electric charge, the electric current undergoes a variation over time resulting in electromagnetic radiation. Charge acceleration is obtained when a time varying exciting current exists while deceleration occurs when there is a discontinuity in the current path or a bent. These mechanisms are utilized to produce electromagnetic radiation and is used in wireless signal transmission. Various types of antennas have been developed for several applications. TV broadcast antennas of high height while the cellular phone are just a few millimeters long. The techno logical advancements especially in integrated circuits have allowed the designers to integrate antennas in very small vicinities within the electronic gadget. This research work delineates Rectangular Dielectric Resonator Antenna (RDRA). These aerials are used in several wireless applications like global positioning system (GPS) receivers and radar systems.

1.1 ANTENNA PERFORMANCE PARAMETER

To describe the performance of an antenna, definitions of various parameters are necessary. Some of the basic parameters of antennas are discussed as below:

1.1.1 Reflection Coefficient

The reflection coefficient is another way of expressing mismatch. It is a logarithmic ratio measured in dB that compares the power reflected by the antenna to the power that is fed into the antenna from the transmission line. The relationship between Voltage Standing Wave Ratio (VSWR) and return loss is the following:

$$\text{Return Loss (in dB)} = -20 \log_{10} \left(\frac{\text{VSWR}-1}{\text{VSWR}+1}\right)\text{dB} \quad (1.1)$$

1.1.2 Impedance

The input impedance of the antenna must identically match the characteristic impedance of the transmission line in order to achieve maximum energy transfer between a transmission line and an antenna. If the input impedance of the antenna does not match with the characteristic impedance of the transmission line, a reflected wave will be generated at the antenna terminal and travel back towards the energy source. This reflection of energy results in a reduction in the overall system efficiency. This loss in efficiency will occur if the antenna is used to transmit or receive energy.

1.1.3 Voltage Standing Wave Ratio (VSWR)

VSWR is the ratio between the maximum voltage and the minimum voltage along the transmission line. The VSWR is given by:

$$\text{VSWR} = \frac{1+\Gamma}{1-\Gamma} \quad (1.2)$$

$$\Gamma = \frac{Z_L - Z_0}{Z_L + Z_0} \quad (1.3)$$

where

Γ = reflection coefficient, Z_L = load impedance and Z_0 = characteristic impedance .

The VSWR indicate that how closely or efficiently an antenna's terminal input impedance is matched to the characteristic impedance of the transmission line. The large number of VSWR, the greater the mismatch between the antenna and the transmission line. In many systems, the antenna is required to operate with a VSWR better than 2:1 with 50 Ω impedance. Therefore an antenna VSWR should be closely to the 50Ω of the antenna impedance. The system are perfectly match if the VSWR

equals to 1:1 where there is no power reflected and all the energy are absorbed at their input terminal.

1.1.4 Bandwidth

Bandwidth refers to the range of frequency that the antenna will radiate effectively where the antenna meets a certain set of specification performance criteria. An antenna that operates over a wide frequency range and still maintain satisfactory performance must have compensating circuits switched into the system to maintain impedance matching. The relationship between VSWR and the bandwidth are shown in Fig.1.1. As shown in Fig. 1.1 operating bandwidth of 3.8 GHz for reflection coefficient below -10dB is obtained for a frequency range starting from 3.7 to 7.5 GHz. VSWR ratio is less than 2 is obtained from the same frequency range

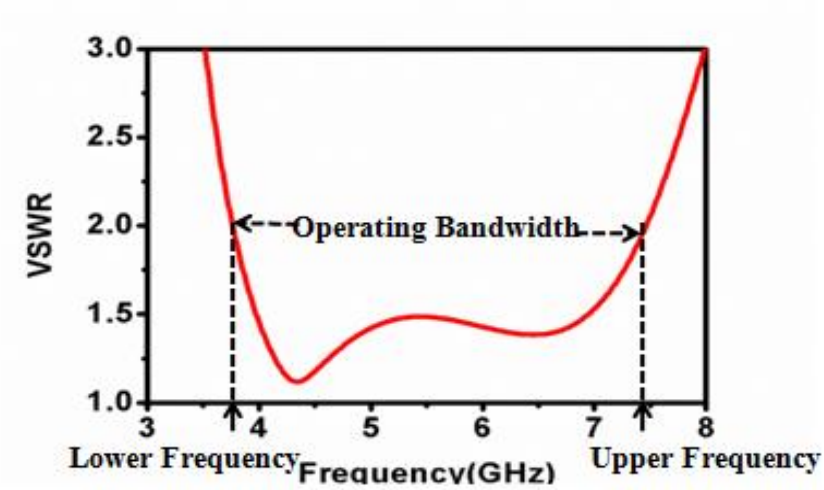

Fig.1.1. Frequency Response of Antenna [Taruna et al. MAPAN 2021]

To determine the bandwidth on the input return loss graph, the difference in frequency is taken at the points where the curve cut the -10dB level. The difference then divided by the resonant frequency to give the percentage bandwidth. In a similar manner, VSWR bandwidth is taken to be the range of frequency that corresponds to a VSWR of less than 2. These can be expressed by:

$$10\text{ dB Bandwidth} = \frac{f_U - f_l}{f_r} \tag{1.4}$$

where f_U = upper frequency, f_l = lower frequency and f_r = operating frequency

1.1.5 Radiation pattern and Half power beam width (HPBW)

Radiation pattern of an antenna affects system coverage and performance. The radiation pattern of antenna simply describes how an antenna focuses or directs the energy it radiates or receives. All antennas do not radiate more total energy than is delivered to their input connector. Antenna radiation pattern are typically presented in the form of a polar plot for a 360° angular pattern in one of two sweep planes and it is presented on a relative power dB scale as shown in Fig.1.2.

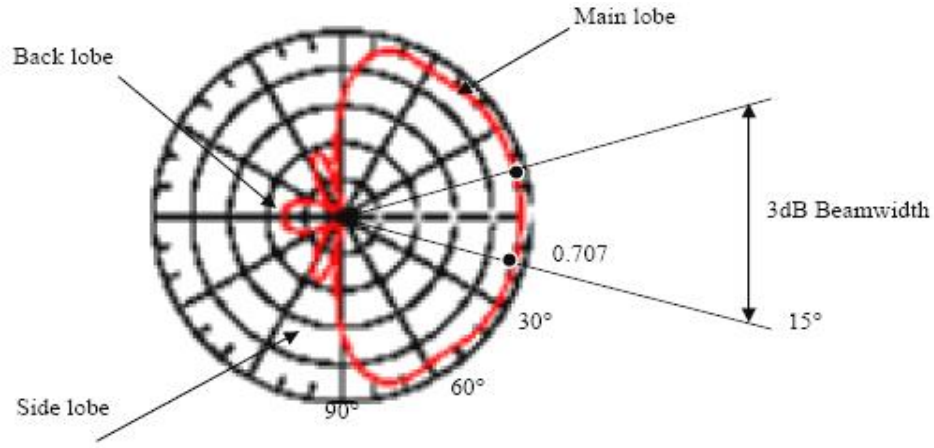

Fig.1.2 Radiation Pattern and Half Power Beam Width [1-2]

From Fig.1.2, it can be observed that the field strength drops to 0.707 (measure in μ (V/m)) of the maximum voltage at the center of the lobe. These points are known as the half power points. The other radiation pattern properties of significance are the antenna's side lobes, back lobes and front to back ratio (f/b). Generally it is impossible to eliminate antenna side lobes and back lobes completely. Antenna side and back lobes affect antenna and system performance in several ways. At a transmitter, energy delivered to side and back lobes maybe directed towards other receive systems causing interference. At receiver, energy from other transmit sites may be receive through the side and back lobes causing interference within the system.

1.1.6 Directivity

Directivity of an antenna is the ratio of the radiation intensity in a given direction from the antenna to the radiation intensity averaged over direction. The average radiation intensity is equal to the total power radiated by the antenna divided by 4π. If the direction is not specified, the direction of maximum radiation is implied. It can be expressed as:

$$D = \frac{4\pi U}{P_{rad}} \tag{1.5}$$

where D = Directivity , U = Radiation intensity (W/unit solid angle), P_{rad} = Total radiated power (W)

1.1.7 Efficiency

Radiation Efficiency of an antenna can be expressed as ratio of power radiated by antenna to the net power received by the antenna to the connected transmitter**.**

$$\text{Efficiency } \eta = \frac{R_{radiated}}{R_{radiated} + R_{dielectric}} \quad (1.6)$$

where $R_{radiated}$ = radiation resistance, $R_{dielectric}$= dielectric resistance

1.1.8 Gain

Absolute gain of an antenna is define as "the ratio of the intensity, in a given direction, to the radiation intensity that would be obtain if the power accepted by the antenna were radiated isotropically. The radiation intensity corresponding to the isotropically radiated power is equal to the power accepted (input) by the antenna divided by 4π.

Relationship between Gain, Directivity and Efficiency can be expressed by eq. given as below:

$$\text{Gain} = \eta D \quad (1.7)$$

where η = Efficiency of antenna

D=Directivity of antenna

1.1.9 Polarization

Polarization is refers to the direction in space of the E-Field (electric vector) portion of the electromagnetic wave being radiated by the transmission system. Low frequency antennas are vertically polarized because of ground effect (reflected waves) and physical construction methods while high frequency antennas are generally horizontally polarized. Polarization may be classified as linear, circular and elliptical. If the vector that describes the electric field at a point in space as a function of time is always directed along a line, the field is said to be linear polarized. When the electric field traces is an ellipse, the field is said to be elliptically polarized. Linear and Circular Polarizations are special cases of elliptical because they can be obtained when the ellipse becomes a straight line or a circle. The figure of electric field is traced in a clockwise (CW) or counterclockwise (CCW) sense. Clockwise rotation of the electric field vector is designated as right-hand polarization and counterclockwise as left-hand polarization.

Instigation of miniaturization of electronic circuitry (VLSI) enables the wireless systems to achieve new epitome in terms of speed, efficiency and adequacy in contemporary communication systems. Low profile and compact wideband antennas are required in upcoming wireless technologies. Micro-strip Patch antennas have emerged as a potential candidate due to their light weight, conformability, low cost and ease of fabrication [4]. These antennas can be integrated with printed strip -line feed networks and active devices. However, use of metal in MPA antenna alleviate losses which subsequently reduces gain and efficiency of antenna.

Dielectric Resonator Antennas presented virtuous features such as high radiation efficiencies with high Q-factor, high gain, small size, light weight and low cost. DRAs offer high degree of flexibility versatility over wide range of frequencies. DRA's have another important factors such as low power losses and high power handling capacity than a microstrip antenna (MSA) [246]. These are easy to fabricate and their operating bandwidth can be varied over wide range by choosing resonator parameters such as permittivity and loss tangent. DRA technology is emerging as a revolution in various fields including WBAN, Wi-Max, WLAN and cognitive radio. Simple coupling schemes are adopted for their integration into different planar techniques and their performance is easily optimized. DRA operates in TE, TM and HEM modes and its impedance bandwidth is superior to microstrip antenna (MSA). The dimension of a DRA is proportional to guided wavelength and is of the order of $\frac{\lambda_0}{\sqrt{\varepsilon_r}}$, Where, λ_0=Free space wavelength and ε_r = Relative Permittivity of the dielectric material ($10 \leq \epsilon r \leq 100$)]. Table 1.1 Provides a comparison between Microstrip Patch Antenna and Dielectric Resonator Antenna [1-6].

Table 1.1 Comparison between MPA and DRA

S.no.	Microstrip Patch Antenna (MPA)	Dielectric Resonator Antenna (DRA)
1.	Patch size varied from $\lambda/2$ to $\lambda/3$, and the thickness of dielectric substrate is in the range of 0.003λ to 0.05λ.	The size of DRA is proportional to $\lambda_o/\sqrt{\varepsilon_r}$ where λ_0 is the free space wavelength at resonant frequency and ε_r is the dielectric constant of the material.
2.	Radiation Efficiency of micro-strip is less on the account of surface wave and conductor	High efficiency in a DRA can be achieved due to less surface wave losses low conductor losses.

	losses occurring due to presence of metal.	
3.	Patch length and dielectric constant determines the resonating frequency of antenna.	Aspect ratio with fixed dielectric constant determines the resonant frequency of DRA.
4.	Microstrip Patch is highly compatible with every kind of feeding mechanism.	Variety of feeding mechanisms and their compatibility with contemporary fabrication technique make them ideal candidate for communication devices.
5.	At higher microwave frequencies the sizes of MSA go beyond the practical limits.	The size of the DRA remains within practical limits at higher frequency as the aspect ratio and dielectric constant provides the antenna designer additional degrees of freedom.

Dielectric Resonator Antennas can be considered as a suitable candidate for millimeter wave application due to minor conductor losses [1]. DRA is a combination of partial metalized surface along with high permittivity that can be utilized as small and low profile antenna at lower microwave frequency bands. Investigations on various DRA shapes like Hemispherical, Cylindrical and Rectangle. High permittivity (≥ 20) material used for fabrication of Dielectric Resonator restrict its use as microwave oscillators and filter and was considered energy storing element rather than a radiator. In order to provide litheness in DR structure, various fusion shapes like H, stair cased, multi segment etc. are realized. Metal absence along with ceramic structure enables DRA as an ardent aerial structure for green electronics and built-in module in various microwave circuits of green communication devices.

Dielectric Resonator Antenna find relevance in applications related to compact and miniaturized microwave circuitry in a variety of microwave frequency bands such as C, X, UWB etc. In year 2002, the FCC declaration of $3.1 - 10.6$ GHzfrequency band for UWB technology refurbish the field of research and development further in to the domain [143]. As a result of Federal Communications Commission regulation, a system

can be termed as UWB system if it possess a signal with a minimum of 500 MHz band width or alternatively fractional bandwidth greater than 20%.

Due to inclusion of Ultra Wideband Frequency Bands, the telecom industry is also looking for antennas capable of rejecting free bands allocated in FCC declaration. UWB technology is capable of supporting high bandwidth and high data rates, which makes it an integral part of modern wireless communication along with military and defense applications. This characteristic of band notch in antenna find its application in dejecting bands in short range applications such as blue tooth. Re-configurability is an important feature that can be achieved in a system with the help of antennas [146-152]. With re-configurable systems, an antenna can exhibit variant bandwidth and radiation characteristics. The biggest challenge is to design such systems which are appropriately suitable for UWB applications with free band rejection property with reconfigurability in current scenario [119-140]. The diverse properties of dielectric resonator structures and especially rectangular shapes offers flexibility to alter key parameters of antenna such as impedance bandwidth, co-polarization and cross-polarization levels. All these characteristics proves DRA as an promising candidate in competitive wireless communication technologies.

1.2 DRA WORKING PRINCIPLE & SHAPES of DRA

Working of DRA can be understood by considering it as a magnetic dipole in which radiation process starts from the reflection of input EM waves which in turn forms the standing waves [1-2]. Removal of conducting metallic walls facilitates EM energy radiates into the free space. Fringing effect is observed in DRA when magnetic field starts out of perforated magnetic walls which are constituted by outer edges of the DRA. Absence of conducting walls not only reduces the conductor losses but also increases the efficiency of the antenna. The Fig. 1.3 shows a Rectangular Dielectric Resonator antenna with dimensions a, b and d.

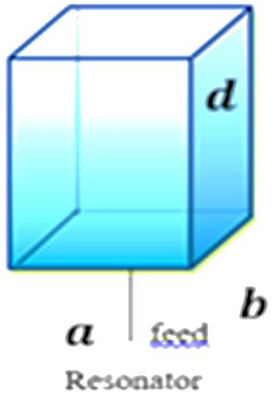

Fig 1.3 Ceramic rectangular DRA with a, b, and d dimensions [1-2]

1.2.1 The Hemispherical DRA

The geometrical representation of Hemispherical DRA with dielectric material of permittivity "ε_r" and radius of "a" units as shown in Fig. 1.4 [1]. The DRA is mounted over ground plane directly onto a lower permittivity substrate. Micro-strip feed line is used to couple electromagnetic power to the hemispherical radiator. Analysis of hemispherical DRA is carried out by assuming the ground plane possesses infinite conductivity and is extended till infinity. As a result of this assumption, it can be considered as an isolated hemispherical DRA with radius as 'a' units. In this DRA , primarily two radiation modes can be observed i.e. transverse electric (TE) and transverse magnetic (TM) modes [14] . When the radial component of electric field E_r becomes zero a TE mode is generated. Similarly for radial magnetic field H_r reducing to zero a TM mode is propagated.

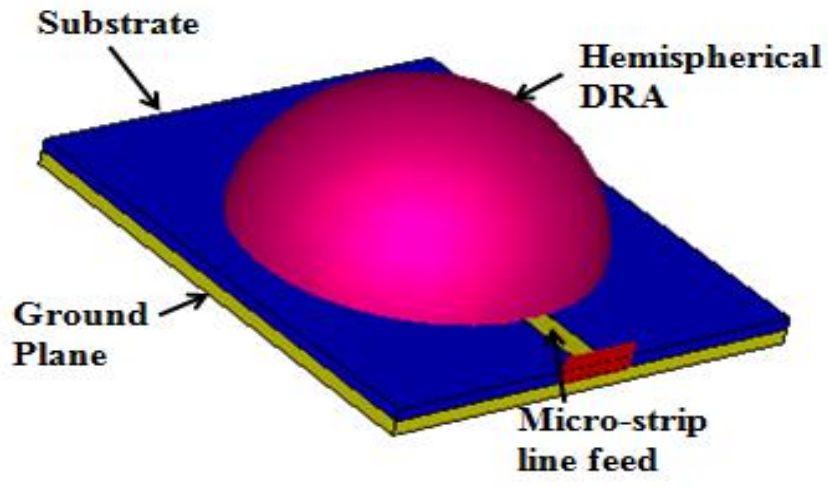

Fig. 1.4 Geometrical Representation of Hemispherical DRA [1]

In a classic hemispherical DRA, the lowest order or dominant mode is identified as TE_{111} mode. The radiation pattern of hemispherical antenna in far field is much similar to a horizontal short magnetic dipole. The Characteristic eq. (1.8) helps in calculating the resonant frequency and the quality factor given as:

$$\frac{J_{1/2}(\sqrt{\varepsilon_r}k_0 a)}{J_{3/2}(\sqrt{\varepsilon_r}k_0 a)} = \frac{H^{(2)}_{1/2}(k_0\ a)}{\sqrt{\varepsilon_r}H^{(2)}_{1/2}(k_0\ a)} \tag{1.8}$$

where J(x) is defined as first order Bessel function and $H^{(2)}$ (x) is the second order Hankel function and k_0 denotes the free space wave number. The eq. (1.8) is transcendental in nature and the solution for k_0, further guides towards the determination of the resonant frequency of the antenna, as given by eq. (1.9)

$$f_{GHz} = \frac{4.7731\ \mathrm{Re}(k_0\, a)}{a_{cm}} \tag{1.9}$$

where frequency is expressed in GHz and radius in cm. The radiation Q- factor can be calculated using eq. (1.10):

$$Q = \frac{\mathrm{Re}(k_0\, a)}{2\ \mathrm{Im}(k_0\, a)} \tag{1.10}$$

As per [1], the Q-factor and Re ($k_o a$) can also be determined using below mentioned eq. (1.11) and (1.12):

$$\mathrm{Re}(k_0\, a) = 2.8316\varepsilon_r^{-0.47829} \tag{1.11}$$

$$Q = 0.08 + 0.796\varepsilon_r + 0.01226\varepsilon_r^2 - 3.10^{-5}\varepsilon_r^3 \tag{1.12}$$

In eq. (1.12) ε_r denotes the relative dielectric constant.

The impedance bandwidth of DRA of any shape utilizing eq. (1.13)

$$BW = \Delta f / f_o = (s - 1)/\sqrt{sQ} \tag{1.13}$$

Where Δf denotes the absolute bandwidth, f_o the resonant frequency and s denotes the voltage standing wave ratio.

By employing a co-axial probe fed technique to hemispherical DRA can easily convert it into Short electric dipole [14]. Coupling mechanisms has a distinctive effect on the input impedance of the hemi spherical DRA and provides the deviation of Q-factor from isolated dielectric sphere. A probe fed hemispherical DRA generates TM_{101} fundamental mode which supports the above theory. The Q-factor and resonant frequency of DRA operating in TM_{101} can be found by using the following transcendental eq. (1.14) as:

$$\frac{1}{\sqrt{\sqrt{\varepsilon_r}k_0 a}} = \frac{J_{1/2}(\sqrt{\varepsilon_r}k_0 a)}{J_{3/2}(\sqrt{\varepsilon_r}k_0 a)} = \frac{\sqrt{\varepsilon_r}}{k_0 a} = \sqrt{\varepsilon_r}\frac{H^{(2)}_{1/2}(k_0\ a)}{\sqrt{\varepsilon_r}H^{(2)}_{1/2}(k_0\ a)} \quad (1.14)$$

On the determination of the wave number, k_o the other two parameters resonant frequency and Q-factor can be easily obtained using eq. (1.9) and (1.10) respectively. Curve fitting techniques and the operating frequencies can be employed in designing Hemispherical DRAs as per the eq. provides ease for antenna designers. The design strategy for both TE and TM modes is quite similar to each other.

1.2.2 Cylindrical DRA Insight

The cylindrical DR got popular as "Puck" and is used extensively in the microwave circuitry as filters, oscillators or energy storage device. Probe feed technique was first introduced to cylindrical DRA to verify its radiation characteristics which resulted in highly efficient antennas for microwave and millimeter wave applications. From a designer's point of view, this antenna provides additional flexibility in the form of aspect ratio a/h and dielectric constant ε_r, where 'a' and 'h' denote the radius and height of the DRA respectively. Most important parameter of this DRA is aspect ratio which determines the values of Q-factor and k_0a at any given dielectric constant [1]. These features strengthen antenna designer to create an elevated meager DRA operating at the same resonant frequency as that of a wide base but thin DRA. On the other hand, the Q-factor will be unlike in these two cases. This feature of cylindrical DRA gives an edge at hemi spherical DRAs. Figure 1.5 shows the geometrical representation of a typical cylindrical DRA with aspect ratio a/h.

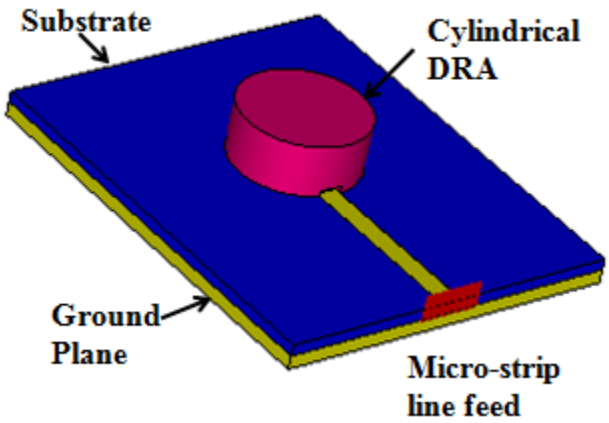

Fig. 1.5 Geometrical Representation of Cylindrical DRA [1,2]

Modes in cylindrical DRA can be segregated in to TE, TM and hybrid modes along with degree of freedom it provides with aspect ratio and permittivity. The hybrid

modes are represented as EH mode if magnetic field component in *z*-axis H_z is rampant and HE in case of dominant electric field component E_z along *z*-axis. The commonly used radiating modes of cylindrical DRA are $TM_{01\delta}$, $TE_{01\delta}$ and $HE_{11\delta}$ modes. The subscripts in the modes depict the variations in fields along Azimuthal (ϕ), radial (r) and Axial (z) directions respectively as in case of cylindrical coordinate system. The range of δ varies from 0 and 1. The lower order modes are assigned with 0 and as the dielectric constant approaches higher values the δ assumes the value 1. The modes of cylindrical dielectric resonator antennas can be chosen such that it operates as electric short monopole, magnetic short dipole, horizontal short magnetic dipole etc [16]. The clear-cut solution for electric field of cylindrical DRA divergent to the exact field solutions in the case of hemi spherical DRA is given, however fields are evaluated by making an assumption that the magnetic field component along *z*-axis (H_z) is zero. The tangential field components (both electric and magnetic) are continuous in nature in the surfaces parallel to *z*-axis.

The eq. (1.15), (1.16) and (1.17) are used to calculate the Q-factor as well as the resonant frequency with excited $TE_{01\delta}$, $TM_{01\delta}$ and $HE_{11\delta}$ modes respectively.

For $TE_{01\delta}$ Mode

$$f = \frac{2.327}{\sqrt{\varepsilon_r+1}}\left\{1 + .2123\frac{a}{h} - 0.00898\left(\frac{a}{h}\right)^2\right\} \quad (1.15)$$

For $TM_{01\delta}$ Mode

$$Q=0.008721\varepsilon_r{}^{0.888413}e^{0.0397475\varepsilon r}\left\{1-\left(0.3-0.2\frac{a}{h}\right)\left(\frac{38-\varepsilon_r}{28}\right)\right\}x \quad \left\{9.498186\frac{a}{h}+ 2058.33\left(\frac{a}{h}\right)^{4.322261} e^{-3.50099\left(\frac{a}{h}\right)}\right\} \quad (1.16)$$

For $HE_{11\delta}$ Mode

$$Q=0.01007\varepsilon_r{}^{1.3}\frac{a}{h}\left\{1+100e^{-2.05\left(\frac{a}{2h}-\frac{1}{80}\left(\frac{a}{h}\right)^2\right)}\right\} \quad (1.17)$$

1.2.3 The Rectangular DRA

Radiating ceramic structure of rectangle cross section is usually refers as rectangular dielectric resonator. It comprised of three dimensions length *d*, width *w* and height *h* as depicted in Fig 1.6. This structure is referred as RDRA (Rectangular dielectric resonator) in upcoming chapters and deliberations on the same structure is done in entire thesis. RDRA provides high degree of freedom to antenna designers. It

can be termed as most versatile shape among all other DRA's [10]. RDRA structure provides extended flexibility in terms of selecting the ratios w/h and w/d independently in order to obtain the desired bandwidth and profile. Consequentially tall, wide or thin aspect ratios can be chosen as per demand of application. Selection of aspect ratio decides the Q-factor of antenna which in turn provides a greater degree of flexibilty to the antenna designers [13].

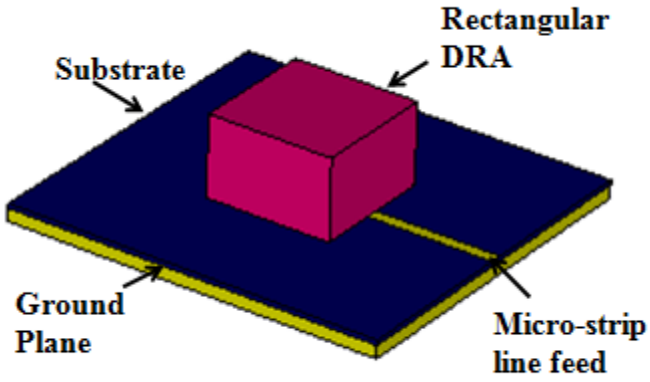

Fig. 1.6 Geometrical Representation of Rectangular DRA[1,2]

In both cylindrical DRA and RDRA, the field configurations are assumed to be equivalent to secluded RDRA with width w and height b=2h (by applying method of images to the charge on infinite ground plane similarity). All four walls of RDRA normal to xy-plane are hypothetically considered to be a case of perfect magnetic walls *i.e.* along the direction of propagating wave in the dielectric guide. The tangential components of electric and magnetic fields are continuous and perpendicular to propagating wave direction. TE and TM modes are the only radiating modes of any isolated RDRA. When the RDRA is erected upon the ground plane typically TE modes are excited. These modes radiate similar to short magnetic dipole antennas and the generated mode configurations can be TE^x, TE^y and TE^z along x, y and z directions respectively. The operating or resonant frequency of RDRA is directly proportional to its dimensions. For example, the lowest order TE modes for condition w>d>b are $TE^x_{\delta 11}$, $TE^y_{\delta 11}$ and $TE^z_{\delta 11}$ representing the variation of fields along *x*, *y* and *z* directions respectively as shown in figure (1.2.3). Let f_o be the resonant frequency for the mode $TE^x_{\delta 11}$ and can be found by employing the following under mentioned of transcendental eq. (1.18):

$$k_x \tan(k_x d|2)=\sqrt{(\varepsilon_r - 1)k_o^2 - k_x^2} \qquad (1.18)$$

where $k_o = \frac{2\pi}{\lambda_o} = \frac{2\pi f_o}{c}$, $k_y = \frac{\pi}{w}$ and $k_x^2 + k_y^2 + k_z^2 = \varepsilon_r k_o^2$

Similar eq. can be used to determine the resonant frequencies of $TE^{y}_{\delta 11}$ and $TE^{z}_{\delta 11}$modes. The next section discusses about the guiding relations to calculate the radiation Q-factor and resonant frequency of any given RDRA.

1.2.4 Determination of Q-Factor and Resonant Frequency

The curve fitting method is quite accurate and provides several combinations for aspect ratios such as w/b and d/b, dielectric constant (ε_r) and at desired quality factor (Q) [13]. The expression used for the determination of above parameter consisting of normalized frequency (F) and given as per eq.

$$F = \frac{2\pi f_o \sqrt{\varepsilon_r}}{c} \qquad (1.19)$$

From the above eq.1.19, the resonant frequency can be estimated in close approximation without solving the transcendental eq. Also the Q-factor of RDRA can be calculated from the relation:

$$Q_e = \frac{Q}{\varepsilon_r^3} \qquad (1.20)$$

where Q_e is the normalized quality factor.

1.3 DRA COUPLING METHODS

The coupling or feeding mechanism is a pivotal element in exciting the desired mode in a DRA [87-89]. It not only affects the input impedance but also varies other radiation characteristics. The feeding mechanisms have a huge brunt on the resonance frequency and the Q-factor of DRA. Some of the common coupling mechanisms are:

- Aperture Coupling [37,44]
- Probe Coupling [45-49]
- Microstrip line Coupling [22-26]
- Coplanar Coupling [56,78]
- Dielectric Image Guide (DIG) Coupling [114]

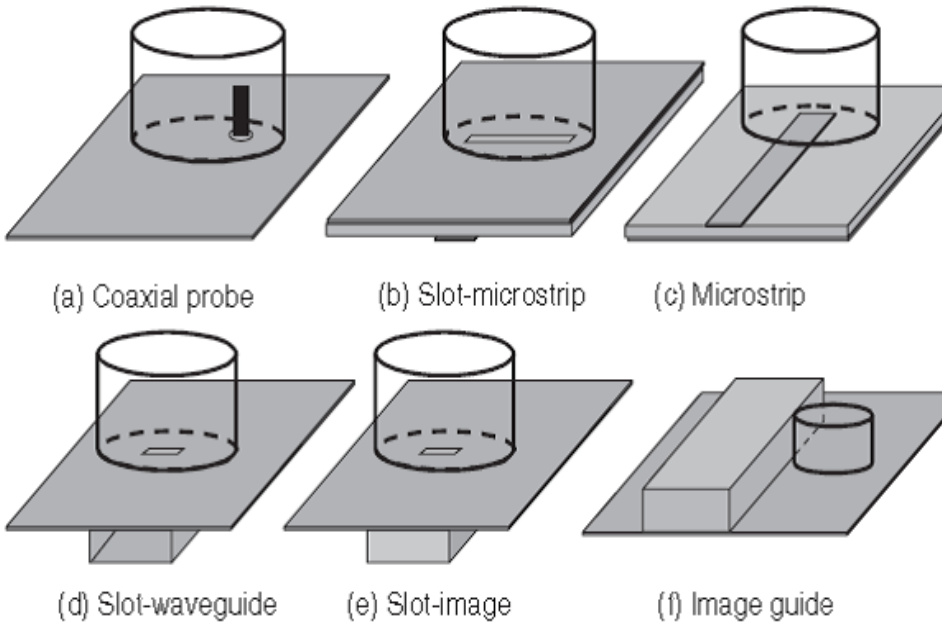

Fig. 1.7 Various Coupling Mechanism of DRA[1-3]

Fig 1.7 shows various coupling mechanism of DRA. In order to ensure practical viability of DRA, it is crucial to couple EM energy into or out of the DRA with the aid of port mechanism [1-2] . The type and number of modes excited in DRA depends upon the feeding method and position of DRA with respect to feed. Figure of Merit for a DRA is resolute by recognition of parameters like the excited modes, frequency response and the extent of coupling. The coupling source is typically considered as an electric or magnetic current and by employing the reciprocity theorem (alongwith suitable boundary conditions) magnitude of coupling (χ) among source and DRA fields can be determined.

In case of electric source:

$$\chi \propto \int (E_{DRA} . J_s) dV \tag{1.21}$$

and magnetic source:

$$\chi \propto \int (H_{DRA} . M_s) dV \tag{1.22}$$

V denotes the volume acquired by the source inside which the currents exist, and E_{DRA} and H_{DRA} are the respective electric and magnetic DRA fields. The eq. (1.21) and (1.22) suggest that the feeds should be positioned in the closed proximities of strong electric/magnetic fields inside the dielectric resonator element respectively to attain optimum coupling.

The coupling techniques also influences the Q-factor of any DRA. So an external Q-Factor (Q_{ext}) in terms of χ is given as:

$$Q_{ext} = \frac{Q}{\chi} \tag{1.23}$$

$$Q_l = \left(\frac{1}{Q} + \frac{1}{Q_{ext}}\right)^{-1} \tag{1.24}$$

Q denoted the unloaded quality factor associated with the DRA independent of any applied coupling mechanism. The maximum transfer of power is obtained when χ attains the value 1 and it is known as critical coupling condition. However, with $\chi < 1$ the condition is termed as under coupled and for $\chi > 1$ the condition is called overcoupled.

1.3.1 Micro strip line

The most ordinary way for coupling to dielectric resonator antenna in microwave circuit is by micro strip line. The amount of coupling from the micro strip line can be controlled by adjusting the lateral distance of the DRA with respect to the micro strip line and on the dielectric constant of the dielectric substrate [22-26] . There are two methods of micro strip line coupling named as side coupling and direct coupling. Figure 1.8 shows micro strip line coupling to the DRA. This feeding mechanism offers ease integrations with the other microwave circuit but produce unwanted air gap between the DRA and the substrate.

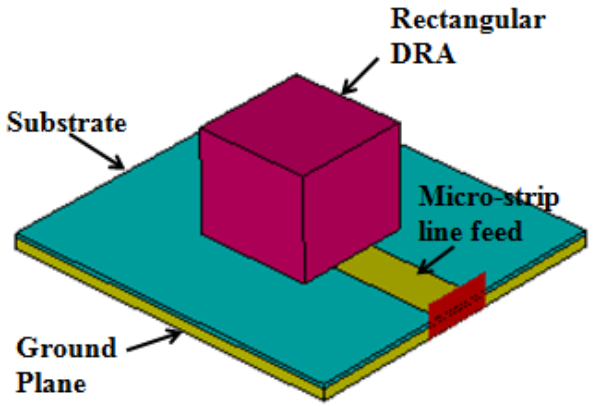

Fig. 1.8 Geometrical Representation of Micro-strip feed line [1-3]

1.3.2 Coaxial Probe

Co-axial probe feed is popularly known as probe feed, it is a very simple technique generally used to feed dielectric resonator antennas as shown in Fig. 1.9. There are two ways with which a probe can be connected to the DRA. It can either be

placed adjacent to DRA or can be fixed firmly with its surrounding mass. In order to optimize the coupling either height or position of the probe can be altered [38]. Depending upon the position of the probe, numerous modes can be excited. In the probe which is located adjacent to the DRA, the magnetic fields of the $TE_{11\delta}$ mode of the rectangular DRA is excited and radiate like horizontal magnetic dipole. In case of a probe located in the middle of a cylindrical DRA, the TE_{011} mode is excited and radiate like a vertical dipole [2]. The advantage offered by probe coupling is that it can be couple directly into a 50Ω system without the requirement of a matching network.

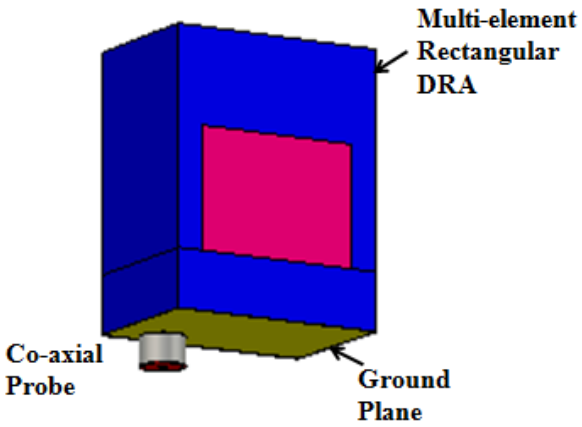

Fig 1.9 Geometrical Representation of Co-axial feed line [-3]

1.3.3 Aperture Coupled DRA

Aperture coupling is the feeding method which couples the DRA with incurring minimum losses as shown in Fig.1.10. This is a technique that can be excited through an aperture in the ground plane which can be feed by a transmission line (micro strip or coaxial) or a waveguide [37]. Any shape of aperture can be chosen but rectangular cross section has an edge over other shapes. The amount of coupling can be controlled by properly selecting the length and width of the slot and varying the position of DRA on the slot [44]. The primary advantage offered from this method is that due to the isolated radiating aperture from the feed preventing itself from any unwanted coupling. Normally, a higher dielectric material is used for the substrate less dielectric constant material is used for the top dielectric resonator patch for optimization radiation of the antenna. Dimensions of slot are determined with the following equations:

$$\text{Slot Width} = 0.022\lambda \quad (1.25)$$

$$\text{Slot Length} = 0.202\lambda. \quad (1.26)$$

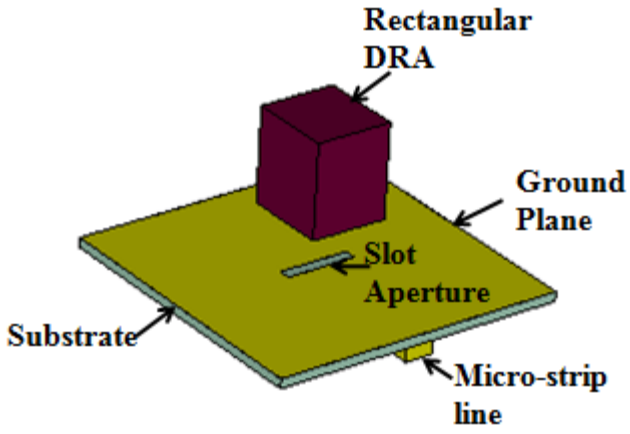

Fig 1.10 Geometrical Representation of Aperture feed line[1,2]

1.3.4 CPW fed DRA

Co-Planar feeds is used to couple electromagnetic power to the DRA. Fig. 1.11 shows rectangular DRA coupled to a co-planar loop [56]. The coupling level can be adjusted by positioning the DRA over the loop. The coupling behavior of the co-planar loop is similar to that of the coaxial probe but the loop offers the advantage of being non-obtrusive [78]. By moving the loop from the edge of the DRA to the center, one can couple into either the $TE_{11\delta}$ mode or the TM_{011} mode of the rectangular DRA.

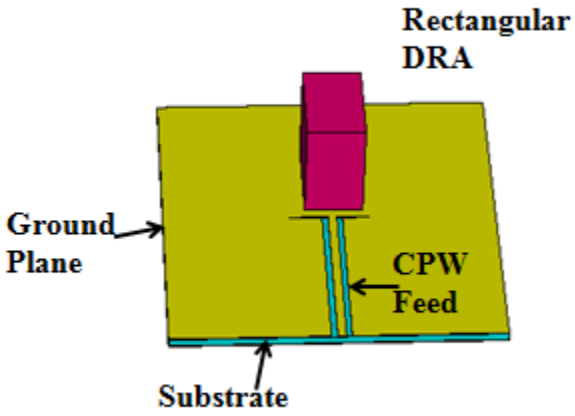

Fig 1.11 Geometrical Representation of CPW feed line[1,2]

1.4 ULTRA-WIDEBAND TECHNOLOGY

Federal Communication Commission (FCC) of United States established new rules and regulations in 2002 for implementation of ultra-wideband (UWB) technology to be used in unlicensed applications. As per these regulations, any frequency band ranging from $3.1 - 10.6$ GHz was assigned to indoor and short distance wireless UWB communication applications. Numerous merits of UWB technology attracted privileged acceptances throughout microwave wireless industry around the world in recent times [17-52]. UWB technology emerged as a boom not only in higher data rate and gain wireless personal area network (WPAN) systems but also in low data rate positioning and location purposes. Bio-medical applications in this frequency spectrum indeed keep this technology at an edge.

1.4.1 Frequency Bandwidth exploration in UWB Concepts

Impedance bandwidth of any antenna is determined via two methods. Either return loss of antenna should be greater than $10\ dB$ or with voltage standing wave ratio (VSWR) should be less than 2 over entire frequency range or bandwidth. In context to the aforesaid, the difference between upper level of frequency and lower level of frequency defines the bandwidth of the given frequency span, given as eq. (1.27)

$$BW = f_U - f_L \tag{1.27}$$

Where f_U and f_L are known as upper frequency and lower frequency levels respectively.

Fractional bandwidth or percentage bandwidth is another key parameter of the antenna performance in UWB region. In order to obtain the fractional bandwidth, first and foremost the center frequency is to be found out. However, the arithmetic mean (F_c), with first term as f_U upper and last term as f_L determines the fractional bandwidth where linear scaling is considered and is given by eq. (1.28)

$$F_c = \frac{f_U + f_L}{2} \tag{1.28}$$

In addition to above, the other term center frequency if found to be geometric mean of upper and lower frequency values in case of logarithmic scale consideration i.e. $F_c = \sqrt{f_U . f_L}$. The ratio of impedance bandwidth to center frequency is known as relative or fractional bandwidth (FB) and can be calculated using eq. (1.29)

$$FB = \frac{BW}{F_C} \tag{1.29}$$

The fractional bandwidth (*FB*) in percent is given using the below mentioned eq. (1.29)

$$\% \text{ FB} = \left(\frac{\text{BW}}{\text{F}_\text{c}}\right) \text{X } 100 \ \% \tag{1.30}$$

Consequent to the above eq., the narrow band, wideband and ultra wideband frequency antenna operations are classified as:

$$\text{Narrowband} \quad [\text{FB} < 1\ \%]$$

$$\text{Wideband} \quad [1\% < \text{FB} < 20\ \%]$$

$$\text{Ultra-wideband} \quad [\text{FB} > 20\ \%]$$

The bandwidth of any conventional antenna or other microwave circuit is given by percentage bandwidth. The Ratio Bandwidth (*RB*) is expressed using eq. (1.29)

$$\text{RB} = \frac{\text{BW}}{\text{f}_\text{L}} \tag{1.31}$$

It is also represented as R: 1, where eq. (1.30) gives the value R

$$\text{R} = \frac{\text{f}_\text{H}}{\text{f}_\text{L}} \tag{1.32}$$

The factors which influence significantly the impedance bandwidth of antenna are substrate thickness as well as the dielectric constant of the substrate used [94-95]. Increment in the substrate thickness yields high bandwidth irrespective to low dielectric constant of the substrate. Augmentation in substrate thickness causes interfacing issue of antenna element with other microwave circuit elements. Thick dielectric substrates pretense the demerits such as surface wave losses leading to enhanced inductive impedance magnitude in the input impedance of the antenna thereby generating counterfeit resonances. The UWB antenna should have constant gain and omni-directional radiation patterns over the entire operating band. The time domain behavior of antenna should also be verified. Antennas required for UWB range should have constant group delay and linear phase response throughout the operating frequency band.

1.5 RE-CONFIGURABILITY, BAND NOTCH CREATION, AND TUNABILTY IN UWB SYSTEMS

Re-Configurability is a distinctive property of antenna that makes it stand apart from other types of antenna. Re-configurable antennas are implemented by changing radiated fields of the antenna's effective aperture. Deliberate arrangements are made to vary antenna currents or radiating edges [119-142]. These amendments cause change in antenna's characteristics. Re-configurable antenna often lacks in good

gain, stable radiation pattern and satisfactory impedance bandwidth. Re-configurability can be of four types:

a) Frequency of operation
b) Re-configurable radiation pattern
c) Re-configurable polarization behavior
d) Combination of any of these

Re-configurability can be achieved by the two methods:

a) Switch based methods like PIN diode and MEMS
b) Non-Switched methods like Graphene and Magneto Hydro Dynamic (MHD) antenna.

Combination of UWB element with narrow band resonant structures will result in unwanted band blockage. Calculated narrow band resonators are inserted in path of UWB system so that a multiband system can be implemented [143-152]. This multiband system has a special feature of rejecting tuned resonating frequency of tuned circuit. Fig. 1.12 shows structure of UWB system with filter structure. This kind of arrangement not only reduces the interfacing inside the microwave communication system but also reduces the overall cost and complexity of the system. Deployment of unallocated blue-tooth and Wi-Fi and WLAN bands makes UWB technology vulnerable to the allocated user. Hence, the need for band notch creation becomes more influential in this scenario where trillions of data is present over the internet. Band notch filters amalgamation with UWB system keeps it safe and reduce complexity of overall system.

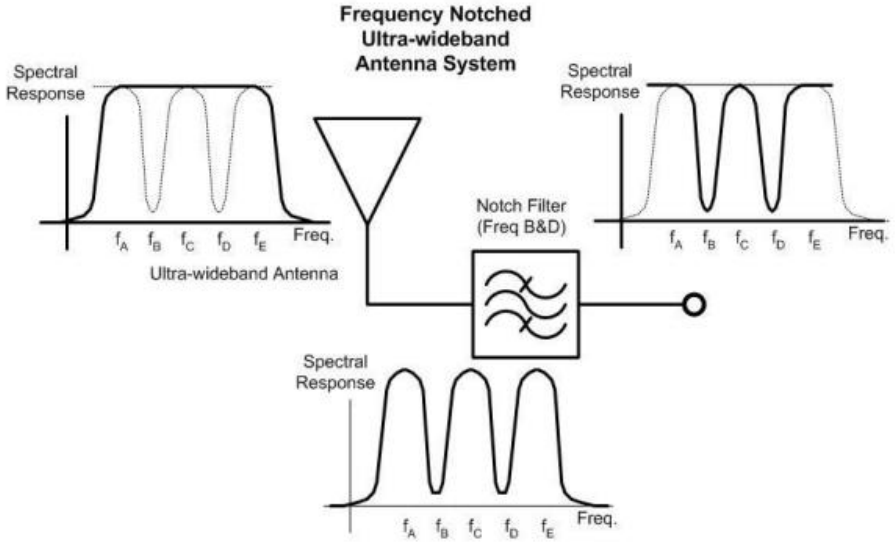

Fig. 1.12 represents UWB antenna with notch filter implementation [Wikipedia.com]

Tunability is the re-configurability achieved by material-based method. Graphene is a honeycomb structure material that changes its conductivity by applied gate voltage which in turn changes the impedance that consequents in varying resonant frequency. The implementation of UWB antennas with tunable notched frequency reduces the system size as well as the cost. Obtaining the tunability in the band-notch frequency can be achieved by changing the physical parameters of antenna in the microwave devices.

1.6 BIO MEDICAL APPLICATIONS OF DRA

Microwave techniques are attracting numerous researchers to apply their acquired knowledge and skills to serve the humanity. Body area Networks generally known as BAN networks not only utilizes an effective data acquisition system but also provide an efficient mechanism to have a distant watch on health issues of concerned person**.**

1.7 MOTIVATION

Recent advancements in Wireless communication technologies have totally transformed the outlook of our society towards sharing and accessing the information via wireless media. Exponentially increasing modern day consumers are expecting super wide bandwidth and high data rate along with high speed information with excellent information quality from the contemporary communication systems. High radiation efficiency, wideband characteristics, low dissipation loss and low cross polarization values are some of the major attractive features of DRA. These ceramic devices can be efficiently integrated with any type of micro strip circuits & patch antennas, feeding mechanisms and also support various gain enhancement techniques such as arrays, Partial/defective ground structure etc.

Numerous approaches to accommodate all or few of these above mentioned qualities have been analyzed by various researchers in different extents. There are few antennas which are catering these requirements. There is still a research gap to fulfill all the prerequisites.

This research work is particularly motivated by effervescent demand of compact, low profile, highly efficient, ease to fabricate, high data rates, fast networks and cost effective microwave aerials that can be employed in wideband and ultra wideband (UWB) devices.

1.8 OBJECTIVES OF THESIS

Main objectives of thesis are as follows:

1. To investigate the design procedures of simple shaped DRAs and various feeding mechanisms.
2. To design and analyze various feeding techniques for providing the degree of freedom to designers for achieving size reduction, bandwidth and support for lower order excitation.
3. To create band notch and attain re-configurability with application in antenna.
4. To design and develop DRA to obtain wideband and UWB applications.

1.9 METHODOLOGY

A deliberate and robust methodology is required to take the research in right direction. The very first step in this process was reviewing state of art of DRA. Analyzing different shapes along with application of various feed mechanisms to get the desired response is accomplished by carrying out an extensive literature survey. Design and development of numerous UWB and wide band structures for various wireless communication technologies and applications have been thoroughly analyzed. Various DRA structures are proposed in the line of the research objectives.

The design optimization, performance analysis and parametric study of the proposed antenna structures have been carried out using finite integration technique based Microwave CST Studio 2018 & HFSS software.

All simulated and optimized designs are fabricated using low cost UV Lithography PCB Fabrication Technique. The measurements of the developed antenna structures are carried out using equipment like Vector Network Analyzer (Agilent PNL 5230 series), Radiation Pattern and Gain AUT (Antenna Under Test) arrangement consisting of movable rotary antenna mounts, microwave signal source and spectrum analyzer, manufactured by company Rohde and Schwarz. At the end, the comparison of simulated and measured results of proposed antenna structures are analyzed and discussed.

1.10 ORGANIZATION OF RESEARCH WORK

The dissertation is fragmented into six chapters.

Chapter 1 is the introduction section of the research work. Antenna parameters along with fundamental shapes of DRA along with their transcendental design eq. have been discussed in this chapter. Feeding Mechanism available for these DRA shapes are

also discussed. Bandwidth and related terms are effectively explained in this unit. Objectives with acquired Methodology and Dissertation fragmentation is presented by this chapter.

Chapter 2 consists of the fundamental concepts of dielectric resonator antennas along with the exhaustive literature survey aligned with the scope of the presented literature. The survey highlights the evolution of DR technology and enlists the prominent historical advancements hitherto. This chapter depicts the latest trends in the DRA technology. It presents the single, dual, multi and UWB band antennas design techniques for various modern day wireless applications. Several methods to achieve reconfigurability in DRA systems is incorporated in this unit. Band Notch creation along with Tunability achievement Methods have been studied. Comprehensive study of DRA used in Bio-Medical applications have been studied in this chapter.

Chapter 3 describes the bandwidth enhancement techniques of the Rectangular DRA. Analysis of various modes and their merging is carried out to implement ultra wide band characteristics. Coaxial feed technique along with multi segmented RDRA is implemented to achieve Ultra wide bandwidth with enhanced gain. Hybridization of Ring Rectangular Dielectric Resonator Antenna with multiple ring patch structure is designed which operates at a frequency band of 5.4-15 GHz. Impedance bandwidth of 94.1 % is achieved with the hybridization of patch and Dielectric Resonator antenna along with slotted ground structure.

Chapter 4 investigates the reconfigurable property of band notch creation in antenna. Rectangular Magneto Hydrodynamic antenna is designed and analyzed to enhance bandwidth and gain. A simple low profile DRA in conjunction with wide band patch has been proposed to create band notch in the UWB frequency range to avoid unnecessary interference. A new material graphene is implemented with UWB structure to create tunable band notches. The antenna structure is numerically analyzed using full wave simulator CST microwave studio and its electrical equivalent circuit is drawn using the circuit theory approach.

Chapter 5 investigates the design of RDRA to develop the smart data acquisition system. This chapter presents two designs operating in Lower European Band (3.7-7.4 GHz) and UWB (5.4-15 GHz) respectively. Radiation characteristics of these antennas are highly suitable for body centric applications especially for early detection of breast cancer. Antennas are designed for on body WBAN technologies and simulated using CST Microwave Studio 2018.

Chapter 6 finally summarizes the results, the concluding interpretation and contribution in implementing new understanding about different characteristic of RDRAs along with the future works/scope in context to the proposed research.

CHAPTER 2

LITERATURE SURVEY

2.1 Introduction

Modern wireless communication technology has taken an exponential leap in design and fabrication of low profile, compact and wide band antennas in GHZ range. A plethora of empirical formulations and equations are available for implementation of highly vigorous aerials for various applications. These ceramic resonators segregated as filters and oscillators only due to its high permittivity with dielectric constant $\varepsilon > 20$ [1]. Due to high Q-factor ranging from 50 to 500, Dielectric Resonator was suitable candidate for energy storage device but not as radiator. Apprehension of DRA as radiating element was furbished but not implemented as antenna widely until Luk and Leung conducted a systematic study on these devices [2-4]. DRA established itself among all type radiators as a device that can cater all needs of any microwave communication system. Ceramic radiator also called as 'Puck' functions as radiator in which four conducting walls are removed. Application of suitable coupling mechanism with proper mode excitement makes DRA an efficient radiator [6-7].

Today's society is an information-oriented society which not only requires wide bandwidth but also large data rates with fluent space allocations. DRA presented itself as a caterer to fulfil all these demands with displaying merits like low dissipation loss, low profile, wideband nature, ease of fabrication, high radiation efficiency, easy integration with other miniaturized microwave circuits, versatile excitation techniques, greater degree of freedom for antenna designers etc. [8]. Inherent properties of DRA give ample space to all designers to create numerous wide bands, multi band and ultra-wide band antennas [9-10]. Bandwidth of these antennas can be augmented with lowering down of Q-factor. Multi-Element and Multi-Segment DR and Perfect electrical conducting (PEC) layers are also used to increase bandwidth.

In order to filter out unwanted bands from ultra-wide band response, filters are required for band rejection. Inclusion of filter is a costly process which increases space complexity of the system. Band notch creation is a property achieved by antenna to remove unwanted band of frequencies or a single frequency component from the system without usage of additional filter. Reconfigurability achieved in terms of reflection coefficient response can be a determining factor of overall microwave communication

circuit. Various switch-based methods have been proposed to obtain the reconfigurability in antenna but advent of new materials in THz region makes tunability comfortable. With the evolution of DRA and involved fabrication techniques applications of these ceramics have entered in the field of Bio-Medical applications. The upcoming sections of this chapters discuss the implementation of the DRA technology in the design and development of Wideband and Ultra-wideband antennas along with specific applications.

In order to develop devices at higher microwave frequency bands the materials used should hold the qualities like lesser dissipation loss, stable/low temperature coefficients, higher efficiencies and adaptability to interface with multiple design and fabrication technologies. Some areas can be marked as potential applications of DRA such as Global Positioning System (GPS), Direct Broadcast Service(DBS), High speed LTE, Defence Applications, Navigation and Meteorological measurements, Collision Avoidance Systems(CAS), Unmanned Guided Vehicles (UGV/UAV) and Healthcare Services etc.

2.2 TRENDS IN DIELECTRIC RESONATOR ANTENNA STRUCTURES

In 1939, a renowned physicist Richtmeyer observed that non-metalized dielectric objects can work in a similar fashion like metallic cavities often termed as Dielectric Resonators [3]. Although theory have been postulated long before but practically relevant work in direction of DRA implementation started after 1960's. Initially dielectric compounds have been appropriate for RF filters and oscillators due to higher Q factor values. In 1983, Long et al started actual methodological experimentation with DRA [21]. A radiator comprised of blocks of ceramics material operating in microwave frequency and with dielectric permittivity $\varepsilon_r \geq 10$ is known as dielectric resonator antenna. Appropriate feeding mechanism along with excitation of desired modes makes DRA a viable and efficient radiator in comparison to present low gain antennas like microstrip, monopoles and dipoles.

Jean Van Bladel [6] presented the confined and non-confined modes existence inside DRA. A lossless material with high permittivity was assumed and using orthogonality and variational properties excitations techniques were demonstrated. In extension of his previous work, scattering phenomenon was presented. Expressions for resonant frequencies with scattering from a spherical cross section have been studied [7].

Glisson [8] proposed the surface integral equation formulation and the method of moments to analyse an isolated Dielectric resonator. Accuracy of calculation in

resonant frequencies and Q-factors for both symmetric and hybrid modes have been postulated.

R.K.Mongia & Prakash Bhartia [9] proposed a wide-ranging review of the modes and the radiation characteristics of DRAs of various shapes such as cylindrical, cylindrical ring, spherical, and rectangular. Closed form expression for given resonant frequencies and Q-factor have been derived for cylindrical DRA.

Luk et al. [10] presented theoretical concept of a hemispherical DRA with coaxial feed technique. Authors calculate exact Green function due to probe current and provide a method to excite TE_{111}. Impact of probe displacement and probe length was investigated in this research paper.

Fang et al. [11] presented the design procedure of single/dual/wideband DRA's. Theoretical aspects of mode merging techniques are very well explained in this research paper.

Mongia et al. [12] presented a theoretical as well as experimental investigation on DR fabricated with dielectric constant of values 20 and 80. Lower order mode generation and determination of resonant frequencies associated with these modes have been determined along with Q-factor. Probe fed and slot fed techniques have been used to excite the DRA and it was observed that slot coupled technique have very less cross polarization levels as compared to probe fed technique.

Mongia et al. [13] devise an accurate method for determining resonant frequency of CDRA. Transcendental equations are proposed to determine other parameters such as stored energy, fields outside the antenna and Q factors of DRA. Two different CDRA termed as A and B designed with different material and their performances are evaluated.

Luk and Leung [14] proposed Green function analysis of mutual impedances of two Hemi Spherical DRAs. Experimental and Simulated results are found in good agreement while Two DRs were fabricated with permittivity 9.5.

Chow et al. [15] experimentally observed performance of 2 x 2 array comprised of two CDRs with permittivity 9.5. This aperture coupled array is excited by HE110 mode and a peak gain of 8.9 dBi is achieved with low cross polarization level.

Petosa et al. [16] proposed a comprehensive approach towards the DRA technology keeping various parameters in context such as bandwidth enhancement schemes, generation of circular polarization through feeding techniques and increment in gain. An exemplary differentiation between linear to planar array in terms of

reduction in number of elements which leads to reducing the losses due to feed distribution. Use of Aperture coupled feed with coaxial feed have been analyzed to achieve circular polarization. A detailed composition of various domain antennas such as notched RDRA, multi segmented DRA and the short circuited RDRA are discussed in this research paper.

2.3 BANDWIDTH ENHANCEMENT TECHNIQUES OF DRA

Dielectric resonator antenna emerged as an efficient substitute of micro-strip patch antenna due to low loss & volume, high radiation efficiency and low metallic losses. Various research groups are contributing towards progress of this metal free radiator from 1980's onwards. Metallic losses along with narrow bandwidth were the major disadvantage offered by micro-strip antenna. Various researchers have proposed numerous DRA designs in direction of enhancing bandwidth width of the antenna with negligible losses due to metal free nature of the device. All of the bandwidth enhancement techniques of DRA can be divided into three major parts:

- Combining multiple DRA's together or joining them in segments.
- Manipulating ground plane by either partially reducing dimensions or creating slots and strips.
- Applying Different shapes, feeding mechanisms along-with Hybridization to enhance bandwidth.

All these techniques solely function on lowering Q-factor of the DRA. Q-factor of DRA decides the energy stored in tank circuit and consequently radiating efficiency of the antenna. In early 1990's, arrays were considered to be the best option for bandwidth and gain augmentation. However, cost consideration for some commercial applications makes it difficult to employ arrays in each scenario. Hence, that need was catered by infusing different permittivity in one element or creating slabs of different permittivity in one structure.

2.3.1 Review on Multi segment Multi Element DRA

Multi segmented DRA can be defined as a resonator with low permittivity substrate under which one or more segments with different permittivity, are inserted to alter the impedance. Multi element is relatively new concept keeping slab structure in mind. In this concept, multiple thin slabs of varying permittivity are stacked on one another to get high impedance and significant reduction in size.

In 1979, Verplankel and Bladel [17] removed inner portion of the circular DRA and proposed that by changing the ratio of inner to outer radii Q-factor can be lowered which in turn reduces the amount of stored energy and subsequently increasing the bandwidth. Same concept was implemented by Apisak Ittipiboon [18] in rectangular geometry in slot fed antenna by creating a notch within antenna and inserting high dielectric slab in that structure. Enhancement of this design was achieved by forming array of proposed MSRDRA, radiating from 10.1-15 GHz with excellent radiation properties.

Petosa et al. [19] implements a micro-strip fed MSRDRA design with 9 substrate inserted for Ku band operations. Lowering the Q factor reduces amount of stored energy in the radiator thus enhances the bandwidth of the structure. This phenomenon can be achieved either by employing multiple segments or multiple elements in form of thin slabs.

Ruan et al. [20] proposed a multi-segment cylindrical structure for wideband characteristics. Both DRA segments with varying size are placed one inside other and are excited by probe fed technique. Broadband radiation pattern with 67%impedance bandwidth is achieved through this design.

Young et al. [21] proposed a study on coaxial probe fed rectangular as well as cylindrical DRA. Material used for fabrication of the device is Eccostock Hik 500 of dielectric constants 8, 12, 16 and 20 with radius as 12.7 mm and a/d ratio of 0.35. Stable radiation pattern with 30% impedance bandwidth is obtained with this design.

Gao et al. [22] investigated a wideband DRA which consists of a RDR having dielectric constant of 10.2 and a rectangular slot. A CPW fed antenna erected on RT Duroid substrate of permittivity 6.1 and height 1.25 mm. Transverse Electric mode was excited in the structure and bandwidth of 28.9% ranging from 4.7 - 6.30 GHz was obtained. The gain of 3.8 dBi is obtained along with stable radiation pattern of antenna. In this research work, the evolution of DRA from a simple RDRA to a T-shape DRA is represented by electric field advancements of the device. Fig. 2.3.1 shows the geographical structure of DRA. Fig.2.3.2 shows comparison of simulated and measured reflection co-efficient of proposed DRA with Annular MPA.

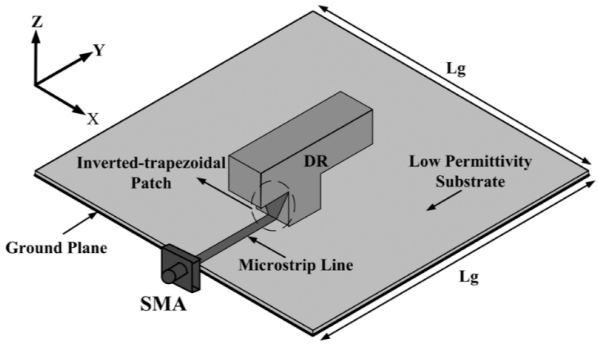

Fig. 2.3.1. Geometry of proposed antenna [22]

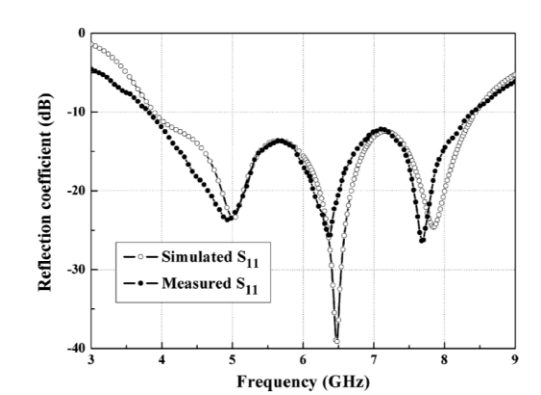

Fig. 2.3.2 Comparison of Simulated and Measured Input Reflection Coefficient of Proposed Ring DRA with Annular-Shaped Microstrip Feed

Liang et al [23] proposed a three segmented L-shape wideband antenna made up of dielectric material of constant 9.8. A square substrate with inverted trapezoidal patch yields a bandwidth of 3.87-8.17 GHz and a high gain of 5.0-8.5 dBi. Presented structure is designed for C, WLAN frequency bands with stable radiation pattern.

A dual band split antenna is reported for dual band application. Excitation of two subsequent modes TE_{111} and TE_{113} enables this device radiating for Wi-Max (3.4-3.7 GHz) and WLAN (5.15-5.35 GHz). Radiation Efficiency of 94%, high gain of 8.4 dBi along with low cross polarization levels have been achieved through the design [24].

A multi-segment cylindrical DRA loaded with a conducting patch is presented for wireless sensor networks [25]. The antenna is fabricated using dielectric material Rogers 3210 and Fr4 having dielectric constants 10.2 and 4.3 respectively. Inclusion of patch reduces the overall electrical size of DRA which provides efficiency of 95% with high gain of 6.8dBi.

Pan et al. [26] proposed a C band antenna fed with a microstrip slot which provides an impedance bandwidth of 40%. Key point of this radiator is its high gain of

9 dBi. Antenna is fabricated with ECCOSTOCK HiK dielectric material having ε_{r1} = 15 in combination with another material having ε_{r1} = 2.2.

Abedian et al. [27] proposed a compact U-shape microstrip fed, Z-shaped T-Shape DR is presented which provides an impedance bandwidth of 110% ranging from 3.14-10.9 GHz. This TSDR consists of a stacked structure with one upper layer with low ε_{rup} = 3.54 and a lower layer ε_{rlw} = 15 which yields excellent Omni-directional radiation pattern. Fig. 2.3.3 shows proposed antenna geometry and Fig. 2.3.4 shows simulated and measured co-efficient result.

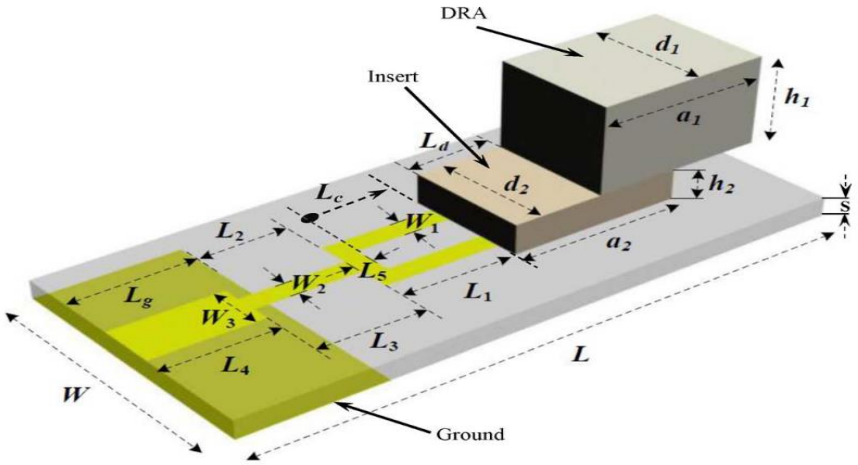

Fig. 2.3.3 Geometry of proposed antenna Top view [27]

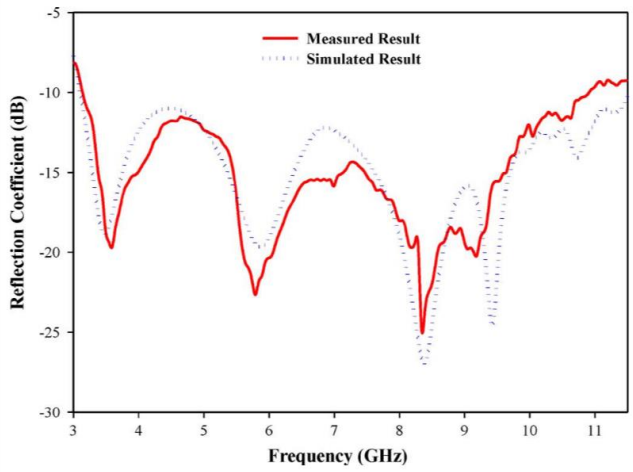

Fig. 2.3.4 Simulated and Measured Reflection Coefficient

Ghosal et al. [28] fabricated a Stacked DRA with metamaterial structure to achieve reconfigurability. Two cylinders with upper radius of 0.64 cm with lower radius of 0.32 is stacked with each other. Partial ground structure with a slot provides a bandwidth from 4-10 GHz. Band notch creation for the frequency bands of (5.25 - 5.8)

GHZ (covering 5.2 GHz and 5.8 GHz WLAN), (7.21 - 7.8) GHz is achieved with employing two split ring resonators structures in the design.

Sankaranarayanan et al. [29] proposed a bi conical structure with volume of 7.58 cm^3 made up of TMM 10i material of ε_r = 9.8, by joining two conical sections from base to base. This design achieved a size reduction of 74% with bandwidth enhancement of bandwidth ranging from 2.8-7.38 GHz yielding an impedance bandwidth of 93.1% . Fig. 2.3.5 shows proposed antenna geometry and Fig. 2.3.6 shows simulated and measured co-efficient result.

Fig. 2.3.5 Fabricated prototype of antenna [30]

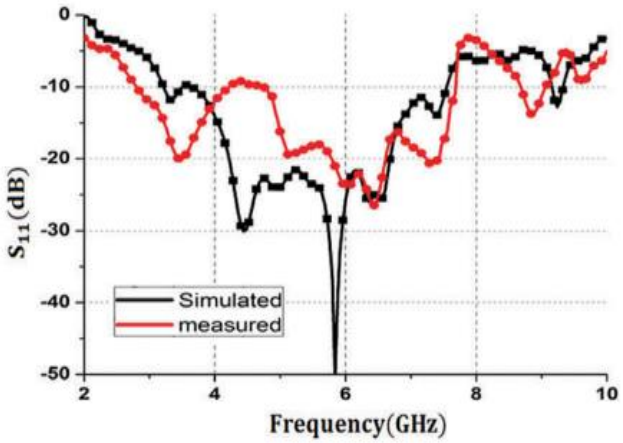

Fig. 2.3.6 Simulated and Measured Reflection Coefficient

Fakhte et al. [30-31] presented a novel technique of enhancing gain in the boresight direction by creating grooves in the side walls of the DRA. This is a stacked structure with 10 layers fabricated using dielectric material of ε_r = 10 of thickness 1.575 mm pressed onto each other mechanically. An impedance bandwidth of 21% is achieved with a maximum gain of 9.6 dBi. Author extended this same work by

presenting aperture-coupled uniaxial anisotropic DRA displays an impedance bandwidth of 20.65% between 3.17 and 3.9 GHz and a peak broadside gain of 8.24 dBi.

Ullah et al. [32] proposed a CDRA, which is constituted by four sections and employ variance in permittivity. A T-stub along with micro-strip line is implemented to place four 90^o pie shape sectors in such a way that, two similar permittivity sectors of ε_{r1} = 15and ε_{r2} = 10.5 are positioned in non-adjacent quadrant. Optimization of all parameters of this structure yields a wide bandwidth of 56 % with frequency ranging from 12.1 GHz to 21.65 GHz.

P. Rezaei et al. [33] presented a two segment RDRA structure separated by a metal plate which offers a size reduction 0f 41.5% in volume. Variation in aspect ratio of this DRA yields 76.8% impedance bandwidth at 3.32– 7.46 GHz frequency band.

Thamae et al. [34] proposed a novel shape bow tie antenna which is mounted on the surface of the 60 x 60 mm^2 ground plane. This structure radiates for a frequency range of 4.194-6.944 GHz. DR is fabricated using Rogers TMM10i with ε_r = 10. Co-axial feed antenna provides impedance bandwidth of 49.4% due to shape deformation of the DRA.

Ge et al. [35] experimentally verified the fact that impedance bandwidth can be enhanced by involving full length low permittivity material in between DR and ground plane. This structure provides the entire UWB range assigned by FCC, starting from 31 -10.6 GHz. This design yields an impedance bandwidth of 109.5% with a volume of 12.8 x 15.2 mm^3. Fig. 2.3.7 shows top view and isometric view of DRA and Fig. 2.3.8 shows simulated and measured co-efficient result.

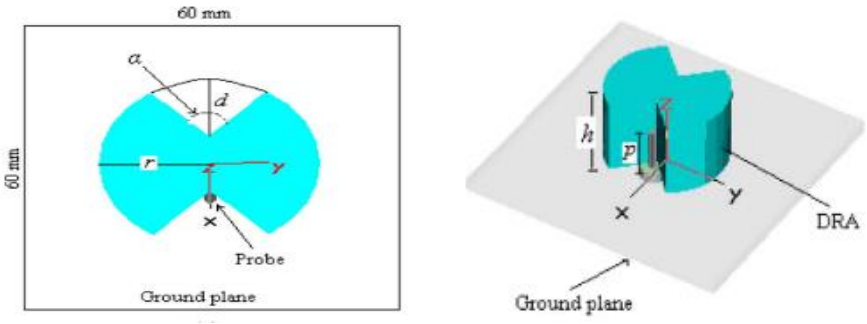

Fig. 2.3.7 (a) Top View of the DRA (b) Isometric View of DRA [34]

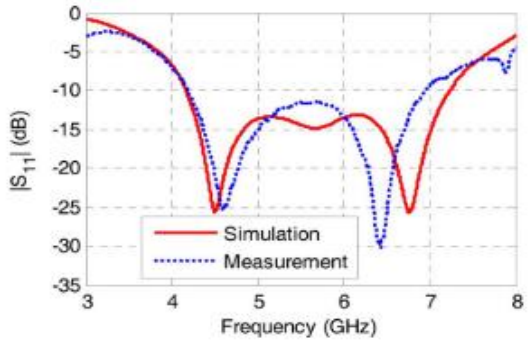

Fig. 2.3.8 Simulated and Measured Reflection Coefficient

Yang et al. [36] presented a cylindrical DRA with foam material placed beneath the cylindrical segment to obtain wide bandwidth response. This design is fabricated from Rogers TMM10i with dielectric constant 9.8 mounted on ground plane fed by 50 Ω shorted to inverted trapezoidal conformal patch. Impedance bandwidth of 75% along with consistent radiation patterns and the gain from 4.8 to 6.5 dBi is achieved through this design.

Zebiri et al. [37] proposed an aperture coupled cylindrical DRA for UWB design. The structure is developed on FR4 substrate relative permittivity of 4.5. Cylindrical Dielectric Resonators are fabricated from alumina material having dielectric constant 9.4. Offset coupling scheme is employed in order to get impedance bandwidth of 21% ranging from 5.9 to 7.3 GHz in lower band and 53% from 8.7 to 15 GHz across of the upper band. Excellent gain of 12 dBi is obtained by this design. Fig. 2.3.9 shows top view and side view of Aperture coupled Asymmetric DRA and Fig. 2.3.10 shows simulated and measured co-efficient result.

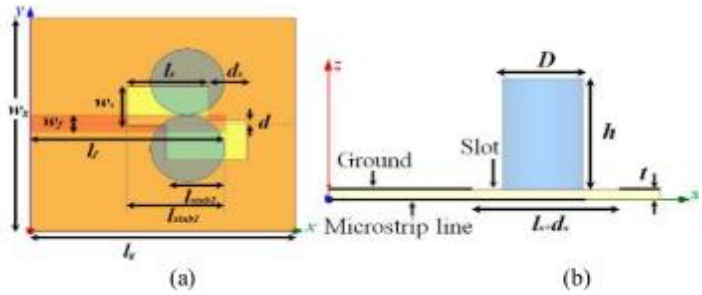

Fig. 2.3.9 Aperture coupled Asymmetric DRA (a) Top View Aperture coupled Asymmetric DRA (a) Top View [37]

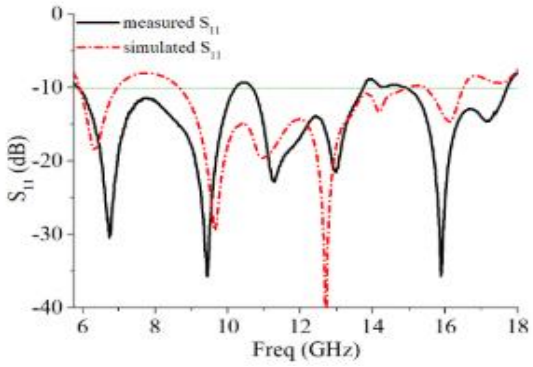

Figure 2.3.10 Measured and simulated Reflection Coefficient of the DRA.

Chaudhary et al. [38] presented RDRA for wide band applications. Antenna is fed with co-axial probe has two layers. An impedance bandwidth of 58.7% with in average gain of 6.99 dBi in frequency range of 6.0-11.5 GHz.

Kishk et al. [39] proposed a wide band stacked antenna with two segments with ring structure. Lower segment is of low dielectric constant (4.3) while upper segment is of high dielectric constant (10.5) with high value of radius. This structure offers a bandwidth of 35% by exciting $HEM_{11\delta}$ mode with resonant frequencies 10.57 GHz and 9.8 GHz respectively.

Kishk [40] proposed a bandwidth enhancement scheme of DRA. Robust design, broadband radiation pattern with impedance bandwidth of 50% are the advantages offered by this design.

Buerkle et al. [41] presented an aperture coupled RDRA which is fabricated with dielectric of permittivity 12. This DRA is mounted on substrate Rogers RT5880 of dielectric constant 2.2. Impedance bandwidth of 29% with broadside radiation pattern is obtained with structure. Stacking of this aperture coupled device can be done to enhance the bandwidth further.

Walsh et al. [42] proposed combination of two bandwidth enhancement techniques with stacking DRs and developing embedded DR. Two cylindrical DRs with upper and lower structure are embedded with plug CDR of different dielectric constant. Structure consists of upper CDR of permittivity of 20, lower shell CDR of permittivity 12 and plug CDR having dielectric constant of 1 similar to air gap. This structure has reduced its volume to one third if it is compared with former stacked DRA and provide impedance bandwidth of 16.5%. Having said that, addition of conformal microstrip is added in the inner side of lower DRA, which makes design complex to make. Table 2.3.1 indicates main multi-segment DRA's proposed till now.

Table 2.3.1 Multi-segment DRA for Bandwidth Enhancement

Ref. No	Author (Year of Publication)	Shape of DRA	Bandwidth(GHz)	Resonant frequency	Type of feed
43	R.K Mongia in 1989	Half Split Cylinder	6.6-7.6	6.87	Co-axial
44	Antar et al. in 1993	Half split Cylinder	7.08-7.83	7.43	Slot coupling
45	M.T.K.Tarn et al. in 1999	Cylindrical Sector	1.68-2.30	1.8	Co-axial
46	Kishk et al. in 2001	Half Split Cylinder	1.7-2.3	2.1	Co-axial
47	Guha et al. in 2006	4 element Cylinder	3.4	3.4	Co-axial
33	P. Rezaei et al. in 2006	Two segment RDRA	3.32-7.456	5.84	Microstrip Line feed
48	Guha et al. in 2012	Half hemisphere	2.8-4.2	3.7	Co-axial
49	Pinku Ranjan et al. in 2018	Triangular shape MEMS	5.1-8.0	7.65	Co-axial
50	Fan Wang et al. in 2019	1x 9 array of RDRA	5.42-16.5	11.2	Co-axial
51	Ankit Roy et al. in 2019	RDRA with air gap and metallic layer	10.97-23.33	20.75	Co-axial
52	Pinku Ranjan et al. in 2020	MEMS h-CDRA	5.3-13.0	6.4	Co-axial

It is observed widely on the basis of Table 2.3.1, while designing the Multi Segment DRA gain is trade off in lieu of increasing the bandwidth. Various design methodologies tabulated in the above table lead to the conclusion that gain is compromised on account of bandwidth increment. Fabrication material and design parameters of Multi segment DRA should be chosen in such a manner so that high efficiency of antenna is achieved with desired bandwidth and gain properties**.**

2.3.2 Review on Defected Ground Structure

Ground plane and its dimensions have a significant impact on antenna's radiation characteristics. The mention of term DGS literally implies defects created in ground plane of the antenna. Compact geometrical slots embedded in the ground plane of microwave circuits are referred as DGS. Defected ground structure is implemented by slotting of ground beneath micro-strip line, CPW fed line and Cavity backed up resonators. Etching slots in ground plane alters slot impedance which in turn alters the micro-strip line impedance. Change in impedance causes change in Q-factor subsequently enhancing bandwidth of DRA. A single defect unit cell or number of periodic or aperiodic defects that can be inscribed on ground plane can be taken as defected ground structure [53-55].

In 1999, Park et al. [56] first introduces a dumbbell shape slot in ground plane in implementing a low pass filter. Afterwards DGS technique is employed for implementation of filters, amplifiers, Co-planar wave guide, Wide band antennas and Band notch creation in wide band width. Defected ground structure technique has been widely utilised by micro-strip antenna designers but not much work is done in case of Dielectric resonator antenna. A research gap still exists in implementing defected ground structure in amalgamation with DRA [57-62].

M. Abedian et al. [63] proposed an UWB DRA fed by U-shape line. Dielectric resonator antenna is fabricated by ε_r =10 and is mounted on a by Rogers 3003 substrate of permittivity. Two WLAN and Wi-MAX band notches are created by incorporating T shaped strip at the back of the antenna in between the two RDR and a stub on the opposite side. This structure provides impedance bandwidth of 122% ranging from 3.03 to 12.52 GHz. Omni directional radiation pattern with stable gain and radiation efficiency above 95% can be considered as key factors of the design.

Kshirsagar et al. [64] proposed a two segmented design fed with common microstrip. In this novel concept, both segments are placed side by side with a slot

cutting in ground. This entire arrangement provides a bandwidth of 131.24% ranging from 2.8-13.49. Proposed structure is best suited for various S, C, X, WLAN and Wi-Max band applications.

Kshirsagar et al. [65] presented a novel shape DRA which consists of a rectangular block. Subsequently, four asymmetrical rectangle shapes blocks have been taken out from that block to provide an overall bandwidth of 2.8-12 GHz. Conformal strip fed antenna is erected on the ground plane of dimension 30 x 30x 20 mm3 with FR4 material of ε_r = 4.3. Impedance bandwidth of 124.32% with an efficiency of 93% and maximum gain of 8.3 dBi is achieved with the prototype of the antenna. Fig. 2.3.11 shows top, front and rear view of a proposed DRA symmetrically placed of on a DGS and Fig. 2.3.12 shows simulated and measured co-efficient result.

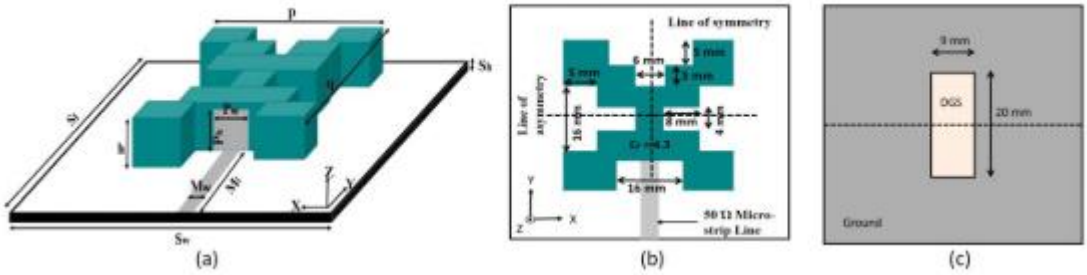

Fig. 2.3.11 Schematic diagram of a proposed DRA symmetrically placed on a Defected Ground Structure: (a) Front, (b) Top and (c) Rear views [65]

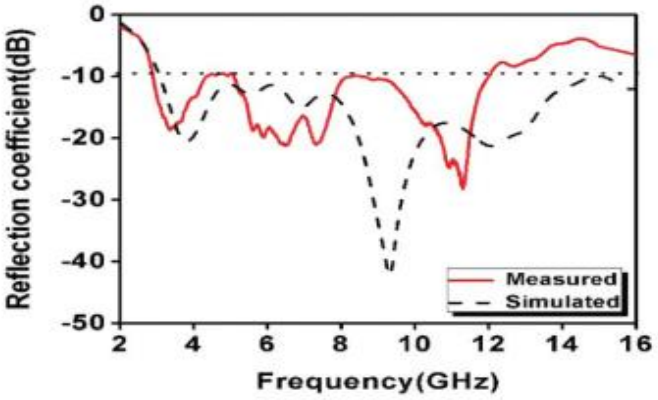

Fig 2.3.12 Measured and Simulated Reflection coefficient

P. Sharma et al. [66] presented a Turtle shaped DRA with 9 layers stacked upon each other giving an impression of turtle. This design provides an impedance bandwidth of 114% for a frequency ranging from 3 -10.9 GHz. Peak efficiency at 3 GHz is obtained in total operating bandwidth of 7.9 GHz.

S.K. Yadav et al. [67] proposed a p shape transformer for impedance matching. Microstrip fed antenna radiates for a frequency range of 3.1-11.1GHz. An average gain of 4.6 dBi along with stable radiation patterns have been obtained in this DRA. Dual polarization property of this antenna gives an edge to it. This antenna basically offers elliptical polarization property and axial ratio bandwidth of 5.1 GHz. Fig. 2.3.13 shows top and panoramic view of a proposed DRA and Fig. 2.3.14 shows simulated and measured co-efficient result.

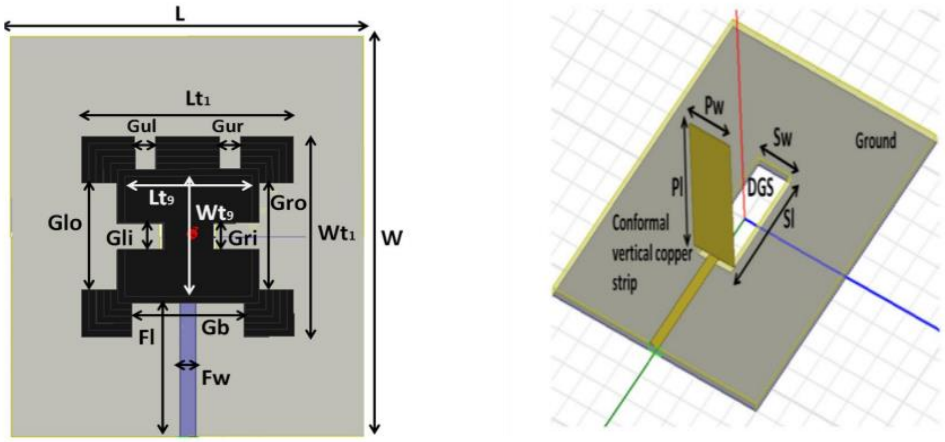

(a) (b)

Fig. 2.3.13 Geometry of proposed antenna (a) Top view and (b) Panoramic view [111]

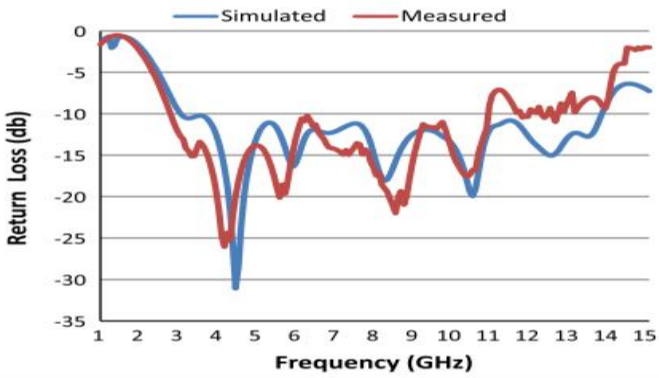

Fig. 2.3.14 Comparison of Simulated and Measured Reflection Coefficient

G. Kaur et al. [68] presented a low profile and compact DRA for early detection of breast cancer, which utilize DGS technique. As shown in Fig2.3.13 DGS employed in this antenna is a combination of step structure and slot consequence in bandwidth of 8.3 GHz ranging from 4.3-12.6. Presented low profile design not only provide low cross polarization but also yields high radiation efficiency. A typical combination of

asymmetrical dumbbell shape feed with defected ground structure makes this antenna proficient. Table 2.3.2 indicates prominent DRA's using DGS technique for Bandwidth enhancement. Fig. 2.3.15 shows microstri feed line, reduced ground plane with slots and front view of cubical shaped DRA. and Fig. 2.3.16 shows simulated and measured co-efficient result.

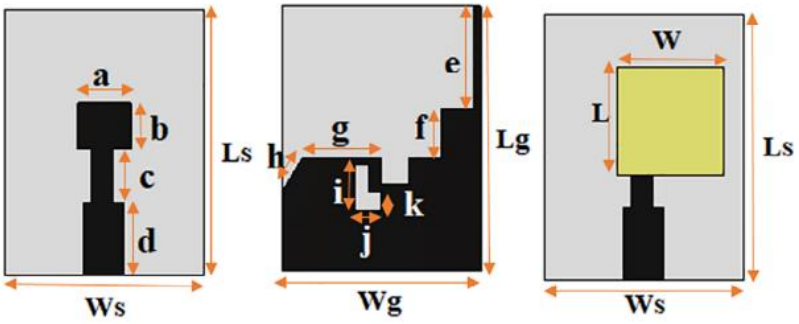

(a) (b) (c)

Fig 2.3.15 Cubical-shaped dielectric resonator antennas (a) Microstrip feed line (b) Reduced ground plane with slots (c) Front View [68]

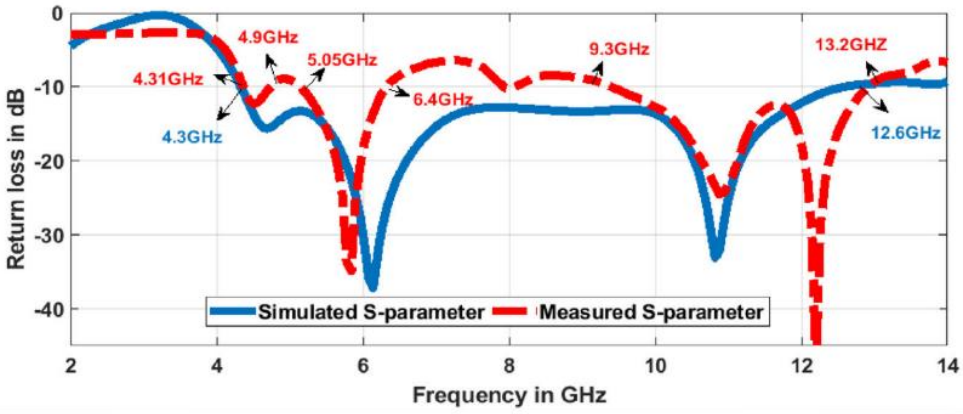

Fig. 2.3.16 Measured and Simulated Reflection Coefficient

Table 2.3.2 DGS based Bandwidth Enhanced DRA

Ref. No	Author Name [Year]	Shape of DRA	Bandwidth [GHz]	Feed Type	Antenna Size [mm]
63	Abedian et al. in 2015	Rectangular	3.03-12.52	U-shape line	20x30x6
64	Kshirasagar et al. in 2018	Rectangular	2.8-13.49.	Conformal strip	60x60x15
65	Kshirasagar et al. in 2018	Rectangular	2.8-12	Conformal strip	30x30x20

66	P. Sharma et al. in 2019	Turtle shape	3-10.9	Conformal Strip fed	60 x50x 15.15
67	S.K.Yadavet al. in 2020	Om shape	3.1-11.1	P-Type Transformer	50 x 40x4.87
68	Gagandeep Kaur et al. in 2020	Cubical Shape	4.3-12.6	Asymmetric Stub feed	20x15x4

2.3.3 Review on Hybridization Techniques of Bandwidth Enhancements

In last three decades, scientists have proposed numerous methods to enhance bandwidth of dielectric resonator antenna. Previous sections of this chapter is dedicated to augmentation of bandwidth via multi-segmentation and defected ground structure methods. This particular section throws light on bandwidth enhancement by employing following methods:-

- Exploring different shapes of DRA
- Application of different feed mechanisms
- Usage of metallic strips and walls to alter boundary conditions
- Hybridization of micro-strip patch antenna and DRA
- Making use of Arrays to enhance gain as well as bandwidth.

A comprehensive study of all categories mentioned above has been carried out to get the idea for a novel research.

Alireza Motevasselian [69] presented a co axial fed circularly polarized circular DRA excited by external tape helix. Co axial feed was connected to the helix by creating a hole in the ground plane. A compact and easy to fabricate antenna is presented which provides a 3dB axial ratio bandwidth of 6.4% for a center frequency of 3.5GH.

Li et al. [70] presented a puck of cylindrical shape with dimension D=49mm, H=22mm and ε_r=10. This design makes use of coaxial feeding which is loaded with Alford Loop. Alford Loop is a circular patch with four twisted legs. Coaxial fed probe makes this design to behave as electric dipole while Alford Loop makes it a magnetic dipole. When electric fields of electric and magnetic dipoles are equal in magnitude and in phase quadrature, they produce circularly polarized Omni-directional radiation pattern for WLAN applications.

Chu et al. [71] devised a CDRA made up of Eccostock material of ε_r = 10 with air infusion radiating in four different bands such as DCS, PCS, UMTS, WLAN with

frequency ranging from 1.6 -2.75 GHz. Unconventional shape of DRA is the primary reason for reduction in Q-factor which leads to increase in bandwidth. Inverted L-shape DRA provides a high gain of 7.25-8.61 dBi with omnidirectional radiation pattern.

Denidni et al. [72] presents a L-shape, triangular wide band DRA fabricated with material Rogers TMM10 of dielectric constant 9.2. This probe fed antenna covers an impedance bandwidth of 38% covering important wireless communication bands such as DCS, PCS, UMTS and WLAN.

A cross T shape antenna with trapezoidal conformal patch is applied to get a bandwidth of 3.57-7.57 GHz with an impedance bandwidth of 71.8%. A high gain of 3.23-7.3 dBi is obtained through the entire operating bandwidth. In another research work, author proposed an asymmetrical T-shape DRA with inverted trapezoidal feed conformal strip is employed for a bandwidth of 75.1% ranging from 3.81-8.39 GHz [73-74].

S. Maity et al. [75] presented a novel triangular shape of DRA with a high bandwidth of 4.33-7.02 GHz. An impedance bandwidth of 47.4% with broadside radiation pattern is obtained with proposed structure. Fig. 2.3.17 shows panoramic and top view of proposed DRA. and Fig. 2.3.18 shows simulated and measured co-efficient result.

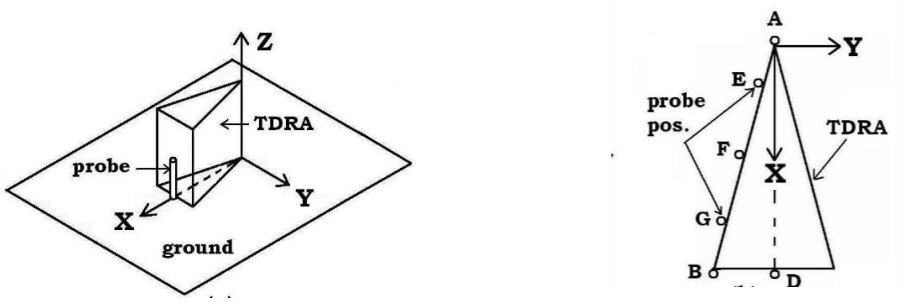

Fig. 2.3.17 Geometry of Proposed Antenna (a) Panoramic (b) Top view [75]

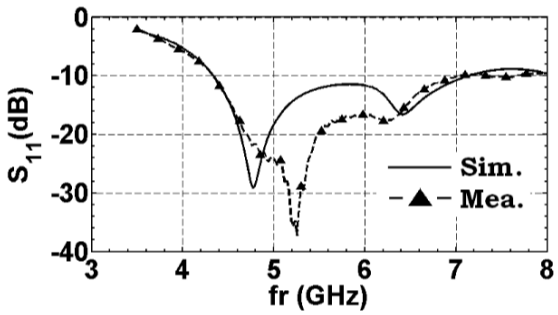

Fig. 2.3.18 Comparison of Simulated and Measured Input Reflection Coefficient

Chaudhary et al. [76] presented an annular ring fed DRA with an impedance bandwidth of 66.72% ranging from 3.49-7.20 GHz along with a measured average gain of 4.31dBi. This cylindrical DRA arrangement yields a good radiation efficiency with stable radiation pattern.

Ryu & Kishk [77] proposed a novel design of "A"shape DRA inserted in substrate after cutting a part of it. Excellent radiation pattern with an impedance bandwidth of 93%. This antenna radiates for frequency ranging from 3.53-9.675 GHz with peak efficiency of 95% and a high gain of 4 dBi. Fig. 2.3.19 shows top and side view of proposed DRA. and Fig. 2.3.20 shows simulated and measured co-efficient result

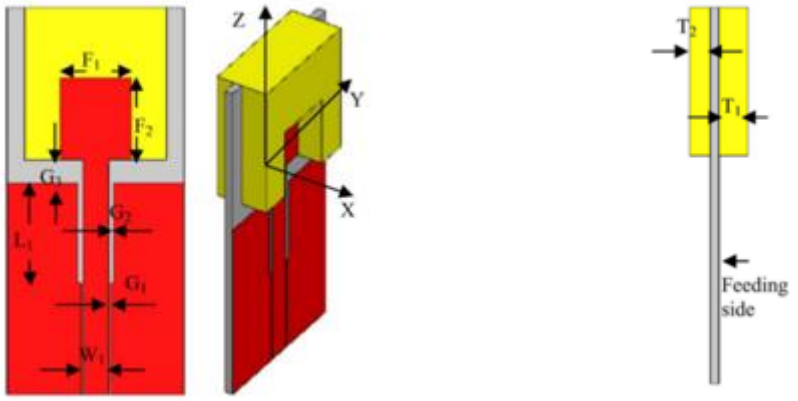

(a) (b)

Fig. 2.3.19 Geometry of proposed antenna (a) Top view and (b) Side view [78]

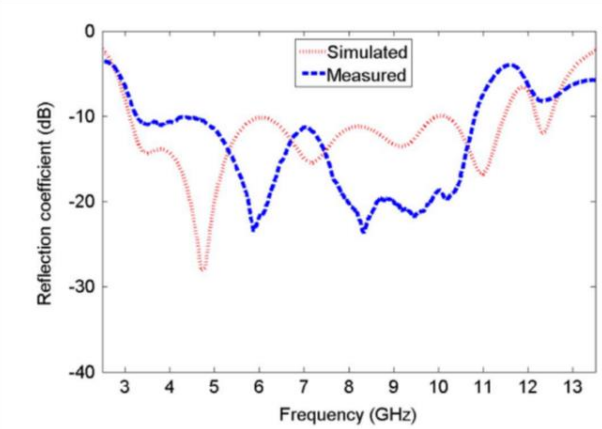

Fig. 2.3.20 Simulated and Measured Reflection Coefficient

In 2013, a CPW fed antenna is reported which is resonating from 3.1-10.6 GHz with omni directional radiation properties with low cross polarization level. A-shape radiator with a combination of patch is extremely suitable for UWB techniques [78].

Polarization can be defined as figure of merit, which can determine the application zone of any device. To render this requirement L-shape Compact DRA is presented. This structure is fed by combining trapezoidal shape feed from bottom in conjunction with coaxial probe. DR is fabricated by 2.56-mm-thick RO3010 dielectric with a size reduction by a factor of 6.7%. This antenna offers a measured bandwidth of 72% with broadband radiation pattern [79].

Elmegri et al. [80] carried out investigations on elliptical aperture coupling fed to CDRA which is fabricated with ε_r = 9.8. which yields an impedance bandwidth of 23% ranging from 9.97 GHz to 12.56 GHz. Omni directional radiation pattern with a peak gain of 7.3 dBi with creation of band notch at 10.57 GHz is given in this research work.

In 2010, Fang et al. [81] proposed a coaxial probe fed hollow RDRA. Meandered rat race junctions are placed in between RDRA's. Antenna radiates at 2.4 GHz for WLAN applications and provide impedance bandwidth of 10% ranging from 2.24-2.49 GHz with a high gain of 6.3 dBi. Stable radiation patterns with low cross polarization are key features of this design.

Asma Majeed et al. [82] proposed a balanced UWB antenna with L-section feeding technique along with a T-shape slot. Dielectric constant for the materials used for fabrication of DR have a permittivity of 9.4. Material chosen for substrate have permittivity of 4.5. The antenna radiates for a frequency range of 6.4 - 11.7 GHz with 58 % impedance bandwidth. Measured gain was found to be 2.66 dBi which is suitable for UWB applications.

Pahadsingh et al. [83] experimented with CDRA with a hexagonal feed mechanism in amalgamation with rectangular and micro strip line. This antenna was designed for cognitive radio applications. Fabrication material availed for this DRA is Eccostock Hick material of dielectric constant 10 and is mounted on a FR4 substrate of permittivity 4.3. This antenna has a bandwidth of 2 to 12 GHz and CDRA resonates in tri bands 4.93-5.4 GHz, 5.9 - 6.7 GHz and 9.28-10.2 GHz. Combination of these two elements results in increase in efficiency and gain.

Weng et al. [84] reported a RDRA fed with micro strip. Material used for this DRA is of relative permittivity of 9.8 and is mounted on the substrate of dielectric constant 2.65. The structure resonates in the frequency range from 2.4 GHz to 4.5 GHz extracting 61% bandwidth with consistent radiation patterns. Peak gain of 7dbi is obtained via this design.

Simons and Lee [85] observed the impact of parasitic elements in CPW fed DRA. Cylindrical DRA is developed from material having εr = 36 and were placed on RT Duroid 5880 substrate of relative permittivity 2.2. With excitation of TE110 and TE113 modes, 2.5% and 3.7% bandwidth increments are achieved. Stacking effect of CDR resulted in 5.3% further improvement in bandwidth.

Lambrecht et al. [86] investigated various features of mutual coupling in RDRA structures. Analysis was performed on coupling of slot/slot, slot/CPW, CPW/probe. Fabrication material used for RDRA have dielectric constant of 10. Peak gain of 6dBi is obtained by this design.

Anand Sharma et al. [87] proposed a cylindrical structure radiating for triple frequencies. Two hybrid modes are radiated within the CDRA. This novel ψ shaped microstrip feedline yields two frequency bands at frequencies 2.5-3.02, 3.76-3.86, and 4.38-4.72 GHz. Antenna is fabricated using alumina ceramic of dielectric constant 9.8 mounted on FR4 substrate of relative permittivity 4.4. Fig. 2.3.21 shows psi-shaped microstrip line and isometric view of Realized CDRA and Fig. 2.3.22 shows simulated and measured co-efficient result.

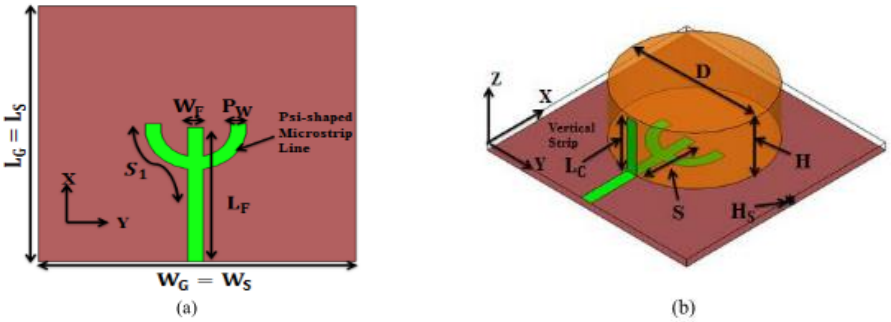

Fig. 2.3.21 Schematic Diagram of Proposed CDRA (a) Psi-Shaped Microstrip Line (b) Isometric View of Realized CDRA [87]

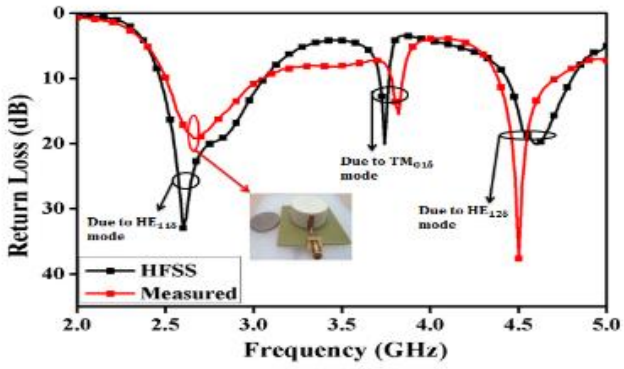

Fig. 2.3.22 Measured and Simulated Return Loss variation of Proposed Antenna

Liang et al. [88] experimented with a RDRA mounted on a concave structure ground plane which is implemented using TMM 10i (ε_r=9.8) material. Air gap formed between concave ground structure is skillfully utilized in enhancement of bandwidth of 55% ranging from 3.8-5.77 GHz with good radiation pattern. With a height of 10.5 mm this device provides a satisfactory gain of 3.7-6.2 dBi in the entire operating bandwidth.

Fang et al. [89] proposed a rectangular DRA of dielectric material of ε_r=9.8 which provides an impedance bandwidth of 56%. This antenna covers the bandwidth of WLAN (2.4-2.48 GHz) and Wi-MAX (3.4-3.7GHz) for commercial applications.

Guha et al. [90] proposed a novel concept of hybridizing monopole antenna with Pawn shape dielectric resonator. This combination of DRA and hybrid monopole impedance bandwidth of 122% is achieved and a gain in the range of 4 to 6 dBi is achieved.

Dong et al. [91] presented a RDRA loaded with two printed patches. Hybridization of these radiators yield an impedance bandwidth of 25.6% ranging from 1.7-2.2 GHz. Key features of this strip fed design are high gain of 8.2 dBi and very good radiation patterns with low cross polarization.

Ullah et al. [92] presented a novel technique of producing circular polarization in RDRA by employing H-shape conformal feed. This feed mechanism provides a 2:1 VSWR bandwidth of 6.95-8.68 with a 5dB gain. Good radiation properties and circular polarization can be considered as key points of this design. Fig. 2.3.23 shows schematic diagram of proposed CDRA and Fig. 2.3.24 shows simulated and measured co-efficient result.

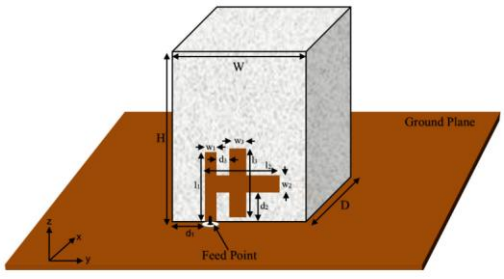

Fig. 2.3.23 Schematic Diagram of Proposed CDRA

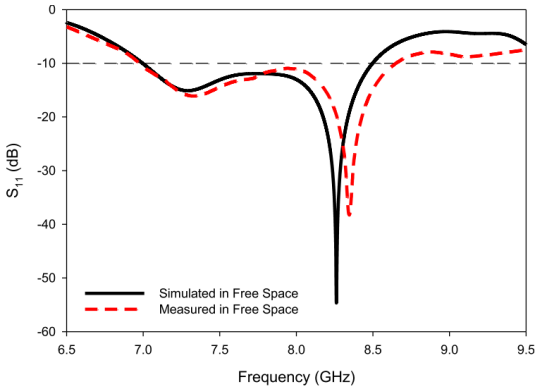

Fig. 2.3.24 Simulated and Measured Reflection Coefficient

Guha et al. [93] utilizes a trough-shaped air cavity in the ground plane of DRA to fiddle with its electric boundaries in order to excite higher radiating modes. HEM111 remained unaffected by new higher mode creation and which in turn consequents in dual band broadside radiating DRA. DRA is fabricated using ECCOSTOCK Hik material and providing frequency 3.8, 6.6 and 7.5 GHz.

Leung et al. [94] presented a cavity backed cylindrical DRA ed by slot aperture technique where aperture is coupled to the microstrip line with a microstrip like tuning stub. Cylindrical DRA of dimension diameter = 6.1 mm and h=11.5mm is fabricated to resonate at a frequency of 5.57 GHz. High gain of 5.5 dBi is obtained at a frequency of 6.3 GHz. Back radiations in this design is blocked by using a hemispherical cavity at the back end.

Sreedevi et al. [95] observed high dielectric constant properties of DRA that can be used to make GHz devices. DRA is fabricated using dielectric constant of 48 and diameter of 24.15 and height h = 6.81 mm. An impedance bandwidth of 18% with frequency range from 2.54-3.04 GHz for a center frequency of 2.68 GHz.

Saed et al. [96] presented a low-profile rectangular DRA with dimensions l = w = 10mm and h = 2.5 mm and is fabricated by the material Rogers RT/Duroid 3010 substrates that have dielectric constant ε_r = 10.2. This research work demonstrated that if top surface of DRA is covered with patch then resonant frequency get shifted downwards and provide bandwidth of 39%. On the contrary, uncovered DRA provides a bandwidth of 5% only.

Hashmi et al. [97] presented a high gain antenna by employing EBG resonator antenna. A small superstructure area of dimension1.5λ0 x 1.5 λ0 is also integrated with

feed to have a bandwidth of 22% with excellent gain of 18.2dBi. A footprint reduction of 85% is achieved along with a bandwidth improvement of 3-4%.

Kishk et al. [98] proposed an inverted cone DRA made up of material with dielectric constant of 12 with coaxial feed mechanism. Impedance bandwidth of 50% with low cross polarization level is achieved with this design.

Gupta et al. [99] compared the results obtained by loading DRA to rectangular and circular patch antennas. Bandwidth enhancement of 18% with circular patch and 13 %with rectangular patch is obtained via this design.

Yuan Gao et al. [100] proposed a compact wideband RDRA integrated with circular loop for RF applications. Rectangular geometry of antenna is chosen to obtain impedance bandwidth of 23% with broadside gain of 5dBi. The RDRA was developed from material having dielectric constant 10.2 and was mounted on FR4 substrate of 2.2 permittivity. Omni directional radiation pattern with low cross polarization levels is achieved with the proposed structure.

Guha et al. [101] proposed a modified frame for designing of UWB Dielectric resonator antenna. Additionally, an annular dielectric ring resonator fed with electric monopole was also presented. An UWB design radiating in range 5 to 13 GHz is proposed with probe excitation along with monopole.

Mongia et al. [102] presented an annular shape DRA excited by monopole antenna. The DR is developed from material having dielectric constant 20. An impedance bandwidth of 2.5% is obtained with size reduction but including monopole in design consequents in degradation in gain, cross polarization levels and radiation efficiency.

Kumar et al. [103] presented a microstrip fed, conical CDRA fabricated with dielectric constant 20.8 which is mounted on substrate of permittivity 4. Antenna offered impedance bandwidth of 35.25%with peak gain of 3.73dBi. In this article increases the dielectric constant to 88.68 and it yields an impedance bandwidth of 14.65% with peak gain of 4.74dBi. Application of vertical and horizontal conducting strips enhances cross polarization and decreases radiation efficiency.

A novel concept of Dielectric Resonator Antenna oscillator (DRAO) was proposed by Eng Hock Lim and Kwok Wa Leung. The rectangular is fabricated using Eccostock Hik material having dielectric constant 6 and erected on Duroid substrate of permittivity 2.94 [104].

Simon et al. [105] proposed a CPW fed CDRA fabricated with ZrSnTiO4 material with permittivity 36 erected on a RT Duroid substrate of dielectric constant 2.2. With addition of parasitic CDR bandwidth enhanced from 2.5% to 3.7%.

Mongia et al. [106] have proposed accurate measurement of theoretical aspects of resonant frequency as well as Q-factor of DRA. Two different CDRA termed as A, B are designed with different material, and their performances are evaluated in.

Sreekantan et al. [107] proposed a variety of DRs implemented material with permittivity 84. These structures include annular, Cylindrical and Rectangular DRA. It was concluded that cylindrical DRA has less bandwidth as compared to annular and RDRA.

Zainud Deen et al. [108] presented a hexagonal shape DRA for RFID applications. Two structures with single element and in array format are designed which not only provide high gain but also broadband radiation patterns. Gain of 7.62dBi is reported with single element structure and gain of 9.5 dBi is reported with array structure. Table 2.3.3 Indicates hybrid techniques to enhance bandwidth of DRA.

Table 2.3.3 Mixed Methods implemented DRA designs to Enhance Bandwidth

Ref. No.	Author Name [Year]	Shape of DRA	Type of feed	Bandwidth [GHz]	Peak Gain [dBi]	Antenna Size [mm]
72	Denidni et al. in 2005	L-shape	Probe feed	1.71-2.51	8.7	32x24
88	Liang et al. in 2008	Cross T shape	Trapezoidal conformal microstrip	3.56-7.57	7.57	60 x60x11
71	Chu et al. in 2009	Inverted L	Probe feed	1.6-2.75	8.61	28 x28
81	Fanget al. in 2011	Rectangular DRA	Strip fed	2.25-4.40	8.03	26x18.8 x 41.51
100	Gao et al. in 2012	T shape	Inverted	3.81-8.39	7.35	60x60x12.8

			Trapezoidal conformal microstrip			
75	Maity et al. in 2016	Triangle shape	Co-axial feed	4.3 – 7.02	5	140 x140x19
87	Sharma et al. in 2016	Cylindrical	ψ shape feed	2.5–3.02, 3.76–3.86, and 4.38–4.72	4.38-4.72	50x 50 x 12
91	Dong et al. in 2018	Rectangular DRA	Microstrip line	1.7–2.2	8.2	67x67x34
92	Illahi et al. in 2019	RDRA	H shape conformal feed	6.95–8.68	5	50x50x15
67	Yadav et al. in 2020	Om shaped	$\lambda/4$ P-type transformer	3.1-11.1	4.6	50 x 40x4.87

2.3.4. Review on Array Structure

Array can be defined as a combination of multiple, distributed antennas working as a single unit to perform desired tasks. In case of antenna, combination of multiple elements fed with a specific phase relationship is implemented to get the increased value of bandwidth and gain. Polarization diversity and beam steering capabilities are recently added features of the antenna arrays. Arrays can be mainly divided into two types:

- Broadside array is a group of half wave dipoles kept $\lambda/2$ distance apart. Property of this array is that it gives highly directional radiation pattern in perpendicular direction of plane of the array.
- End fire array is another kind of array in which bi-directional radiation patterns are achieved in a plane parallel to the plane of the array.

In order to understand the behavioral aspects of multiple antennas grouped together, a study of array is done in the following sections. This study not only dissolve the concept of multiple antennas grouped together to high get high gain and bandwidth but also bring forth the beam steering and polarization diversity concepts into the picture.

Wael M. Abdel-Wahab [109], simulated an array of 8-elements fed with a planar Surface Integrated Waveguide. This high gain and large bandwidth design is used for efficient millimetre wave band applications. An equivalent transmission line model is proposed for this type of high Q surface integrated waveguide model.

Nikkhah et al. [110] investigated Electronically Steerable Phase Shift Array Radiators (ESPAR Arrays) with analog beam steering capability with a scan angle of $\pm$30 degree. YAGI UDA antenna is used as a base for this structure. In this structure, two driven elements along with two parasitic elements are electromagnetically coupled to each other. In this phased array mutual coupling among elements decides the phase shift which consequents due to reactance changed by capacitive action of antenna.

Nikkah et al. [111] proposed a high gain, aperture coupled rectangular dielectric resonator array. This structure was designed to implement two types of arrays. H-plane rectangular dielectric resonating antenna array to which electromagnetic coupling is driven by driven element is fed by a narrow aperture from the substrate and the microstrip line is used to provide excitation signal. Another version of this array was fed by a cross shaped feed in which parasitic elements are placed in a cross shape to the driven elements. Due to these two arrangements, two different radiation patterns are obtained. H plane array yields broadside radiation pattern and cross shaped yields vane beam radiation pattern. Presence of parasitic element resulted in low gain due to energy wasted. Hence gain obtained by simple design is much more as compared to array structure implemented. This design is best suitable design for applications which needs pattern diversity such as LTE.

Petosa et al. [112] investigated a linear array constitutes of rectangular DRA excited by microstrip feed line. Objective of this research was to enhance gain. This objective was fulfilled with the construction of 10 element array where each element was spaced by a distance L= 25.4mm, approximately λg apart, placed adjacent to the microstrip feed printed on substrate of dielectric constant 2.2. Duroid material of relative permittivity 10.8 was utilized in order to fabricate the RDRA. Peak gain of 13.2 dBi at a frequency of 8.2 GHz with low cross polarization levels in radiation pattern is achieved by antenna array.

Larose et al. [113] proposed another planar array of MSRDRA fed by branch line microstrip. This array is implemented with RDR of permittivity 10 each and the optimized value of relative permittivity for dielectric inserts was 40. Materials used for top-most and bottom-most layer used for branch line is Rogers 3003 of dielectric constant 3. An exceptionally good gain of 15.4 dBi along with wideband response of 17% in X-band is achieved by this design.

Asem S. Al-Zoubi et al. [114] proposed tapered DIG feeding technique to excite RDRA array. At first single element DRA is fed by Dielectric image guide method in which narrow rectangular slots were used for impedance matching. Afterwards 7-element array with rectangular radiating slots along with reflector slots are added to improve to impedance matching. Another design with 15 elements array is designed in this research work. A perfect electric conducting wall is placed above DIG as reflector in order to reduce the back radiation. An exceptionally good gain of 10.27 dBi for 7-elements and 13.0 dBi for 15 elements is obtained through this array.

Leung et al. [115] makes an array arrangement to enhance gain of the entire structure. Single element of array structure is fabricated with permittivity of 16 and mounted on a substrate with dielectric constant = 2.33. Maximum gain obtained by this array is 10.8 dBi.

Chow et al. [116] experimentally verified performance of 2 x 2 array comprised of two CDRs with permittivity 9.5. This aperture coupled array is excited by HE_{110} mode and a peak gain of 8.9 dBi is achieved with low cross polarization level.

Petosa et al. [117-118] reported a microstrip fed linear array of 10 element RDR made by material having permittivity 10.8 and the microstrip was etched on Duroid substrate of dielectric constant 2.2.A peak gain of 13.2 with low cross polarization levels have been obtained via this design. An end fire array of identical CDRs is implemented which provide 35% impedance bandwidth.

2.4 REVIEW on RE-CONFIGURABILITY and BAND NOTCH CREATION

Last four decades have witnessed exponential growth in the demand of multimode reconfigurable antennas to render the requirement of modern wireless communication systems. Frequency-Agility or popularly known as Re-configurability of any antenna represents dynamic tuning of antenna in frequency, polarization and radiation characteristic domain through any switching mechanism [119]. Frequency agility interprets the shifting of resonant frequency of the antenna while polarization

diversity signifies alterations in polarization without hampering the smooth operation of device. Advantages offered by reconfigurable antennas include interoperability and compatibility of structure with varying conditions offered by wireless communication networks [120].

In 1983, Daniel Schaubert proposed and patented a reconfigurable array of micro-strip antennas. In that array, a part of the conducting patch was removed from the center which provides frequency as well as polarization reversal. Due to permanent etching of the conductor, this method was considerably slow and complicated to attain frequency-agility. Various methods to get reconfigurable antennas with fast switching speed, have been proposed by numerous researchers. Switching technique can be viewed as the contrivance through which antenna can alter its characteristics [121-124]. Fig. 2.4.1 shows characterization of Re-configurable witching techniques.

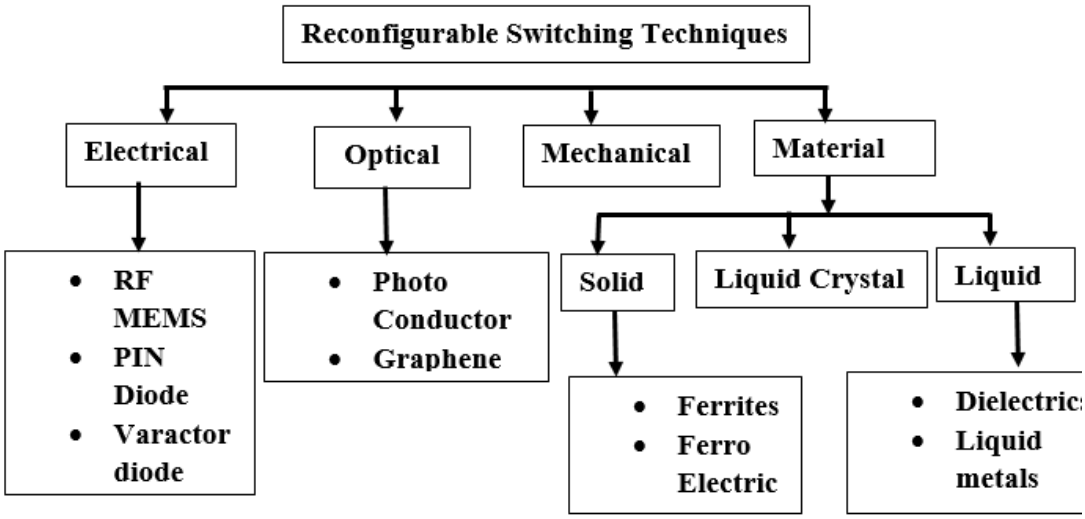

Fig.2.4.1 Categorization of antenna reconfiguration techniques

Most popular and practically feasible technique amongst all these reconfigure techniques is Electrical switching technique. RF-MEMS reconfigure the antennas with the help of nano-scaled devices and offers a good isolation with minimum power consumption. Switching speed of this technique lags behind PIN diode technique where diode mechanism makes it suitable to achieve faster switching speed ranging from 1-100 ns as compared to RF-MEMS ranging from 1-200μs. Varactor diode offers continuous tuning ability due to changing capacitance and high speed. Advantages offered by electrical switching have only disadvantage of requiring high voltage

consumption. Biasing circuits of antenna add losses and deteriorate radiation patterns [119].

Optical switching techniques includes LASER diodes at GHz regime and use of graphene at THz frequency region. These devices do not need biasing lines but LASER diode is bulky in size which makes design spacious and heavy. Graphene is emerging as new material for achieving tunabilty and re-configurability at THz regime. Applied Chemical potential voltage can be varied to change the permittivity of graphene and thus changing the properties of device. Physical or mechanical switches are easy way out to eradicate biasing and interference problem. However, slow response time and difficult integration with antenna makes it a cumbersome deal [120].

Material based switching technique has solid ferrite and ferroelectric materials which makes use of electric and magnetic fields to achieve agility in device. Main advantage of these devices is their large permittivity and permeability, which helps to achieve wide tuning range with size reduction. Liquid crystals are voltage-controlled devices. Variation in voltage subsequently alters the permittivity of antenna and changes radiation properties. Main concern associated with these devices is to maintain a particular temperature (20-35 °C) otherwise crystal loses its properties. Liquid metal-based switching technique is a relatively new method of switching but is still gathering attention of scientists and researchers. High conductivity, low losses, conformability are key advantages of this technique but still suffers from low switching speed and power handling constraints [125-126].

Liquid dielectric material switching technique-based antennas promises to offer fluidity and conformability. Following points are worth mentioning about these antennas

- These antennas are conformal, low cost, transparent and biocompatible.
- Physical and chemical both kind of re-configurability can be achieved through this design. Height, volume and shape of the liquid along with chemical composition decide the reconfigurable factor of the antenna.
- Liquid assisted antennas make use of water as dielectric material to modify local currents to reconfigure a metal base antenna.
- Conductivity of the water can be enhanced by adding salts (NaCl, KCl) which in turn increases the bandwidth ad tuning range of antenna.
- A microfluidic container or cavity (independent of shape) has to be placed near the location of maximum electric field or current to maximize the tuning range.

Magneto Hydrodynamic antenna is one such liquid assisted antenna used with NaCl to increase the conductivity of the antenna. An oscillating rectangular fluid frame consisting of conducting fluid has been radiating under controlled electric field and magnetic field applied. Fluid molecules oscillate due to impact ionization inside the fluid and contribute to radiate energy. Resonant frequency depends on velocity of the fluid, volume, type of fluid, shape of tube, chemical properties of fluid used, magnetic bias and electric bias conditions. It has resulted into large design space for antenna reconfigurability mechanisms i.e., frequency reconfigurability, polarization reconfigurability and pattern reconfigurability. Based on perturbation techniques, current in the fluid can be computed by fixing probe position at any arbitrary position. The Maxwell's Equations, Navier Stokes Equations and Equations of mass conservation are used to analyze the structure with conducting fluid with EM fields. These have been expressed as partial differential equations for the stream function, electric and magnetic fields. These equations are first order in time which helps us to predict velocity field of the fluid in the near field region and electromagnetic field in the far field region. Microwave fluids i.e., Silicon oil or Naphthenic oil can be used as substrate based on permittivity characteristics desired for Rectangular MHD Antenna [127-129].

Earlier study of Re-configurable antennas has been confined to microstrip patch antennas only. A few designs on dielectric resonator antenna, have been proposed in literature hitherto. Upcoming section of this chapter is dedicated to state of art of DRA in reconfigurable paradigm. An exhaustive study of DRA proposed are studied to get an- idea of contemporary techniques being employed in today's reconfigurable systems.

Mohammad et al. [130-131] presented UWB DRA with additional band notch characteristics. Cylindrical shape of DRA is erected on to FR4 substrate with high permittivity 4.4 and thickness of 1.64 mm. Impedance bandwidth of 113% with a notched band of 3.2 -3.8 GHz is obtained in the bandwidth of 3.3-12 GHz. Radiation efficiency of 68% with a peak gain of 7.5 dBi is obtained via this design. Omnidirectional radiation pattern with low cross polarization levels have been achieved. Another stacked approach with dual band notch creation is proposed. Materials used for fabrication are Rogers TMM10 and RT/Duroid 5880, whose dielectric constants are 9.2 (ε_2) and 2.2 (ε_1), respectively. The impedance bandwidth of VSWR< 2 covers the frequency range of 2.9–12 GHz, with a band notch of 5.2–6.1 GHz.

Shahine et al. [132] presented reconfigurable DRA with WB and notch band characteristics. Two implementations of DRA's have been designed. In first design, CDRA is placed on a Rogers3203 substrate with dielectric constant 3.02. CDR is fabricated from TCI-ceramic K12 material with permittivity 12 and is fed with bevel shape patch. Partial ground plane structure with split ring resonator is incorporated to attain dual band notch characteristics. For second design, the CDR made of Glycerine material of permittivity 42.5 is placed on a FR4 epoxy substrate of dielectric constant 4.3. Rotation of DRA at various angles ranging from -75^o, 15^o, 45^o, and 90^o is done which in turn resonates at different reconfigurable frequencies given as per rotation angle 3.6 GHz, 4.0 GHz, 4.1 GHz, and 4.25 GHz respectively. The peak measured gain the antenna is 5dBi.

Asem S. Al-Zoubi et al. [133] experimented with tapered DIG feeding technique to excite RDRA array. At first single element DRA is fed by Dielectric image guide method in which narrow rectangular slots were used for impedance matching. Afterwards 7-element array with rectangular radiating slots along with reflector slots are added to improve to impedance matching. Another design with 15 elements array is designed and presented in this research. A perfect electric conducting wall is placed above DIG as reflector in order to reduce the back radiation. An exceptionally good gain of 10.27 dBi for 7-elements and 13.0 dBi for 15 elements is obtained through this array.

Abhishek Singh et al. [134] proposed a dual probe fed mechanism for cylindrical DRA. Comparison of singly fed DRA with doubly fed DRA is done in this research paper. A detailed comparison in terms of bandwidth and gain is done in this design. Impedance bandwidth of 82% with high cross polarization level is achieved with single fed scheme. At first, CDRA is designed with one probe feed which provides impedance bandwidth of 68% with a measured gain of 6.7 dBi with low cross polarization level. Fabrication material used for construction of CDR have dielectric constant 10.2 which is mounted on the substrate backed by a circular ground plane of relative permittivity 2.1.

Hady et al. [135] proposed a dual polarized cylindrical DRA with a peak measured gain of the antenna was 4.8dBi with radiation efficiency of 96.4%. This CDRA is fabricated with material of relative permittivity 32 and placed on a substrate of dielectric constant 6.15. Circularly as well as vertically polarized antenna is implemented for GPS and WLAN applications. Hybrid mode through co-axial probe is

generated to produce circular polarization while two L-shaped printed lines are used for TM mode excitation to generate vertical polarization. The circular polarized and vertical polarized bandwidths were found to be 7% and 17.2% respectively.

Meng Zou et al. [136] proposed a comprehensive study on co-axial feed mechanism of the RDRA. Two resonances with two different modes are observed. TE_{121} mode is excited at first resonance while TE_{211} mode was excited at second resonance. Omnidirectional radiation pattern is obtained with this structure.

S. Danesh et al. [137] investigates a reconfigurable antenna fabricated with Taconic substrate of dimension $40 \times 45 \times 1.57$ mm^3 has a dielectric constant of $\varepsilon_r = 15$. A U-shape microstrip line is used to couple electromagnetic energy to the device. Switching method of re-configurability is used to obtain two types of responses from the antenna. At its ON state, impedance bandwidth of 49% (4.12-6.8) is achieved while in the counter state bandwidth achieved is 25% (6.90-8.85) GHz. Average efficiency of 93% with peak gain of 6.25 dBi is achieved via this arrangement.

Chair et al. [70] investigates a cylindrical DRA made up of material of dielectric constant of 10.2 with diameter of 10mm and height of 5mm.First exciting technique is J-shaped and another is Hook-shaped probe which are applied after creating a recess in its bottom. When antenna is excited by J-shape probe then bandwidth obtained is 8.2-11.5 GHz with an impedance bandwidth of 33.5%. With Hook shape excitation, wideband response with 31%impedance bandwidth with range from 8.2-11.5 GHz is obtained. Table 2.4.1 highlights prominent reconfigurable techniques and implemented DRA's. Fig. 2.4.2 shows top of the DRA and Fig. 2.4.3 shows simulated and measured co-efficient result.

.

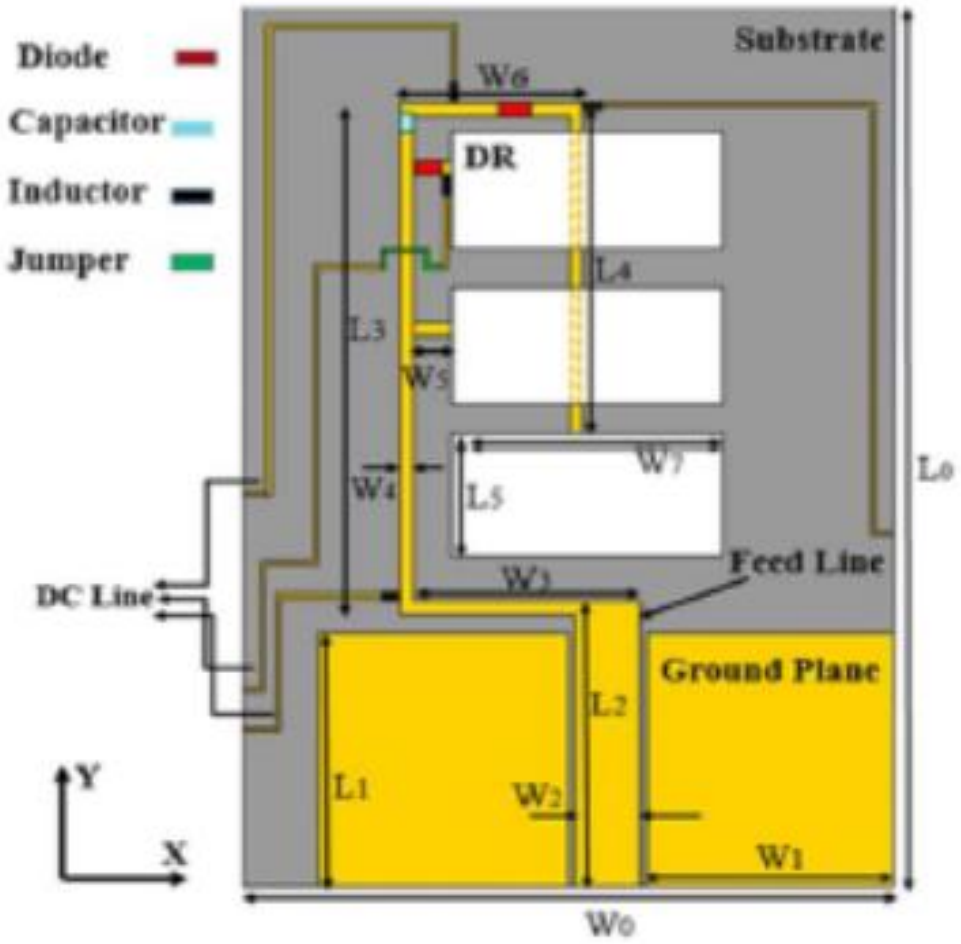

Fig. 2.4.2 Top View of the DRA [137]

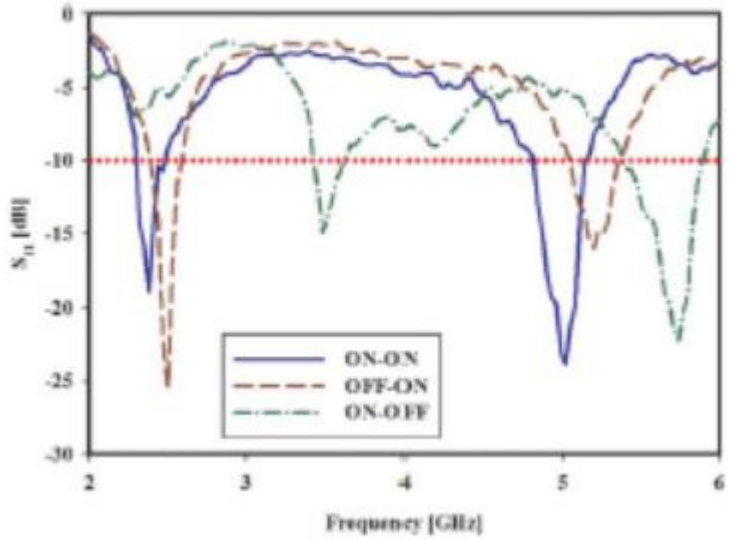

Fig. 2.4.3 Simulated and Measured Reflection Coefficient

Table 2.4.1 Reconfigurable DRA in present state of art

Ref. No	Author Year	Frequency	Tuning Technique	Peak Gain	Dimension
138	Kefee et al. in 2007	0.05-0.1	Water	NA	800x300x550
139	Huff et al. in 2010	2.5-4.5	Colloidal Dispersion	NA	R=28, H=30
140	Hao et al. in 2011	2.12-2.87	Chip Capacitor	7.06	100x100x15
137	Danesh et al. in 2013	3.45-6.77	PIN	4.86	33x45x2.8
141	Tang et al.in 2019	13.34-18.53	Metallic Pillar	8.53	20x20x3
142	Kausha et al.in 2020	3.6,2.6,1.8	PIN diode	3.8	20x36x4.8

It is inferred from the table 2.4 that the reconfigurability in DRA is achieved either with Metallic pillars [141] or connecting PIN Diode [142] or by creating changes in the overall permittivity and permeability of the medium [138-140]. All these methods alter the properties of the antenna without physical changes consequence in simplicity in fabrication and less space requirement.

2.4.1 Review on Band -Notch Multi-Mode &Multi-Band Reconfigurable antennas

Multi-Mode and Multi-band reconfigurable antennas are emerging rapidly in wireless communication. In 2002, Federal Communication Commission approved unlicensed band of frequency from 3.1-10.6 GHz for indoor short-range communication. UWB technology is gaining momentum due to large bandwidth availability which subsequently provides high data rates. FCC assigned IEEE 802.11 and 802.16 standards for narrow frequency bands. Table 2.4.2 summarize the band structure in ultra wide band technology [143].

Table 2.4.2. Summarizing Narrow Band Structure in UWB Technology

Sr. No	Band Name	Frequency Range (GHz)
1.	WLAN	5.15-5.35 5.725-5.825
2.	Wi-MAX	3.3-3.6 5.25-5.825
3.	C-band	3.7-4.2 5.925-6.425
4.	X-band	7.25-7.745

Co-existence of multiple devices within UWB band causes an electro-magnetic interference. To avoid this kind of intrusion, antenna structure must retain band rejection capability. This property is known as band notch or band selection property. A plethora of techniques is available for band notch creation in micro-strip patch antennas [144-146]. However, there still exists an exuberant need for implementing such techniques in DRA. Fig. 2.4.4 shows top of the DRA and Fig. 2.4.5 shows simulated and measured co-efficient result.

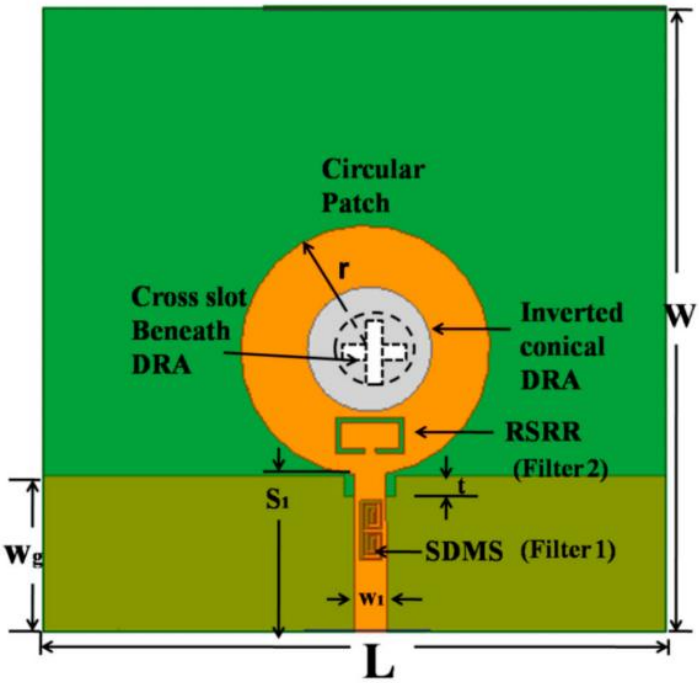

Fig 2.4.4 Top View of the DRA [150]

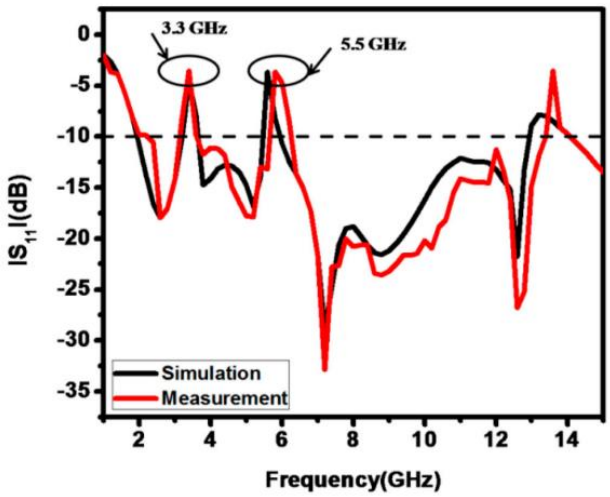

Fig 2.4.5 Simulated and Measured Reflection Coefficient

Table 2.4.3 highlights the latest work done in obtaining multi band antennas by notching bands.

Table 2.4.3 Band Notch DRA's in present state of Art

Ref. No.	Author (Year)	Dimensions (mm^3)	Peak Gain (dB)	Band Notch Created	Band Covered (GHz)	Notch creation Method
147	Vashistha et al. in 2014	25x9.2x4	NM	Single	5.725	T-shape slot in ground plane
148	Weng et al. in 2014	90x90x19	9.8	Single	5-6	Short circuited strips with slot etched in feeding
27	Abedian et al. in 2015	12x30x6	5	Dual	3.22-4.06 4.84-5.96	Slotted ground plane with inverted T-shape stub with parasitic patch

149	Shao et al. in 2015	100x100x15.5	5.4	Single	5.2-6.1	Slot creation in feeding patch
150	Dash et al. in 2018	60x60x10	6	Dual	3.3-2.75 5.2-5.6	Slotting in ground plane and feeding patch
151	Liu et al. in 2019	24x28x5.6	4.1	Dual	5.3-5.84 8.74-8.98	Varactor diode with slot in feed.
152	Afifi et al. in 2020	30 x30x9.8	5.2	Dual	2.5/5.2 3.5 4./4.8	Vertical Metallic strip pairs (VMSP)

2.5 REVIEW BASED ON GRAPHENE BASED TUNABILITY

Nano Plasmonic devices are emerging as a revolutionary contrivance to mitigate modern communication system requirements such as High Data Transfer Rates and Ultra High Band Width. Optical metallic antennas have a variety of photonic applications such as Sensitive Biosensing and Fluoroscense analysis. To harvest energy from sun, low-cost solar cells and Hybrid Plasmonic SOI configurations have been implemented. Various properties including Quantum efficiency of a Nano patch antenna with four different geometries is explained in for optical Plasmonic enhancement of light emission for targeted applications [153-157].

Undeniably, noble metals can be looked upon as the best accessible Plasmonic material, but due to large ohmic losses and hard tunability puts a constraint in the feasibility of these materials to be used in optoelectronic applications.

Presently, Graphene is attracting most attention in 2D material for applications in THz band. Graphene is a planar atomic material which is encapsulated in a hexagonal structure and extracted from graphite. Graphene is termed as that exceptional semiconductor that has zero band-gap structure with exuberant electrical and optical characteristics. Most important characteristics that Graphene offers is its tunability.

Change in chemical potential changes the conductivity of the material which in turn tune the frequency response of the antenna. Chemical potential can be changed either by altering the doping concentration or by applying external bias. Graphene is emerging as a new substitute for material to be used in THz frequency applications. Over last decade, many Graphene based devices including modulators, phase shifters, amplifiers, Graphene scattering devices, reconfigurable Plasmonic antennas and MIMO systems, leaky wave antennas, THz filters and reflect array antenna have been proposed [158-176].

Arduous exertions are being done by the researchers in order to get adequate material for application in the field of optoelectronics. This investigation leads to one highly significant stream called hybridization. Process of hybridizing noble metals with other materials in order to target specific Plasmonic applications to analyze the impacts over spontaneous emissions and absorptions. Success of these systems are mainly determined by suitable and precise means of tuning the Plasmon resonance of a Nanostructure while keeping the electromagnetic characteristics intact. The technique employing enhancement region Hybridization of noble metals with silicon or glass have been reported in past to target specific applications such as Time domain spectroscopy of thin metal gold film with silicon at the metal insulator percolation transition [177-178].

Graphene has been projected as a highly suitable substitute for noble metals in field of Plasmonics due to its superior properties, yet not much work has been done on the amalgamation of both legendary materials to enrich the field of electronics. Metallic nano structures are combined with graphene to provide a mean of electrically tunable device in optoelectronic field. A quantitative analysis of the Patch antenna presented in this research work can be done with the help of classic Metal –Insulator- Metal (MIM) fabry-perot cavity model. Many researchers are working either towards mathematically modelling of the optoelectronic devices like Eigen Analysis, Matrix Mesh Analysis or deriving these components from their RF counterparts. Unprecedented amount of work i.e., Quality factor variations, Resonant tunneling in Nano cavity have already achieved on this simplest MIM cavity [179-184].

Patch Antennas have gained immense popularity due to their planar structure and ease in fabrication for RF and microwave range. Reconfigurable and Tunable Graphene based patch antenna, with PBG high gain antennas have also been proposed. Along with simple geometries, fractal geometries have also been widespread in RF

range. Lately elliptical metallic patch antenna with high gain and large impedance bandwidth have been reported [225-227]. Table 2.5 gives the comparison between THz patch antennas.

Table 2.5 Comparison Table of THz Patch Antennas

Ref. No.	Dimensions (λ^3)	Shape of Patch	Author (year)	Gain (dB)	Bandwidth (THz)
227	$2.47\lambda_0 \times 2.479\lambda_0 \times 0.011\lambda_0$	Fractal Circular	S.Das in 2020	12.89	9.9(0.1-10)
226	$12\boldsymbol{\lambda}_0 \times 9\boldsymbol{\lambda}_0 \times 1.2\boldsymbol{\lambda}_0$	Elliptical	Singhal et al in 2020	9.5	9(0.3-9.3)THz
209	$6.6\boldsymbol{\lambda}_0 \times 5\boldsymbol{\lambda}_0 \times 0.67\boldsymbol{\lambda}_0$	Elliptical	Singhal et al. in 2019	12	5(0.46-5.46)

2.6 REVIEW on BIO-MEDICAL APPLICATIONS of DRA

Wireless Body Area Network (WBAN) is one special kind of sensor which is designed to work independently to unite with other medical sensors and appliances which are placed inside or outside of human body. Wireless Body Area Networks are essential amalgamation of tiny sensors and gateway nodes which connect sensors to external wireless communication server. Popular wireless technologies available for medical monitoring are Zigbee, WLAN, GSM and Bluetooth. Revitalization of short range UWB technology resulted as a boon for WBAN application due to its low transmitted power, robust and secure communication with high channel capacity [228-230].

Various metallic patch sensors have been proposed in literature for WBAN applications for great performance but low gain offered due to metallic loses and low efficiency provided by this antenna. Recently Dielectric Resonator Antennas (DRA) is catching eyes of researchers due to its promising features such as radiation efficiencies with high Q, high gain, small size, light weight and low cost. Various shape DRA structures have been proposed by scientists to be used as sensors in WBAN systems. Apart from offering numerous merits, mechanical processing and stability are still a matter of concern for DR antenna designers. In order to extract virtuous features of both

antennas, Hybridization emerges as the best possible solution for the present scenario. Hybridization of both elements yields high efficiency, high gain, low cross polarization levels and stability which are mandatory features required for the sensing unit of the WBAN communication systems. Stepped microstrip fed mechanism is used to improve impedance matching of antenna. Ring shape patches have been an ardent candidate to enhance the bandwidth of structures. Defected ground structure are one of the prudent techniques used to enhance bandwidth of the antenna [231-249].Table 2.6 compare the radiators proposed for BAN networks.

Table 2.6 Radiators Proposed for BAN Networks

Ref. No	Author (year)	Dimensions (mm3)	Band width (%)GHz	Gain (dBi)	Efficiency (%)	Type of radiator
234	Jiang et al. in 2014 2014	35x37x1.6	2.3-2.46	6.2	NM	Microstrip Patch
232	Samal et al. in2019	39x42x3.14	3.5-4.3 6.6-10.2	5.42	NM	Wearable textile microstrip
250	Kwashik et al. in 2018	40x34x2.7	2.7-19.5	6	87.2	Textile Patch
235	Simorangkir et al. in 2016	85x75x3	4.95	7.4	85	Patch
241	A. Iqbal et al. in 2017	40x40x7	5.4	5.4	92	Cylindrical DRA
251	Alampanis et al. in 2009	Radius=30 Height=12.5	3.4-5.0	NM	NM	Conical DRA
243	M S Iqbal et al. in 2015	6x24x11.9	4.4-9.7	5.2	FG	RDRA

242	A. R. .Chandran et al. in 2014	20x 20x13.2	2.45	1.84	94.6	DRA
239	Tahsen et al. in 2016	60x60x12.7	5.4-6.2	8.3	97	Cylindrical DRA
240	Mashaddi et al. in 2010	60x60x12.7	4.2-6.8	NM	NM	Bow-tie DRA
230	R.Alaskalani et al. in 2016	Hybrid, Ground Radius =40 Height= 19	3-13	4.5	NM	Caped Monopole with DRA
92.	Illahi et al. in 2020	60x60x15	6.95-8.68	5	NM	Rectangular DRA

2.6.1 Review Based on BREAST CANCER DETECTION SENSORS

According to WHO Report 2020 breast cancer is the most commonly occurring cancer among women. At present about 2.10 million women are being affected each year globally and having high mortality rate. In 2018 it was estimated that 627000 died from breast cancer, which is approximately 16% of all cancer deaths among women. In order to improve breast screenings, their outcomes and survival rate, early stage detection is critical. It is reported that in every four minute, an Indian woman is diagnosed with breast cancer. The survival rate is 60% in India while 90% in USA. An early detection may lead to better health care and almost 70% of cases can be cured with well-defined treatment and protocols [252-254].

Contemporary techniques being used for breast cancer detection are X-ray mammography, Ultrasound, Magnetic Resonance Image, Positron Emission Tomography and Microwave imaging. X-ray Mammography technique exposes the malign tissue with low energy X-rays for early detection but it suffers from needless and intrusive follow ups with false positive test results. Moreover patient has to expose to radiations along with compression of breast, which makes this technique highly

uncomfortable. Ultrasound technique makes use of sound waves of frequency higher than 24 KHz but its low resolution makes this secondary technique for mammography. MRI process makes use of radio waves and strong magnetic field to create impressions of the inside body. In this process amount of energy absorption of malign, benign and normal tissue varies and that is recorded by data acquisition system. This is pre-surgery procedure and is very expensive hence this cannot be used for early detection. Positron Emission Tomography (PET) is a process of injecting contrast liquid of radioactive element with glucose or glycoprotein to soft tissues of breast. Nutrients are absorbed by tumor tissues and positrons are ejected. Mapping of these positrons provide image for tumor in breast but PET also suffers from lower resolutions due to dependency on body's inherent characteristics [256-257].

Microwave imaging techniques transmit high frequency radio waves towards the affected area and retrieve those reflected and scattered radio waves to identify shape and size of tumor. This technique has no radiation and ionizing properties as compare to X-ray Mammography and have exceptionally low cost in comparison to MRI. Technically microwave imaging is the most comfortable, high resolution and low cost technique that can be used for early detection of cancer. It can be bifurcated into two parts according to the approach devised to acquire the tumor image. One is Microwave Tomography (MT), in which data can be collected at remote location by estimation of permittivity distribution inside the breast. It makes use of inverse scattering algorithms which in turn increases system complexity and time taken to produce output. On the other hand second less complex approach of microwave imaging is known as Ground Penetrated Radar (GPR) approach. UWB Radar Microwave imaging system steers a short pulse along ultra wide band width, and response in form of scattered wave is collected and processed through various Focusing Algorithms. Main component of Radar based detection scheme is aerial structures due to which waves will be transmitted and received [258-266].

In order to eradicate these problems number of wearable, on body microstrip antennas have been proposed which are operating in Lower European Band (3-5.5 GHz) with high bandwidth, efficiency and radiation pattern [267-270].

In 1960, Jack. H. Raymond proposed his views on scattered waves that can identify the properties of dielectric material. Afterwards Toro Uno proposed his work on conductivity and permittivity profile estimation of a one dimensional inhomogeneous medium using inverse scattering matrix. It was the high time when

Researcher group like Luk and Lueng, Mongia et all were working towards the Dielectric resonators which were prime candidates for TE mode propagation. Uno's work was progressed by Tie Jun Cui by using a two –step Inverse scattering algorithm for a lossy inhomogeneous medium. In early 5 years of 20th century, both academia and industry were rigorously searching for image reconstruction methods for both TE and TM waves. Franceschini et al., proposed a iterative method for image reconstruction from the scatterers of TE waves. This proposal of image reconstruction technology worked as the boom for dielectric resonator antenna to use it as a biomedical sensor [271-275]. Table 2.6.1 provides a detailed study on literature related to microwave imaging used for breast cancer detection technologies.

Table 2.6.1 Sensor comparison for early detection of Breast Cancer

Ref.	Type of antenna	Bandwidth	Classification	Domain
276	BAVA Stacked Substrate Approach	2-12 GHz	Multi-static	Frequency
277	Stair shaped 2009	7-12 GHz	Mono-static	Frequency
278	BAVA Single Element	1.16-6.92 GHz	Multi-static	Time
279	Slot antenna Array	3.5-15 GHz	Mono-static	Frequency
280	Array of 16 UWB antenna	3-10 GHz	Multi-static	Time
281	(TWTLTAs)	2-4 GHz	Multi-static	Time
78	L shape DRA	2.6-5.52 GHz	Multi-Static	Frequency
282	Vivaldi Structure	1-4 GHz	Multi-Static	Both
283	(TWTLTAs)	2-4 GHz	Multi-Static	Time
284	H -Shape DRA	3.47-9.62 GHz	Mono-Static	Frequency

285	Slotted patch antenna with stair shape	2.4-4.7 GHz	Mono-static	Frequency
286	CPW fed Slotted Patch antenna	2-6.5 GHz	Multi-Static	Time
287	Two antenna with metamaterial with AMC CPW fed 5 x 5 array.	3.1-7.6 GHz	Multi-Static	Frequency
288	Vivaldi Antenna with 9 antenna array	2.8-7 GHz	Multi-Static	Frequency
289	Rectangular DRA	22.5-27 GHz	Mono-Static	Frequency
290	Stacked substrate antenna	4.9-10.9 GHz	Mono-Static	Frequency
68.	Cubicle shaped	4.3-12.6 GHz	Mono-static	Frequency

CHAPTER 3

BANDWIDTH ENHANCEMENT TECHNIQUES of DRA

INTRODUCTION

Modern wireless information-oriented society needs wide bandwidth to support huge data transfers and locate the frequency bands. In order to meet these requirements, low profile, ultra wideband & efficient radiators are required. DRA (Dielectric Resonator Antenna) is a lossless radiator displaying various merits like wideband nature, compactness in size, light weight offering high temperature stability, low cost and ease of fabrication [1-2]. DRA displays high radiating efficiencies due to absence of any kind of conductors in the radiator. These dielectric radiators are highly compatible with every kind of transmission lines such as coaxial probe, micro-strip line, micro-strip slot, coupled or aperture coupled, coplanar waveguide and dielectric image guide method [22, 37, 78, 114].

In last 25 years, numerous techniques have been devised to increase the bandwidth of the DRA with a stable gain. These techniques can be broadly divided in three categories one is lowering the Q-factor of the DRA second is making use of external matching networks to increase the impedance bandwidth and combination of multiple DRA's in one form or another. Array formation is the best way to increase bandwidth and maintain high gain at the same time [111-115]. One of the methods used for the improvement in impedance bandwidth is the stacked DRA. In stacked DRA method, two or more different samples of same or different dimensions and dielectric materials are stacked vertically. It is possible to have different combination of shapes such as a dielectric disk, a rectangular and a triangle DRA in the stacked antenna [118].

3.1 BANDWIDTH ENHANCEMENT USING MSRDRA

Multi Segmented DRA makes use of alteration in the permittivity of the material. Generally high permittivity material is inserted below low permittivity material which changes the overall permittivity. Combination of low and high values of permittivity should be such that Q-factor of the antenna is reduced [18-25]. Insertion of blocks within the yoke of antenna yields extremely high bandwidth due to increase in effective permittivity of the antenna. Bladel [7] started the concept with a circular DRA. In this particular design ratio of inner to outer radii is changed and the impact on bandwidth is recorded. Pinku Ranjan et al. [52] makes use of stacked dielectric slabs

of different permittivity to enhance the bandwidth. A Multi segmented DRA with Ultra wide band-width is presented in this chapter. In this DRA four segments of different permittivity are inserted in base segment. Base segment is made up of material Alumina with dielectric constant =9.4, which can also be addressed as Yoke of the structure.

3.1.1 Geometry and Design of MSRDRA

Fig. 3.1.1 shows the geometric configuration of MSRDRA (Multi Segment Rectangular Dielectric Resonator Antenna). A multilayer multi segment RDRA is designed having a ground of 40 x 40 x 0.02 mm^3 and a substrate material of FR4 epoxy having permittivity of 4.4 with dimensions of 10 x 15 x 3.2 mm^3. Rectangular DRA is made of alumina with permittivity of 9.4. Coaxial feed coupling method is used for feeding of the structure. In this method the excitation is done by inner most conductors of the coaxial.

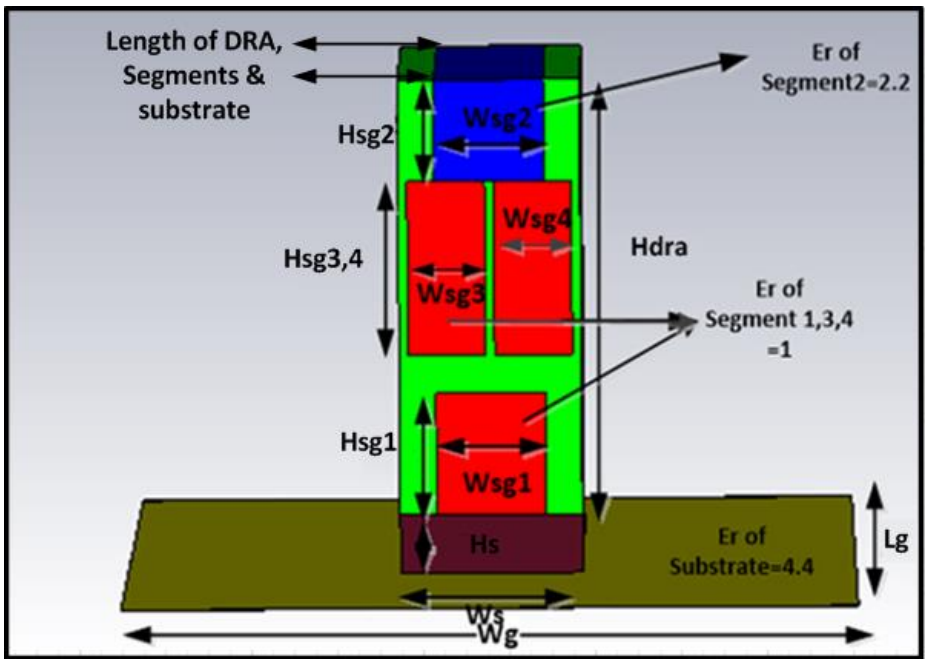

Fig. 3.1.1 Geometrical Configuration of the MSRDRA

Reported MSRDRA consists of four segments inserted into a main rectangular DRA of dimension W_s (DRA width) = 10mm, H_{dra} (DRA height) = 24mm and a length of 15mm which is common for segments (W_{sg}) and substrate (H_s). DRA is made up of Alumina with dielectric constant ($\boldsymbol{\varepsilon_r}$) of 9.4 which is placed on a substrate of material FR4 $\boldsymbol{\varepsilon_r}$=4.4 with dimensions 10 x 15 x 3.2 mm^3. Segment 2 is made up of material RT5880 of dielectric constant $\boldsymbol{\varepsilon_r}$=2.2 and dimensions of W_{sg1}= 6mm, Length = 15mm and H_{sg1}= 5.2 mm. Segment 1, 3 and 4 are of dielectric material foam with dielectric constant of 1. Dimensions of segment 1 are 6 x 15 x 6.75 mm^3 while segment 3 and 4 have same dimensions but different positions. Length of segment 3 and 4 is 15 mm with

height of 9.6mm and width of 4.25mm. $W_g = L_g = 40$mm represents ground dimensions upon which entire DRA structure is designed.

The Q factor RDRA without air cavity was determined. The Q factor of the cavity induced RDRA is given by the following equation (3.1) [13]:

$$\varepsilon_{eff} = \frac{\varepsilon_{r1}+\varepsilon_{r2}+\varepsilon_{r3}}{3} \quad (3.1)$$

Where the cavity RDRA is divided in to three segments of dielectric constants $\varepsilon_{r1}, \varepsilon_{r2}$ and ε_{r3}.

Lowering of Q-factor is achieved by varying permittivity of the RDRA by generating lower order modes in the boundaries of changing medium. Further simulated result comparisons are discussed in upcoming sections of the chapter. A graphical representation showing comparison between all stages is included in Fig. 3.1.9.

3.1.2 Results and Discussions of MSRDRA

Proposed antenna displays tremendous impedance bandwidth of 128% with a sustainable gain of 5 dB over entire bandwidth. Multi segmentation is regarded as one of the most prudent techniques to increase the bandwidth of the antenna. In the presented design, four segments are inserted one by one and their effect on bandwidth parameter is observed. This section consists of graphs and table that summarizes the exact results attained by the proposed structure.

Fig. 3.1.2(a) shows the geometry of proposed RDRA in a form of chunk when no segment is inserted. Fig. 3.1.2(b). shows S11 (Return loss) parameter of the RDRA without any segment and displays a bandwidth of 2.66 GHz with a frequency range from 5.57 GHz to 8.23 GHz with a gain of 6.82 dB.

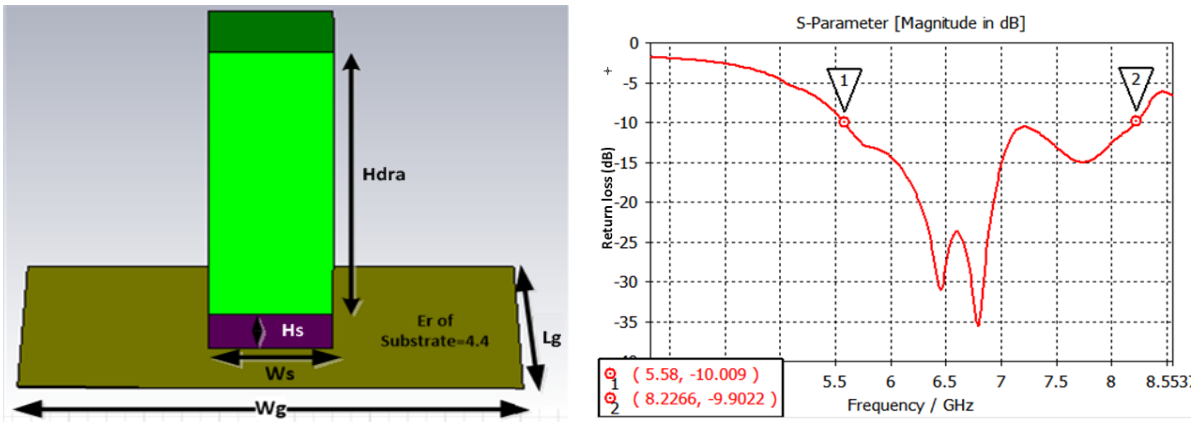

(a) (b)

Fig. 3.1.2 (a) Geometry of RDRA with No Segment (b) S11 Response of the RDRA with No Segment.

Fig. 3.1.3(a) illustrate the geometry of RDRA when one segment of dielectric material foam is inserted. This segment have dimensions of 6 x 15 x 6.75 mm^3. Fig. 3.1.3(b) represents S11 parameter of the RDRA when one segment is inserted and gives a bandwidth of 2.78 GHz with a frequency range from 7.96 GHz to 10.74 GHz and have a gain of 5.46 dB. Fig. 3.1.3 (a) indicates the geometry of RDRA when second segment is inserted. This segment is made up of material RT5880 of dielectric constant 2.2.

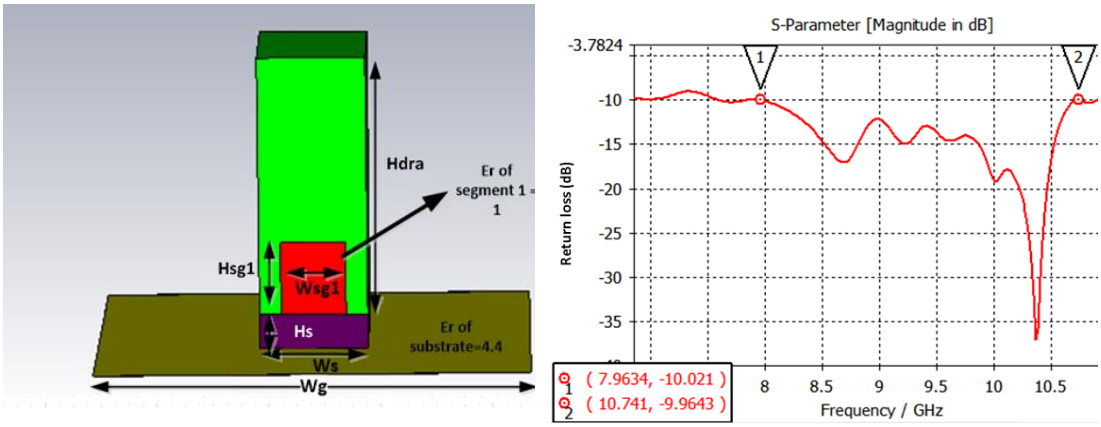

(a) (b)

Fig. 3.1.3(a) Geometry of RDRA with one segment. (b) S11 response of the RDRA with one segment.

Fig. 3.1.4 (b) displays S11 parameter of the RDRA when two segments are inserted and this insertion yields dual band antenna with frequency range of 7.02 - 11.58 GHz and 12.57 - 19.17 GHz with bandwidth of 4.4 GHz and 6.6 GHz and have a gain of 6.42 dB.

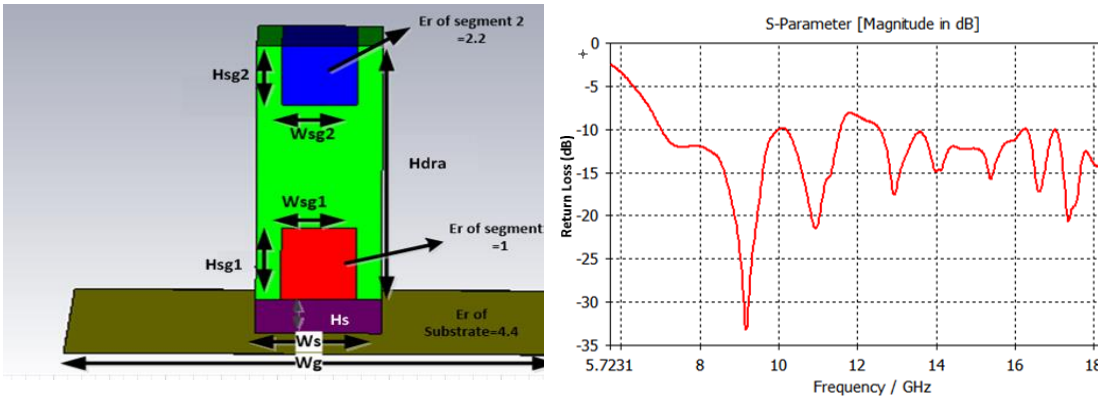

(a) (b)

Fig. 3.1.4(a) Geometry of RDRA with two segments. (b) S11 response of the RDRA with two segments.

Fig. 3.1.5(a) represents the geometry of RDRA when third segment is inserted. Segment 3 is made up of dielectric material foam. Fig. 3.1.4(b) illustrates S11 parameter of the RDRA when three segments are inserted and shows a dual band

antenna which have frequency range of 6.81 GHz - 11.87 GHz and 12.41-19.10 GHz with bandwidth of 5.06 GHz and 6.69 GHz and a gain of 5.41 dB.

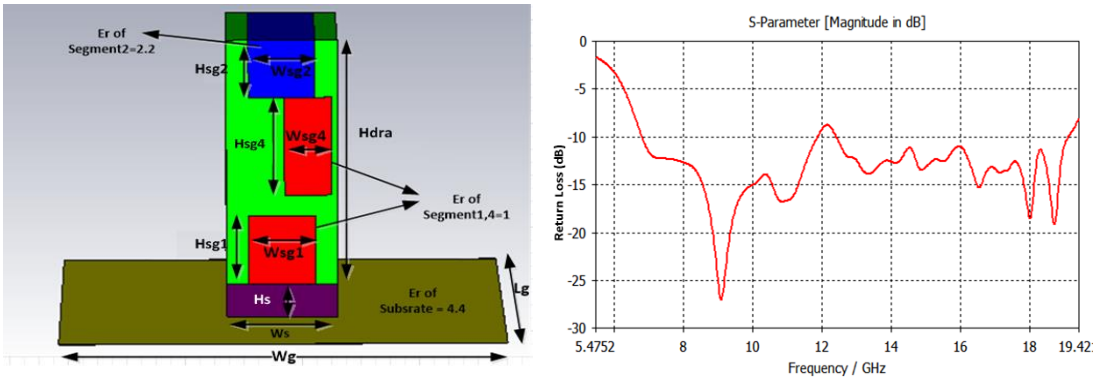

(a) (b)

Fig.3.1.5 (a) Geometry of RDRA with three segments.(b) S11 response of the RDRA with three segments.

Fig. 3.1.6(a). displays the geometry of RDRA when fourth segment of dielectric material foam is inserted. Fig. 3.1.6(b) Demonstrates a bandwidth of 11.92 GHz with a frequency range from 7.03-18.95 GHz and a gain of 5.25 dB.

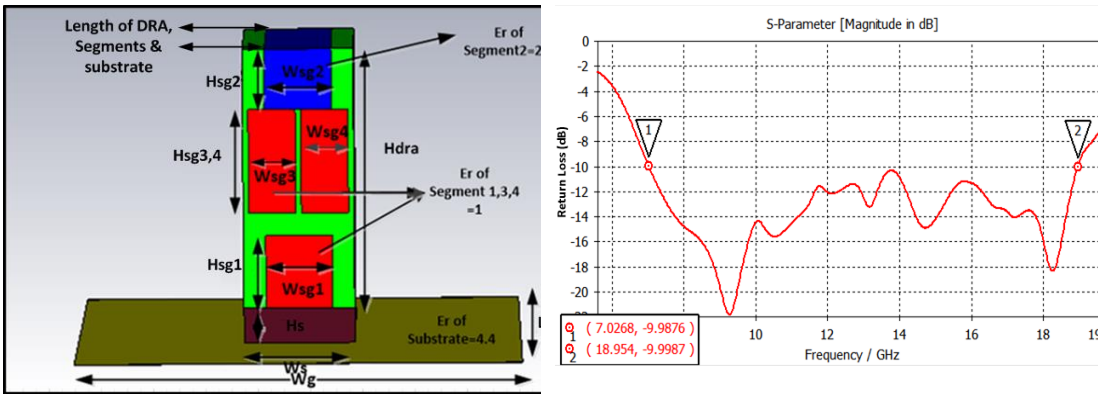

(a) (b)

Fig. 3.1.6(a) Geometry of RDRA with four segment. (b) S11 response of the RDRA with four segment.

Fig.3.1.7 (a) displays radiation efficiency of antenna. Radiation efficiency determines the amount of impedance matched in the antenna. It can be observed from the Fig. 3.1.7(a) that radiation efficiency of antenna is high in overall operating bandwidth of the antenna. An average efficiency of 94% is obtained through this structure. Fig. 3.1.7(b) shows gain vs frequency response of the antenna. Excellent stability in gain is attained in this antenna. Amalgamation of various dielectric values results in multimode resonance in antenna which in turn increases bandwidth of the antenna with a sustained value of gain of value 5.25 dB.

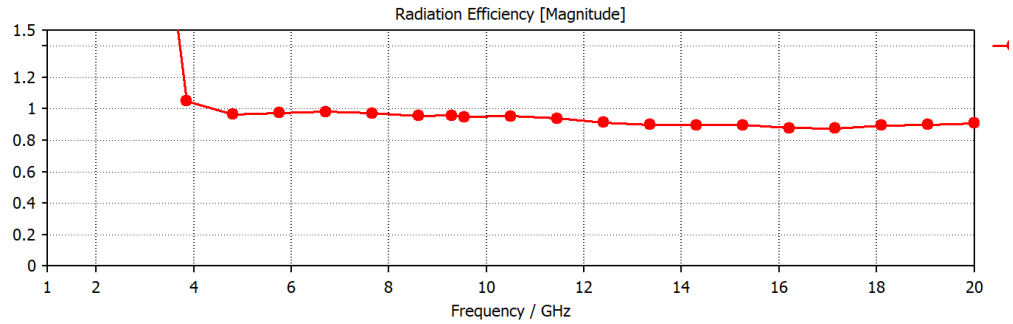

Fig 3.1.7(a) Radiation Efficiency of the antenna.

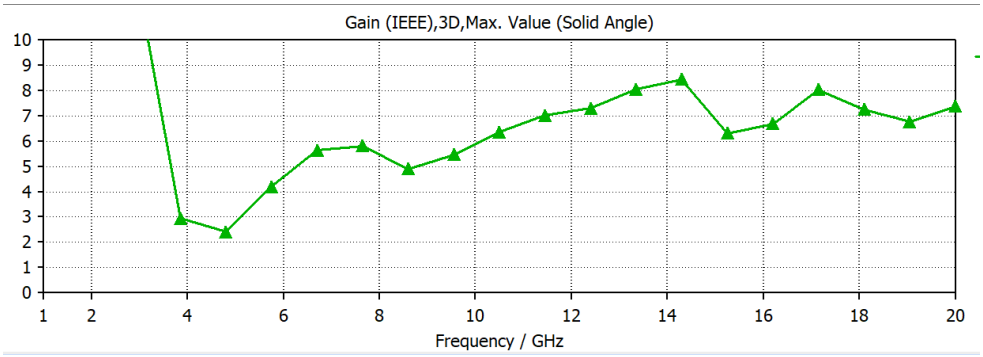

Fig 3.1.7(b) Gain v/s Frequency response of the antenna.

Fig.3.1.8 (a) represents the 3-D radiation Pattern of the antenna. This radiation pattern is sampled from the entire range at 9.29 GHz. Feeding mechanism plays an important role in deciding radiation characteristics of the antenna. Probe fed mechanism generates TE modes in the antenna .In this antenna feed structure is provided in Y-direction hence Z-direction is the direction of propagation of the wave. It can be observed from the Fig. 3.1.8(a) that the wave front of the radiated wave is in z-direction concentrating E-field in this particular direction only. Next is broadband radiation pattern of antenna of the antenna. Multiple lobes can be viewed in this radiation pattern. At higher frequencies, higher order harmonics are generated. Due to the reverberation, fringing of fields occurs and multiple lobes are generated. However, despite of getting multiple lobes Omni-directional coverage can be seen from the figure 3.1.8(b).

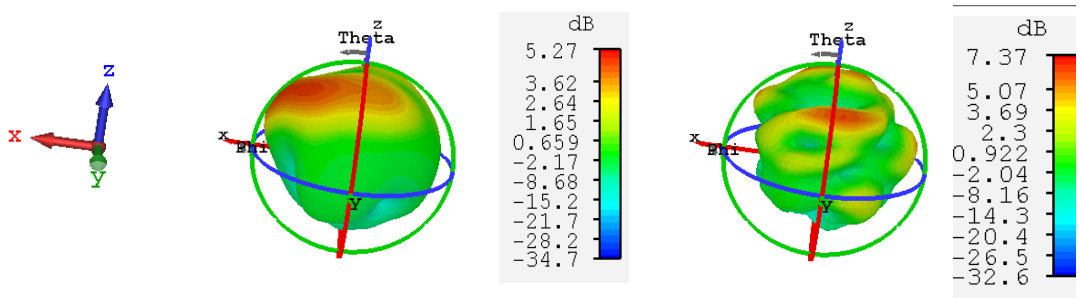

(a) (b)

Fig. 3.1.8 (a) Radiation Pattern at 9.29 GHz and (b) Broadband Radiation Pattern

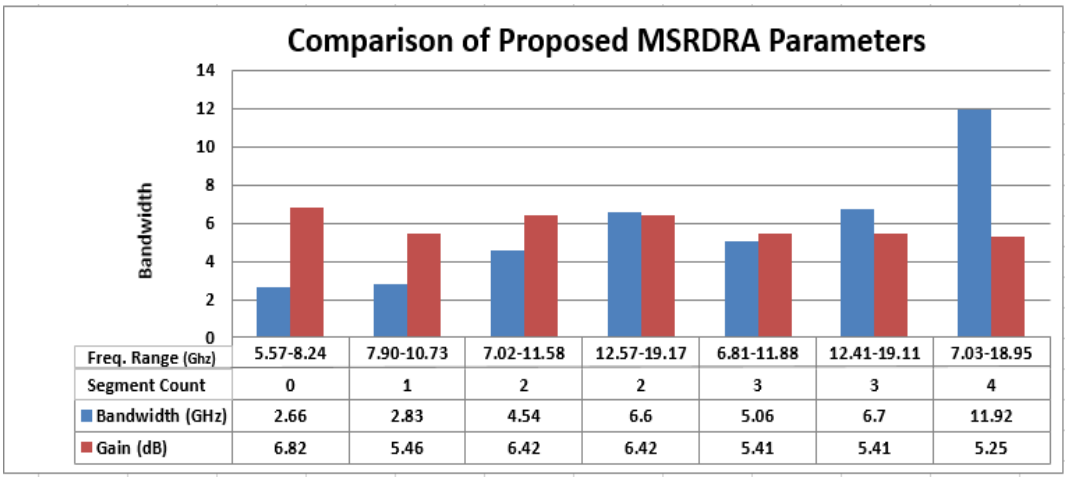

Freq. Range (Ghz)	5.57-8.24	7.90-10.73	7.02-11.58	12.57-19.17	6.81-11.88	12.41-19.11	7.03-18.95
Segment Count	0	1	2	2	3	3	4
Bandwidth (GHz)	2.66	2.83	4.54	6.6	5.06	6.7	11.92
Gain (dB)	6.82	5.46	6.42	6.42	5.41	5.41	5.25

Fig. 3.1.9 Comparison of proposed MSRDRA parameters.

3.2 BAND WIDTH ENHANCEMENT of DRA with DEFECTED GROUND STRUCTURE

3.2.1 Geometry of DRA with Defected Ground Structure

Fig 3.2.1 represents the geometrical aspects of the antenna. Presented structure is implemented with FR4 substrate $\varepsilon_r = 4.4$ with dimensions of 26 x 20 x 1.6 mm^3. Ultra Wide band in this antenna is achieved with the application of partial ground structure of dimension 11 x 20 x 0.018 mm^3. Fig. 3.2.1(a) represents Top view of antenna which shows DRA and feed implementation of structure. Fig. 3.2.1(b) represents the side view of the antenna with proposed heights of substrate and DRA. Fig. 3.2.1(c) represents the ground structure with embedded slots of the antenna.

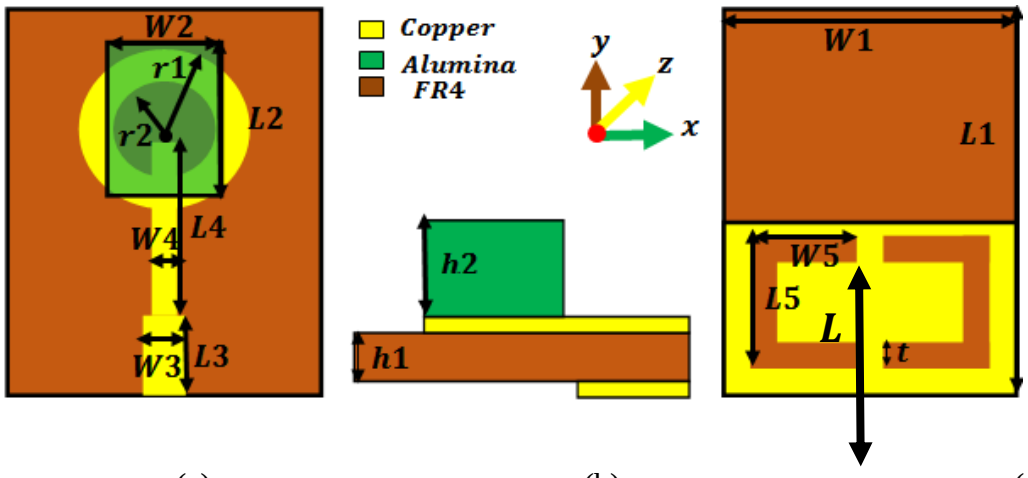

(a) (b) (c)

Fig. 3.2.1(a) Top View (b) Side view (c) Bottom view of DRA

Table 3.2.1. The dimensions of the antenna structure

(Units of dimensions is mm)

Parameter	Dimensions	Parameter	Dimensions
$\mathbf{L_1}$	26	L_5	9
$\mathbf{W_1}$	18	W_5	6.75
$\mathbf{L_2}$	9.6	h_1	1.6
$\mathbf{W_2}$	4.6	h_2	10.6
$\mathbf{L_3}$	5	r_1	4.5
$\mathbf{W_3}$	2	r_2	3.75
$\mathbf{L_4}$	7.4	t	1
$\mathbf{W_4}$	1.4	L	11

3.2.2 Results and Discussions of DRA with Defected Ground Structure

Reflection coefficient is a true measure of the total amount of power coupled by the antenna in space. A good reflection coefficient ensures the good radiation properties of any radiator. Fig. 3.2.2 (a) represents reflection coefficient parameters of the proposed antenna. Proposed structure (PS) represents hybridization of patch, feed and DRA. Patch only configuration (PO) represents dual band design of 4.5-6.3 GHz and 9-13 GHz. From the Fig. 3.2.2, it can be seen that antenna has reflection coefficient below -10 dB from a frequency range of 5-14.1 GHz

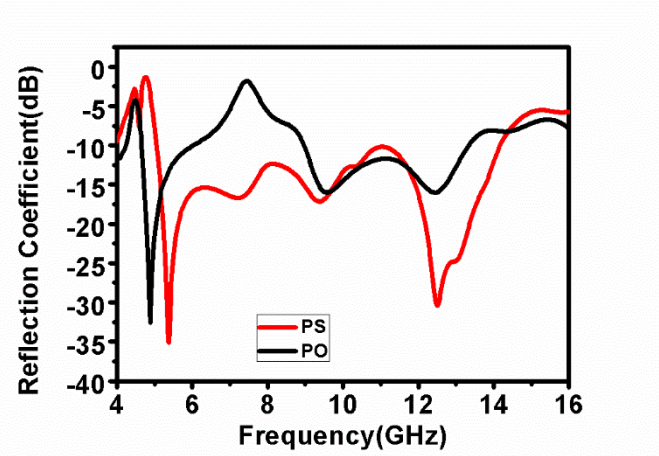

Fig. 3.2.2 Reflection coefficient of Proposed Structure (PS) and Patch Only (PO) configuration of antenna.

3.2.3 Radiation Pattern

Fig. 3.2.3 shows the radiation pattern of the antenna at 5.3 GHz, 9.3 GHz, 12.5 GHz and overall broadband radiation pattern of the antenna. It can be observed from

the Fig. 3.2.3 (a) that the proposed antenna is radiating like magnetic monopole antenna. At 9.3 GHz radiating pattern is concentrated in elevation plane, but at higher frequencies i.e. at 12.5 GHz Multiple lobes have been formed in radiation pattern of the antenna. Higher order modes at higher frequencies results in multiple lobe formation of the antenna.

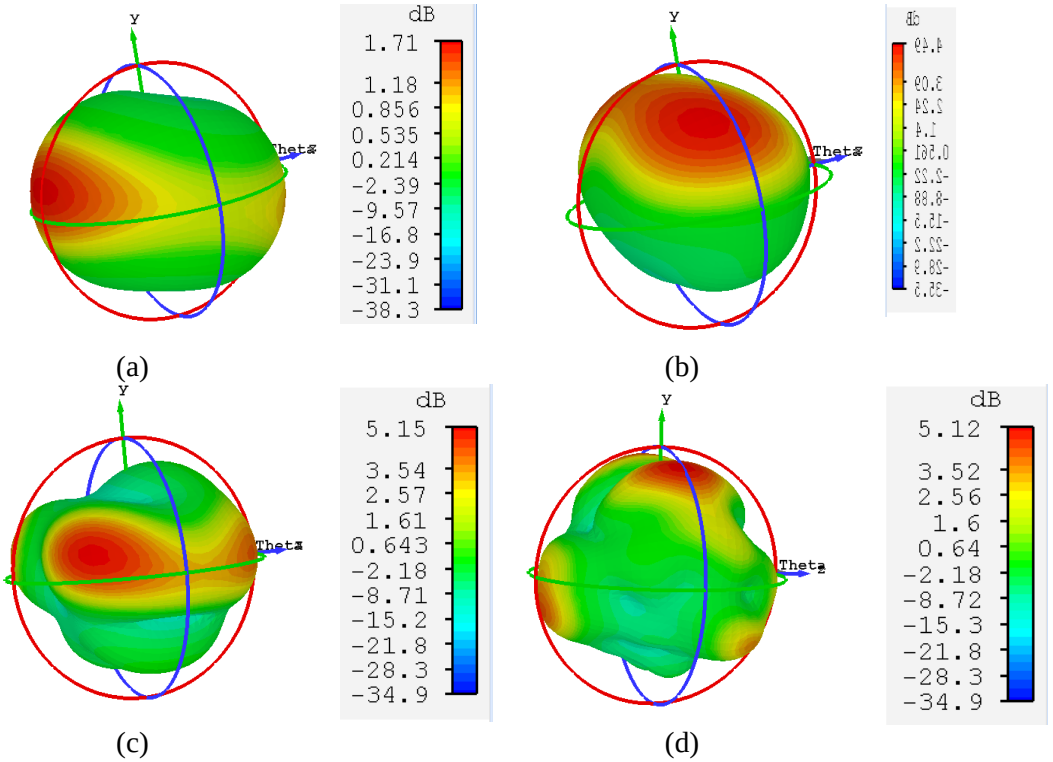

Fig. 3.2.3 (a) Radiation Pattern at 5.3 GHz and (b) 9.3 GHz (c) 12.57 GHz (d) Broadband respectively.

Fig. 3.2.4 (a) shows curve of gain plotted against frequency. It is apparent from this figure that with Patch Only (PO) configuration average as well as overall peak gain is less as compare to Proposed Hybrid Structure (PHS). Peak gain of 2.5 dB is achieved with the proposed radiator. Fig. 3.2.4 (b) represents radiation efficiency of antenna. Radiation efficiency is very important parameter which signifies the role of radiator as sensor in the entire system. Peak Radiation Efficiency of 99% is obtained with this design. It is also observed that with hybrid structure, peak efficiency as well as overall efficiency of the system is increased.

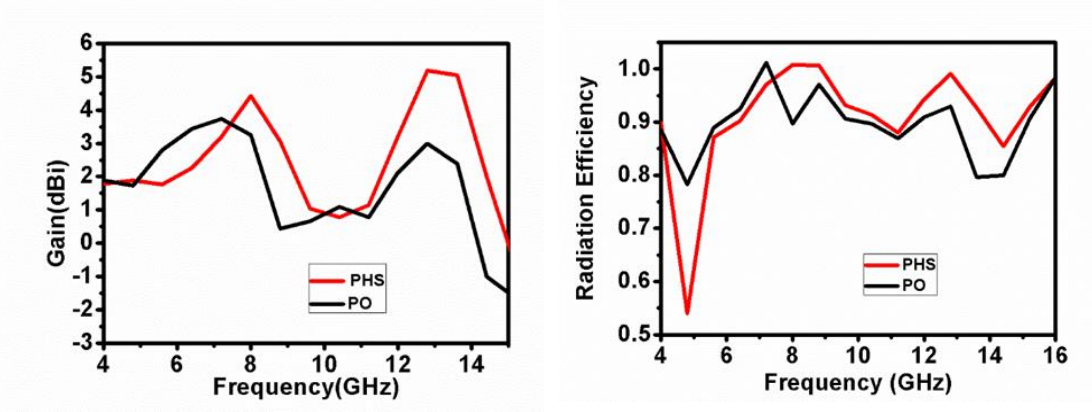

(a) (b)

Fig. 3.2.4 (a) Gain of the antenna (b) Radiation Efficiency

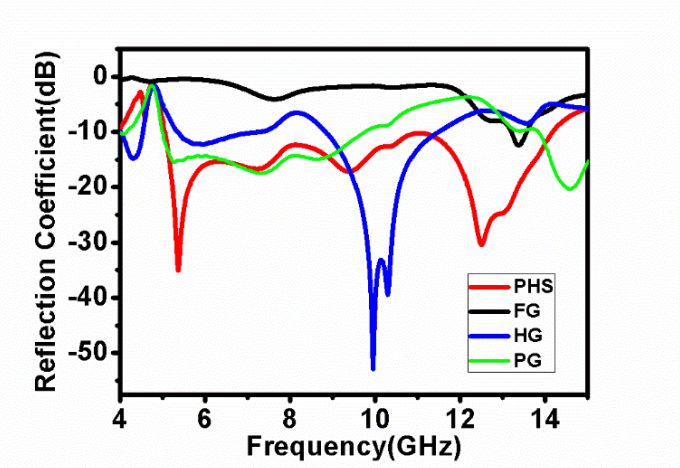

Fig 3.2.5 Variation in dimensions of Ground Plane

3.2.4 Impact of ground on bandwidth

Ground of any planar structure plays an important role in determining reflection coefficient characteristics of antenna. The proposed antenna makes use of partial ground structure. Fig. 3.2.5 represents the impact of reducing the ground dimensions. Full ground (FG), of dimension L1=23 mm is taken and it has been observed that antenna is slightly radiating for a single band of 13 GHz to 13.7 GHz. When length of antenna is reduced, antenna behaves as a tuned circuit for some specific range of frequencies depending upon structure. Hence after reducing the length of the ground to half L1=11 mm, Antenna radiates for a frequency range of 9 to 11 GHz. In Partial Ground (PG) Structure configuration where length L1= 11mm is taken , antenna resonates for a wide band of 5-10 GHz. Proposed Hybrid Structure (PHS) configuration makes use of two symmetrical C-slots in the ground plane which yields a bandwidth of 5-14.1 GHz. Table 3.2.2 shows antenna dimensions with variation in ground.

Table 3.2.2 Impact of Ground Dimensions on Band Width

Sr. No.	Configuration	Dimension of ground(mm)	Bandwidth (GHz)
1.	FG	26	13-13.7
2.	HG	13	9-11
3.	PG	11	5-10
4.	PHS (Partial Ground with slots)	11	5-14.1

3.2.5 Fabricated Results

(a) (b)

Fig. 3.2.6 (a) Fabricated Microstrip Patch (b) Ground plane of antenna without DRA

Fig.3.2.6 (a) represents fabricated ground plane of the patch antenna on FR4 substrate. Fig.3.2.6 (b) represents front annular ring shape patch with stepped feeding mechanism. Fig.3.2.7 (a) shows the Proposed Hybrid Structure (PHS) where DRA is instituted upon the patch antenna. Fig.3.2.7 (b) represents the measured Reflection Coefficient of the antenna.

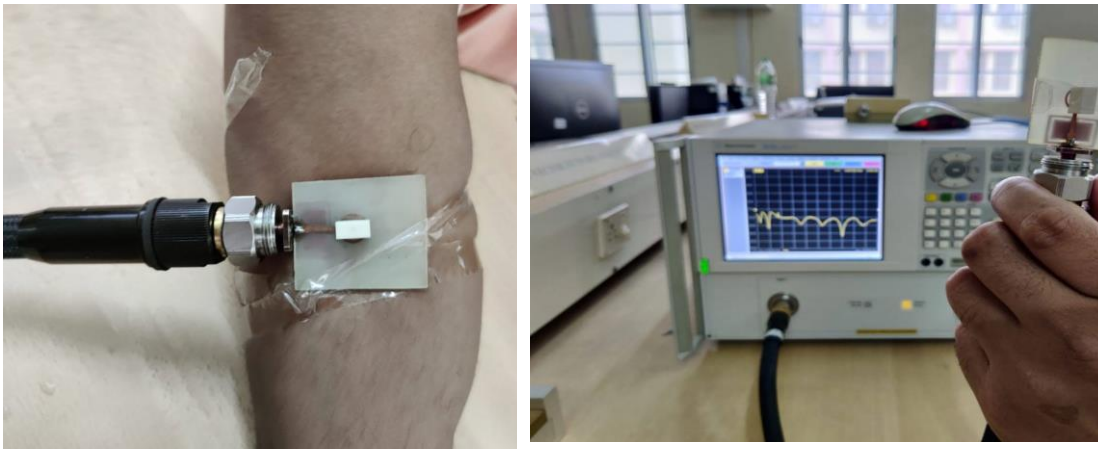

(a) (b)

Fig. 3.2.7 (a) Assembled antenna with DRA (b) Measured S11 parameter

Fig. 3.2.8 shows Comparison of Simulated and Measured (a) Reflection Coefficient (b) Gain of the antenna. It is observed that the simulated and the measured reflection coefficient responses are in close approximation with each other. However, in case of gain measurement, much lower gain value is obtained due to conductor losses.

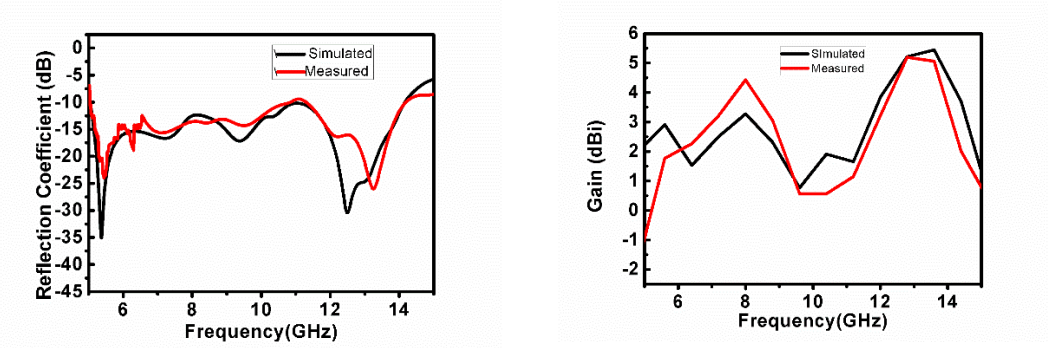

(a) **(b)**

Fig. 3.2.8 Comparitive Graph of Measured and Simulated (a) Reflection Coefficient (b) Gain

3.3 CONCLUSION

Presented multi segmented antenna is a compact and novel design which provides high gain > 5 dB and a high bandwidth of 11.92 GHz. A minimum bandwidth of 2.67 GHz is achieved when no segment is inserted, when four segments are inserted then it shows a high bandwidth of 11.92 GHz. Hence it is concluded from the design that by inserting up to four segment the bandwidth is increased and show ultra wideband properties. Availability of materials used and simple design are key features of this antenna. The presented results demonstrate that the rectangular DRA with four segments can be considered as a promising alternative for antennas applied at X and Ku band frequency operations.

A novel and unique combination of Patch and Dielectric resonator antenna has been proposed in this research work. Stepped micro-strip fed mechanism is used to improve impedance matching of antenna. Annular Ring shape patch has been an ardent candidate to enhance the bandwidth of antenna and this property is utilized in the presented article. Rectangular shape dielectric resonator antenna is designed and analyzed in conjunction with ring shape patch with defected ground structure. A compact DRA, ring shaped patch with slotted partial ground structure can be perfectly employed as a sensing node for WBAN technology along with gateway nodes. High gain of 5.1 dB along with average efficiency of 90% throughout the operating bandwidth has been obtained. Proposed structure is best suited for Off-body communication due to high bandwidth, gain, light weight and compact size.

CHAPTER 4

RECONFIGURABLE, BAND NOTCH AND TUNABLE ANTENNAS

INTRODUCTION

Last two decades have witnessesd exponential increase in demand of Reconfigurable and band notch antennas. Researchers across the globe have proposed numerous antennas such as planar microstrip patch antennas, helical antennas, loop anteenas, and dish antennas, to cater high bandwidth and constant gain requirements.

Among all available radiators, Dielectric Resonator Antenna (DRA) is evolving as a prolific, ultra wideband, low profile and efficient radiator. DRA is a lossless radiator which provides various merits like wideband nature, compactness in size, light weight offering high temperature stability, low cost and ease of fabrication [1]. DRA displays high radiating efficiencies due to absence of any kind of conductors in the radiator. Moreover, these dielectric radiators are highly compatible with every kind of transmission lines such as coaxial probe, micro-strip line, micro-strip slot, coupled or aperture coupled, coplanar waveguide and dielectric image guide method [114,133].

Multi band systems are increasing popularity due to the requirements of the present scenario of wireless communication systems. Reconfigurable aerials are those structures that can alter its resonant frequency and other radiation characteristics such as polarization and radiation patterns [120-142]. Various methods are deviced to achieve such capacity in any system can be divided into mainly two parts:

i. Switch based techniques
ii. Non-switch based techniques.

In Switch Based Techniques, electrical configurability is most popular technique. This technique makes use of PIN diode & Varactor diode as a switching element [119]. All these devices use techniques suffer from power consumption and biasing circuit problems.

Non-switch based techniques include Optical, Liquid Dielectric (Ferrite Base, Ferroelectric Base), and Liquid Assisted Dielectric. Performance and Bulky structure of Ferroelectric material make it difficult to handle [125-126]. Optical system include photonic band gap semiconductor including graphene. The various advantages offered by Liquid Dielectric Systems are both Chemical and Physical Re-configurability. These systems can take any size due to conformability and their quantity can be varied by

varying size of micro cavities. The another way of achieving re-configurability is Chemical Composition of Water. Higher permittivity of DRA yields high bandwidth. This permittivity can be changed by adding salt to the water. Various salts such as NaCl and KCl can be added to increase permittivity and conductivity of the antenna. In this research work. This thesis proposed Liquid Assisted Antenna is proposed which is known as Magneto Hydro Dynamic Antenna.

4.1 Rectangular Moat shaped MHD Antenna

A rotating fluid frame Antenna consisting of conducting fluid is taken which is radiating under controlled electric field and magnetic field conditions. In this conducting fluid, water molecules oscillates due to impact ionization inside the fluid which further contribute to radiate energy. Resonant frequency depends on volume, type of fluid, shape of tube, chemical properties of fluid used, DC magnetic bias and electric bias conditions Current in the fluid has been derived from probe feeding network excited at the Centre of the cube$\left(\frac{a}{2},\frac{a}{2},0\right)$. Power flux has also been computed in the far field region.

The modes of MHD antenna can be characterized as fields pattern set up due to excitation inside resonator tube. An oscillating rectangular fluid frame consisting of conducting fluid has been radiating under controlled electric field and magnetic field. Fluid molecules oscillate due to impact ionization inside the fluid and contribute to radiate energy. Resonant frequency depends on velocity of the fluid, volume, type of fluid, shape of tube, chemical properties of fluid used, magnetic bias and electric bias conditions. Hence, it has resulted into large design space for antenna reconfigurability mechanisms i.e. frequency reconfigurability, polarization reconfigurability and pattern reconfigurability. Based on perturbation techniques, current in the fluid can be computed by fixing probe position at any arbitrary position. Maxwell's Equations, Navier Stokes equations and Equations of Mass Conservation for the conducting fluid with EM field have been analytically derived to calculate fields of antenna. These are expressed as partial differential equations for the electric and magnetic fields. These equations are first order in time which helps us to predict velocity field of the fluid in the near field region and electromagnetic field in the far field region.

4.1.1 Mathematical modelling of RDRA structure Liquid Assisted Structure

Before starting mathematical modelling of MHD antenna, few assumption are to be made.

ξ = Variable length of probe for RF excitation.

$\nabla \times \mathbf{B} = \mu J + \mu\varepsilon\frac{\partial \boldsymbol{E}}{\partial \boldsymbol{t}}$ (Maxwell's equation) and this is combined with $\nabla \times \mathbf{E} = -\frac{\partial \boldsymbol{B}}{\partial \boldsymbol{t}}$ and the MHD equations are simultaneously solved for (**v, E, B).**

Here J = Current density, v = Fluid Velocity inside polypropelene tube, E= Electric field intensity and B= magnetic flux density.

Current and power radiated has been computed in the rectangular fluid frame and far field. Assumptions based on probe position under perfect match. The coordinates has been assumed at the center of the cube i.e. $\left(\frac{a}{2}, \frac{a}{2}, 0\right)$. In order to calculate electric and magnetic field equations, first magnetic vector potential ($\mathbf{A_z}$) has to be calculated. The magnetic vector potential ($\mathbf{A_z}$) can be written as :

$$\mathbf{A_z\ (\omega, x, y, z)} = \frac{\mu Io}{4\pi}\int_0^d \frac{e^{-jk|r - a/2\,\hat{x} - b/2\,\hat{y} - \xi\,\hat{z}|}}{|r - a/2\,\hat{x} - b/2\,\hat{y} - \xi\,\hat{z}|}\, d\xi \qquad (4.1)$$

Let $\mathbf{C} = \frac{\mu}{4\pi}$, k =ω/c and ξ = variable probe length inside the fluid

$$\mathbf{A_z} = I_o \int_0^d \frac{\exp\{-j\,k\,((x - a/2)^2 + (y - a/2)^2 + (z - \xi)^2)}{((x - a/2)^2 + (y - a/2)^2 + (z - \xi)^2)^{1/2}}\} d\xi \qquad (4.2)$$

$$\mathbf{A_z\ (w, x, y, z)} = 2CI_o \exp(-jkr_o) \exp\frac{\left(\frac{jkd}{2}\cos\theta_o\right)\ \sin\left(\frac{kd\cos\theta_o}{2}\right)}{kr_o\cos\theta_o} \qquad (4.3)$$

Here, (r, θ, Φ) are spherical polar coordinates

With help of calculated magnetic vector potential, Electric field vector in time domain can be given as:

E (t, x, y, z)

$$= \frac{w}{r_o^3}\,|P(\theta_o)|\,\sin\left(wt - kr_o + \Psi(\theta_o)\right)\left((x - a/2)^2 + (y - a/2)^2\right) + \left(x - \frac{a}{2}\right)) z\hat{x} + \{-\frac{w((y - a/2)\ z)}{r_o^3}\} \qquad (4.4)$$

B (t, x, y, z)

$$= -\frac{k\left(X - \frac{a}{2}\right)}{r_o^2}\,|P(\theta_o)|\,\sin\left(wt - kr_o + \Psi(\theta_o)\right)\hat{y} + \frac{k\left(y - \frac{a}{2}\right)}{r_o^2}\,|P(\theta_o)|\,\sin\left(wt - kr_o + \Psi(\theta_o)\right)\hat{x} \qquad (4.5)$$

where, $|P(\theta_o)| = \frac{2CI_o}{k\cos\theta_o}\ Sin\ \left(\frac{kd\ Cos\theta_o}{2}\right)$

and $\Psi(\theta_o) = \frac{kd\cos\theta_o}{2}$

Eq. (4.1-4.5) have provided the idea to device an algorithm for defining resonant modes, radiation patterns current distribution into the fluid frame.

4.1.2 Software Based Design of Antenna

Fig. 4.1.1 shows geometry of DRA and Square Annular Ring MHD.

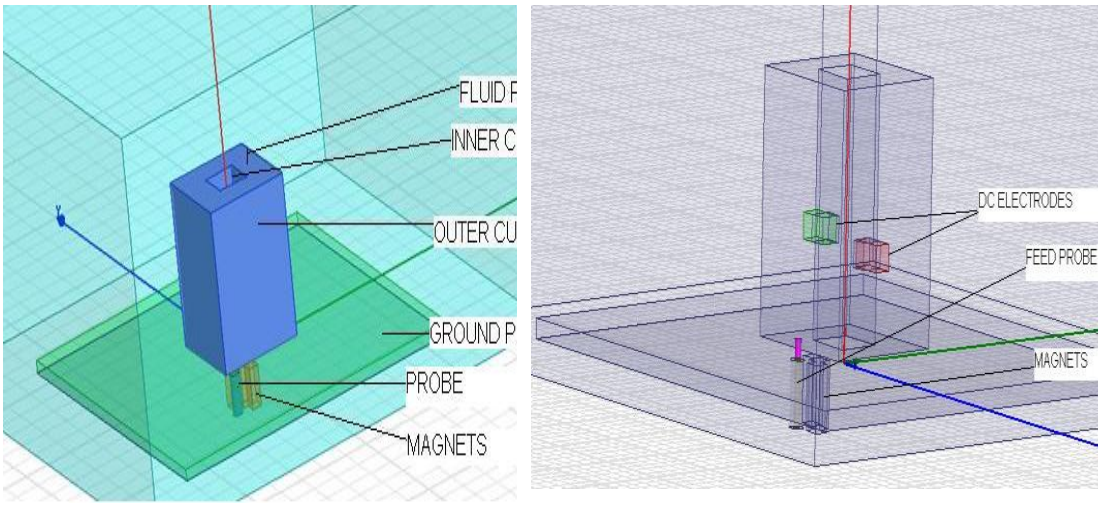

(a) (b)

Fig. 4.1.1 (a) Geometrical structure of DRA (b) Geometry of Square Annular Ring MHD shows Magnetic and Electric bias.

Table 4.1.1 Dimensions of Rectangular MHD Antenna

S.No.	Object Name	Size (dx, dy, dz)mm	Centre position
1.	Ground Plane	60x60	-30,-30,0
2.	Substrate(permittivity.=4.4, FR 4 epoxy)	60x60x1.52	-30,-30,0
3.	Central DRA Box9 (material 2 permittivity = 25)	16.4x16.4x20	-8.2,-8.2,1.52
4.	Cavity box 10	6x6x20	-3,-3,1.52
5.	Box 6 ferrite	2x2x-5	-2,-6.2,0
6.	Box 7 ferrite	2x2x-5	-4.5,-2.5,0
7.	Box 8 ferrite	2x2x-5`	-2.8,-4,0
8.	Coax	R=1, h=-5 vacuum	-4.5,-4.5,0
9.	Feed probe	R=.44 h=-.5 pec	-4.5,-4.5,0
10.	Feed	R=.44, h=1.52 pec	-4.5,-4.5,0
11.	Magnetic Bias	1100 Tesla	

Table 4.1.1 shows the dimensions of the antenna designed and simulated. The maximum dimensions of antenna are 60 x 60 x 20 mm^3. Probe fed technique is being utilized along with ferrite material to provide magnetic bias.

4.1.3 Results and Discussions for MHD Antenna

From the above proposed parameters used for simulation, return loss of -18dB at 22.5 GHz is achieved as shown in Fig. 4.1.2. Here the simple water is taken as fluid element. Permittivity of plane water not only depends upon ambient temperature but also on the polar characteristics. In our case, Non-Polarized water is used which have a permittivity of range 75- 80.10 providing stable temperature. Here, a wide bandwidth of 18.5-34 GHz is obtained as shown in Fig. 4.1.2.

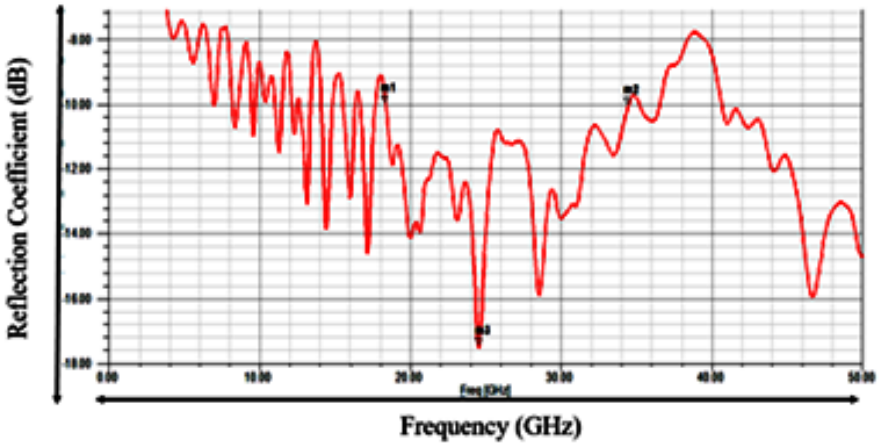

Fig. 4.1.2 Optimized Return Loss results -18dB at 22.5GHz when simple water is taken as fluid element.

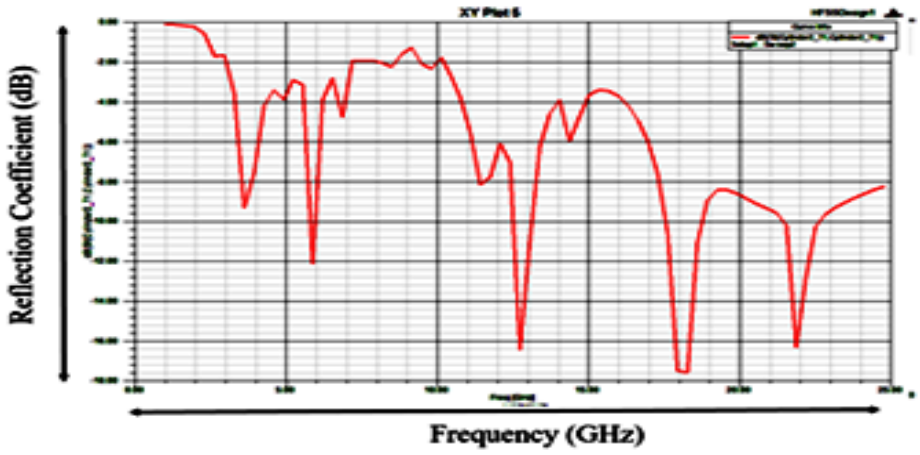

Fig. 4.1.3 Return Loss results for various frequency bands when NaCl is taken as fluid element.

On the other hand, when this plane water is replaced by saline water, permittivity of water gets fix at 80 at room temperature and it consequence in varying chemical properties of water. After adding salt, UWB antenna changed to multi band antenna. . When fluid is taken as NaCl, the multiband frequencies obtained are 6, 11.85,

18 and 22 GHz. These resonating frequencies can be varied if concentration and properties of salt will be changed.

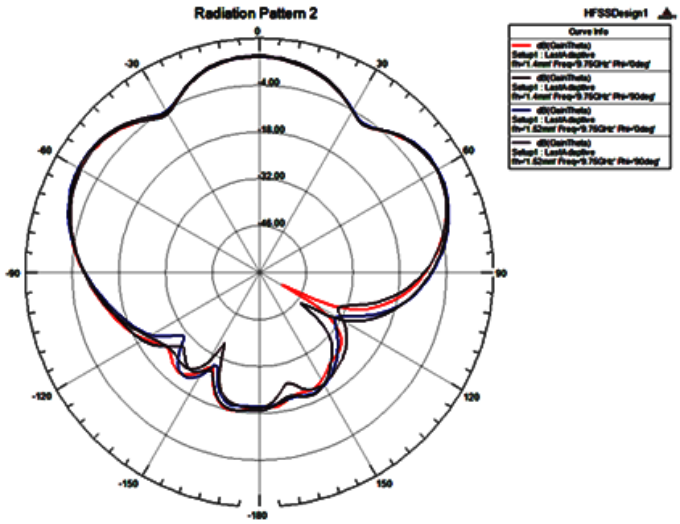

Fig. 4.1.4 Obtained radiation pattern of X-Y plane of antenna

Fig. 4.1.4 represents the radiation pattern of the antenna at 9.75 GHz. Gain of the antenna at this frequency for different angles is shown in Fig.4.1.4.

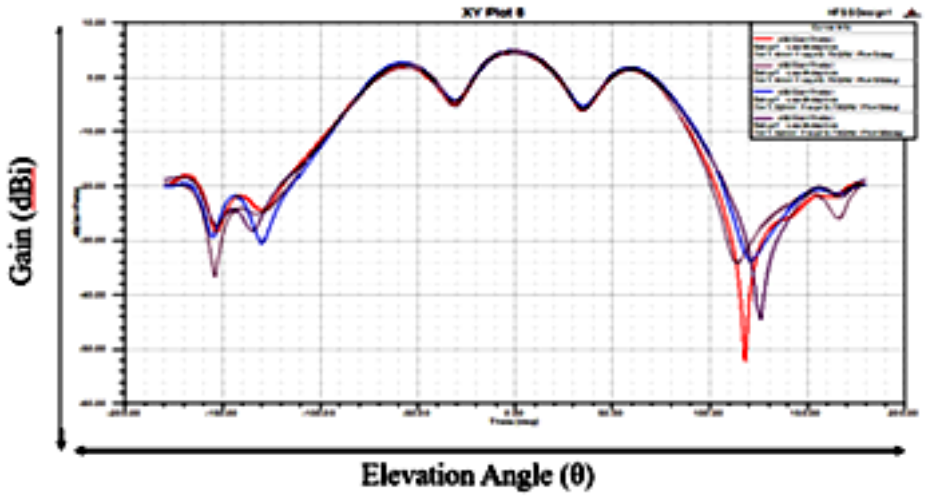

Fig. 4.1.5 Gain obtained by the antenna at different Elevation Angle

4.1.4. Parametric Analysis of Antenna

Numerous iterations have been performed on HFSS by simulating various sweeps. Probe insertion inside the fluid decides the impedance of antenna, which subsequently decides the multiband characteristic of the antenna. The resonant frequency and generated modes created are changed with the insertion of the probe

inside the antenna. Table 4.1.2 given below depicts the immersion of probe and its impact on frequency.

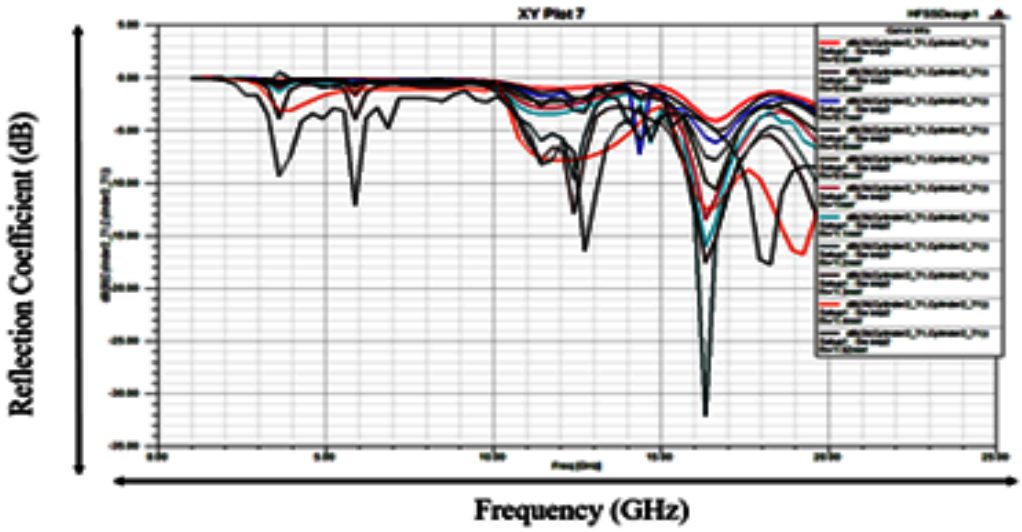

Fig. 4.1.6 Return Loss Graph for frequencies when different probe lengths are taken

Table 4.1.2 Parametric Variation of Probe Inside Fluid

Sr. No.	Insertion of probe inside fluid	Resonating frequency
1.	0.9	16.75
2.	1	16.35
3.	1.1	16-17
4.	1.2	16-17
5.	1.3	12.75-13.75,16-17
6.	1.4	15.75-17.1
7.	1.52	6,12.25-13,16-17

Fig. 4.1.5.1 shows return loss when different probe lengths are taken. Liquid Assisted Antennas have created a space in reconfigurable antennas due to their conformal shapes and physical as well as chemical properties of fluid. The proposed MHD Square Annular Rings antenna offers multiband, multiple resonant frequencies.

4.2 BAND NOTCH CREATION with DRA

Multi-mode and Multi band techniques are rejuvenating the concept of wireless communication and its usage. FCC approved unlicensed band from 3.1-10.6 GHz and also a few narrow bands to be used as free bands [143]. This free unlicensed band enables intruder to demolish network security. To avoid this interference antenna must possess band rejection capabilities. A variety of designs either by creating slots or by implementing hybridization have been proposed in literature to accommodate the need

of band notch creation [146-152]. This section of the chapter describes a novel method with high radiation efficiency to achieve band notch**.**

Many techniques have been devised to suppress unwanted signal interference in WLAN and Wi-Fi and ITU bands of UWB system provided by FCC in the frequency range 3-10 GHz. Insertion of stubs and parasitic strips [142] and slots [146] with altered feed mechanism is serving the purpose. In this work, a detail investigation on Fork shape feed, low profile DRA is carried out. A compact, miniaturized, antenna is proposed which not only solve the space constraint of the UWB systems but also can be fitted into any hand held device for 4.2-16.6 GHz range. DGS technique of bandwidth enhancement is applied in the design. Partial ground structure with a slot in center and use of conducting strip not only increases the bandwidth but also increases gain of the antenna. Incorporation of the asymmetric ring in DRA reduces the quality factor of DRA, which in turn improve cross and co polarization of the design.

4.2.1 Antenna Geometry and Design

The geometric configuration of a ARDRA (Asymmetric Rectangular Dielectric Resonator Antenna) is shown in Fig. 4.2.1 A compact RDRA is designed with a ground plane of dimension 10 x 24 mm^2 and a substrate material of FR4 epoxy, permittivity of 4.4 with dimensions of 20 x 24 x 1.6 mm^3. Rectangular DRA is made of TMM13i with permittivity of 12.8. Feeding mechanism used here is microstrip plus conjunction with fork shape feed coupling method.

In this design, A rectangular slotted DRA is chosen along with defected ground structure base. Slots and strips are invariably used to provide impedance matching of the antenna to free space. In this particular antenna, partial ground structure is taken and is slotted to enhance the bandwidth of structure. A conducting strip is inserted in the slot in order to get impedance matching. Slots provide capacitive effect on the impedance of the structure. Insertion of strip provides inductive reactance which cumulatively make tank circuit in cohesion with entire structure. Frequency correspond to a slot etched, is written as:

$$f_n = \frac{c}{2S_n\sqrt{\varepsilon_r+1/2}} \tag{4.7}$$

Where f_n is the notch frequency, c is the speed of light and ε_r is the relative permittivity of the substrate. The effective length S_n for notches n from 1 to 4 are made nearly equal to half of the guided wavelength at the notched frequency of the band are calculated as

$$S_n = (M_n+\frac{G}{2})+2L_n\text{-}G \quad (4.8)$$

where L_n is the slot's vertical length, M_n is the biggest dimension of the part being cut and G is the width of the etched slot.

Fig. 4.2.1 (c) shows the feed section of the DRA. This design is basically a combination of trishool shaped Patch and Slotted DRA. This combination makes a perfectly compact and highly efficient antenna for UWB applications. This antenna provides band notch at entire WLAN band ranging from 5.2-5.8 GHz.

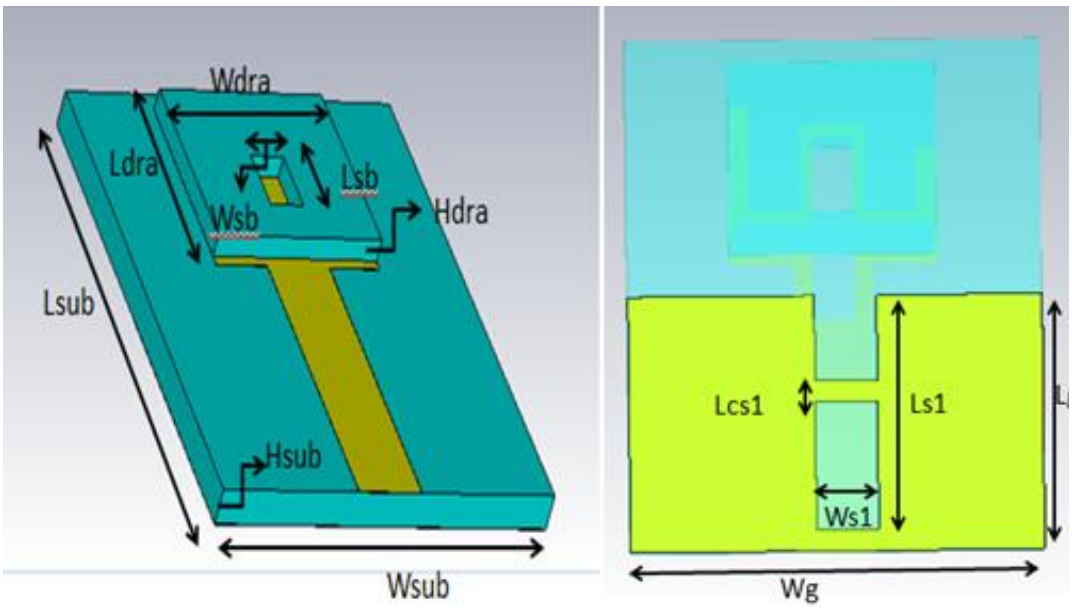

(a) (b)

Fig. 4.2.1 (a) Top View (b) Bottom View of the antenna

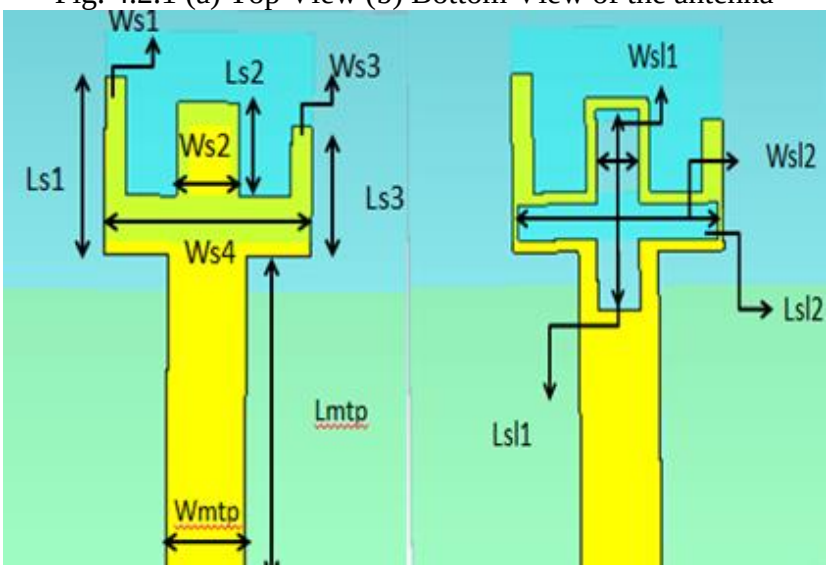

(c) (d)

Fig. 4.2.1(c) Without slot feed structure (d) with slot feed structure

Table 4.2.1 Dimension table of the DRA

S.no.	Antenna Part	Dimensions(mm)	Material used
1.	Substrate	W_{sub} x L_{sub} x H_{sub} = 20x24x1.6	FR4(εr =4.4)
2.	Fork shape feed	W_{s1} x L_{s1} =1x7.5	Copper
		W_{s2} x L_{s2} =1x5.5	
		W_{s3} x L_{s3} =3x4	
		W_{s4} =1.5	
3.	Ground	W_g x L_g =20x10	
		W_{s1} x L_{s1} =3.5x11	
		L_{cs1}=1	
4.	DRA	W_{dra} x L_{dra} xH_{dra} =10x9x1	TMM13 i(εr =12.8)
		W_{sb} x L_{sb} =2x3	
5.	Slots in fork	W_{sl1} x L_{sl1} = 2x8.5	
		W_{sl2} x L_{sl2} = 1.5x9.5	

Table 4.2.1 depicts the dimensional table of the concerned DRA. This antenna is simulated on both the software to get the validity of the design from CST and HFSS Software.

4.2.2. Results And Discussion for Band Notch DRA

In this design, a slotted DRA is loaded onto a wide band patch. UWB frequency response is obtained with the amalgamation of the various modes excited via Patch and DRA combination. DRA is slotted to improve the radiation pattern of the antenna. Fig 4.2.1(c) shows with and without slotted patch responsible for creating notch in the entire operating bandwidth.

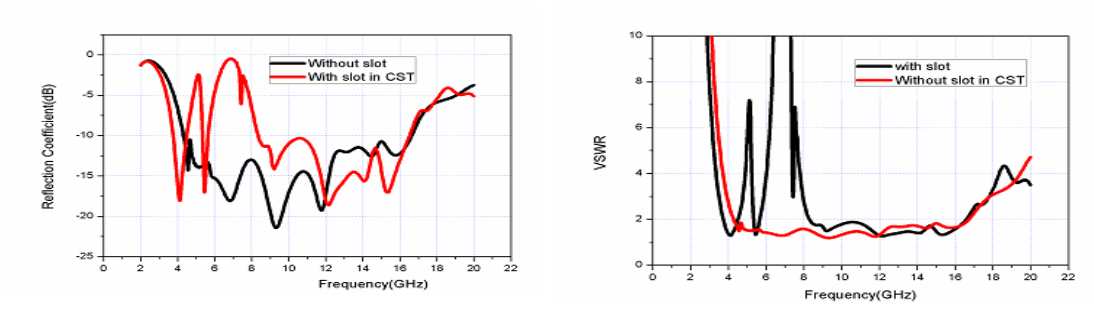

(a) (b)

Fig.4.2.2 (a) S11 with and without Slot in CST (b) VSWR with and without slot in CST.

Fig. 4.2.2(a) represents reflection coefficient of the Antenna with and without slot. It can be easily observed from the above that without slot in feed mechanism antenna radiates from 4.2 -16.6 GHz. Application of "+"shape slot in feed yields exact band notch at 5.2-5.8 GHz, which excludes WLAN bad from the entire bandwidth. Fig. 4.2.3 (b) represents Voltage Standing Wave comparison of the structure with and without slot.

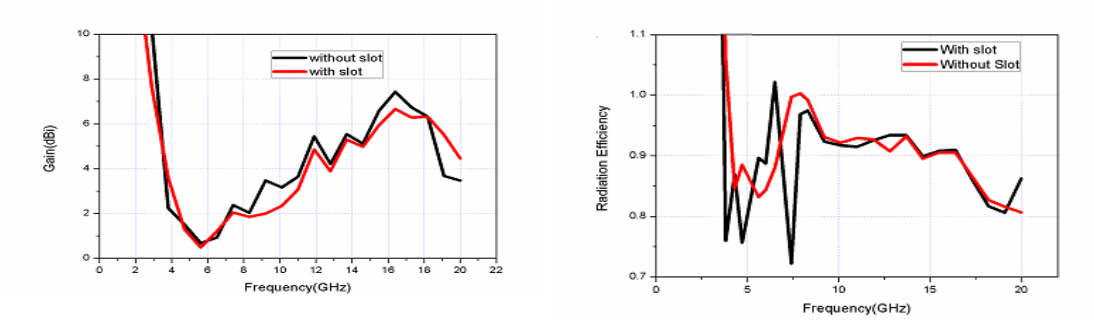

(a) (b)

Fig.4.2.3 (a) Gain Drop in DRA with and without Slot (b) Depicts Drop in Efficiency at Band Rejection Frequencies

Fig. 4.2.3 represents Gain and Radiation Efficiency comparison of the antenna. In Fig 4.2.3 (a) gain is dropped with slot due to energy losses occurred in tank circuit formed due to slots. This is the important characteristic of band notch antennas. Creation of slot creates a tank circuit for a particular frequency. This tank circuit store that energy inside it rather than radiating it. It has been observed that there is a declination in the efficiency due to creation of notches.

Radiation pattern is the primitive property of antenna which decides the future usage of antenna. Depending upon the radiation pattern, antenna is categorized as monopole and dipole antenna. Presented antenna has broadband monopole radiation

patterns in both azimuthal and elevation plane. Fig. 4.2.4 shows the E-field and H-field at 4.5 GHZ and 7.5 GHz. Radiation pattern is plotted for $0° \leq \theta \leq 360°$ in $\phi = 0° \; and \; 90°$ plane.

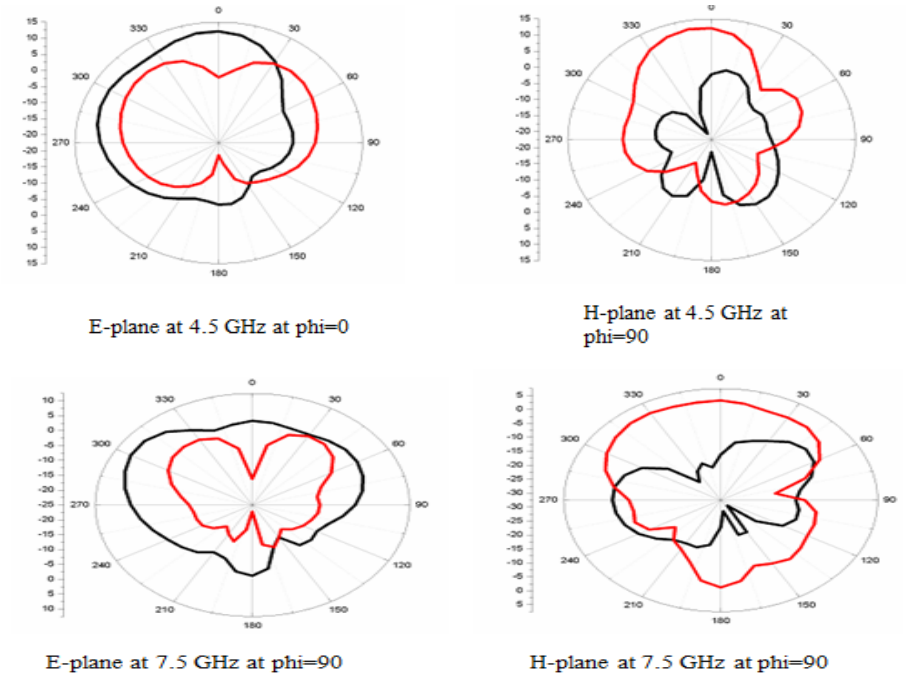

Fig. 4.2.4 (a) and (b) Co-polarized and Cross Polarized Simulated Radiation Patterns in $\phi = 0^o$ and $\phi = 90^o$ Planes at Operating Frequency 4.5 and 7.5 GHz of the Band Notch DRA.

4.3 TUNABLE ANTENNA WITH GRAPHENE

THz frequency band is being investigated due to its ability of providing the wide bandwidth and higher data transfer rate. This is the frequency spectrum being investigated for the biomedical applications. Researchers are implementing different devices for realizing the THz communication systems like modulator, filter, power divider and antennas. The realization of wireless communication is not possible without an antenna. Numerous antennas have been developed for THz applications. Plasmonic antennas have the potential of confinement of the non-local electromagnetic wave to localized energy. THz metallic antennas have a variety of applications such as sensitive bio-sensing and fluorescence analysis, plasmon enhanced spectroscopy and sensitive molecular detection, infrared photo-detection, nano-network biosensors and rectennas. Various properties including quantum efficiency of a nano-patch antenna with four different geometries is explained in for optical plasmonic enhancement of light emission. Noble metals can be looked upon as the best accessible plasmonic material.

Currently, the mian development of THz and optical antennas is based on the metallic compounds. The resarchers are still searching the techniques of implementing the plasmonic antennas for THz applications. At THz frequncy spectrum, the antennas are being developed with the defferent fearures like wide-bandwidth, reconfigurable radiation pattern, multi-band response and multi-input-muti-output characteristics. The ultra-wideband (UWB) antennas are being utilized in high data transfer communication systems, radar systems and electromagnetic interference sensor at the microwave frequencies. Very few antennas have been reported with UWB response covering the THz frequency spectrum. A GaAS and Metal based wideband antenna was implemented for operating at THz frequency spectrum [185-208]. A metallic antenna with radiating elliptical metallic patch is implemented for covering the bandwidth around 1-7 THz. For obtaining the Ultra Wide Band response in THZ spectrum,there is still scope for further investigations.

The reconfigurability of antenna response remains another challenge at THz frequency. A number of antennas have been implemented with the reconfigurable characteristics at THz frequency utilizing the graphene material in the main radiator. However, the practical implementation of these antennas is still like tusker's teeth. Conversely, utilizing the metals in the implementation of nanoscale antennas is still reliable. Implementing a UWB antenna does not need reconfigurability in frequency response. Hence, utilization of metals in the implementation of UWB antenna for THz frequency is justifiable. However, the conductivity of metals is reduced at THz frequency. The performance of metallic antennas can be enhanced by hybridizing with fluorophores to increase emission and absorption rate. Hybridization of silicon and gold nano particles enhances the near-field intensity and scattering. In order to obtain the reconfigurability, the metallic structures are combined with the 2D material like graphene. Metallic nano-structures combined with graphene provide a mean of electrically tunable characteristic. A reconfigurable graphene loaded metallic patch was reported to get modulation intensity of more than 30% and bandwidth augmentation of 8% [209-214].

Moreover, filters play an important role in the wideband communication system. Restricting a particular set of frequency and allowing other becomes important for avoiding the interference. However, the utilization of filters in the communication systems increases structural complexities and cost. These structural complexities are overcome by the implementation of antennas with band Notch characteristics. The

implementation of UWB antennas with tunable notched frequency reduces the system size as well as the cost. Tunability in the band-notch frequency can be done by changing the physical parameters of antenna in the microwave devices [215-217]]. But, it is unrealizable to change the physical parameters of antenna at the nano-scale sized dimensions. Thus, the literature reveals several issues (1) implementation of nano-antenna with UWB response (2) obtaining the band-notch characteristics and (3) tunability of the notched frequency band.

In this research work, a nano-antenna is designed for operating at THz frequency spectrum with UWB response. The antenna dimensions are selected to operate with the large number of modes having resonant frequency close to each other. A simple monopole nano-antenna with rectangular patch and half-ground structure can provide the UWB response. The impedance bandwidth of antenna is further improved by utilizing the defective ground structure (DGS). DGS is well known technique for the enhancement of impedance bandwidth of antennas at microwave frequencies. After implementing the UWB antenna, two graphene nano-ribbons are placed at the top of metallic patch for obtaining the band-notch characteristics. Depending upon the size and location of the applied graphene nano-ribbons, UWB response of antenna can be set with single/dual/triple notched band. The main feature of utilizing the graphene based nano-ribbons is electrical tunability by applying an external electrostatic DC gate voltage. The tunability of surface conductivity of graphene nano-ribbons provides the tunability in the notched frequency band keeping the operating frequency range of antenna unchanged. The tuning of notched frequency band by keeping the operating frequency band of the metallic antenna unchanged makes the problem more interesting. The proposed research work shows the novel utilization of graphene nano-ribbons for fortifying the advancements of wireless communication systems. The antenna structure is numerically analyzed using full wave simulator CST microwave studio and its electrical equivalent circuit is drawn using the circuit theory approach [206]. The antenna structure is further designed by considering all the practical parameters in manner that it could be fabricated in the near future.

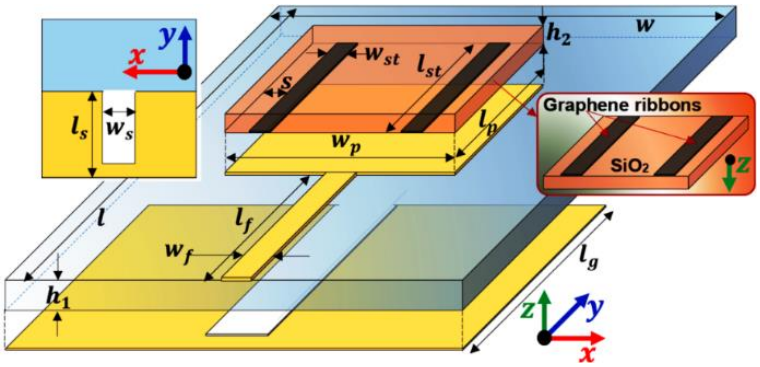

Fig. 4.3.1 The antenna structure.

Table 4.3 The dimensions of antenna structure

(Units of dimensions is μm)

Parameter	Dimension	Parameter	Dimension	Parameter	Dimension	Parameter	Dimension
$\mathbf{l_g}$	12	w_s	3	w_{st}	1	l_{st}	7
w	20	l_s	11	w_p	10	l_p	7.5
l	24	l_f	13.5	h_2	0.3	S	2
$\mathbf{h_1}$	1.6	w_f	4				

4.3.1 Nano-Antenna with UWB response

Fig. 4.3.1 shows the geometry of proposed UWB antenna. The antenna structure contains a metallic patch connected with the 50Ω nano-strip feedline. The material for the metallic radiator and transmission line can be selected as silver with the dispersive properties according to the Drude's model as $\epsilon_{Ag} = \epsilon_o \left[\epsilon_\infty + \frac{f_p^2}{f(f+i\gamma)}\right]$, assuming $\epsilon_\infty = 5, f_p = 2175$ THz and $\gamma/\pi = 4.35$ THz [204]. Here, the parameters $\epsilon_{Ag}, f_p, \gamma, \epsilon_\infty$ are permittivity of the silver, plasma frequency, collision frequency and offset of the real part of dielectric constant respectively and ϵ_o is free space permittivity. The dispersive properties of nanostrip are selected such that the transmission losses could be mitigated at the THz frequency range. The silver metal having thickness of the order of atomic level or several multiple times of atomic level can be grown on the silicon dioxide (SiO_2) substrate having the relative permittivity $\epsilon_s = 3.8$ at the THz frequency regime. This whole structure is supported by the perfect electrical conducting ground plane with

the slot of length $l_s \times w_s$. For any resonant mode, the dimensions of radiating patch can be selected using equation (4.9) [4].

$$f_r = \frac{c}{2\sqrt{\epsilon_{eff}}}\sqrt{\left(\frac{m}{l_p}\right)^2 + \left(\frac{n}{w_p}\right)^2} \quad (4.9)$$

Here, m and n are the integers showing the half-wave variations of field along the length and width of radiating patch. The formula for resonant frequency uses the effective permittivity due to non-homogenous medium at both sides of the nano-strip patch and it is given as

$\varepsilon_{eff} = \frac{\varepsilon_s+1}{2} + \frac{\varepsilon_s-1}{2}\left[1 + 12\frac{h_1}{w_p}\right]^{-1/2}$.

The dimensions of antenna structure can be further optimized to excite the higher order mode at the nearby resonant frequencies so that the UWB response can be obtained.. Fig.4.3.2 (a) shows the evolution of antenna providing UWB response. Fig. 4.3.2 (b) shows the S_{11}-parameter response of antennas and the performance of all these antennas is reported in Table-4.3.1. The antenna having radiating nano-patch supported by full-ground (FG) plane is represented by antenna-1 in Fig. 4.3.2(a). This antenna provides no radiation due to poor impedance matching. Reducing the size of ground approximately to half improves the impedance matching and this antenna provides the wideband response. The antenna with half-ground (HG) is represented by antenna-2 in Fig. 4.3.2(b). In the third case (antenna-3), the antenna with half-ground is further optimized by inserting the nano-slot in the ground plane. The insertion of the slot in the ground provides the ultra-wideband response. The enhancement of impedance bandwidth by inserting the slot in the ground plane is well known at microwave frequency [216]. This specifically is referred as the defective ground structure (DGS). However, implementing the antenna structure with DGS may be difficult in the case of nano-scale dimensions due to the fabrication complexities. In the proposed antenna, the nano-slot is inserted with the sufficiently large dimensions so that it may not offer the fabrication complexities and the effect of quantum conductance can be mitigated [220].

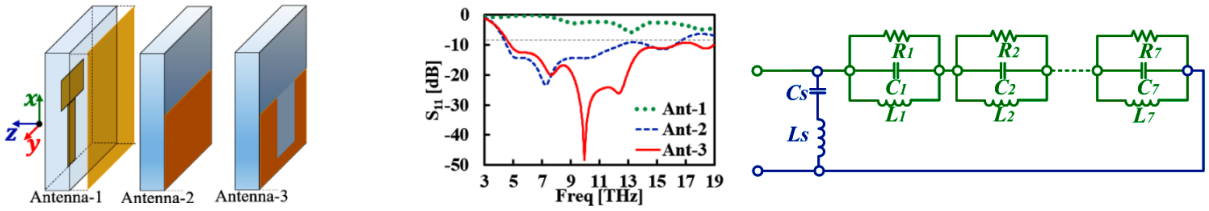

(a) (b)

Fig. 4.3.2 (a) Antenna Evolution, (b) S-parameter Response and (c) Electrical Equivalent circuit of UWB antenna.

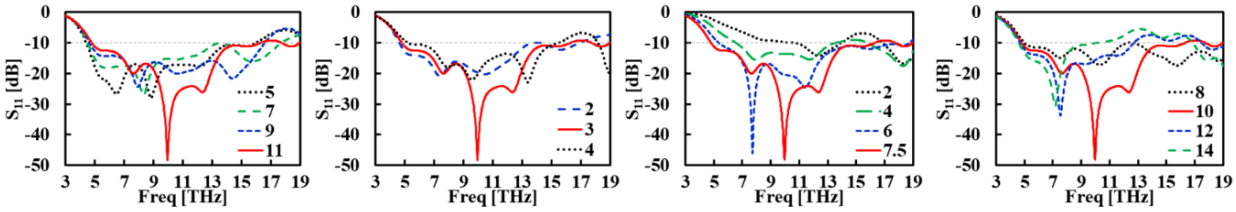

(a) (b) (c) (d)

Fig. 4.3.3 S-Parameter Response of UWB Antenna with Variable (a) l_s, (b) w_s, (c) l_p and (d) w_p.

The operation of antenna can be understood by drawing its electrical equivalent circuit model using circuit theory approach as shown in Fig. 4.3.2(c) [206]. The dimensions of antenna are selected to operate with the multiple modes having resonant frequency nearby to each other.

Table 4.3.1. Performance of antennas

Antenna	Impedance bandwidth (%)	Gain (dBi)
Antenna 1	0	–
Antenna2	94.65 $(4.48 - 12.53\ THz)$	$2.4 - 5.8$
Antenna 3	119.86 $(4.76 - 19\ THz)$	$2.3 - 6.4$

Each mode can be represented by a parallel RLC resonance circuit. All these resonant circuits are cascaded together to represent the generation of multiple modes. The incorporation of slot in the ground plane leads to change the effective capacitances and inductances of the patch by adding capacitance C_{sl} and inductance L_{sl}. Changing the slotted area changes these circuit parameters which leads to tune the resonant frequency of the excited modes and hence the impedance bandwidth. Fig. 4.3.3(a) and (b) shows the effect of variation in the slot area by varying its length (l_{sl}) and width (w_{sl}), respectively. It can be observed in the S-parameter response that insertion of nano-slot in the ground plane and varying its dimensions improves the impedance bandwidth at the higher frequency. At the lower frequency till 10 THz, the antenna

response is approximately unaffected. Fig. 4.3.3(c) and (d) shows the S-parameters response of antenna with the variation in the dimensions of radiating patch. The increment in the aperture of metallic patch leads to generate the higher order modes with the resonant frequencies nearby to each other. The dimensions of antenna are set to obtain the UWB response, its response can further be advanced by adding the graphene nano-ribbons for obtaining the tunable band-notch operation as given in the next section.

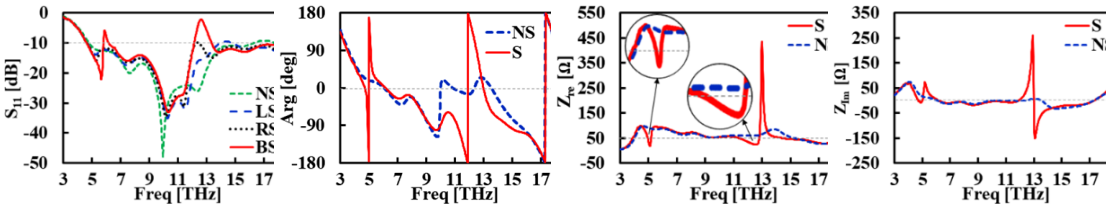

(a) (b) (c) (d)

Fig. 4.3.4 Effect of placing the dielectric slab with grown graphene nano-ribbons on (a) S_{11}-parameter response and (b) it's phase, (c) real and (d) imaginary part of impedance ($\mu_c = 0.1\ eV, \tau = 1\ ps$ and $T = 300K$).

4.3.2 The Tunable Dual-Band Notch Characteristics

Two graphene nano-ribbons are placed above the metallic patch for obtaining the tunable band-notch characteristics in UWB response. The graphene nano-ribbons can be grown either on the metallic patch or on the SiO_2 slab separately and placed above the metallic patch with the interaction of metal and graphene as shown in Fig. 4.3.1. The tunability in the band-notch frequency can be obtained by applying the electrostatic voltage on the graphene nano-ribbons with the support of metallic ground. There is an interface between metal and graphene nano-ribbon. This maintains the uniformity of the applied gate voltage throughout the surface area of graphene nano-ribbons. The effect of adding the graphene nano-ribbons on S-parameter response of antenna is shown in Fig. 4.3.4 (a). The antenna without graphene nano-ribbon (NS-no ribbons), single nano-ribbon (either left side (LS) ribbon or right side (RS)) provides the UWB response without notched band. The application of both side (BS) graphene nano-ribbons provides the dual-band notch characteristics in the frequency bands $5.02 - 5.52$ THz and $12.16 - 13.34$ THz. The parameters of graphene are selected as chemical potential $\mu_c = 0.1$ with relaxation time $\tau = 1$ ps at temperature $T = 300$ K. Fig. 4.3.4(b) shows the phase plot of S-parameter response of antenna. The phase of

reflection coefficient is changed and take a rotation of 360° at the frequency of band-notch after adding the graphene nano-ribbons in the antenna structure. This can be regarded as the addition of poles and zeros in the transfer function of electrical equivalent circuit of antenna. The impedance plot shown in Fig. 4.3.4 (a) represents its real and imaginary part without (NS) and with graphene nano-ribbons (S). Analysis of impedance plot is represented in Fig. 4.3.4 (a). It has been observed in the impedance plot that multiple modes are excited in antenna to provide the ultra-wideband response. There are probably seven identified modes represented by $M_1, M_2 \ldots . M_7$.

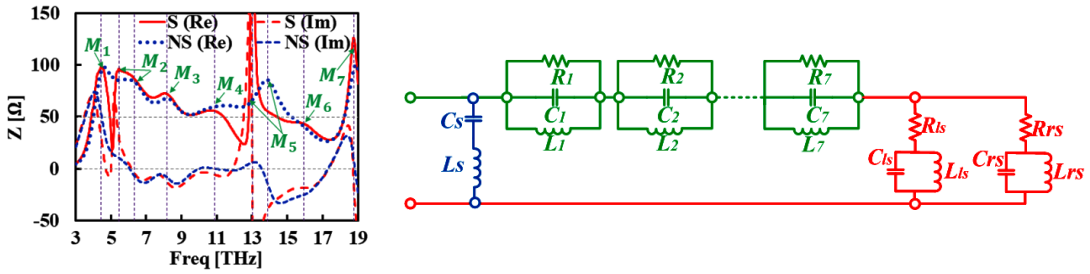

(a) (b)

Fig. 4.3.5 (a) Impedance Plot of the Antenna with and without Graphene Nano-Ribbons showing the generation of multiple modes and (b) Equivalent Circuit of Antenna with Graphene Nano-Ribbons.

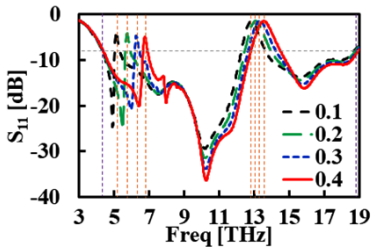

Fig. 4.3.6 Antenna Response with variable μ_c.

Addition of graphene nano-ribbons in the antenna structure provides the dip of real part of impedance in the notched band region at 5.04 THz and 12.21 THz (Fig. (4.3.4(c)). It is interesting to observe that addition of graphene nano-ribbons only affects the position of two modes M_2 and M_5. The operating frequency of mode M_2 and M_5 is 6.26 and 13.86 THz respectively in the antenna without graphene nano-ribbons. Addition of graphene ribbons shifts the resonant frequency of these modes to the lower side. Consequently, the modes M_2 and M_5 start resonating at 5.42 and 12.97 THz respectively. Fig. 4.3.5(b) shows the electrical equivalent circuit model of antenna drawn using circuit theory approach. There are seven resonating parallel RLC circuits having resonant frequency equal to modes from M_1 to M_7. These parallel resonance

circuits are cascaded representing the wide-band operation of the antenna. Two parallel LC circuit in series with R represent the band-notch filter corresponding to graphene nano-ribbons. The lumped parameters R_{ls}, L_{ls} and C_{ls} are representing the left side graphene ribbon and R_{rs}, L_{rs} and C_{rs} are representing the ride side graphene ribbon. The total impedance of antenna can be written as equation (4.14).

$$Z_p = Z_1 + Z_2 + Z_3 + Z_4 + Z_5 + Z_6 + Z_7 \tag{4.10}$$

$$Z_{nr} = Z_{LS} || Z_{RS} \tag{4.11}$$

$$Z_{LS} = R_{LS} + \left(X_{L_{LS}} \sim X_{C_{Ls}}\right) \text{ and } Z_{RS} = R_{RS} + \left(X_{L_{RS}} \sim X_{C_{RS}}\right) \tag{4.12}$$

$$Z_s = \left(X_{L_s} \sim X_{C_s}\right) \tag{4.13}$$

$$Z = Z_s || (Z_p + Z_{nr}) \tag{4.14}$$

where Z_p represents the impedance offered by metallic patch, Z_{nr} is impedance offered by graphene nano-ribbons and Z is the total impedance of the antenna with graphene nano-ribbons. The main feature of graphene is tunability of its electrical characteristics by applying the electrostatic field externally. The electrostatic field is applied normally to obtain the tunability in its chemical potential (μ_c) and the surface conductivity (σ_g) in this proposed antenna structure. The application of electrostatic field on thin layer of monolayer graphene with thickness 0.34 nm makes the off-diagonal component zero in two dimensional tensor matrix of σ_g. The spatial dispersion is assumed to be absent in the THz frequency region. Applying the Kubo's Formulism, the expression for σ_g can be written using Drude's model as given in equation (4.15).

$$\sigma_s(\omega) = \frac{j2e^2 k_b T}{\pi h^2 (\omega + i\tau^{-1})} \ln\left[2\cosh\left(\frac{E_F}{2k_b T}\right)\right] + \frac{e^2}{4h}\left[\frac{1}{2} + \frac{1}{\pi}\arctan\left(\frac{h\omega - 2E_F}{2k_B t}\right) - \frac{j}{2\pi}\ln\frac{(h\omega + 2E_F)^2}{(h\omega - 2E_F)^2 + 4(k_B T)^2}\right] \tag{4.15}$$

where e is electronic charge, k_b represents Boltzmann's constant, T is the temperature, ω is the frequency, τ is carrier relaxation lifetime, h represents reduced planck's constant, E_F represents Fermi level which is dependent upon graphene charge carrier concentration. Equation (4.16) contains both the inter and intraband terms of σ_g. The intraband part remains significantly small in the lower THz region. Hence, its intraband term is considered to find the electrical characteristics of graphene nano-ribbons. In Fig. 4.3.5(b), two parallel tank circuits are having the equal voltage at the corresponding node hence changing the applied voltage changes the value of circuits parameters of graphene strip. The variation in the frequency dependent components of

band-notch tank circuit changes the frequency of notched band. Fig. 4.3.6 shows the variation of notched band frequency by varying the chemical potential (μ_c) of graphene. On varying μ_c by changing the applied voltage changes the notched band frequency keeping the operating band of antenna intact.

The effect of introducing the graphene nano-ribbons can be further understood by E −field distribution on the antenna shown in Fig. 4.3.7 and Fig.4.3.8. Fig. 4.3.7 shows the field distribution on antenna without graphene nano-ribbons Fig. 4.3.8 shows the field after addition of the graphene nano-ribbons. It can be observed in Fig. 4.3.8 that electric field is heavily confined in the area of metallic patch nearby to the graphene nano-ribbons. Comparing Fig. 4.3.7 and 4.3.8 , it can be concluded that the operating mode of antenna remains same at all the frequency in both the cases without and with the graphene nano-ribbons except at frequency 5.42 THz and 12.97 THz which is nearest to the notched band shown in Fig. 4.3.7 (b), 4.3.8 (b) and Fig. 4.3.7 (e), 4.3.8 (e), respectively. At these frequencies, the radiating edge and surface of antenna is drastically changed after applying the graphene nano-ribbons. The field distribution shows the operation of antenna with horizontal magnetic dipoles.

Furthermore, the size and location of the applied graphene nano-ribbons decides the number of created notches and their frequency location. Fig. 4.3.9 shows the effect of varying the size and location of the applied graphene nano-ribbons. Fig. 4.3.9 (a) shows the effect of varying the size of graphene nano-ribbons by changing their offset from the bottom edge of the metallic radiator. It can be observed in the S-parameter response that reducing the metal graphene interaction area by increasing the offset changes the operating passband. At the zero offset converts the ultra-wideband response in to the narrow triple band with wide notches between the operating passbands. For the value of offset 0.5 μm provides the defined narrow dual-band notch operation with ultra-wideband characteristics. Increasing the offset to 1.5 μm omits the first notched band and antenna provides the UWB response with single band-notch characteristics near the frequency around 14 THz. Fig. 4.3.9 (b) shows the effect of varying the location of varying the location of the graphene nano-ribbons by varying s which is offset from the side edge of radiator. In previous discussion it is found the application of two graphene nano-ribbons together provides the UWB response with dual-band notch operation . Hence, the location of both ribbons is varied together by changing s with equal separation from the sides of the radiating patch. Placing the graphene nano-ribbons at

the size edges of radiating patch sinks fringing fields responsible for radiations and antenna provide very narrow band operation. Increasing s provides the fringing field from the side edges of metallic radiators and UWB response is achieved with the dual band-notch characteristics.

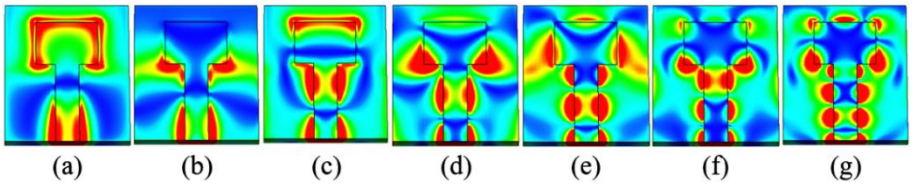

Fig. 4.3.7 E −field distribution on antenna without graphene nano-ribbons at frequency (a) 4.36 THz (b) 6.26 THz (c) 8.21THz (d) 10.90 THz (e) 13.86THz (f) 16 THz (g) 18.85 THz.

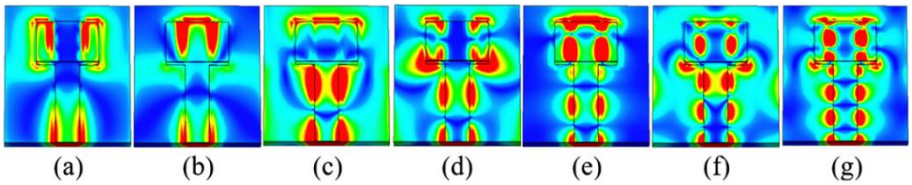

Fig. 4.3.8 E −field distribution on antenna with graphene nano-ribbons at frequency (a) 4.36THz (b) 5.42 THz (c) 8.21THz (d) 10.90 THz (e) 12.97THz (f) 16 THz (g) 18.85 THz.

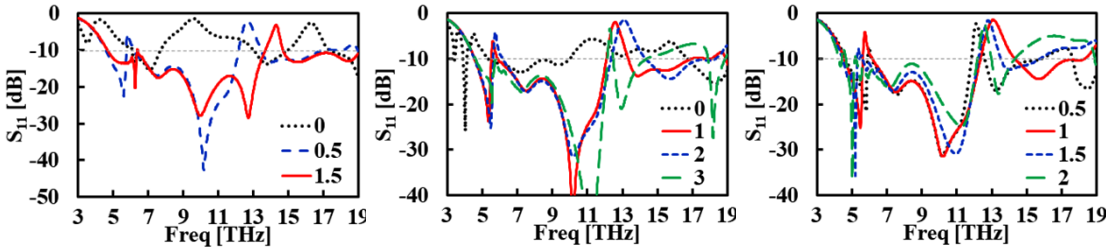

Fig. 4.3.9 S_{11}-parameter response of antenna with (a) different values of offset of graphene nano-ribbons from the bottom edge of metallic radiator, (b) variable s and (c) variable w_{st}.

However, increasing s narrow downs the upper notched band and reduces the reflection coefficient in the lower notched frequency band and converts the antenna response in the UWB with single band-notch. Thus, suitable choice of s can provide the

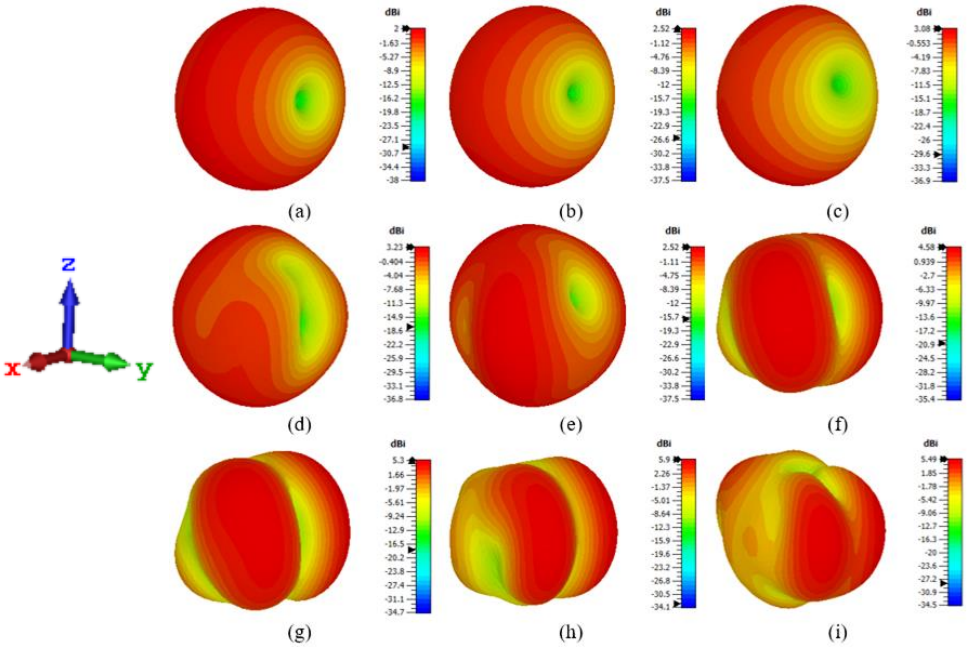

Fig. 4.3.10. Radiation pattern of antenna at frequency (a) 4.36, (b) 5.42, (c) 6.86, (d) 8.21, (e) 10.90, (f) 12.97, (g) 13.86, (h) 16 and (i) 18.85 THz.

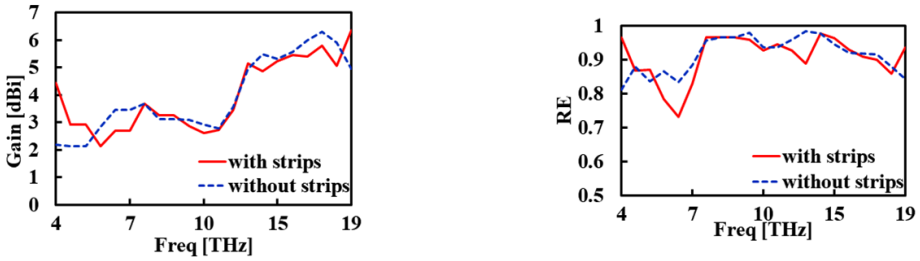

Fig. 4.3.11 (a) Gain and (b) radiation efficiency of antenna with and without graphene nano-ribbons.

notched band with desired frequency range. Fig. 4.3.9(c) shows the effect of variation in width of graphene nano-ribbons (w_{st}) on S-parameter response. Increasing w_{st} reduces the reflection coefficient at the frequency of first band-notch and antenna provides the UWB response with single band notch characteristics.

Fig. 4.3.10 shows the radiation pattern of antenna at the resonant frequencies covering whole passband. It can be observed in the plot that antenna provides the monopole like radiation pattern with the omni-directional coverage due to generation of horizontal magnetic dipoles in antenna. The generation of the horizontal magnetic dipole along the $y-$axis provides the radiation with the coverage $0° \leq \theta \leq 360°$ in $\phi = 0°$ plane. The radiation pattern of antenna remains consistent throughout the passband. However, the ration pattern has the increased directivity with reduced beam width at higher frequencies, as expected. Fig. 4.3.11 (a) shows the gain plot of antenna

$\theta = 90°$ in $\phi = 0°$ plane. Fig. 4.3.11 (b) shows the radiation efficiency of antenna as a function of frequency. The main limitation of nanoscale antennas is reduced efficiency due to the metallic losses and low conductivity of metals. The selection of dispersive properties of materials used in the proposed antenna in the reported manner provides the higher radiation efficiency. The proposed antenna provides the radiation efficiency more than 80% throughout the passband.

4.4 CONCLUSION

In this research work, Reconfigurable antennas with dual band characteristics have been designed. Magneto Hydrodynamic antenna with Saline water as fluid element is simulated for multi band frequency. Antenna characteristics can be changed by changing chemical composition of water,

A compact and low profile solution of the space constraint of Ultra wide band technology of the wireless communication. This design provides high peak gain of 6.4 dB and a high bandwidth of 12.24 GHz ranging from 4.2-16.6 GHz. Average radiation efficiency is above 90% and group delay provided is also <1.2 ns.

CHAPTER 5

BIO-MEDICAL APPLICATIONS OF DRA

5.1 INTRODUCTION

Ultra Wide Band technology has specifically endowed Radio sensor technology in information retrieval of physiological conditions measured among various human organs. Radio sensors possess several characteristics in comparison of the contemporary counterparts, due to which they are ardent candidate for detection of early stage of breast cancer. Last two decades have witnessed extension of breast cancer as a cause of mortality among women worldwide. According to WHO report 2020 about 2.10 million women globally are being affected each year due to this deadly disease [252]. It was approximated in 2018 that 627000 women died due to breast cancer which is approximately 16% of all cancers death among women [253-254]. Situation is quite complicated in India because for same number of cancer affected women with survival rate 60% here, while in USA it is 90%. Early stage detection is a powerful tool that can be employed to increase survival rate and leading towards better health care treatment and protocols.

Modern-day techniques used for breast cancer detection are X-ray Mammography, Ultrasound, Magnetic Resonance Image (MRI), Positrons Emission Tomography and Microwave Imaging [255]. The very first profound technique that is still in maximum use is X- ray mammography but it suffers from excessive number of trials and false positive test results. Apart from risk of high radiation exposure, this process deals with compression of affected breast which makes it highly uncomfortable [256]. Ultrasound technique makes use of sound waves but its low resolution doesn't yield accurate results. It is regarded as secondary technique after mammography. MRI is an accurate process of retrieving image of inside body with the help of radio waves and strong magnetic field. This is a pre surgery procedure and is not feasible for a major segment of society to make it repetitive due to high cost. Positron Emission Tomography (PET) makes use of a mixture of radioactive element with glucose or glycoprotein to soft tissues of breast. Nutrients are absorbed by tumour and positrons are ejected in this process. Positrons are mapped and image is formed but this process also suffers from low resolution.

Microwave imaging emerges as a substitute for all of these abovementioned contemporary techniques with its virtuous characteristics such as unique operating

principle with no harmful radiation exposure, low cost and high resolution. In this technique, high frequency radio waves are incident on affected area and reflected waves are accumulated by data acquisition system [257-258]. According to the mechanism involved in image recreation and data collection, microwave imaging can be divided into two parts. Microwave Tomography is the first process in which difference in permittivity distribution is used to produce results in image form [259]. Scattering Algorithms are being used by this technique, but it increases both complexity and time to form image which makes it a tedious approach towards early detection of breast cancer. A rather simple approach i. e. Ground Penetrating Radar (GPR) which incident high frequency electromagnetic waves and collect scattered and reverted waves [9]. It works on Impulse Radio Transmission and Reception method of UWB Technology [260]. In this RADAR based technology, first data collection takes place and further it is processed via Focussing Algorithms (FA) and afterwards image is recreated by entire system.

Efficiency of a Radar Microwave Imaging system depends upon its sensitivity towards the electrical properties of malign and benign tissues. Few first studies which consider homogeneous breast tissue, suggested that the contrast between normal tissue and the malignant tissue is 5:1 [267-268]. Specific Absorption Rate can be defined as a measure for electromagnetic energy absorbed by biological tissue mass when exposed to radiating device such as mobile phones. On the other hand, penetrating tissue losses has to be overcome in the operating frequency range and they should not exceed beyond 4dB/cm. In a nut shell, it can be determined that the type of sensor GPR system has to use should have low tissue penetrating loss and low values of Specific Absorption Rate (SAR) along with high efficiency and resolution. All these issues have been addressed by various researchers worldwide. Numerous radiators such as Micro strip Patch Antenna (MPA) or Dielectric Resonator Antenna (DRA) have been proposed to mitigate these shortcomings.

In this work, a novel and unique hybridization of Patch and Dielectric resonator antenna has been proposed. Stepped micro strip fed mechanism is used to improve impedance matching of antenna. Ring shape patches have been an ardent candidate to enhance the bandwidth of antenna and this property is utilised in the presented article. Ring Rectangular shape dielectric resonator antenna is designed and analysed in conjunction with jumbled ring shape patch with defected ground structure. Defected ground structure are one of the prudent techniques used to enhance bandwidth of the antenna.

A compact RRDRA, multiple and jumbled ring shaped patch with slotted and stripped partial ground structure can be perfectly employed as a sensor for Early detection of breast cancer along with gateway nodes. As far as frequency domain parameters are concerned, high gain of 5.7 dB along with average efficiency of 90% throughout the operating bandwidth has been obtained. Proposed structure is best suited for sensing unit and efficient communication due to its high bandwidth, gain, light weight and compact size.

5.1.1 Design and Development of DRA with Circular Patches.

Fig. 5.1.1 represents the geometrical aspects of the antenna. Presented structure is implemented with FR4 substrate $\boldsymbol{\varepsilon_r = 4.4}$ with dimensions of 18 x 26 x 1.6 mm^3. A Ring Rectangular Dielectric Resonator Antenna of material Alumina ceramic having the relative permittivity of 9.8 is instituted upon the substrate having dimensions as per the Table 5.1.1. A novel feed mechanism is proposed to excite higher order modes so that operating bandwidth of frequency 5.4-15 GHz can be achieved. As shown in Fig 5.1.1 (b), stepped structure of micro strip feed is being utilized in order to obtain impedance matching. Multiple rings are employed in conjunction with DRA to enhance bandwidth of the antenna. Fig. 5.1.1 (a) represents Top view of antenna which shows DRA and feed implementation of structure. Fig 5.1.1 (b) shows the jumbled ring structure of antenna without DRA. Fig. 5.1.1 (c) represents the side view of the antenna with proposed heights of substrate and DRA. Fig. 5.1.1 (c) represents the defected structure of the antenna.

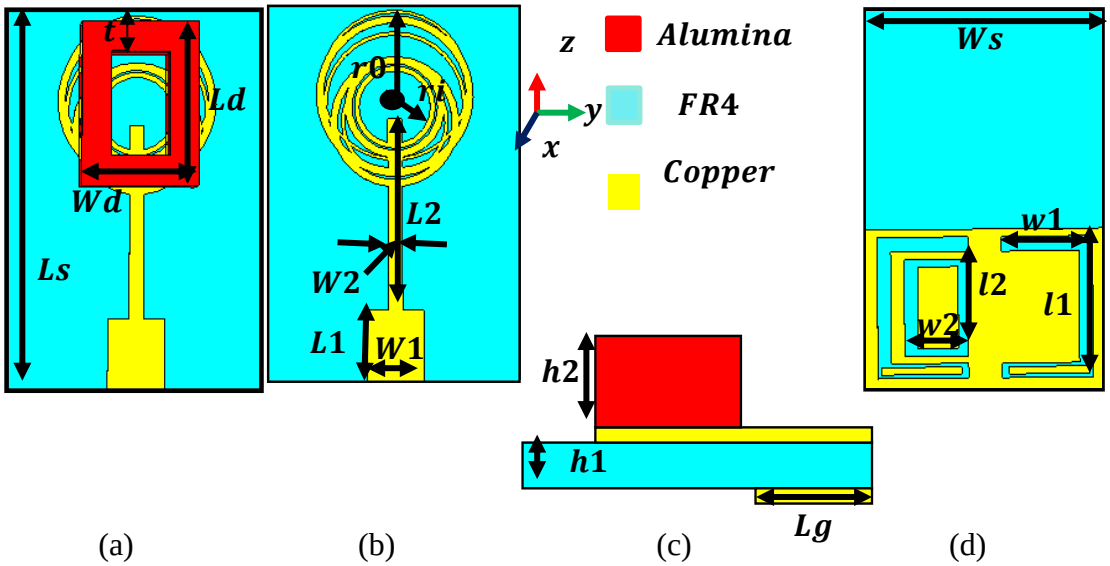

(a) (b) (c) (d)

Fig 5.1.1 Depicts (a) Top View, (b) Top View without DRA, (c) Side view, (d) Bottom View

Table 5.1.1 Dimensions of the Proposed Structure

Parameter	Dimensions (mm)	Parameter	Dimensions (mm)
L_1	5	$\boldsymbol{l_1}$	9
W_1	4	$\boldsymbol{w_1}$	6.75
L_2	7.2	$\boldsymbol{h_1}$	1.6
W_2	1	$\boldsymbol{h_2}$	12
L_s	26	$\boldsymbol{r_i}$	2.5
W_s	18	$\boldsymbol{r_0}$	5.5
L_d	11	$\boldsymbol{l_2}$	6.75
W_d	8	$\boldsymbol{w_2}$	4.75
t	2	$\boldsymbol{L_g}$	11

5.1.2. Theoretical Consideration of DRA with Circular Patches

In this design, annular ring patch is chosen at first step to implement the hybrid sensor. Ring patch antenna offers dual band properties along with better impedance matching and improved radiation properties. The mathematical analysis of a ring patch can be done with the expression of Resonant frequency

$$\boldsymbol{f_{rnm} = \frac{X_{nm} \times c}{2\pi\sqrt{\epsilon_r}}} \quad (5.1)$$

where c = 3× $\mathbf{10^{10}}$ is velocity of light in cm/sec

$\boldsymbol{X_{nm}}$ is the first order Bessel function root and depends on the mode of the patch.

For $\boldsymbol{TM_{11}}$ mode , the value of the value of = 0.6773.

$$\boldsymbol{X_{nm} = K_{nm} \times a} \quad (5.2)$$

Where n= azimuthal variation

And m indicates field variation across the ring width.

The above expressions provide accurate values when $\frac{\boldsymbol{b-a}}{\boldsymbol{b+a}}$ < 0.35 and b = 2 ×a ×c conditions are met. ‘a’ and ‘b’ are the inner and outer radii of the ring. If the fringing effect is also considered then the resonant frequency is given by

$$\boldsymbol{f_{rnm} = \frac{X_{nm} \times c}{2 \times \pi \times a \times \sqrt{\epsilon_{re}}}} \quad (\mathbf{5.3})$$

$$\boldsymbol{\epsilon_{re} = \frac{\epsilon_r + 1}{2} + \frac{\epsilon_r - 1}{2} \left[1 + 10 \times \frac{h}{w}\right]^{-\frac{1}{2}}} \quad (5.4)$$

where ϵ_{re} is the effective dielectric constant

and w = b-a, is the width of the ring.

Dimensions of ring shaped patch are chosen according to eq. (5.1) and eq. (5.2), but in order to get desired response from the radiator, modification in the geometry has been done. Hybrid senor proposed in this paper is a combination of patch and ring shaped rectangular dielectric resonator [RRDRA]. RRDRA offers advantages of low Q factor due to drilled rectangle in between of rectangular DRA, that's why it is best suited as an antenna element in terms of gain and operating frequency and efficiency. Proposed rectangular geometry of DRA is chosen due to the agility offered by this structure. With proper selection of antenna dimensions i.e. length L_d, width W_d and height h_2 desired antenna response can be achieved. Q-factor of RDRA depends upon aspect ratio of the structure. Presented antenna makes use of lowest order mode of RDRA i.e. TE^x_{111} mode. Resonant frequency for this particular mode can be determined with the following transcendental eq.

$$k_x \tan(k_x Ld|2) = \sqrt{(\varepsilon_r - 1)k_o^2 - k_x^2} \quad (5.5)$$

Where $k_o = \frac{2\pi}{\lambda_o} = \frac{2\pi f_o}{c}$, ky = $\frac{\pi}{Wd}$ and $k_x^2 + k_y^2 + k_z^2 = \varepsilon_r k_o^2$

Selection of aspect ratio $\frac{Wd}{h2}$ and $\frac{Ld}{h2}$ along with dielectric constant (ε_r), is important in determining the resonant frequency of antenna. The expression used for the determination of above parameter consisting of normalized frequency (F) is given by equation (5.6):

$$F = \frac{2\pi f_o \sqrt{\varepsilon_r}}{c} \quad (5.6)$$

Versatility of this sensor increased due to amalgamation of inherent properties of micro strip patch antenna with Dielectric resonator antenna. Micro strip patch offers easy to fabricate approach with high impedance bandwidth on the other hand DRA offers low losses, high efficiency and high gain. Combination of multiple ring patch antenna with RRDRA is yields best frequency response with a bandwidth of 9.6 GHz with a high gain of 5.7 dB and average efficiency of 90% throughout the operating range. Hybridisation extracts best characteristics among both radiators and offers the best possible sensor for breast cancer detection technology.

5.1.3 Results and Discussions for DRA with Circular Patches

Reflection coefficient determines the total amount of power coupled by the antenna in space. Good reflection coefficient is a figure of merit to understand radiation

properties of any radiator. Fig. 5.1.2 (a) represents simulated reflection coefficient parameters of the proposed antenna with and without DRA. It can be seen that antenna has reflection coefficient below -10 dB from a frequency range of 5.4-15 GHz as a whole structure. Without DRA Structure is not radiating from 7.1-7.8 GHz. RRDRA incorporated in the structure not only enhanced the bandwidth of the system but also increase overall characteristics of the sensor. Fig. 5.1.2 (b) represents comparative Voltage Standing Wave Ratio (VSWR) of the antenna.

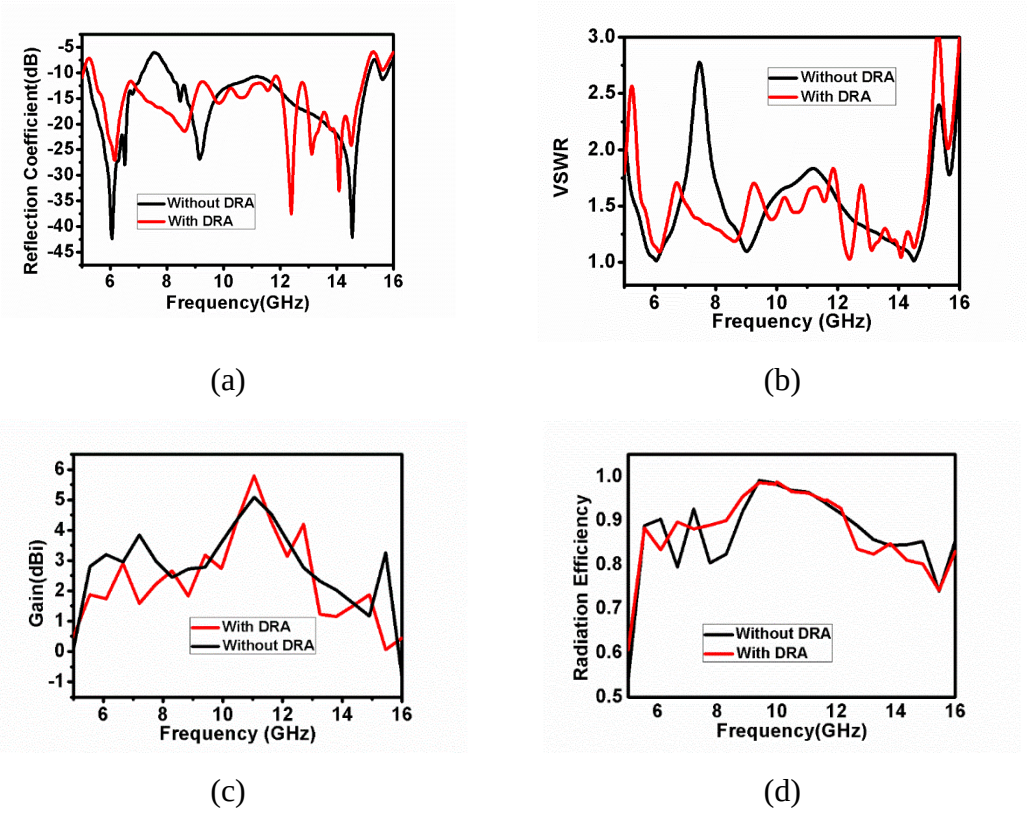

(a) (b)

(c) (d)

Fig. 5.1.2 (a) Reflection Coefficient comparison, (b) VSWR comparison, (c) Gain comparison, (d) Radiation Efficiency comparison

It can be observed from the Fig. 5.1.2(b) that a typical 2:1 ratio of VSWR has been achieved by proposed structure which again indicates excellent tuning of the radiator. With and without DRA comparison of VSWR clearly indicate the significance of DRA in the structure. Fig.5.1.2 (c) represents comparative gain of antenna with respect to the frequency. The figure shows curve of gain plotted against frequency. 14% increment in peak gain is achieved with the proposed radiator. This is due to the effect of enhanced capacitive reactance on addition of RRDR. It is interesting to note that with DRA, average as well as peak gain is high as compare to without DRA configuration. Radiation Efficiency is a significant parameter in determining overall response of the antenna. Fig 5.1.2 (d) depicts the radiation efficiency of antenna with and without DRA.

It is interesting to note that With DRA, overall radiation efficiency of the system stabilize, if it is compare with, only patch configuration. Peak efficiency of 99% is achieved throughout the operating bandwidth of the system.

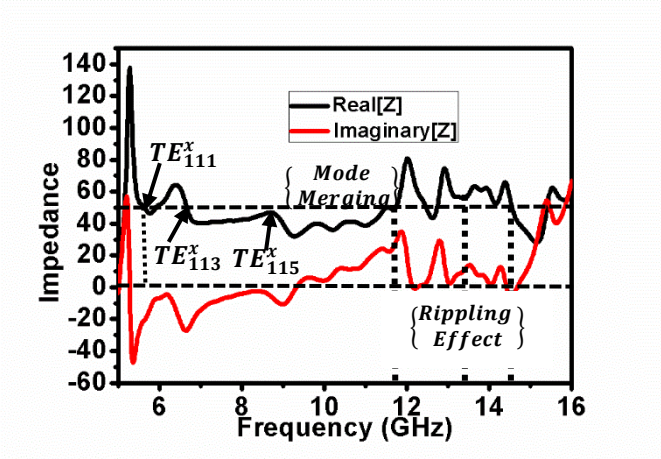

Fig. 5.1.3 Impedance Plot of the Proposed Structure

Proposed antenna is designed and simulated using transcendental eq. (5.5) and (5.6) for a theoretical frequency of 6 GHz. is chosen in such a manner so that Antenna radiate in its fundamental mode i.e. $\boldsymbol{TE^x_{111}}$.

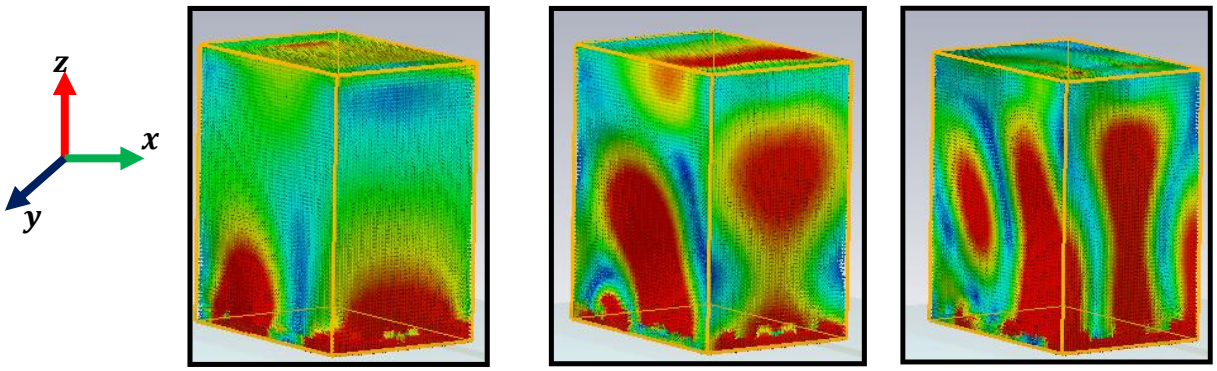

(a) (b) (c)

Fig. 5.1.4 represents E field distribution inside RDRA at (a) 6 GHz (b) 10 GHz and (c) 13.8 GHz

Fig. 5.1.4 represents the plot of electric field inside RDRA. Antenna is theoretically designed to radiate at a frequency of 6GHz. As can be seen from Fig. 5.1.3 real part of impedance is plotted against a line segment drawn at 50 GHz. It can be observed from this figure that fundamental mode of the antenna in simulation, is in the considerable agreement with the theoretical calculation. Fig. 5.1.4 (a) represents the fundamental mode $\boldsymbol{TE^x_{111}}$ of the DRA. Further two other modes $\boldsymbol{TE^x_{113}}$ and $\boldsymbol{TE^x_{115}}$ are generated as can be seen from Fig. 5.1.4 (b). As depicted in Fig. 5.1.3, Mode merging of these three modes happens till 11 GHz and afterwards due to generation of higher

order modes rippling effect is encountered by the system. Merged modes and rippled modes are shown in Fig. 5.1.4 (c). Rippling effect occurs due to generation of higher order modes at higher frequencies which affects the stability of the UWB system.

5.1.4 Radiation Pattern of DRA with Circular Patches

Fig. 5.1.5 represents the radiation pattern achieved by the proposed antenna. It is evident from the pattern that at 6 GHz antenna is behaving as magnetic monopole antenna. Good Cross-polarization and Co-polarization levels are obtained at frequency 6 GHz,10 GHz and 13.8 GHz. Fig. 5.1.5 rippling effect is also evident from the radiation pattern of 13.8 GHz. Due to generations of higher order modes irregularity in radiation pattern of the antenna can be observed.

(a)

(b)

(c)

Fig. 5.1.5 a) Radiation Pattern with Co-Polarization and Cross Polarization (Simulated and measured) in $\phi = \boldsymbol{\theta^o}$ and $\phi = 90^{\boldsymbol{o}}$ planes at 6GHz, (b) Radiation Pattern with Co-Polarizationand Cross Polarization (Simulated and measured) in $\phi = \boldsymbol{\theta^o}$ and $\phi = 90^o$ planes at 10 GHz and (c) Radiation Pattern with Co-Polarization and Cross Polarization (Simulated and measured) in $\phi = \boldsymbol{\theta^o}$ and $\phi = 90^o$ planes at 13.8 GHz.

5.1.5 Parametric Analysis of DRA with Circular Patches

Evolution stages of the antenna are depicted in the Fig. 5.1.6. Annular ring slot is subtracted from patch antenna shown in Fig. 5.1.6 (a). In next step Fig.5.1.6 (c) two ring structures are added in the base structure. In Fig. 5.1.6 (d) and (e) represents the successive stages of the structure. Fig.5.1.6 (e) represents final stage of the patch proposed in this letter. Dimensions and the operation performed to get the desired response is shown in Table 5.1.2. In this table with every subscript $\boldsymbol{r}$ represents the width of the ring to be added in the base ring. Including external and internal radius of the ring patch, Table 5.1.5.1 displays the centre position of the ring in Cartesian coordinate system. Reflection Coefficient response of the Antenna for various stages is shown in Fig. 5.1.5.2(a). Response of various stages in terms of bandwidth is depicted in Table 5.1.2 For first stage, With DRA and defected ground structure, sensor behaves as a dual wide band antenna for frequency ranging from7.8-11 GHz, 11.7-13.89 GHz.

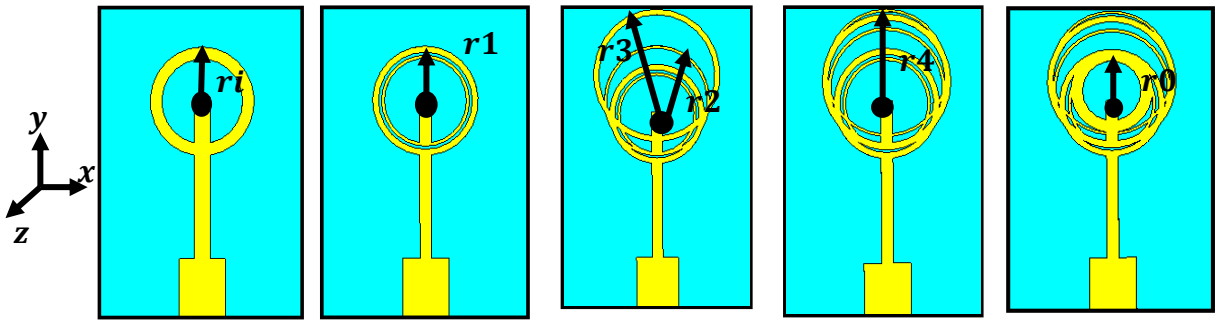

(a) (b) (c) (d) (e)

Fig. 5.1.6 Evolution of the Patch to be used in sensor

Table 5.1.2 Dimensions of the Jumbled ring structure

Sr.No	Ring Name	Operation performed	Internal radius (mm)	External Radius (mm)	Position (In coordinates x,y)
1.	$\boldsymbol{r_i}$	Base ring	3.5	4.5	0,5
2.	$\boldsymbol{r_1}$	Subtraction	4	3.75	0,5
3.	$\boldsymbol{r_2}$	Addition	5	4.75	0,6.2
4.	$\boldsymbol{r_3}$	Addition	5.2	5	0,7.5
5.	$\boldsymbol{r_4}$	Addition	5.5	6	0,6.8
6.	$\boldsymbol{r_5}$	Addition	3.5	2.5	0,6

In second step, when annular ring is subtracted from the base ring then antenna behaves as a triple band resonator. In intermediate two stages, two more rings of width r_3 *and* r_4 are added. Addition of these rings makes antenna performance to be viewed as Dual Wide band antenna. With every successive stage and addition of more rings, antenna behaves as ultra wide band antenna for frequency ranging from 5.4-15 GHz. Multiple mode resonance phenomenon of DRA is used in this structure in order to get the wide impedance bandwidth.

Table 5.1.3 Variation in Bandwidth with variation in Patch

Sr. No	Configuration	Bandwidth (GHz)
1.	5.1.6 (a)	7.8-11,11.7-13.89
2.	5.1.6 (b)	7.2-7.4, 8.3-, 10.1,10.2-13
3.	5.1.6 (c)	7-7.8,8.3-13.5
4.	5.1.6 (d)	5.3-6.4, 7-15
5.	5.1.6 (e)	5.4-15

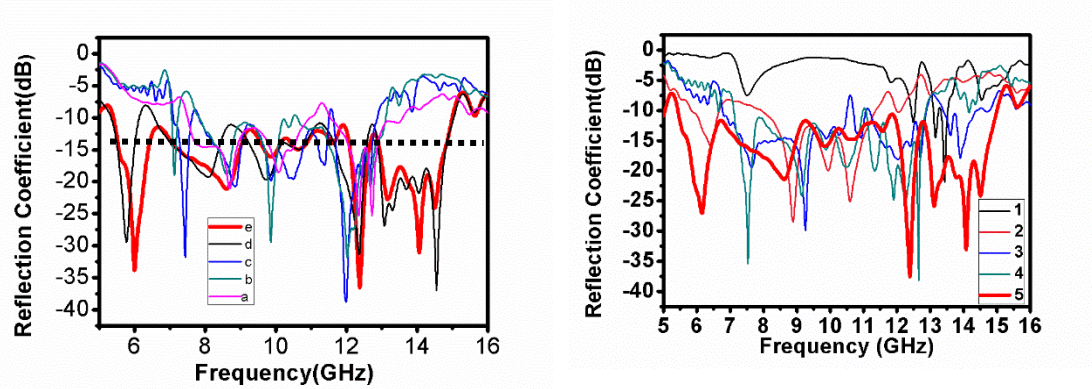

(a) (b)

Fig. 5.1.7 (a) Various response of patch from evolution stages, (b) Response of various ground structures

5.1.6. Impact of Ground on antenna performance

Ground of any planar structure can be viewed as pivotal element in deciding radiating characteristics of antenna. The proposed antenna makes use of partial ground structure along with strips and slots. Fig. 5.1.8 illustrates all phases of the ground which are implemented to achieve high impedance bandwidth.

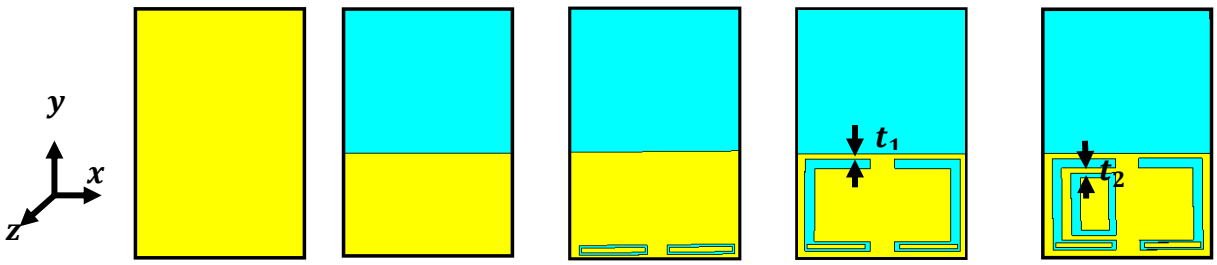

(a) (b) (c) (d) (e)

Fig. 5.1.8 Various modifications in partial ground structure

Fig. 5.1.8 (a) represents the impact of reducing the ground dimensions. Full ground dimensions (L1=26 mm) is taken and it has been observed that with patch and DRA, structure is resonating for1 GHz i.e. from 13-14 GHz. Fig. 5.1.8 (b) represent reduced length ground of the structure. While length of antenna is reduced, antenna behaves as a tuned circuit for some specific range of frequencies depending upon structure. Hence after reducing the length of the ground to little less than half (L1=11 mm), antenna starts resonating from 8-11 GHz. Fig 5.1.8 (c) represents the slot of dimension $\boldsymbol{l_1}$ and $\boldsymbol{w_1}$ is hewed off in ground plane with a thickness of 1mm. In that slot a strip of dimension 6mm x 0.5 mm is inserted. With this insertion, antenna starts behaving as dual wide band antenna. Next step Fig. 5.1.8 (d), combines two C shape slot and its mirroring in the ground plane. Due to this mirror slotting antenna behaves as ultra wide band antenna and starts resonating from 7-13 GHz as shown in Fig. 5.1.7 (b). At last step as shown in Fig. 5.1.8 (e) a rectangular slot of varying thickness along X-axis ($\boldsymbol{t_1}$) and Y-axis ($\boldsymbol{t_2}$) is inserted in the ground plane.

Table 5.1.4 Variation in Bandwidth due to Defected Ground Structure

Sr. No.	Ground Configuration	Frequency Range (GHz)
1.	(a) Full Ground	13-14
2.	(b) Less than half ground	8-11.5
3.	(c) With one slot And Strip inside	6.5-10.5, 10.9-14.3
4.	(d) Mirror C image	7.2-13.1
5.	(e)With additional rectangle slot	5.4-15

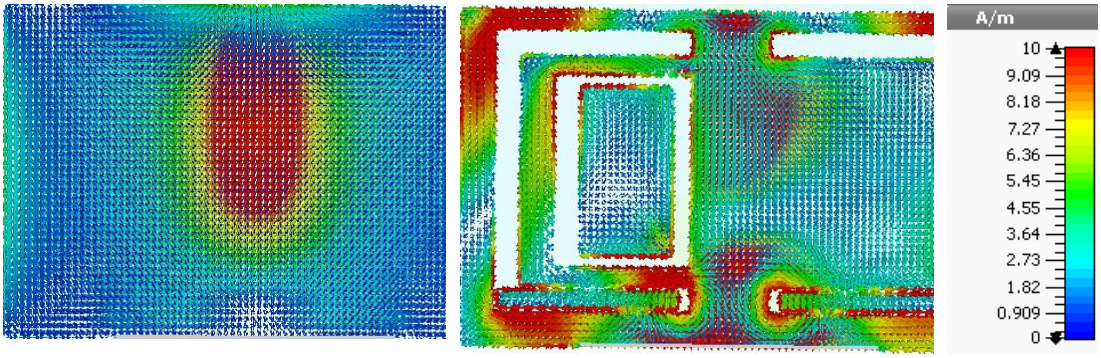

(a) (b)

Fig 5.1.9 Current Density Of Ground Plane (a) Without slot (b) With slot

With insertion of final slot, Structure starts resonating at a frequency of 5.4-15 GHz. Fig. 5.1.9 (b) represents graphical depiction of the reflection coefficients of the various structures simulated. Impedance matching of any structure can be achieved by varying reactive component of the structure. A slot and strip insertion provides key methods to vary the overall impedance of the structure, which is employed in this sensor implementation. Table 5.1.4 Describes all ground configurations and their corresponding frequency ranges for which antenna is radiating. Fig. 5.1.9 (a) represents the current density of the ground without slot (a) and with slot (b). It is evident from the Fig. 5.1.9 (b) that the current density in the ground increases with the number of slot. Fig.5.1.9 depicts the current density at 6 GHz which is the dominant mode of the radiator.

5.1.7 Stepped Microstrip Parametric Variation

Micro strip feed mechanism offers advantage of ease in fabrication, reliable, and simple method to excite the planar structures. In the proposed work, Stepped micro strip feed line is used to achieve impedance matching.

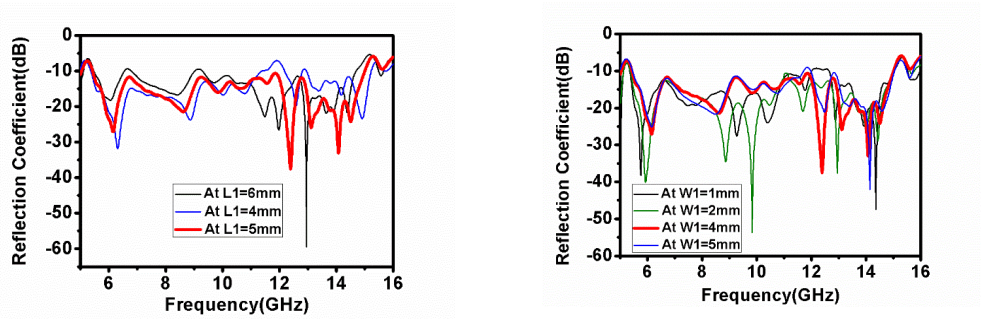

(a) (b)

Fig. 5.1.10 (a) Length variation of Micro strip feed (b) Width variation of Micro strip feed

Fig. 5.1.10 (a) and 5.1.10 (b) represents variation in the Length ($\boldsymbol{L_1}$) and width ($\boldsymbol{W_1}$) respectively and their corresponding impact on the reflection coefficient of antenna. In Fig 5.1.10 (a), value of $\boldsymbol{L_1}$ is varied from 5 mm, 4mm and 6 mm. At both 4mm and 6mm, proper impedance matching is not being obtained. For the proposed value of 5mm, proper matching occurs. Bandwidth of 5.4-15 GHz is obtained with 5mm length. Fig. 5.1.10(b) depicts the width variation of the micro strip feed. It is evident from the figure that for all values of strip line except 4mm, reflection coefficient is not displaying good matching characteristics. For W_1=1mm, antenna radiates for same frequency range but reflection coefficient factor is poor in that case.

5.1.8 Phantom Design and SAR Calculation

Specific Absorption Ratio can be defined as a measure for electromagnetic energy absorbed by biological tissue mass when exposed to radiating device.

SAR= $\frac{\boldsymbol{P}}{\boldsymbol{\rho}} = \frac{\boldsymbol{\sigma E^2}}{\boldsymbol{2\rho}} = \frac{\boldsymbol{J^2}}{\boldsymbol{2\rho\sigma}}$

Where $\boldsymbol{P}$ = Power loss density, $\boldsymbol{E}$ = Electric field strength

$\boldsymbol{J}$=Current density, $\boldsymbol{\sigma}$ = Conductivity, $\boldsymbol{\rho}$ = Density

Table 5.1.5 Material properties of the multilayer human tissue model

Parameter	Skin	Fat	Tumour
$\boldsymbol{\epsilon_r}$	36.8	4.84	54.9
$\boldsymbol{\sigma}$(S/m)	2.34	0.262	4
Density(kg/m3)	1109	911	1058

Phantom designed for measuring the SAR for the presented structure is shown in Fig. 5.1.5 and the material properties for the phantom is tabulated in Table 5.1.5 Phantom is designed with three layer structure. Skin Fat and tumour. Properties of the particular layer are shown in Fig.5.1.11. Mass Averaged SAR method used in presented paper is taken as 1g of tissue method. In this method 1.6W/kg averaged over 1g of tissue. Simulated averaged mass obtained with phantom is 0.6 W/kg , which is quite good for early detection of breast cancer .

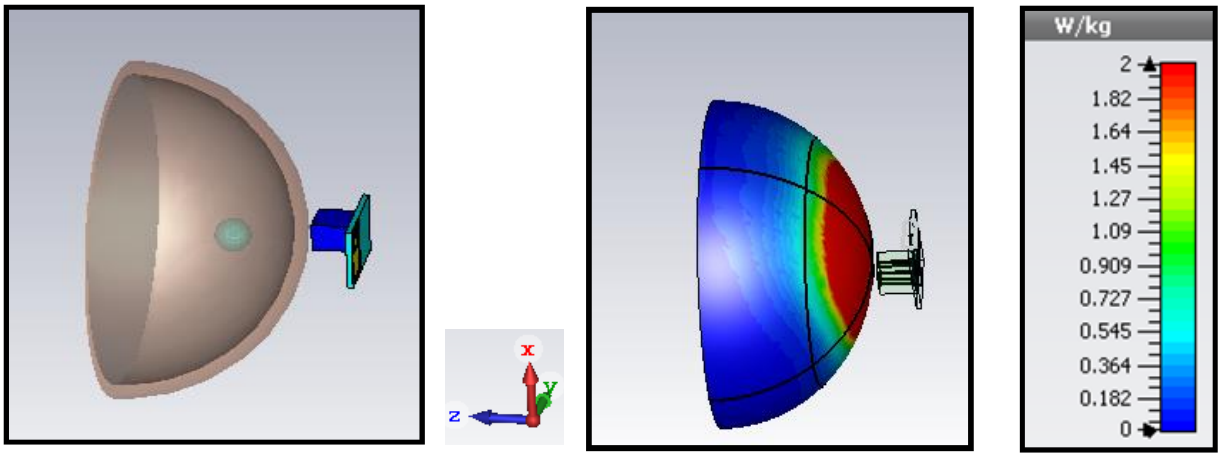

(a) (b)

Fig.5.1.11 Breast Phantom for calculation of SAR

5.2 DRA with SYMMETRICAL L-SHAPE STUB MICROSTRIP FEED

5.2.1 Design of DRA with Symmetrical L-shape stub microstrip feed

In this research work, rectangular geometry of DRA is chosen due to the agility offered by this structure. With proper selection of antenna dimensions i.e. length (L5), width (W5) and height (H2), desired antenna response can be achieved. Q-factor of RDRA depends upon aspect ratio of the structure. Presented antenna makes use of lowest order mode of RDRA i.e. TE^{x}_{111} mode. Resonant frequency for this particular mode can be determined with eq. 5.5 and eq. 5.6. With these equations the resonant frequency is calculated. Table 5.2.1 shows dimensions of proposed antenna. Fig. 5.2.1 represents the geometrical aspects of the antenna. Presented structure is implemented with FR4 substrate $\varepsilon_r = 4.4$ with substrate dimensions of 26 x 20 x 1.6mm^3. In this design, Ultra Wide bandwidth response is achieved with the application of partial ground structure of dimension 13 x 20 x 0.018 mm^3. A Ring Dielectric resonator antenna of material Alumina ceramic having the relative permittivity of 9.8 is instituted upon the substrate having dimensions as per the Table 5.2.1. A novel feed mechanism is presented in this work to excite lower order modes so that operating bandwidth between the frequency 3.7-7.4 GHz is obtained. Two extended stub structures along with slot in between is proposed which is primitive way of obtaining impedance matching of antenna. Fig. 5.2.1. (a) represents Top view of antenna with DRA and feed implementation of structure. Fig. 5.2.1. (b) represents the side view of the antenna with proposed heights of substrate and DRA. Fig. 5.2.1 (c) represents the feed structure of the antenna.

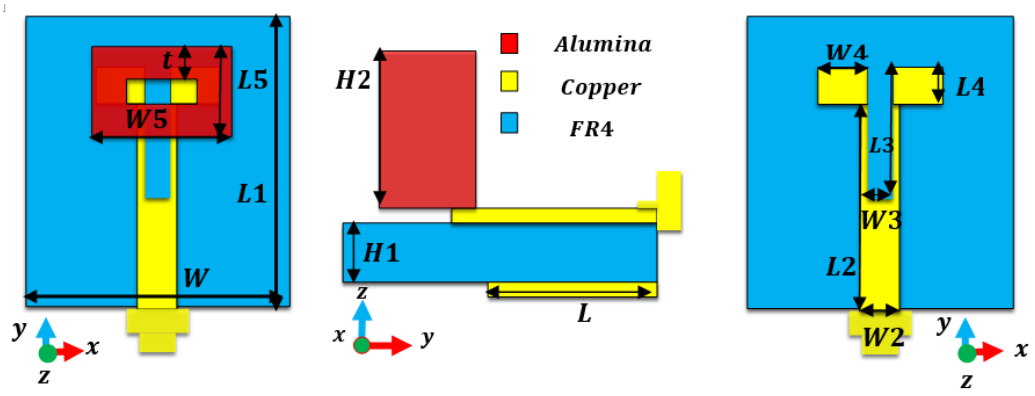

(a) (b) (c)

Fig.5.2.1 (a) Top View (b) Side View (c) Feed structure of Antenna

Table 5.2.1. Dimensions of the Proposed Structure

Parameter	Dimension(mm)	Parameter	Dimension(mm)
L1	26	L4	3.25
W1	20	W4	3.5
H1	1.6	L5	6
L2	18.5	W5	10
W2	4	t	2
L3	12.5	H2	10
W3	2	L	13

5.2.2 Optimization of the feed

Fig.5.2.2 represents evolution stages of the feed mechanism of the antenna. Fig. 5.2.2 (a) shows simple rectangular micro-strip feed line, which is used for impedance matching of the antenna to free space. Fig. 5.2.2 (a) and (b) shows imaginary impedance and corresponding reflection coefficient of the antenna.

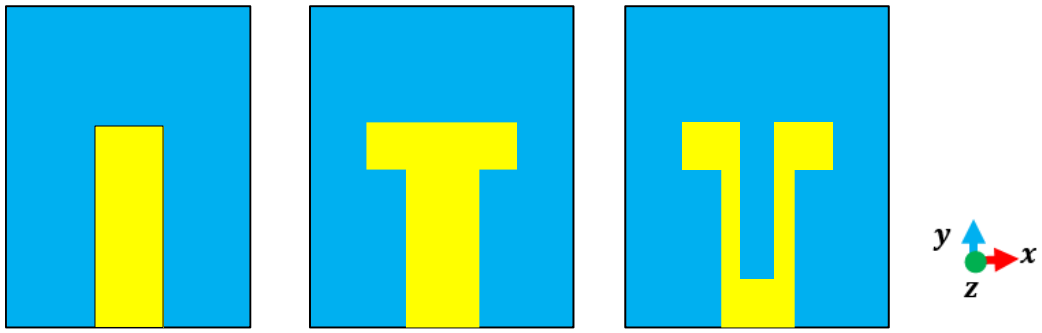

(a) (b) (c)

Fig. 5.2.2 (a) Simple feed (b) Inductive feed (c) Capacitive feed

It is observed from Fig. 5.2.3 (b) that for simple feed mechanism, antenna starts resonating from 6.3 GHz. Bandwidth of the antenna is shifted from higher to lower frequency due to high tissue losses occurrence at higher frequencies. An inductive stub is embedded at the end of simple rectangular feed. This results in shifting the entire frequency towards the left and providing a bandwidth of 3.4-7 GHz.

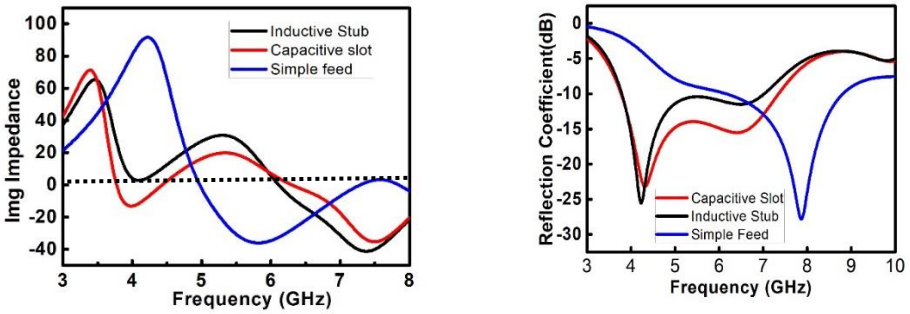

(a) (b)

Fig. 5.2.3 (a) Imaginary Impedance of the three stages (b) Reflection coefficients of the three stages.

Fig. 5.2.3 displays evolution stages of impedance of the proposed antenna. A simple feed is applied to the RDRA which yields a single band response of antenna. A T-type structure acts as inductive stub, which enhances impedance bandwidth of the circuit as shown in fig. 5.2.3(b). In order to further enhance the bandwidth of the antenna a capacitive slot is cut in centre of the rectangle feed which subsequently increases the bandwidth of the antenna. Fig. 5.2.3(b) shows the frequency range of 3.4-7 GHz. Bandwidth of 3.7-7.4 GHz is obtained with the structure of the antenna. Fig. 5.2.4 shows the electrical equivalent circuit for the entire structure of antenna.

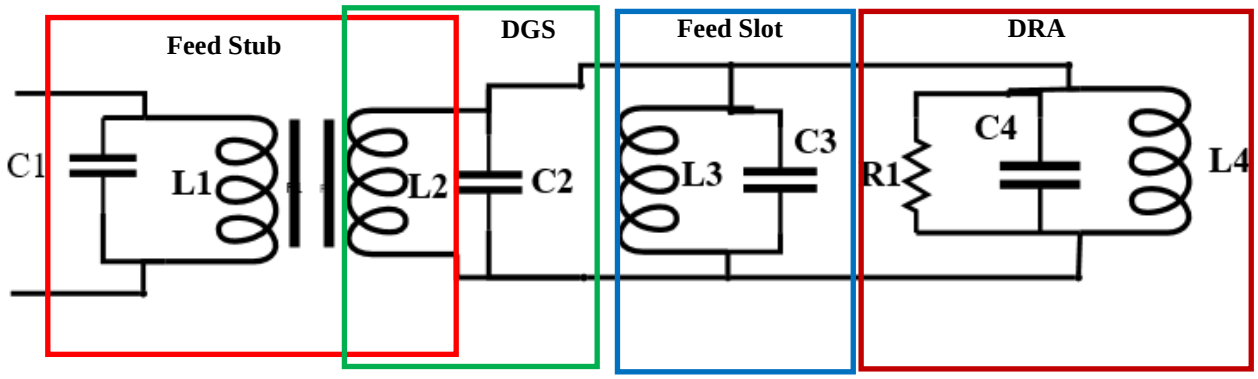

Fig.5.2.4 Electrical equivalent circuit of Structure

5.2.3 Fabricated Prototype of Antenna

Fig. 5.2.5 (a) represents the fabricated prototype of antenna proto type of antenna. Vector Network Analyzer of Agilent technologies is used to measure reflection coefficient of the antenna. Fig. 5.2.5 (b) shows the measured reflection coefficient while (c) shows the close-up of VNA screen.

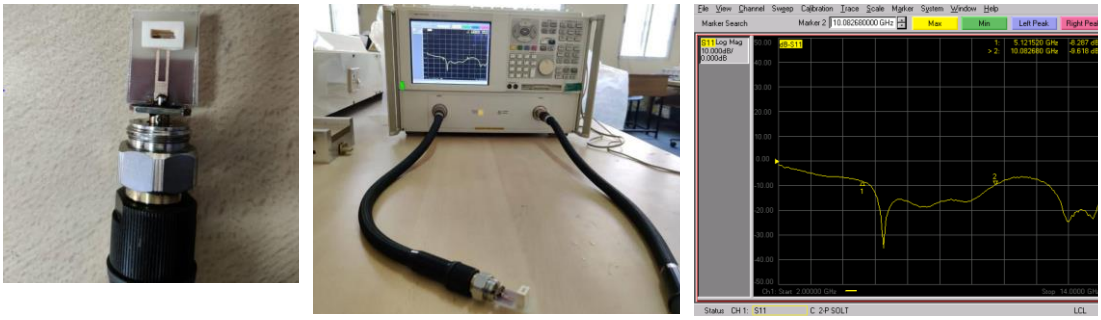

(a) (b) (c)

Fig. 5.2.5 (a) Fabricated prototype of antenna (b) Measured Refection-coefficient (c) Screen shot of VNA

5.2.4 Results and Discussions

Reflection coefficient is a true measure of the total amount of power coupled by the antenna in space**.** Fig. 5.2.6 (a) represents simulated reflection coefficient parameters of the proposed antenna. It can be observed from the figure that antenna has reflection coefficient below -10 dB from a frequency range of 3.7-7.4 GHz. Measured and Simulated graphs are almost identical and shows a great degree of coherence. Simulated Graph shows better impedance matching as compare to measured S11. This can be attributed to the wire losses occurred at the time of measurement. Fig. 5.2.6 (b) represents impedance graph of the structure. Modes shown in the diagram displays varying nature of electric field inside the DRA.It is evident from the Fig. 5.2.6 (b) that multi-mode and UWB is yielding due to generation of lower order modes and their merging. Further Fig. 5.2.6 (b) represents that at frequency 4.1 GHz dominant TE^{x}_{111} mode is generated and at 5.2 GHz TE^{x}_{113} mode is generated.

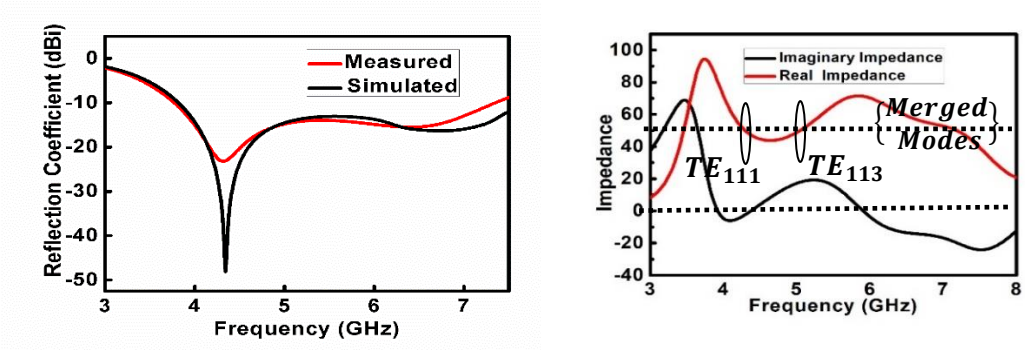

(a) (b)

Fig.5.2.6 (a) represents comparison between measured and simulated parameter (b) impedance plot of the antenna.

Fig. 5.2.7 represents the electric field distribution inside the proposed antenna structure. Generation of these modes is quite visible in Fig. 5.2.7(a) and (b). Fig. 5.2.7 (c) shows mode merging phenomenon inside DR structure. Multiple merging of radiating modes is evident from the above Fig.5.2.6 (c) due to the induced inductances by feeding method and this leads to the generation of successive TE^{x}_{111} modes at 4.1GHz. Subsequently, at higher frequencies the interaction between various components of electric fields increases significantly thereby leading to generation of higher order modes. However, clear separation of modes excited inside the DR (dielectric resonator) can be seen at frequencies 4.1 GHz and 5.2 GHz respectively.

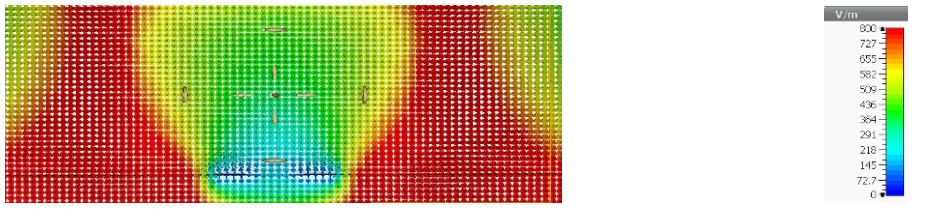

(a) TE^{x}_{111} mode

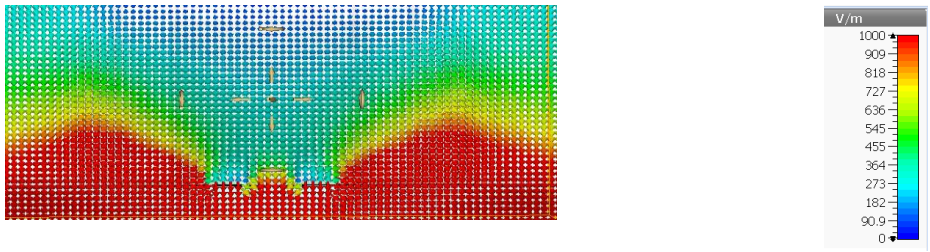

(b) TE^{x}_{113} mode

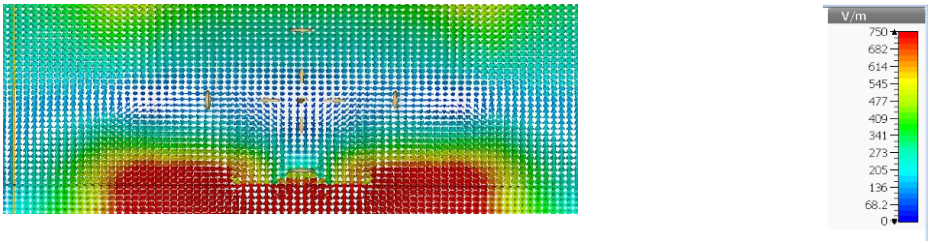

(c) Merged modes of DRA

Figure 5.2.7 (a) Electric field at configuration at 4.1 (b) 5.2 and (c) 6.8 GHz

Fig. 5.2.8 (a) represents comparison of measured and simulated gain of the antenna with respect to frequency. Peak gain of 2.5 dB is achieved with the proposed radiator. Fig.5.2.8 (b) represents radiation efficiency of antenna. It is interesting to observe that presented DRA reflects exceptionally high radiation efficiency in the operating bandwidth. An average radiation efficiency of 92% is obtained with this sensor.

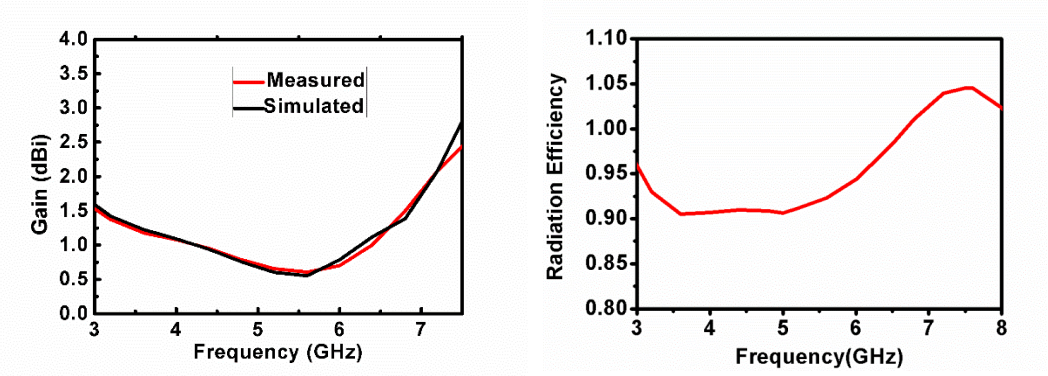

(a) (b)

Fig. 5.2.8 (a) Gain (b) Radiation Efficiency of Antenna

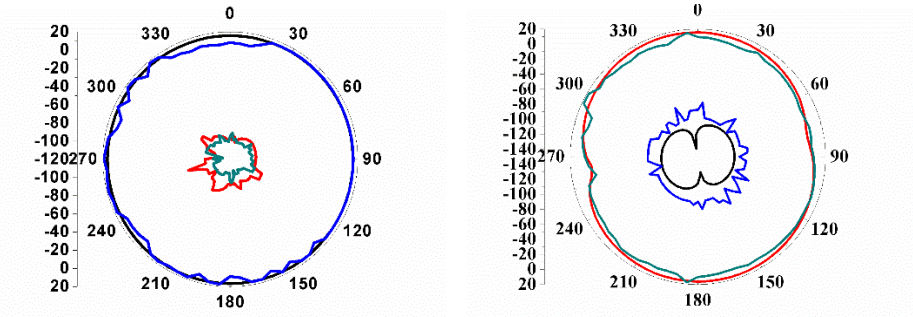

(a) (b)

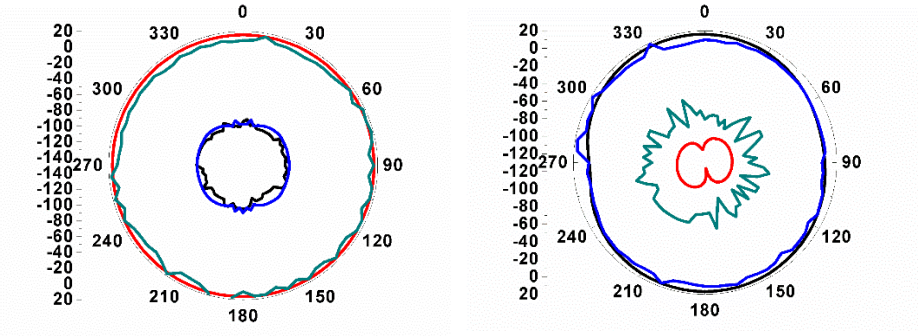

(c) (d)

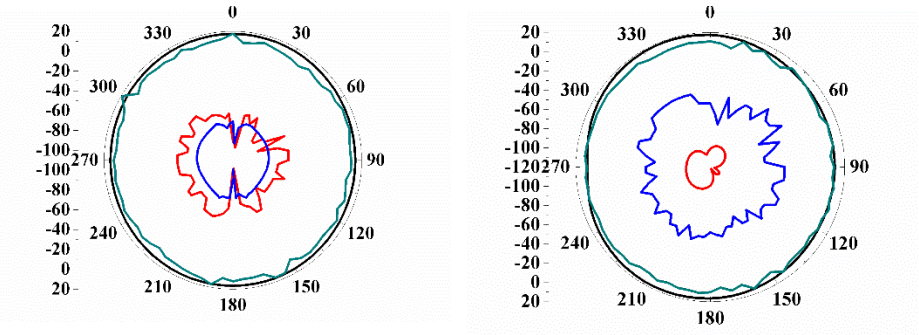

(e) (f)

Figure 5.2.9 Simulated and measured Co-polarization and Cross-polarization radiation patterns of the proposed antenna structures at frequencies 4.1, 5.2 and 6.8 GHz respectively along $\phi = 0^o$ and $\phi = 90^o$.

Fairly close agreement is obtained between the simulated and the measured reflection coefficients. Fig.5.2.9 shows the simulated and the measured radiation patterns in $\phi = 0^o$ and $\phi = 90^o$ planes, with co-polarization and cross-polarization effects at 4.1 GHz, 5.2 GHz and 6.8 GHz respectively.

The field patterns are broadband and stable throughout the entire frequency range and with significantly low cross polarization levels along bore sight direction.

5.3 CONCLUSION

In this research work, the antenna structure highlights the hybridization of Ring Rectangular Dielectric Resonator [RRDR] placed on multiple ring patch, which operates at a frequency band of 5.4-15 GHz. Impedance bandwidth of 94.1% is achieved with the hybridization of patch and dielectric resonator antenna along with slotted ground structure. A peak gain of 5.7 dBi and high efficiency of 95% is achieved over the entire operating band which presented hybrid antenna is highly suitable for wearable and On-body communication. Breast Phantom is designed and Specific

Absorption Rate (SAR) is calculated to check the feasibility of contemplated structure. Acceptable SAR and ringing free impulse response makes this antenna suitable for primitive breast cancer detection as well as Wireless Body Area Networks.

A novel feed Ring rectangular Dielectric Resonator Antenna (RRDRA) is presented as a sensing element for Radar based microwave imaging Breast Cancer Detection technique. Proposed antenna is purposefully designed to radiate in Lower European Band so that penetrating tissue losses can be confined. This antenna offers peak radiation efficiency of 99%, which makes it a strong candidate to be used as high resolution sensor. Impedance bandwidth of 67% and a constant gain of 2.5 dBi over the entire operating bandwidth make it a perfect choice for On-Body and wearable sensors.

CHAPTER 6

CONCLUSIONS AND FUTURE SCOPES

6.1 CONCLUSION

Exponential increase in the requirement for ultra wide band application antennas results in research and development of dielectric resonator antennas. Dielectric Resonators provides numerous advantages such as flexibility in design, simplicity of fabrication, less conductor & surface losses, augmented bandwidth and efficiency with reduced size. Plethora of feeding mechanisms and easy amalgamation with contemporary technologies make them a profound candidate in wireless communication system. DRAs not only provide resourceful coverage requirements but also have the ability to operate across wide range of frequencies in the range 1.3 GHz - 40 GHz. Excitation of several radiating modes can be impelled within the RDRA which makes them suitable to be used over numerous applications in modern-day wireless technologies. Reduction in the size of DRA is supported by availability of wide range of materials with dielectric constants from ε_r~8 to 100 which in turn enables the antenna designers to try different designs suitable for various telecom applications. The research work encompasses around proficient utilization and involvement of the above mentioned characteristics such as feeding mechanisms and excitation of various modes inside the RDRAs towards implementation of highly professional antennas for latest wireless communication devices & systems. The completion of proposed dissertation outcomes may find relevance in the analysis and synthesis of numerous novel dielectric resonator antennas predominantly derived from rectangular dielectric resonator antennas.

This research work explores various advantages offered by rectangular geometry of the Dielectric Resonator Antennas. The main objective of this work is to miniaturize and improve the performance of RDRA. The key highlights of this research is based on investigation on Bandwidth enhancement schemes, Band notch creation, Tunability with graphene and Re-configurability. The dissertation explore in-depth details of bandwidth enhancement schemes such as Multi segmentation in both fluidic and solid state RDRA, DGS, Strips and slots. Band notch creation and tunability have been proposed in this work. Breast cancer detection application using DRA technology proved to be a considerable factor in health care services. Sensor for early detection of breast cancer have been implemented in this research work.

A thorough study of literature on the development, design and analysis of DRA has been carried out. At first, shortcomings of patch antenna have been pointed out. The lack of higher gain and low efficiency problem for single element can be eradicated with the usage of DRA. Various shapes of DRA along with feeding arrangements have been explored in this state of art and it was concluded that RDRA offered a tremendous freedom in choosing the design parameters.

Multi-segmentation is the technique is used to enhance bandwidth with sustainable gain characteristics. In this research work, dielectric segment is loaded by another dielectric segment thus making it a stacked structure. In this research work, a multi segment coaxial feed rectangular DRA is demonstrated with four segments. This antenna can be considered as a promising alternative for antennas applied at X and Ku band frequency operations. Impedance bandwidth of 37.5% is achieved when no segment is inserted in rectangle DRA. Four segments with different dielectric permittivity are added which yields an impedance bandwidth of 91.89%. Hence, Multi segmentation provides relative increment of 145% in bandwidth of RDRA.

Defected ground structure bandwidth is applied to increase bandwidth and reduce size of the antenna. Combination of wide band annular patch with narrow band DRA yields relative size reduction of 19% and bandwidth increment of 76%. Impedance bandwidth of 95%, peak efficiency of 90 % and peak gain of 5.1 dB is a achieved through this design.

Reconfigurability is a desirable attribute in antenna system which changes radiation properties of antenna. In this research work, Liquid Assisted Antenna is simulated and analyzed. Chemical and physical property of water are investigated in this antenna. Magneto hydrodynamic antenna is proposed with polypropelene tube filled with air, plain water and NaCl added water. A multiband antenna with frequency tunability is obtained with this design. When simple water is taken as fluid element, an UWB antenna with frequency range of 18.5-34 GHz is achieved. With the addition of NaCl makes this antenna multiband resonating at frequencies at 6 GHz, 11.85 GHz, 18 GHz and 22 GHz.

Evolution of Ultra Wide Band Technology has spiked up the problem of electromagnetic interference in free bands such as Wi-Fi and WLAN wireless systems. These interferences decreases performance of UWB system and requires filtration process. Integration of filter in UWB system yields cost and complexity of the system. In this research work, an UWB trishool shaped patch antenna is implemented which

provides an impedance bandwidth of 119%. With the inclusion of dielectric slab produces two band notches at 3.8-4.4 GHz and 5.2-5.8 GHz respectively.

Graphene based tunability is achieved with UWB nano antenna for THz frequencies. An UWB antenna implemented provides a bandwidth of 119.86%. Application of graphene based nano ribbons provides tunable band notches at 5.02-5.52 THz and 12.16-13.34 THz. These notches can be tuned by changing chemical potential of the graphene.

Hybridization combines effervescent qualities of Microstrip Patch and Dielectric Resonator antenna. In this research work, hybridization of multiple ring circular patch antenna is done with RRDRA. Hybridization of both resonators is simulated get a peak efficiency of 95%. High Impedance bandwidth of 94.1% is achieved with this technique. In comparison of simple DRA, hybridization of DRA and patch provides a relative size reduction of 10% and relative bandwidth enhancement of 82%.

Feeding Mechanism have a great impact on antenna's characteristics. A symmetrical L-stub feed along with partial ground structure is implemented in DRA design. An impedance bandwidth of 67% with 99% peak efficiency is achieved through this design. Relative size reduction of 20% and Bandwidth increment of 70 % is achieved through this design.

6.2 FUTURE SCOPE

In this research work, Bandwidth Enhancement, Size Reduction and Reconfigurable techniques have been studied and implemented in Dielectric Resonator Antennas. Further aspects of this work can be comprehended with the following points for better understanding of the applications of Dielectric Resonator Antenna.

Future prospect of designed DRA in the proposed research work can be helpful in the territory of various microwave communication devices as well as modern wireless technologies deliberate for ultra fast short range and UWB communication systems.

Rectangular geometry have been explored in this work for Bio-Medical applications. Further, more geometrical patterns within realm of rectangle geometry can be traversed to enhance characteristics of antenna in health domain only.

Presented work has been focused on GHz frequency range. Tera Hertz (THz) regime (0.1 -30 THz) can be explored for future applications of DRA's. Absence of

metallic parts in DRA make it a favorable component of wireless industry for THz frequency range.

Re-configurability of antenna has been achieved in this work either by using grapheme on microstrip and by using fluid in MHD antenna. This very concept will be extremely rewarding with DRA in THz frequency range. Graphene based, finite size millimeter wave antennas and additional microwave circuits intended for some specific purposes like NFC, Bluetooth, Wi/max, WLAN, 5G etc. Apart from these various other properties of dielectric resonators like ferrite structure, FSS enclosures, array configurations, and higher dielectric constants can be utilized for the design of antennas applicable in biomedical spheres.

Meta Materials are synthetic man made materials which paves path for realistic materials with strong chirality, perfectly absorbing metamaterials, and low index metamaterials that are excellent for beam-forming applications. These materials can be used in combination with DRA to enhance gain, band width and reduction in size of the device implemented.

Multiple Input Multiple Output (MIMO) signifies new ways of providing high data transfer rates. Presented research work can be extended in implementing MIMO structures in DRA.

REFERENCES

[1] A. Petosa, “Dielectric Resonator Antenna Handbook” Artech House, 2007.

[2] Kwai Man Luk, K. W. Leung, “Dielectric Resonator Antennas” Research Studies Press, 2003.

[3] Roger .F. Harington, “Time-Harmonic Electromagnetic Fields” Wiley, 2001.

[4] Constantine A. Balanis, “Antenna Theory: Analysis and Design” Wiley, 1996.

[5] D.M. Pozar, “Microwave engineering 4th Edition” John Wiley & Sons 2012.

[6] Jean Van Bladel, “The Excitations of dielectric resonators of very high permittivity”, IEEE trans. Vol. MTT-23, No.2, pp. 199-208, February 1975.

[7] Jean Van Bladel,” The Excitations of dielectric resonators of very high permittivity”, IEEE trans. Vol. MTT-23, No.2, pp. 208-218, February 1975.

[8] Allen W. Glisson, Darko Kajfez, and Joseph James,“ Evaluation of modes in Dielectric resonator using a surface integral equation formulation”, IEEE trans. MTT, Vol. MTT-31, No. 12, pp. 1023-1029, December 1983.

[9] R.K.Mongia, Prakash Bhartia, “ Dielectric Resonator Antennas - A review and general design relations for resonant frequencies and bandwidth,” International journal of microwave and millimeter wave computer aided engineering, John-Wiley & sons Inc., Vol. 4, No. 3, pp. 230-247, July 1994.

[10] K. M. Luk, W. K. Leung, and K. W. Leung, “Mutual Impedance of Hemispherical Dielectric Resonator Antennas,” IEEE Transactions on Antennas and Propagation, Vol. 42, No. 12, pp. 1652–1654, December 1994.

[11] X.S Fang, K.W. Leung, “Designs of single-, dual-, Wide-band rectangular Dielectric resonator antennas,” IEEE Transaction on Antenna and Propagation, Vol.59, No.6, pp. 2409-2414, June 2011.

[12] R.K. Mongia and A. Ittipiboon, “Theoretical and experimental investigations on rectangular dielectric resonator antennas,” IEEE Transactions on Antennas and Propagation, Vol. 45, No. 9, pp. 1348–1356, September 1997.

[13] R.K. Mongia, P. Bhartia, C. L. Larose, and S. R. Mishra, “Accurate Measurement of Q-Factors of Isolated Dielectric Resonators,” IEEE Transactions Microwave Theory and Techniques, vol. 42, no. 8, pp. 1463–1467, 1994.

[14] M. Luk, K. W. Leung, and E. K. N. Yung, “Hemispherical dielectric resonator antenna with a concentric conductor,” IEEE Antennas and Propagation Society International Symposium, 2002.

[15] K.Y. Chow, K.W. Leung, K. M. Luk AND E.K.N. Yung, " Cylindrical Dielectric Resonator Antenna Array", Electronics Letters, Vol. 31, no. 18, pp. no. 1536-1537 , 1995.

[16] Aldo Petosa, Apisak Ittipiboon, Y.M.M. Antar, D.Coscoe, M. Cuhachi, "Recent advancements in DRA technology" IEEE Antennas and Magazine, Vol. 40, No. 3, pp. 35 -48, June 1998.

[17] M. Verplanken and J. van Bladel, "The Magnetic-Dipole Resonances of Ring Resonators of Very High Permittivity," IEEE Trans. Microw. Theory Tech., vol. 27, no. 4, pp. 328–333, 1979, doi: 10.1109/TMTT.1979.1129624.

[18] A. Ittipiboon and R. M. Dave Roscoe, Aldo Petosa, "United States Patent (19) Slot in Ground Plane L-3 thing," no. 19, 1999.

[19] A. Petosa, N. Simons, R. Siushansian, A. Ittipiboon, and M. Cuhaci, "Design and analysis of multisegment dielectric resonator antennas," IEEE Trans. Antennas Propag., vol. 48, no. 5, pp. 738–742, 2000, doi: 10.1109/8.855492.

[20] Y.-F. Ruan, Y.-X. Guo, and X.-Q. Shi, "Wideband dielectric resonator antenna," Microwave and Optical Technology Letters, vol. 48, No. 2, pp. 222- 226, February 2006.

[21] C. S. De Young and S. A. Long, "Wideband Cylindrical and Rectangular Dielectric Resonator Antennas," Antennas and Wireless Propagation Letters, IEEE, vol. 5, pp. 426-429, October 2006.

[22] G. Yuan, O. Ban-Leong, E. Wei-Bin, and A. P. Popov, "A compact wideband hybrid dielectric resonator antenna," Microwave and Wireless Components Letters, IEEE, vol. 16, No. 4, pp. 227-229, April 2006.

[23] X. L. Liang, T. A. Denidni, and L. N. Zhang, "Wideband L-shaped dielectric resonator antenna with a conformal inverted-trapezoidal patch feed," IEEETransaction Antennas Propagation, vol. 57, no. 1, pp. 271–273, January 2009.

[24] T. H. Chang and J. F. Kiang, "Dualband split dielectric resonator antenna," IEEE Transactions on Antennas and Propagation, vol. 55, No. 11 , pp. 3155–3162, November 2007.

[25] M. Chauhan, A. K. Pandey, and B. Mukherjee, "A Novel Compact Cylindrical Dielectric Resonator Antenna for Wireless Sensor Network Application," IEEE Sensors Letter, Vol. 2, No. 2, pp. 1 – 4, June 2018.

[26] Y. M. Pan and S. Y. Zheng, “A Low-Profile Stacked Dielectric Resonator Antenna with High-Gain and Wide Bandwidth,” IEEE Antennas Wireless and Propagation Letter, vol. 15, pp. 68–71, 2016.

[27] M. Abedian, S. K. A. Rahim, and M. Khalily, “Two-segments compact dielectric resonator antenna for UWB application,” IEEE Antennas and Wireless Propagation Letter, vol. 11, pp. 1533–1536, 2012.

[28] R. Ghosal and B. Gupta, “Design of reconfigurable band notched Ultra Wide Band (UWB) stacked DRA using metamaterial structure,” 2015 Int. Conf. Work. Comput. Communication IEMCON 2015, no. Table I, pp. 1–3, 2015.

[29] D. Sankaranarayanan, D. Venkatakiran, and B. Mukherjee, “Compact bi-cone dielectric resonator antenna for ultra-wideband applications–a novel geometry explored,” Electromagnetics, vol. 37, no. 7, pp. 471–481, 2017.

[30] S. Fakhte, H. Oraizi, and L. Matekovits, “Gain improvement of rectangular dielectric resonator antenna by engraving grooves on its side walls,” IEEE Antennas and Wireless Propagation Letters, vol. 16, pp. 2167–2170, 2017.

[31] S. Fakhte, H. Oraizi, and L. Matekovits, “High gain rectangular dielectric resonator antenna using uniaxial material at fundamental mode,” IEEE Transaction on Antennas and Propagation, vol. 65, no. 1, pp. 342–347, January 2017.

[32] U.Ullah et al., “A novel multi-permittivity cylindrical dielectric resonator antenna for wideband applications,” Radioengineering, vol. 23, no. 4, pp. 1071–1076, 2014.

[33] P.Rezaei, , M.Hakkak,and K Forooraghi,.,"Design of Wide-Band Dielectric Resonator Antenna With a Two-Segment Structure." Progress In Electromagnetics Research, Vol. 66, pp. 111–124, 2006.

[34] L. Z. Thamae and Z. Wu, “Broadband bowtie dielectric resonator antenna,” IEEE Transactions on Antennas and Propagations, Vol. 58, No. 11, pp. 3707–3710, November 2010.

[35] Y. Ge, K. P. Esselle, and T. S. Bird, “Compact dielectric resonator antennas with ultrawide 60%-110% bandwidth,” IEEE Transactions on Antennas and Propagation, Vol. 59, No. 9, pp. 3445–3448, September 2011.

[36] Y. Yang, F. Gao, H. Ma, X. Shi, and X. Li, “A Compact Dielectric Resonator Antenna Excited by a Planar Monopole Patch for Wideband Applications,”

International Journal of Antennas and Propagation, Hindawi, Vol. 2016, pp. 1–9, 2016.

[37] C. E. Zebiri, “Offset Aperture-Coupled Double-Cylinder Dielectric Resonator Antenna with Extended Wideband,” IEEE Transactions on Antennas and Propagation, Vol. 65, No. 10, pp. 5617–5622, October 2017.

[38] R. K. Chaudhary, H. B. Baskey, K. V. Srivastava, and A. Biswas, “Synthesis and microwave characterisation of (Zr0.8Sn0.2)TiO4–epoxy composite and its application in wideband stacked rectangular dielectric resonator antenna,” IET Microwaves, Antennas Propagation, Vol. 6, No. 7, pp. 740, 2012.

[39] A. A. Kishk, X. Zhang, A. W. Glisson, and D. Kajfez, “Numerical analysis of stacked dielectric resonator antennas excited by a coaxial probe for wideband applications,” IEEE Transactions on Antennas and Propagation, vol. 51, no. 8, pp. 1996–2006, August 2003.

[40] A. A. Kishk, “Experimental study of broadband embedded dielectric resonator antennas excited by a narrow slot,” IEEE Antennas and Wireless Propagation Letters, Vol. 4, No. 1, pp. 79 – 81, 2005.

[41] A. Buerkle, K. Sarabandi, and H. Mosallaei, “Compact slot and dielectric resonator antenna with dual-resonance, broadband characteristics,” IEEE Transactions on Antennas and Propagation, vol. 53, no. 3, pp. 1020–1027, 2005.

[42] A. G. Walsh, C. S. De Young, and S. A. Long, “An investigation of stacked and embedded cylindrical dielectric resonator antennas,” IEEE Antennas and Wireless Propagion Letters, vol. 5, no. 1, pp. 130–133, 2006.

[43] R. K. Mongia, “Half Split Dielectric Resonator placed on metallic plane for antenna applications,” vol. 25, no. 7, pp. 462–464, 1989.

[44] Y. M. M. Antar and M. Cuhaci, “A Half-Split Cylindrical Dielectric Resonator Antenna Using Slot-Coupling,” IEEE Microw. Guid. Wave Lett., vol. 3, no. 2, pp. 38–39, 1993, doi: 10.1109/75.196034.

[45] M. T. K. Tarn and R. D. Murch, “Compact circular sector and annular sector dielectric resonator antennas,” IEEE Trans. Antennas Propag., vol. 47, no. 5, pp. 837–842, 1999, doi: 10.1109/8.774138.

[46] A. Kishk, A W. Glisson, G. P. Junker, W. M. Ave, and E. Segundo, “Cylindrical Dielectric Resonator Antennas,” Electr. Eng., pp. 97–118, 2001.

[47] D. Guha and Y. M. M. Antar, “Four-element cylindrical dielectric resonator antenna for wideband monopole-like radiation,” IEEE Trans. Antennas Propag., vol. 54, no. 9, pp. 2657–2662, 2006, doi: 10.1109/TAP.2006.880766.

[48] D. Guha, B. Gupta, C. Kumar, and Y. M. M. Antar, “Segmented hemispherical DRA: New geometry characterized and investigated in multi-element composite forms for wideband antenna applications,” IEEE Trans. Antennas Propag., vol. 60, no. 3, pp. 1605–1610, 2012, doi: 10.1109/TAP.2011.2180345.

[49] Pinku Ranjan and R. K. Gangwar, “Probe Feed Multi-Element Multi-Segment Triangular Dielectric Resonator Antenna with RCS Analysis,” J. Circuits, Syst. Comput., vol. 28, no. 12, pp. 1–18, 2019, doi: 10.1142/S0218126619502086.

[50] F. Wang, C. Zhang, H. Sun, and Y. Xiao, “Ultra-Wideband Dielectric Resonator Antenna Design Based on Multilayer Form,” Int. J. Antennas Propag., vol. 2019, 2019, doi: 10.1155/2019/4391474.

[51] A. K. Roy and S. Basu, “Broadband, high gain, narrow width rectangular dielectric resonator antenna with air gap,” J. Electron. Sci. Technol., vol. 17, no. 1, pp. 90–96, 2019, doi: 10.11989/JEST.1674-862X.70728079.

[52] Pinku Ranjan and R. K. Gangwar, “Investigation of wideband multi-element multi-segment half-sectored cylindrical dielectric resonator antenna for wireless applications,” Prog. Electromagn. Res. C, vol. 100, no. January, pp. 31–43, 2020, doi: 10.2528/pierc20010202.

[53] R. Garg, I.Bahl and M. Buzzi,"Microstrip Lines and Strip Lines" Artech House 2013.

[54] J. G.Webster "Wiley Encyclopedia of Electrical and Electronics Engineering" John Wiley & Sons, Hoboken, NJ, USA, 2001, 2013.

[55] M. K. Khandelwal, B. K. Kanaujia, and S. Kumar, “Defected ground structure: Fundamentals, analysis, and applications in modern wireless trends,” Int. J. Antennas Propag., vol. 2017, 2017, doi: 10.1155/2017/2018527.

[56] J. I. Park, J.Kim, J.S.Park, Y.Qian, D. Ahn, T. Itoh “Modeling of a photonic bandgap and its application for the low-pass filter design,” Asia-Pacific Microw. Conf. Proceedings, APMC, vol. 2, pp. 331–334, 1999, doi: 10.1109/apmc.1999.829865.

[57] S. Shi, W. W. Choi, W. Che, K. W. Tam, and Q. Xue, “Ultra-wideband differential bandpass filter with narrow notched band and improved common-

mode suppression by DGS," IEEE Microw. Wirel. Components Lett., vol. 22, no. 4, pp. 185–187, 2012, doi: 10.1109/LMWC.2012.2187885.

[58] J. S. Lim, C. S. Kim, Y. T. Lee, D. Ahn, and S. Nam, "A spiral-shaped defected ground structure for coplanar waveguide," IEEE Microw. Wirel. Components Lett., vol. 12, no. 9, pp. 330–332, 2002, doi: 10.1109/LMWC.2002.803208.

[59] J. Y. Jan and J. W. Su, "Bandwidth enhancement of a printed wide-slot antenna with a rotated slot," IEEE Trans. Antennas Propag., vol. 53, no. 6, pp. 2111–2114, 2005, doi: 10.1109/TAP.2005.848518.

[60] Y. Sung, "Bandwidth enhancement of a microstrip line-fed printed wide-slot antenna with a parasitic center patch," IEEE Trans. Antennas Propag., vol. 60, no. 4, pp. 1712–1716, 2012, doi: 10.1109/TAP.2012.2186224.

[61] K. Y. and J. P. Xu, "Compact ultra-wideband antenna with dual bandstop characteristic," Electron. Lett., vol. 41, no. 2, pp. 40–41, 2005, doi: 10.1049/el.

[62] M. Abdollahvand, G. R. Dadashzadeh, and H. Ebrahimian, "Compact band-rejection printed monopole antenna for UWB application," IEICE Electron. Express, vol. 8, no. 7, pp. 423–428, 2011, doi: 10.1587/elex.8.423.

[63] M. Abedian, S. K. A. Rahim, S. Danesh, S. Hakimi, L. Y. Cheong, and M. H. Jamaluddin, "Novel design of compact UWB dielectric resonator antenna with dual-band-rejection characteristics for WiMAX/WLAN bands," IEEE Antennas and Wireless Propagation Letters, vol. 14, pp. 245–248, September 2015.

[64] P. Kshirsagar, S. Gupta, and B. Mukherjee, "A two-segment rectangular dielectric resonator antenna for ultra-wideband application," Electromagnetics, vol. 38, no. 1, pp. 20–33, 2018.

[65] P. Kshirsagar, S. Gupta, and B. Mukherjee, "Novel design of conformal-strip excited asymmetrical rectangular dielectric resonator antenna for ultra-wide band application," Journal of Microwave Power Electromagnetic Energy, vol. 52, no. 2, pp. 128–141, 2018.

[66] P. Sharma, A. Vaish, and R. S. Yaduvanshi, "The design of a turtle-shaped dielectric resonator antenna for ultrawide-band applications," J. Comput. Electron., vol. 18, no. 4, pp. 1333–1341, 2019, doi: 10.1007/s10825-019-01374-8.

[67] S. K. Yadav, A. Kaur, and R. Khanna, "An ultra wideband 'OM' shaped DRA with a defected ground structure and dual polarization properties for 4G/5G

wireless communications," Int. J. RF Microw. Comput. Eng., vol. 30, no. 8, pp. 1–18, 2020, doi: 10.1002/mmce.22327.

[68] G. Kaur and A. Kaur, "Monostatic radar-based microwave imaging of breast tumor detection using a compact cubical dielectric resonator antenna," Microw. Opt. Technol. Lett., no. January, pp. 1–9, 2020, doi: 10.1002/mop.32557

[69] Alireza Motevasselian, Anders Ellgardt, and B. L. G. Jonsson , " A Circularly Polarized Cylindrical Dielectric Resonator Antenna Using a Helical Exciter" IEEE Transactions on Antennas and Propagation, vol. 61, no. 3, pp. 1439 -1443, March 2013.

[70] Wei Wei Li, Kwok Wa Leung, "Omnidirectional Circularly Polarized Dielectric Resonator Antenna With Top-Loaded Alford Loop for Pattern Diversity Design," IEEE Transactions on Antennas and Propagation, vol. 61, no. 8, pp. 4246 - 4256. August 2013.

[71] L. C. Y. Chu, D. Guha, and Y. M. M. Antar, "Conformal strip-fed shaped cylindrical dielectric resonator: Improved design of a wideband wireless antenna," IEEEAntennas Wireless Propagation Letters, vol. 8, pp. 482–485, March 2009.

[72] T. A. Denidni, Q. Rao, and A. R. Sebak, "Broadband L-shaped dielectric resonator antenna," IEEE Antennas Wireless Propagation Letter, Vol. 4, no. 1, pp. 453–454, December 2005.

[73] Y. Gao, Z. Feng, and L. Zhang, "Compact Asymmetrical T-Shaped Dielectric Resonator," IEEE Transactions on Antenna and Propagation,Vol. 60, No. 3, pp. 1611–1615, March 2012.

[74] Y. Gao, Z. Feng, and L. Zhang, "Compact Asymmetrical T-Shaped Dielectric Resonator," IEEE Transactions on Antenna and Propagation,Vol. 60, No. 3, pp. 1611–1615, March 2012.

[75] S. Maity and B. Gupta, "Experimental Investigations on Wideband Triangular Dielectric Resonator Antenna," IEEE Transactions on Antennas an Propagation, vol. 64, no. 12, pp. 5483–5486, December 2016.

[76] R. K. Chaudhary, S. Member, and R. Kumar, "Wideband Ring Dielectric Resonator Antenna with annular shaped microstrip feed," IEEE Antennas and Wireless propagation letters, vol. 12, pp. 595–598, April 2013.

[77] K. S. Ryu and A. A. Kishk, "UWB Dielectric Resonator Antenna having consistent omnidirectional pattern and low Cross polarization Characteristics,"

IEEE Transactions on Antennas Propagation, Vol. 59, No. 4, pp. 1403–1408, April 2011.

[78] Sabouni and A. A. Kishk, "Dual-polarized, broadside, thin dielectric resonator antenna for microwave imaging," IEEE Antennas and Wireless Propagation Letters, Vol. 12, pp. 380 –383, March 2013.

[79] P. Singhal, B. Dhaniram, and S. Banerjee, "A stacked square patch slotted broadband microstrip antenna," J. Microwaves Optoelectron. (JMOE), Vol. 3, No. 2, pp. 60 – 66, 2003.

[80] F. Elmegri, A. H. Majeed, K. H. Sayidmarie, J. M. Noras, A. S. Abdullah, and R. A. Abd-Alhameed, "Compact Dielectric Resonator Antenna With Band-Notched Characteristics for Ultra-Wideband Applicationnss," Progress in Electromagnetics Research C, Vol. 57, pp. 137–148, 2015.

[81] X. S. Fang, K. W. Leung, E. H. Lim, and R.S. Chen, "Compact Differential Rectangular Dielectric Resonator Antenna," IEEE Antennas and Wireless Propagation Letters, Vol. 9, pp. 662–665, July 2010.

[82] A. H. Majeed, A. S. Abdullah, K. H. Sayidmarie, R. A. Abd-Alhameed, J. M. Noras, and F. Elmegri, "Balanced dual-segment cylindrical dielectric resonator antennas for ultra-wideband applications," IET Microwaves, Antennas Propagation, Vol. 9, No. 13, pp. 1478 – 1486, 2015.

[83] S. Pahadsingh and S. Sahu, "Planar UWB integrated with multi narrowband cylindrical dielectric resonator antenna for cognitive radio application," AEU - Int. J. Electronics and Communication, Vol. 74, pp. 150 – 157, 2017.

[84] Z. Weng, X. Wang, Y. Jiao and F.Zhang, "Wideband Rectangular Dielectric Resonating Antenna[DRA] with slot/fed design", Progress In Electromagnetics Research Letters, Vol. 16, 181–190, Vol. 16, pp. 181–190, August 2010.

[85] R. N. Simons and R. Q. Lee, "Effect of parasitic dielectric resonators on CPW/aperture-coupled dielectric resonator antennas," IEE Proceedings H Microwaves, Antennas Propagation, Vol. 140, No. 5, pp. 336 - 338, 1993.

[86] A. Lambrecht, O. Oestreich, J. Pontes, and W. Wiesbeck, "Dielectric resonator antennas for polarization diversity in base station array applications," 2007 Int. Conf. Electromagn. Adv. Appl. ICEAA'07, pp. 527–530, 2007.

[87] A. Sharma, G. Das, P. Ranjan, N. K. Sahu, and R. K. Gangwar, "Novel Feeding Mechanism to Stimulate Triple Radiating Modes in Cylindrical Dielectric Resonator Antenna," IEEE Access, Vol. 4, pp. 9987–9992, November 2016.

[88] Xian-Ling Liang and Tayeb A. Denidni, “Wideband Rectangular Dielectric Resonator Antenna With a Concave Ground Plane,” Electromagnetics, Vol. 35, No. 5, pp. 355–363, 2015.

[89] X. S. Fang, K. W. Leung, and R. S. Chen, “On the wideband notched rectangular dielectric resonator antenna,” International Workshop on Antenna Technology (iWAT) 2011.

[90] D. Guha, B. Gupta, and Y. M. M. Antar, “New pawn-shaped dielectric ring resonator loaded hybrid monopole antenna for improved ultrawide bandwidth,” IEEE Antennas and Wireless Propagation Letters, Vol. 8, pp. 1178–1181, October 2009.

[91] Dong, L. Xu, W. Lin, and T. Zhang, “A Compact Wide-Band Hybrid Dielectric Resonator Antenna with Enhanced Gain and Low Cross-Polarization,” Int. J. Antennas Propag., vol. 2017, 2017

[92] U. Ullah , M.F.Ain, M.Othman, I.A.Zubir, N.H.Mahyuddin, Z.A.Ahmad, M.Z. Abdullah., “A novel multi-permittivity cylindrical dielectric resonator antenna for wideband applications,” Radioengineering, vol. 23, no. 4, pp. 1071–1076, 2014.

[93] Guha, A. Banerjee, C. Kumar, and Y. M. M. Antar, “New technique to excite higher-order radiating mode in a cylindrical dielectric resonator antenna,” IEEE Antennas Wireless and Propagation Letters, Vol. 13, pp. 15–18, January 2014.

[94] K. W. Leung and C. K. Leung, “Wideband dielectric resonator antenna excited by cavity-backed circular aperture with microstrip tuning fork,” Electronic Letters, Vol. 39, No. 14, pp. 1033, July 2003.

[95] S. K. Menon, B. Lethakumary, P. Mohanan, P. V. Bijumon, and M. T. Sebastian, “Wideband cylindrical dielectric resonator antenna excited using an L-strip feed,” Microwave and Optical Technology Letters, Vol. 42, No. 4, pp. 293–294, June 2004.

[96] M. A. Saed and R. Yadla, “Microstrip - Fed Low Profile and Compact Dielectric Resonator Antennas,” Progress in Electromagnetics Research., Vol. 56, pp. 151–162, 2006.

[97] R.M. Hashmi, B. A. Zeb, and K. P. Esselle, “Wideband high-gain EBG resonator antennas with small footprints and all-dielectric superstructures,” IEEE Transactions on Antennas and Propagation, Vol. 62, No. 6, pp. 2970–2977, June 2014.

[98] A.A. Kishk, Y. Yin, and A. W. Glisson, “Conical dielectric resonator antennas for wide-band applications,” IEEE Transactions on Antennas and Propagation, Vol. 50, No. 4, pp. 469–474, April 2002.

[99] V.Gupta, S. Sinha, S. K. Koul, and B. Bhat, “Wideband dielectric resonator-loaded suspended microstrip patch antennas,” Microwave and Optical Technology Letters, vol. 37, no. 4, pp. 300–302, 2003.

[100] Yuan Gao, Chee-Parmg Chua, Alexandre P. Popov, and Ban-Leong ,'Integrated Wideband Rectangular Dielectric Resonator Antenna for WLAN', IEEE Antennas and Propagation Society International Symposium, 2005.

[101] D. Lee, A. Petosa, D. Guha, Y. M. M. Antar, and A. Ittipiboon, “Improved Design Guidelines for the Ultra Wideband Monopole-Dielectric Resonator Antenna,” IEEE Antennas and Wireless Propagation Letters, vol. 5, pp. 373–376, 2006.

[102] R.K. Mongia,"Novel Electric-Monopole mode dielectric resonator antenna", IEEE Antennas and Propagation Society International Symposium, 1996.

[103] A.V. P. Kumar, V. Hamsakutty, J. Yohannan, and K. T. Mathew, “ A Wideband Conical Beam Cylindrical Dielectric Resonator Antenna,” IEEE Antennas and Wireless Propagation Letters, Vol. 6, pp. 15 - 17, July 2007.

[104] E. H. Lim and K. W. Leung, “Novel utilization of the dielectric resonator antenna as an oscillator load,” IEEE Transactions on Antennas and Propagation, Vol. 55, No. 10, pp. 2686–2691, 2007.

[105] R.N.Simons, and R.Q Lee, “Effect of parasitic Dielectric Resonators on CPW-Aperture-coupled Dielectric Resonator Antenna” IEE proceedings H- Microwave Antennas and Propagation,vol. 140, no.5, 1993.

[106] R. K. Mongia,“Resonant frequency of Cylindrical Dielectric Resonator placed in MIC Environments,” IEEE Transactions Microwave Theory and Techniques, vol. 38, no. 6, pp. 802-804, June 1990.

[107] Sreekantan, Y. K. Ling, and Z. A. Ahmad, “Simulation and Experimental Investigators on Rectangular, Circular and Cylindrical Dielectric Resonator Antenna,” Progress in Electromagnetics Research C, Vol. 7, pp. 151–166, 2009.

[108] H. A. E. Malhat, S. Zainud-deen, N. El-Shalaby, and K. Awadalla, “Dielectric Resonator Antenna Mounted on Cylindrical Ground Plane for Handheld RFID Reader at 5.8 GHz,” Advanced Electromagnetics, vol. 1, no. 3, p. 71, 2012

[109] Wael M. Abdel-Wahab, SafieddinSafavi-Naeini, Dan Busuioc, “ Modelling and Design of Millimetre-Wave High Q-Factor Parallel Feeding Scheme for

Dielectric Resonator Antenna Arrays," IEEE Antennas and Wireless Propagation letters, Vol. 10, pp. 53 - 55, January 2011.

[110] Mohammad Ranjbar Nikkhah, J. Rashed-Mohassel, and Ahmed A. Kishk," Compact Low-Cost Phased Array of Dielectric Resonator Antenna Using Parasitic Elements and Capacitor Loading," IEEE Transactions on Antennas and Propagation, vol. 61, no. 4, pp. 2318 - 2321, April 2013.

[111] Mohammad Ranjbar Nikkhah, J. Rashed-Mohassel, and Ahmed A. Kishk, "High-Gain Aperture Coupled Rectangular Dielectric Resonator Antenna Array Using Parasitic Elements," IEEE Transactions on Antennas and Propagation, Vol. 61, no. 7, pp. 3905 - 3908, July 2013.

[112] J. S. Wight, A. Petosa, R. K. Mongia, and A. Ittipiboon, "Design of microstrip-fed series array of dielectric resonator antennas," Electronics Letters, Vol. 31, No. 16, pp. 1306–1307, August 1995.

[113] R. Larose, A. Ittipiboon, and M. Cuhaci, "Microstrip-fed array of multisegment Dielectric Resoator Antennas,"IEE Proceedings-microwave antennas propagations, vol. 144, no. 6, December 1997.

[114] A. S. Al-Zoubi, A. A. Kishk, and A. W. Glisson, "Aperture coupled rectangular dielectric resonator antenna array fed by dielectric image guide," IEEE Transactions on Antennas and Propagation, Vol. 57, No. 8, pp. 2252–2259, August 2009.

[115] K. W. Leung, H. Y. Lo, K. M. Luk, and E. K. N. Yung, "Two-dimensional cylindrical dielectric resonator antenna array," Electronics Letters, vol. 34, no. 13, pp. 1283 - 1285, June 1998.

[116] K.Y. Chow, K.W. Leung, K. M. Luk AND E.K.N. Yung, " Cylindrical Dielectric Resonator Antenna Array", Electronics Letters, Vol. 31, no. 18, pp. no. 1536-1537 , 1995.

[117] Petosa, R. K. Mongia, A. Ittipiboon, and J. S. Wight, "Investigation of various feed structures for linear arrays of dielectric resonator antennas," IEEE Antennas and Propagation Society International Symposium, 2002

[118] G. DROSSOS, Z.Wu and L.E.Davis "Two-Element End Fire Dielectric Resontor Antenna Array" Electronics letters,Vol. 32, no. 7, pp. 618-619, 1996.

[119] Bernhard, J.T., "Reconfigurable Antennas" Morgan & Claypool Publishers: San Rafael, CA, USA, 2007.

[120] C. G. Christodoulou, Y. Tawk, S. A. Lane, and S. R. Erwin, “Reconfigurable Antennas for Wireless and Space Applications” Ieee, vol. 100, no. 7, pp. 2250–2261, 2012.

[121] Daniel H. Schaubert, “Microstrip Antennas,” Electromagnetics, vol. 12, no. 3–4, pp. 381–401, 1992, doi: 10.1109/9780470545270.

[122] N. O. Parchin, H. J. Basherlou, Y. I. A. Al-Yasir, R. A. Abd-Alhameed, A. M. Abdulkhaleq, and J. M. Noras, “Recent developments of reconfigurable antennas for current and future wireless communication systems,” Electron., vol. 8, no. 2, pp. 1–17, 2019, doi: 10.3390/electronics8020128.

[123] N. Kumar, P. Kumar, and M. Sharma, “Reconfigurable Antenna and Performance Optimization Approach,” Wirel. Pers. Commun., vol. 112, no. 4, pp. 2187–2212, 2020, doi: 10.1007/s11277-020-07145-0.

[124] N. O. Parchin, H. J. Basherlou, Y. I. A. Al-Yasir, A. M. Abdulkhaleq, and R. A. Abd-Alhameed, “Reconfigurable antennas: Switching techniques— a survey,” Electron., vol. 9, no. 2, 2020, doi: 10.3390/electronics9020336.

[125] E. Motovilova and S. Y. Huang, “A review on reconfigurable liquid dielectric antennas,” Materials (Basel)., vol. 13, no. 8, pp. 1–28, 2020, doi: 10.3390/MA13081863.

[126] Tang and J. X. Chen, “Microfluidically Frequency-Reconfigurable Microstrip Patch Antenna and Array,” IEEE Access, vol. 5, pp. 20470–20476, 2017, doi: 10.1109/ACCESS.2017.2756638

[127] Rajveer S Yaduvanshi and Harish Parthasarathy, “Design, Development and Simulations of MHD Equations with its proto type implementations”(IJACSA) International Journal of Advanced Computer Science and Applications,Vol. 1, No. 4, October 2010.

[128] Rajveer S Yaduvanshi and Harish Parthasarathy, “EM Wave transport 2D and 3D investigations” (IJACSA) International Journal of Advanced Computer Science and Applications,Vol. 1, No. 6, December 2010.

[129] Rajveer S Yaduvanshi and Harish Parthasarathy, “Exact solution of 3D Magnetohydrodynamic system with nonlinearity analysis” Jan 2011, IJATIT

[130] Debab Mohamed, and Mahdjoub Zoubir ,” Single Band Notched Characteristics UWB Antenna using a Cylindrical Dielectric Resonator and U-shaped Slot, ” J. Microwave. Optoelectronics. Electromagnetics. Appl. vol.17 no.3 July/Sept. 2018.

[131] P. Singhal, B. Dhaniram, and S. Banerjee, “A stacked square patch slotted broadband microstrip antenna,” J. Microwaves Optoelectron. (JMOE), Vol. 3, No. 2, pp. 60 – 66, 2003.

[132] M. Y. Abou Shahine, M. Al-Husseini, K. Y. Kabalan, and A. El-Hajj, “Dielectric Resonator Antennas With Band Rejection and Frequency Reconfigurability,” Progress in Electromagnetics Research C, Vol. 46, pp. 101–108, 2014.

[133] A. S. Al-Zoubi, A. A. Kishk, and A. W. Glisson, “Aperture coupled rectangular dielectric resonator antenna array fed by dielectric image guide,” IEEE Transactions on Antennas and Propagation, Vol. 57, No. 8, pp. 2252–2259, August 2009.

[134] A. Singh and S. K. Sharma, “Investigations on wideband cylindrical dielectric resonator antenna with directive radiation patterns and low cross polarization,” IEEE Transactions on Antennas and Propagation, Vol. 58, no. 5, pp. 1779–1783, June 2010.

[135] L. K. Hady, A. A. Kishk, and D. Kajfez, “Dual-band compact DRA with circular and monopole-like linear polarizations as a concept for GPS and WLAN applications,” IEEE Transactions on Antennas and Propagation, Vol. 57, No. 9, pp. 2591–2598, September 2009.

[136] M. Zou and J. Pan, “Investigation of Resonant Modes in Wideband Hybrid Omnidirectional Rectangular Dielectric Resonator Antenna,” IEEE Transactions on Antennas and Propagation, Vol. 63, No. 7, pp. 3272–3275, July 2015.

[137] S. Danesh, M. R. Kamarudin, T. A. Rahman, M. Abedian, and M. Khalily, “A wideband frequency reconfigurable rectangular dielectric resonator antenna,” 2016 10th Eur. Conf. Antennas Propagation, EuCAP 2016, pp. 2–5, 2016.

[138] G. O’Keefe and S. P. Kingsley, “Tunability of liquid dielectric resonator antennas,” IEEE Antennas Wirel. Propag. Lett., vol. 6, pp. 533–536, 2007, doi: 10.1109/LAWP.2007.907916.

[139] H. Huff, D. L. Rolando, P. Walters, and J. McDonald, “A frequency reconfigurable dielectric resonator antenna using colloidal dispersions,” IEEE Antennas Wirel. Propag. Lett., vol. 9, pp. 288–290, 2010, doi: 10.1109/LAWP.2010.2046613.

[140] C. X. Hao, B. Li, K. W. Leung, and X. Q. Sheng, “Frequency-tunable differentially fed rectangular dielectric resonator antennas,” IEEE Antennas

Wirel. Propag. Lett., vol. 10, pp884–887, 2011, doi: 10.1109/LAWP.2011.2165929.

[141] C. W. Tong, H. Tang, W. Qin, W. W. Yang, and J. X. Chen, "A Ku band frequency-reconfigurable dielectric resonator antenna using metallic pillars," Microw. Opt. Technol. Lett., vol. 62, no. 4, pp. 1760–1764, 2020, doi: 10.1002/mop.32227.

[142] J. Kosha, W. Mshwat, C.Zebiri, D.Shayad, I.Elfergani, Y.A.Yasir, A.Asharah, A.Ullah, R.A.Alhameed., "Reconfigurable dielectric resonator antenna for gsm, lte, and 5g applications," PervasiveHealth Pervasive Comput. Technol. Healthc., vol. 2, no. October, pp. 1013–1023, 2020, doi: 10.4108/eai.28-6-2020.2298076.

[143] J. C. Mierzwa, "Federal Communications Commission, First Report and Order, Revision of Part 15 of commission's Rule Regarding UWB Transmission System FCC 02–48. Washington, DC, USA; 2002

[144] S. Ullah, C. Ruan, M. S. Sadiq, T. Ul Haq, and W. He, "High efficient and ultra wide band monopole antenna for microwave imaging and communication applications," Sensors (Switzerland), vol. 20, no. 1, pp. 1–11, 2020, doi: 10.3390/s20010115.

[145] J. Park, M. Jeong, N. Hussain, S. Rhee, P. Kim, and N. Kim, "Design and fabrication of triple-band folded dipole antenna for GPS/DCS/WLAN/WiMAX applications," Microw. Opt. Technol. Lett., vol. 61, no. 5, pp. 1328–1332, 2019, doi: 10.1002/mop.31739.

[146] H. U. Bong, M. Jeong, N. Hussain, S. Y. Rhee, S. K. Gil, and N. Kim, "Design of an UWB antenna with two slits for 5G/WLAN-notched bands," Microw. Opt. Technol. Lett., vol. 61, no. 5, pp. 1295–1300, 2019, doi: 10.1002/mop.31670.

[147] V. Vashistha, M. V. Kartikeyan, J. Malik, and R. P. Maheshwari, "Analysis of ultra wide band dielectric resonator antenna with band notch for WLAN communication," 2014 IEEE Students' Conf. Electr. Electron. Comput. Sci. SCEECS 2014, vol. 1, pp. 14–16, 2014, doi: 10.1109/SCEECS.2014.6804499.

[148] Y. F. Wang, T. A. Denidni, Q. S. Zeng, and G. Wei, "Band-notched UWB rectangular dielectric resonator antenna," Electron. Lett., vol. 50, no. 7, pp. 483–484, 2014, doi: 10.1049/el.2014.0188.

[149] Y. Shao, Y. Ge, Y. Chen, and H. Zhang, "Compact Band-Notched Uwb Dielectric Resonator Antennas," Prog. Electromagn. Res. Lett., vol. 52, no. December 2014, pp. 87–92, 2015, doi: 10.2528/pierl14121906.

[150] U. A. Dash and S. Sahu, “UWB Dual-Band Notched Conical Dielectric Resonator Antenna with Improved Gain,” IETE J. Res., vol. 66, no. 5, pp. 643–653, 2020, doi: 10.1080/03772063.2018.1515672.

[151] B. Liu, J. Qiu, L. Chen, and G. Li, “Dual band-notched rectangular dielectric resonator antenna with tunable characteristic,” Electron., vol. 8, no. 5, pp. 1–9, 2019, doi: 10.3390/electronics8050472.

[152] A. I. Afifi, A. B. Abdel-Rahman, A. S. A. El-Hameed, A. Allam, and S. M. Ahmed, “Small Frequency Ratio Multi-Band Dielectric Resonator Antenna Utilizing Vertical Metallic Strip Pairs Feeding Structure,” IEEE Access, vol. 8, pp. 112840–112845, 2020, doi: 10.1109/ACCESS.2020.3002789.

[153] L. Novotny, “Optical Antennas: A New Technology that can Enhance Light-Matter Interactions,” Front. Eng., vol. 39, no. 4, pp. 100–120, 2012.

[154] A. Mohammadi, V. Sandoghdar, and M. Agio, “Gold, copper, silver and aluminum Nanoantennas to enhance spontaneous emission,” J. Comput. Theor. Nanosci., vol. 6, no. 9, pp. 2024–2030, 2009.

[155] S. Obayya, F. O. M. Hameed, N. Fayez Fahmy, and M. Hussein Abdelrazik, Optical Nano-Antennas for Energy Harvesting Salah, no. May 2018. 2015.

[156] A. Nourmohammadi and M. Nikoufard, “Ultra-Wideband Photonic Hybrid Plasmonic Horn Nanoantenna with SOI Configuration,” Silicon, pp. 2–7, 2019.

[157] Z. Wu and Y. Zheng, “Radiative Enhancement of Plasmonic Nanopatch Antennas,” Plasmonics, vol. 11, no. 1, pp. 213–222, 2016.

[158] F. H. L. Koppens, D. E. Chang, and F. J. G. De Abajo, “Graphene Plasmonics : A Platform for Strong LightÀMatter,” Nano Lett., vol. 11, no. 8, pp. 3370–3377, 2011.

[159] B. Sensale-Rodriguez, R. Yan, L. Liu, D. Jena, and H. G. Xing, “Graphene for reconfigurable terahertz optoelectronics,” Proc. IEEE, vol. 101, no. 7, pp. 1705–1716, 2013.

[160] X. Luo, T. Qiu, W. Lu, and Z. Ni, “Plasmons in Graphene: Recent progress and applications,” Mater. Sci. Eng. R Reports, vol. 74, no. 11, pp. 351–376, 2013.

[161] M. P. Ariza and M. Ortiz, “Discrete dislocations in Graphene,” J. Mech. Phys. Solids, vol. 58, no. 5, pp. 710–734, 2010.

[162] L. A. Falkovsky and S. S. Pershoguba, “Optical far-infrared properties of a Graphene monolayer and multilayer,” Phys. Rev. B - Condens. Matter Mater. Phys., vol. 76, no. 15, pp. 1–4, 2007.

[163] G.W. Hanson, “Dyadic Green’s functions for an anisotropic non-local model of biased Graphene,” IEEE Trans. Antennas Propag., vol. 56, no. 3, pp. 747–757, 2008.

[164] T. Low and P. Avouris, “Graphene Plasmonics for Terahertz to Mid-Infrared Applications,” ACS Nano Vol. 8, Issue 2 pp. 1075-1950, February 25, 2014.

[165] D. Correas-Serrano, J. S. Gomez-Diaz, D. L. Sounas, Y. Hadad, A. Alvarez-Melcon, and A. Alu, “Nonreciprocal Graphene Devices and Antennas Based on Spatiotemporal Modulation,” IEEE Antennas Wirel. Propag. Lett., vol. 15, no. c, pp. 1529–1533, 2016.

[166] P. Chen, C. Argyropoulos, and A. Alù, “Terahertz Antenna Phase Shifters Using,” IEEE Trans. Antenna Propag., vol. 61, no. 4, pp. 1528–1537, 2013.

[167] F. Rana, “Graphene Terahertz Plasmon Oscillators Farhan,” vol. 7, no. 1, pp. 91–99, 2008.

[168] M. S. Sharawi, “Printed multi-band MIMO antenna systems and their performance metrics [wireless corner],” IEEE Antennas Propag. Mag., vol. 55, no. 5, pp. 218–232, 2013.

[169] Marc Esquius-Morote, J. S. Gómez-D´ıaz, and J. Perruisseau-Carrier, “Periodically-Modulated Graphene Leaky-Wave Antenna for Electronic Beamscanning at THz,” IEEE Trans. Terahertz Sci. Technol., vol. 4, no. 1, pp. 116–122, 2014.

[170] X. C. Wang, W. S. Zhao, J. Hu, and W. Y. Yin, “Reconfigurable terahertz leaky-wave antenna using Graphene-based high-impedance surface,” IEEE Trans. Nanotechnol., vol. 14, no. 1, pp. 62–69, 2015.

[171] V. Dmitriev, G. Tavares, and C. Nascimento, “Graphene terahertz filter,” SBMO/IEEE MTT-S Int. Microw. Optoelectron. Conf. Proc., vol. 2015-Decem, pp. 5–9, 2015.

[172] E. Carrasco and J. Perruisseau-Carrier, “Reflectarray antenna at terahertz using Graphene,” IEEE Antennas Wirel. Propag. Lett., vol. 12, pp. 253–256, 2013.

[173] Y. Dong, P. Liu, D. Yu, G. Li, and F. Tao, “Dual-Band Reconfigurable Terahertz Patch Antenna with Graphene-Stack-Based Backing Cavity,” IEEE Antennas Wirel. Propag. Lett., vol. 15, no. c, pp. 1541–1544, 2016.

[174] I. Llatser, C. Kremers, A. Cabellos-Aparicio, J. M. Jornet, E. Alarcón, and D. N. Chigrin, “Graphene-based Nano-patch antenna for terahertz radiation,” Photonics Nanostructures - Fundam. Appl., vol. 10, no. 4, pp. 353–358, 2012.

[175] R. Bala and A. Marwaha, “Development of computational model for tunable characteristics of Graphene based triangular patch antenna in THz regime,” J. Comput. Electron., vol. 15, no. 1, pp. 222–227, 2016.

[176] S. Abadal, I. Llatser, A. Mestres, H. Lee, E. Alarcon, and A. Cabellos-Aparicio, “Time-domain analysis of Graphene-based miniaturized antennas for ultra-short-range impulse radio communications,” IEEE Trans. Commun., vol. 63, no. 4, pp. 1470–1482, 2015.

[177] A. Alu and N. Engheta, “Theory, modeling and features of optical Nanoantennas,” IEEE Trans. Antennas Propag., vol. 61, no. 4, pp. 1508–1517, 2013.

[178] M. Walther, D. G. Cooke, C. Sherstan, M. Hajar, M. R. Freeman, and F. A. Hegmann, “Terahertz conductivity of thin gold films at the metal-insulator percolation transition,” Phys. Rev. B - Condens. Matter Mater. Phys., vol. 76, no. 12, pp. 1–9, 2007.

[179] K. D. Paschaloudis, C.L.Zekios, L.Ghisa, P.C.Alliomes, K.E.Zoiras, A.Sharaiha, S.Iezekiel, G.A.Kyrialon., “An Eigenanalysis Study of Tunable THz and Photonic Unbounded Structures Employing Finite Element Method,” IEEE Photonics J., vol. 11, no. 5, pp. 1–20, 2019.

[180] C. Lin, M. A. Swillam, and A. S. Helmy, “Analytical model for metal–insulator–metal mesh waveguide architectures,” J. Opt. Soc. Am. B, vol. 29, no. 11, p. 3157, 2012.

[181] G. S. Unal and M. I. Aksun, “Bridging the gap between RF and optical patch antenna analysis via the cavity model,” Sci. Rep., vol. 5, pp. 1–8, 2015.

[182] J. Yang, C. Sauvan, A. Jouanin, S. Collin, J.-L. Pelouard, and P. Lalanne, “Ultrasmall metal-insulator-metal Nanoresonators: impact of slow-wave effects on the quality factor,” Opt. Express, vol. 20, no. 15, p. 16880, 2012.

[183] J. Park, H. Kim, I.-M. Lee, S. Kim, J. Jung, and B. Lee, “Resonant tunneling of surface Plasmon polariton in the Plasmonic Nano-cavity,” Opt. Express, vol. 16, no. 21, p. 16903, 2008.

[184] A. Chandran, E. S. Barnard, J. S. White, and M. L. Brongersma, “Metal-dielectric-metal surface Plasmon-polariton resonators,” Phys. Rev. B - Condens. Matter Mater. Phys., vol. 85, no. 8, pp. 1–9, 2012.

[185] I. F. Akyildiz, J. M. Jornet, and C. Han, “Terahertz band: Next frontier for wireless communications,” Phys. Commun., vol. 12, pp. 16–32, 2014.

[186] M. Danciu, T. A. Stratulat, C. Stefanescu, G. Dodi, B. I. Tamba, C. T. Mihai, G. D. Stanciu, A. Luca, I. A. Spiridon, L. B. Ungureanu, V. Ianole, I. Ciortescu, C. Mihai, G. Stefanescu, I. Chirilă, R. Ciobanu, and V. L. Drug, "Terahertz spectroscopy and imaging: A cutting-edge method for diagnosing digestive cancers," Materials (Basel)., vol. 12, no. 9, pp. 1–16, 2019.

[187] J. Cheng, F. Fan, and S. Chang, "Recent Progress on Graphene-Functionalized Metasurfaces for Tunable Phase and Polarization Control," Nanomaterials, vol. 9, no. 3, p. 398, 2019.

[188] J. Kim , D. S. Kim, B. Kang, J. Park, Y. M. Bahk , W. T. Kim, J. Rhie, H. Jeon, F. Rotermund, D. S. Kim , "Terahertz Quantum Plasmonics of Nanoslot Antennas in Nonlinear Regime," Nano Lett., 2015.N. Berkovitch, P. Ginzburg, and M. Orenstein, "Nano-plasmonic antennas in the near infrared regime," J. Phys. Condens. Matter, vol. 24, no. 7, 2012.

[189] S. Y. Lee, M. Choo, S. Jung, and W. Hong, "Optically transparent nano-patterned antennas: A review and future directions," Appl. Sci., vol. 8, no. 6, pp. 1–13, 2018.

[190] A. Saeed, S. Panaro, R. Proietti Zaccaria, W. Raja, C. Liberale, M. Dipalo, G. C. Messina, H. Wang, F. De Angelis & A. Toma "Stacked optical antennas for plasmon propagation in a 5 nm-confined cavity," Sci. Rep., vol. 5, no. June, 2015.

[191] P. R. West, S. Ishii, G. V. Naik, N. K. Emani, V. M. Shalaev, and A. Boltasseva, "Searching for better plasmonic materials," Laser Photonics Rev., vol. 4, no. 6, pp. 795–808, 2010.

[192] A. Mohammadi, V. Sandoghdar, and M. Agio, "Gold, copper, silver and aluminum nanoantennas to enhance spontaneous emission," J. Comput. Theor. Nanosci., vol. 6, no. 9, pp. 2024–2030, 2009.

[193] J. F. Herrmann and C. Höppener, "Dumbbell gold nanoparticle dimer antennas with advanced optical properties," Beilstein J. Nanotechnol., vol. 9, no. 1, pp. 2188–2197, 2018.

[194] J. Tong, F. Suo, J. Ma, L. Y. M. Tobing, L. Qian, and D. Hua Zhang, "Surface plasmon enhanced infrared photodetection," Opto-Electronic Adv., vol. 2, no. 1, pp. 18002601–18002610, 2019.

[195] M. Nafari and J. M. Jornet, “Modeling and Performance Analysis of Metallic Plasmonic Nano-Antennas for Wireless Optical Communication in Nanonetworks,” IEEE Access, vol. 5, pp. 6389–6398, 2017.

[196] M. Shanawani, D. Masotti, and A. Costanzo, “THz rectennas and their design rules,” Electron., vol. 6, no. 4, 2017.

[197] Z. Wu and Y. Zheng, “Radiative Enhancement of Plasmonic Nanopatch Antennas,” Plasmonics, vol. 11, no. 1, pp. 213–222, 2016.

[198] Li. Tang S. E. Kocabas, Salman Latif, Ali. K. Okyay, D.Sebastien, Ly-Gagnon, K. C. Saraswat & David A. B. Milleret al., “Nanometre-scale germanium photodetector enhanced by a near-infrared dipole antenna,” Nat. Photonics, vol. 2, no. 4, pp. 226–229, 2008.

[199] A. Devilez, B. Stout, and N. Bonod, “Compact metallo-dielectric optical antenna for ultra directional and enhanced radiative emission,” ACS Nano, vol. 4, no. 6, pp. 3390–3396, 2010.

[200] J. A. Schuller, T. Taubner, and M. L. Brongersma, “Optical antenna thermal emitters,” Nat. Photonics, vol. 3, no. 11, pp. 658–661, 2009.

[201] Y. Yang, D. Zhao, H. Gong, Q. Li, and M. Qiu, “Plasmonic sectoral horn nanoantennas,” Opt. Lett., vol. 39, no. 11, pp. 3204–3207, 2014.

[202] G. Varshney, A. Verma, V. S. Pandey, R. S. Yaduvanshi, and R. Bala, “A Proximity Coupleld Wideband Graphene Antenna with the Generation of Higher Order TM Modes for THz Application,” Opt. Mater. Elsevier, vol. 85, pp. 456–463, 2018.

[203] G. Varshney, S. Gotra, J. Kaur, V. S. Pandey, and R. S. Yaduvanshi, “Obtaining the Circular Polarization in a Nano-Dielectric Resonator Antenna for Photonics Applications,” Semicond. Sci. Technol., vol. 34, no. 7, p. 07LT01, 2019.

[204] G. Varshney, S. Gotra, V. S. Pandey, and R. S. Yaduvanshi, “Proximity-coupled two-port multi-input-multi-output graphene antenna with pattern diversity for THz applications,” Nano Commun. Netw., vol. 21, p. 100246, 2019.

[205] G. Varshney, “Reconfigurable Graphene Antenna for THz Applications: A Mode Conversion Approach,” Nanotechnology, IOP Sci., p. (Accepted), 2019.

[206] S. Gotra, G. Varshney, V. S. Pandey, and R. S. Yaduvanshi, “Super-wideband multi-input–multi-output dielectric resonator antenna,” IET Microwaves Antennas Propag., vol. Accepted, 2019.

[207] B. Andres-Garcia, L. E. Garcia-Mu˜noz, and D. Segovia-Vargas, “Ultra-wideband antenna excited by a photo mixer for terahertz band,” Prog. Electromagn. Res., vol. 114, pp. 1–15, 2011.

[208] S. Singhal, “Ultrawideband elliptical microstrip antenna for terahertz applications,” Microw. Opt. Technol. Lett., vol. 61, no. 10, pp. 2366–2373, 2019.

[209] M. Walther, D. G. Cooke, C. Sherstan, M. Hajar, M. R. Freeman, and F. A. Hegmann, “Terahertz conductivity of thin gold films at the metal-insulator percolation transition,” Phys. Rev. B - Condens. Matter Mater. Phys., vol. 76, no. 12, pp. 1–9, 2007.

[210] A.Rose, T.B.Haong, F.Mcguire, C.Ciraci, D.R. Smith, H.M.Mikikelsen., “Control of radiative processes using tunable plasmonic nanopatch antennas,” Nano Lett., vol. 14, no. 8, pp. 4797–4802, 2014.

[211] G. Lu, Xu. Jianning, W.Te, Z. Jingyi, Hu.Aiqin, B.Gregory, G.Qihuang, “Hybrid metal-dielectric nano-aperture antenna for surface enhanced fluorescence,” Materials (Basel)., vol. 11, no. 8, pp. 1–10, 2018.

[212] A. Kucherik , S.Kutrovskaya, A.Osipov, M.Gerke, I.Chestnov, S.Arakelian, A.S. Shalin, A.B.Evlyukhin, A.V. Kavokin , “Nano-Antennas Based on Silicon-Gold Nanostructures,” Sci. Rep., vol. 9, no. 1, pp. 1–6, 2019.

[213] Y. Yao, M. A. Kats, P. Genevet, Yu. Nanfang, Yi Song, Jing Kong, and F. Capasso., “Broad electrical tuning of graphene-loaded optical antennas,” Nano Lett., 2013.

[214] G. Varshney, S. Gotra, V. S. Pandey, and R. S. Yaduvanshi, “Proximity-Coupled Graphene-Patch-Based Tunable Single-/Dual-Band Notch Filter for THz Applications,” J. Electron. Mater. Springer, vol. 48, no. 8, pp. 4818–4829, 2019.

[215] S. S. Mirmosaei, S. E. Afjei, E. Mehrshahi, and M. M. Fakharian, “A dual band-notched ultra-wideband monopole antenna with spiral-slots and folded SIR-DGS as notch band structures,” Int. J. Microw. Wirel. Technol., vol. 8, no. 8, pp. 1197–1206, 2016.

[216] T. C. Tang and K. H. Lin, “An ultrawideband MIMO antenna with dual band-notched function,” IEEE Antennas Wirel. Propag. Lett., vol. 13, pp. 1076–1079, 2014.

[217] K. Takano, H. Harada, M. Yoshimura, and M. Nakajima, “Quantized conductance observed during sintering of silver nanoparticles by intense terahertz pulses,” Appl. Phys. Lett., vol. 112, no. 16, pp. 1–5, 2018.

[218] C. Balanis, “Antenna Theory - Analysis and Design.” John Willey & Sons, Inc., New York, 1997.

[219] J. W. Haus, D. de Ceglia, M. A. Vincenti, and M. Scalora, “Quantum conductivity for metal–insulator–metal nanostructures,” J. Opt. Soc. Am. B, vol. 31, no. 2, p. 259, 2014.

[220] A. Kucherik, S. Kutrovskaya, A. Osipov, M. Gerke, I. Chestnov, S. Arakelian, A. S. Shalin, A. B. Evlyukhin & A. V. Kavokin. 2019. “Nano-Antennas Based on Silicon-Gold Nanostructures.” Scientific Reports 9(1): 1–6. http://dx.doi.org/10.1038/s41598-018-36851-w.

[221] Bala, Rajni, and Anupma Marwaha. 2012. “Analysis and Design of Terahertz Microstrip Antenna on Photonic Bandgap Material.” Journal of Computational Electronics 11(4): 364–73.

[222] Jha, Kumud Ranjan, and G. Singh. 2010. “Analysis and Design of Rectangular Microstrip Antenna on Two-Layer Substrate Materials at Terahertz Frequency.” Journal of Computational Electronics 9(2): 68–78.

[223] Jha, Kumud Ranjan, and Ghanshyam Singh. 2009. “Improved Performance Analysis of Square Patch Microstrip Antenna at Terahertz Frequency.” ARTCom 2009 - International Conference on Advances in Recent Technologies in Communication and Computing: 676–79.

[224] D. H. Werner and S. Ganguly, “An overview of fractal antenna engineering research,” IEEE Antennas Propag. Mag., vol. 45, no. 1, pp. 38–57, 2003.

[225] Singhal, Sarthak. 2019a. “Elliptical Ring Terahertz Fractal Antenna.” Optik 194(May): 163129. https://doi.org/10.1016/j.ijleo.2019.163129.

[226] S. Das, D. Mitra, S. Ranjan, and B. Chaudhuri, “Fractal Loaded Circular Patch Antenna for Super Wide Band Operation in THz Frequency Region,” Opt. - Int. J. Light Electron Opt., p. 165528, 2020.

[227] P. Van Daele, I. Moerman, and P. Demeester, “Wireless body area networks: Status and opportunities,” 2014 31th URSI Gen. Assem. Sci. Symp. URSI GASS 2014, pp. 2–5, 2014.

[228] Mark, Z. Wang, E. G. Lim, K. L. Man, J. C. Huang, YiWang, and Leach, “Wireless body area network and its applications,” ISOCC 2015 - Int. SoC Des. Conf. SoC Internet Everything, pp. 169–170, 2016.

[229] A. W. Astrin, H. B. Li, and R. Kohno, “Standardization for Body Area Networks,” IEICE Trans. Commun., vol. E92-B, no. 2, pp. 366–372, 2009.

[230] A. Sabban, “Active Compact Wearable Body Area Networks for Wireless Communication, Medical and IoT Applications,” Appl. Syst. Innov., vol. 1, no. 4, p. 46, 2018.

[231] P. B. Samal, P. Jack Soh, and Z. Zakaria, “Compact and Wearable Microstrip-based Textile Antenna with Full Ground Plane Designed for WBAN-UWB 802.15.6 Application,” 13th Eur. Conf. Antennas Propagation, EuCAP 2019, vol. 2019, 2019.

[232] V. S. Ubale and O. S. Lamba, “Flexible Wearable Antennas for Body Area Network,” Int. J. Recent Technol. Eng., vol. 8, no. 5, pp. 1561–1565, 2020.

[233] Z. H. Jiang, D. E. Brocker, P. E. Sieber, and D. H. Werner, “A compact, low-profile metasurface-enabled antenna for wearable medical body-area network devices,” IEEE Trans. Antennas Propag., vol. 62, no. 8, pp. 4021–4030, 2014.

[234] R. B. V. B. Simorangkir, S. M. Abbas, and K. P. Esselle, “A printed UWB antenna with full ground plane for WBAN applications,” 2016 Int. Work. Antenna Technol. iWAT 2016, pp. 127–130, 2016.

[235] Y. M. Pan, K.W.Leung, K.W.Luk , “Design of the millimeter-wave rectangular dielectric resonator antenna using a higher-order mode,” 2015 Int. Work. Antenna Technol. iWAT 2015, vol. 2017, no. 8, pp. 2780–2788, 2017.

[236] X. S. Fang, K. W. Leung, and R. S. Chen, “On the wideband notched rectangular dielectric resonator antenna,” Final Progr. B. Abstr. - iWAT 2011 2011 IEEE Int. Work. Antenna Technol. Small Antennas, Nov. Struct. Innov. Metamaterials, no. 1, pp. 267–270, 2011.

[237] R. Al-askalani, H. F. Hammad, M. Leib, “Investigation on an UWB Antenna combining a Caped-Monopole and a Dielectric Resonator,” IEEE, no. 1, pp. 2–5, 2010.

[238] M. M. Tahseen and A. A. Kishk, “Textile-based wideband flexible wearable dielectric resonator antennas for WLAN-band,” 2016 17th Int. Symp. Antenna Technol. Appl. Electromagn. ANTEM 2016, pp. 6–8, 2016.

[239] S. H. H. Mashhadi, S. M. Y. Abbas, Z. Wu, and L. Z. Thamae, “Transmission characteristics of wearable broadband textile dielectric resonator antennas in body area network,” Proc. 2012 9th Int. Bhurban Conf. Appl. Sci. Technol. IBCAST 2012, no. November, pp. 336–339, 2012.

[240] A. Iqbal and O. A. Saraereh, “Design and analysis of flexible cylindrical dielectric resonator antenna for body centric WiMAX and WLAN applications,” 2016 Loughbrgh. Antennas Propag. Conf. LAPC 2016, pp. 1–4, 2017.

[241] A. R. Chandran, N. Timmons, and J. Morrison, “Compact microstrip line fed dielectric resonator based wearable antenna,” 2014 IEEE Conf. Antenna Meas. Appl. CAMA 2014, pp. 1–4, 2014.

[242] M. S. Iqbal and K. P. Esselle, “A compact wideband dielectric resonator antenna for on-body applications,” Conf. Proc. - 2014 IEEE MTT-S Int. Microw. Work. Ser. RF Wirel. Technol. Biomed. Healthc. Appl. IMWS-Bio 2014, pp. 6–8, 2015.

[243] A. M. Faiz, T. Alves, B. Poussot, and J. M. Laheurte, “Diversity antenna combining slot-loop DRA for BAN applications,” Electron. Lett., vol. 48, no. 1, pp. 7–8, 2012.

[244] A. M. Faiz, N. Gogosh, A. Rehman, M. F. Shafique, B. Poussot, and J. M. Laheurte, “Pattern diversity antenna with high-temperature tolerance for body area networks,” IET Microwaves, Antennas Propag., vol. 10, no. 2, pp. 162–167, 2016.

[245] D. Guha and C. Kumar, “Microstrip Patch versus Dielectric Resonator Antenna Bearing All Commonly Used Feeds,” IEEE antenna propogation Mag., no. February, pp. 45–55, 2016.

[246] R. Zaker, C. Ghobadi, and J. Nourinia, “A modified microstrip-fed two-step tapered monopole antenna for UWB and WLAN applications,” Prog. Electromagn. Res., vol. 77, pp. 137–148, 2007.

[247] A. K. Patel, S. Yadav, A. K. Pandey, and R. Singh, “A wideband rectangular and circular ring-shaped patch antenna with gap coupled meandered parasitic elements for wireless applications,” Int. J. RF Microw. Comput. Eng., vol. 30, no. 1, pp. 1–12, 2020.

[248] F. A. Lalitha Bhavani Konkyana and B. Alapati Sudhakar, “A review on microstrip antennas with defected ground structure techniques for ultra-wideband applications,” Proc. 2019 IEEE Int. Conf. Commun. Signal Process. ICCSP 2019, pp. 930–934, 2019.

[249] Kwashik Shikder and F. Arifin, “A Novel UWB wearable Icon-Type textile antenna for WBAN applications,” ECCE 2017 - Int. Conf. Electr. Comput. Commun. Eng., pp. 886–890, 2017, doi: 10.1109/ECACE.2017.7913028.

[250] G. Almpanis, C. Fumeaux, J. Fröhlich, and R. Vahldieck, “A truncated conical dielectric resonator antenna for body-area network applications,” IEEE Antennas Wirel. Propag. Lett., vol. 8, pp. 279–282, 2009, doi: 10.1109/LAWP.2008.2005213.

[251] WHO. (2020) WHO Report on Cancer.

[252] A. C. Society, Cancer Facts & Figures, The Society, New York, NY, USA, 2016.

[253] K. B. C. Society, Breast Cancer Facts & Figures 2014,Korean Breast Cancer Society, Seoul, South Korea, 2014.

[254] A.L.Siu,“ Screening for breast cancer:U.S. Preventive ser- vices task force recommendation statement,” Annals of Internal Medicine,vol.164, pp.279–296,2016.

[255] D. R. Hooley, “Mammographic Images Showing How Cancer Looks in Each of the Breast Density Categories,” Dense Breast info, http://densebreast-info.org/faqs-for-health-professionals .aspx.

[256] P. M. Meaney, M. W. Fanning, T. Zhou, A. Golnabi, S. D. Geimer, and K. D. Paulsen, “Clinical microwave breast imaging—2D results and the evolution to 3D,” in Proceedings of the 2009 International Conference on Electromagnetics in Advanced Applications (ICEAA’09), pp. 881–884, Torino, Italy, September 2009.

[257] P. M. Meaney, M. W. Fanning, D. Li, S. P. Poplack, and K. D. Paulsen, “A clinical prototype for active microwave imaging of the breast,” IEEE Trans. Microw. Theory Tech., vol. 48, pp. 1841–1853, 2000.

[258] T. M. Grzegorczyk, P. M. Meaney, P. A. Kaufman, R. M. Diflorio-Alexander, and K. D. Paulsen, “Fast 3-D tomographic microwave imaging for breast cancer detection,” IEEE Transactions on Medical Imaging,vol.31,pp. 1584–1592, 2012.

[259] K.-J. Lee, J.-Y. Kim, S.-H. Son, J. Lee, and S. Jeon, “Sensing probe for 3–6 GHz microwave imaging systems,” Electronics Letters, vol.50, pp. 1049-1050,2014.

[260] E. Porter, E. Kirshin, A. Santorelli, M. Coates, and M. Popovı,“Time-domain multistatic radar system for microwave breast screening,” IEEEAntennas andWireless Propagation Letters,vol. 12, pp. 229–232, 2013.

[261] E.C.Fear,P.M.Meaney, andM.A.Stuchly,“Microwaves for breast cancer detection?” IEEE Potentials,vol.22,pp. 12– 18, 2003.

[262] M. Klemm, J. A. Leendertz, D. Gibbins, I. J. Craddock, A. Preece, andR. Benjamin, “Microwave radar-based breast cancer detection: imaging in

inhomogeneous breast phantoms," IEEE Antennas andWireless Propagation Letters,vol.8,pp. 1349–1352, 2009.

[263] J. Bourqui, J. Garrett, and E. Fear, "Measurement and analysis of microwave frequency signals transmitted through the breast," International Journal of Biomedical Imaging,vol.2012, Article ID 562563, 11 pages, 2012.

[264] R. C. Conceicao, H. Medeiros, M. O'Halloran, D. Rodriguez- Herrera, D. Flores-Tapia, and S. Pistorius, "Initial classification of breast tumour phantoms using a UWB radar prototype," in Proceedings ofthe 15th International Conference on Electromag- netics in Advanced Applications (ICEAA '13), pp. 720–723, IEEE, 2013.

[265] N. Simonov, S.-I. Jeon, S.-H. Son, J.-M. Lee, and H.-J. Kim,"3D microwave breast imaging based on multistatic radar concept system," Journal ofElectromagnetic Engineeringand Science,vol. 12, pp. 107–114, 2012.

[266] S. S. Chaudhary, R. K. Mishra, A. Swarup, and J. M. Thomas,"Dielectric properties of normal & malignant human breast tissues at radiowave & microwave frequencies," Indian Journal of Biochemistry and Biophysics,vol.21,pp. 76–79, 1984.

[267] P. M. Meaney, S. A. Pendergrass, M. W. Fanning, and K. D. Paulsen, "Importance of using a reduced contrast coupling medium in 2D microwave breast imaging," Journal ofElectro- magnetic Waves and Applications,vol.17,pp.333–355, 2003.

[268] L. Wang, "Microwave sensors for breast cancer detection," Sensors (Switzerland), vol. 18, no. 2, pp. 1–17, 2018, doi: 10.3390/s18020655.

[269] R. Cicchetti, E. Miozzi, and O. Testa, "Wideband and UWB antennas for wireless applications: A comprehensive review," Int. J. Antennas Propag., vol. 2017, 2017, doi: 10.1155/2017/2390808.

[270] T. Uno and S. Adachi, "Inverse scattering method for one-dimensional inhomogeneous layered media," IEEE Trans. Antennas Propag., vol. 35, no. 12, pp. 1456–1466, 1987, doi: 10.1109/TAP.1987.1144033.

[271] R. K. Mongia, P. Bhartia, C. L. Larose, and S. R. Mishra, "Accurate Measurement of Q-Factors of Isolated Dielectric Resonators," IEEE Trans. Microw. Theory Tech., vol. 42, no. 8, pp. 1463–1467, 1994, doi: 10.1109/22.297807.

[272] T. Jun Cui and C. Hong Liang, "Inverse Scattering Method for One-Dimensional Inhomogeneous Lossy Medium by Using a Microwave Networking Technique,"

IEEE Trans. Microw. Theory Tech., vol. 43, no. 8, pp. 1773–1781, 1995, doi: 10.1109/22.402259.

[273] O. P. Profiles, V. a Mikhnev, and P. Vainikainen, “Two-Step Inverse Scattering Method for,” vol. 48, no. 2, pp. 293–298, 2000.

[274] D. Franceschini, M. Donell, G. Franceschini, and A. Massa, “Iterative image reconstruction of two-dimensional scatterers illuminated by TE waves,” IEEE Trans. Microw. Theory Tech., vol. 54, no. 4, pp. 1484–1494, 2006, doi: 10.1109/TMTT.2006.871921.

[275] J. M. Geffrin, P. Sabouroux, and C. Eyraud, “Free space experimental scattering database continuation: Experimental set-up and measurement precision,” Inverse Probl., vol. 21, no. 6, 2005, doi: 10.1088/0266-5611/21/6/S09.

[276] W. Huang and A. A. Kishk, “Compact dielectric resonator antenna for microwave breast cancer detection,” IET Microwaves, Antennas Propag., vol. 3, no. 4, pp. 638–644, 2009, doi: 10.1049/iet-map.2008.0170.

[277] S. M. Salvador, E. C. Fear, M. Okoniewski, and J. R. Matyas, “Exploring joint tissues with microwave imaging,” IEEE Trans. Microw. Theory Tech., vol. 58, no. 8, pp. 2307–2313, 2010, doi: 10.1109/TMTT.2010.2052662.

[278] T. Kikkawa and T. Sugitani, “Planar UWB antenna array for breast cancer detection,” 2013 7th Eur. Conf. Antennas Propagation, EuCAP 2013, vol. 2, pp. 339–343, 2013.

[279] S. Kwon and S. Lee, “Instantaneous microwave imaging with time-domain measurements for breast cancer detection,” Electron. Lett., vol. 49, no. 10, pp. 653–654, 2013, doi: 10.1049/el.2013.0248.

[280] E. Porter, E. Kirshin, A. Santorelli, M. Coates, and M. Popoví, “Time-domain multistatic radar system for microwave breast screening,” IEEE Antennas Wirel. Propag. Lett., vol. 12, pp. 229–232, 2013, doi: 10.1109/LAWP.2013.2247374.

[281] B. J. Mohammed, A. M. Abbosh, S. Mustafa, and D. Ireland, “Microwave system for head imaging,” IEEE Trans. Instrum. Meas., vol. 63, no. 1, pp. 117–123, 2014, doi: 10.1109/TIM.2013.2277562.

[282] E. Porter, H. Bahrami, A. Santorelli, B. Gosselin, L. A. Rusch, and M. Popovic, “A Wearable Microwave Antenna Array for Time-Domain Breast Tumor Screening,” IEEE Trans. Med. Imaging, vol. 35, no. 6, pp. 1501–1509, 2016, doi: 10.1109/TMI.2016.2518489.

[283] Z. Xu, S. Zhu, R. Wang, and R. Xie, “An H-shape dielectric resonator antenna with U-slot on the patch,” 2016 Prog. Electromagn. Res. Symp. PIERS 2016 - Proc., pp. 4447–4450, 2016, doi: 10.1109/PIERS.2016.7735647.

[284] V. Selvaraj, D. Baskaran, P. H. Rao, P. Srinivasan, and R. Krishnan, “Breast Tissue Tumor Analysis Using Wideband Antenna and Microwave Scattering,” IETE J. Res., vol. 0, no. 0, pp. 1–11, 2018, doi: 10.1080/03772063.2018.1531067.

[285] W. Shao, A. Edalati, T. R. McCollough, and W. J. McCollough, “A Time-Domain Measurement System for UWB Microwave Imaging,” IEEE Trans. Microw. Theory Tech., vol. 66, no. 5, pp. 2265–2275, 2018, doi: 10.1109/TMTT.2018.2801862.

[286] M. Z. Mahmud, M. T. Islam, N. Misran, S. Kibria, and M. Samsuzzaman, “Microwave imaging for breast tumor detection using uniplanar AMC Based CPW-fed microstrip antenna,” IEEE Access, vol. 6, no. c, pp. 44763–44775, 2018, doi: 10.1109/ACCESS.2018.2859434.

[287] M. T. Islam, M. Z. Mahmud, M. T. Islam, S. Kibria, and M. Samsuzzaman, “A Low Cost and Portable Microwave Imaging System for Breast Tumor Detection Using UWB Directional Antenna array,” Sci. Rep., vol. 9, no. 1, pp. 1–13, 2019, doi: 10.1038/s41598-019-51620-z

[288] S. S. Singhwal, B. K. Kanaujia, A. Singh, and J. Kishor, “Novel circularly polarized dielectric resonator antenna for microwave image sensing application,” Microw. Opt. Technol. Lett., vol. 61, no. 7, pp. 1821–1827, 2019, doi: 10.1002/mop.31830.

[289] G. Kaur and A. Kaur, “ Breast tissue tumor detection using ‘ S ’ parameter analysis with an UWB stacked aperture coupled microstrip patch antenna having a ‘ + ’ shaped defected ground structure ,” Int. J. Microw. Wirel. Technol., pp. 1–17, 2019, doi: 10.1017/s1759078719001442.

APPENDIX

TOOLS AND SOFTWARE USED:

1.HIGH FREQUENCY STRUCTURE SIMULATOR (HFSS): Modelling, designing and simulation of dieectric resonator antenna is done on HFSS 15.0 software. Optimization of antenna is done with optimetric tool of this software.

2. CST MICROWAVE STUDIO SIMULATOR: HFSS makes use of FEM (finite element method) method with MoM techniques. On the other hand , CSt makes use of FDTD techniques to converge the result. This technique is more useful in simulating designs at higher frequency. In this thesis,THz regime antennas are simulated using CST Microwave studio.

3. TOOLS FOR MEASUREMENT OF PERFORMANCE PARAMETERS OF ANTENNA:

1. Vector Network Analyzer(VNA): To calculate reflection coefficient of fabricated antenna , Agilent technologies VNA is used as shown in picture below:

Vector Network Analyzer

2. Anechoic Chamber: Measurement of gain, radiation pattern of fabricated antenna is done in AAICTR, New delhi as shown in picture below:

3. Signal Generator and Spectrum Analyzer: Rodhe signal generator and spectrum analyzer is used to generate and measure the spectrum of the signal**.** As shown in pictures below:

Rodhe and Schwarz Signal generator

Rodhe and Schwarz Spectrum Analyzer

4. MICROSOFT EXCEL AND ORIGIN SOFTWARE: Microsoft excel and origin both software are used for plotting graphs of the radiation characteristics of the antenna from simulated and measured data.

BRIEF PROFILE OF RESEARCH SCHOLAR

Taruna Sharma (parashar.taruna@gmail.com) is an agile and innovative Ph.D scholar in Department of Electronics and Communication at J.C. Bose University of Science and Technology, YMCA, Faridabad, India. Her qualification comprises of Diploma, B.E and M.Tech in Electronics and Communication. She has a keen interest in the field of RF Applications, Microwave & RADAR Communication,Optics ,Graphene and related technologies. Her vision is to implement microwave and millimetre antenna technologies to eradicate societal problem.

LIST OF PUBLICATIONS

Paper published in International Journals: 4

International Conference: 4

National Conference:3

Communicated Paper: 1

List of Published Papers in International Journals

Sr. No.	Title of Paper	Name of Journal where published	ISBN/ISSN No.	Volume and Issue	Year	Pages
1.	A novel Hybrid Ultra-Wideband Radio Sensor for Primitive Stage Detection of Breast Cancer	BJIT, Springer Nature	2511-2104	1,2	March 2021	**1-19**
2.	A Versatile Ultra-Wideband Radio Sensor for Early Stage Detection of Breast Cancer	MAPAN, Journal of Metrology Society of India	0970-3950 / 0974-9853	13,5	October 2021	**1-11**
3.	Obtaining the Tunable Band Notch in Ultra Wide Band THz Antenna Using Graphene Nano Ribbons	Optical Engineering	0091-3286	59	April 2020	47103(1-11)
4.	Dual Band Notch, Compact, Low Profile,	International Journal of Engineering and Advanced	2249-8958	10,1	October 2020	167-169

	Hybrid Ultra Wide Band DRA	Technology (IJEAT)				

List of Published Papers in International Conferences

Sr. No.	Title of Paper	Name of International Conference	Year
1.	**Dual band Rectangular Dielectric Resonator Antenna with Partial Ground Structure for Wi-Max/WLAN Applications**	Emerging Technologies: AI, IoT and CPS for Science & Technology Applications	**September, 2021**
1.	Investigation on multi-segment rectangular dielectric resonator antenna for high gain and wide bandwidth for X& Ku band antenna	IEEE international Conference on Signal Processing And Communication Engineering Systems (SPACES) 2018	Jan 2018
2.	Enhanced gain stacked RDRA with conformal trapezoidal patch"	International Conference, "ICPR-_2017" AIACTR, New Delhi	Dec 2017
3.	Design and analysis of MSRDRA for C-band Applications"	International Conference, "ICPR-_2017" AIACTR, New Delhi	Dec 2017
4.	Methodology of controlling resonant modes and results"	International Conference on Sustainable Development through Research in Engineering and Management held in YMCAUST	Dec 2016

List of Published Papers in National Conferences

Sr. No.	Title of Paper	Name of International Conference	Year
1.	Analysis of DRA using various bandwidth broadening techniques	National conference "RSTTMI" held in YMCAUST, Faridabad	March 2016
2.	Design and Analysis of dual frequency UWB rectangular dielectric resonator antenna for S-band application	National Conference on Emerging Trends in Engineering & Technology held in APEEJAY SATYA UNIVERSITY, SOHNA, GURGAON	April 2014
3.	Rectangular fluid frame magneto hydro dynamic antenna	National Conference on RF and Wireless Communication Networks (NCRWCN-2014)	Dec 2014

List of Communicated Papers in International Journals

Sr. No.	Title of Paper	Name of Journal where published	ISBN/ISSN No.	Volume and Issue	Year
1.	Ultra Wide Band Hybrid Antenna for WBAN applications	AEÜ - International Journal of Electronics and Communications	1434-8411	Communicated	2021